

Sheffield Hallam University

Investigation of the pulse time modulation techniques for transmission of wideband signals

ISSA, Abd Al-Kareem M.

Available from the Sheffield Hallam University Research Archive (SHURA) at:

<http://shura.shu.ac.uk/3094/>

A Sheffield Hallam University thesis

This thesis is protected by copyright which belongs to the author.

The content must not be changed in any way or sold commercially in any format or medium without the formal permission of the author.

When referring to this work, full bibliographic details including the author, title, awarding institution and date of the thesis must be given.

Please visit <http://shura.shu.ac.uk/3094/> and <http://shura.shu.ac.uk/information.html> for further details about copyright and re-use permissions.

Investigation of the Pulse Time Modulation Techniques for Transmission of Wideband Signals

Abd Al-Kareem M. Issa

A thesis submitted in partial fulfilment of the
requirement of Sheffield Hallam University for
the degree of Doctor of Philosophy



November 1997

ProQuest Number: 10697166

All rights reserved

INFORMATION TO ALL USERS

The quality of this reproduction is dependent upon the quality of the copy submitted.

In the unlikely event that the author did not send a complete manuscript and there are missing pages, these will be noted. Also, if material had to be removed, a note will indicate the deletion.



ProQuest 10697166

Published by ProQuest LLC (2017). Copyright of the Dissertation is held by the Author.

All rights reserved.

This work is protected against unauthorized copying under Title 17, United States Code
Microform Edition © ProQuest LLC.

ProQuest LLC.
789 East Eisenhower Parkway
P.O. Box 1346
Ann Arbor, MI 48106 – 1346



Declaration

I hereby declare that this thesis is entirely my own work and has not been submitted in support of an application of another degree or qualification of this or any other university, institute of learning or industrial organisation.

Abd Al-Kareem M. Issa

August 1997.

Acknowledgement

The author wishes to express his sincere thanks to his supervisor, Professor Z. Ghassemlooy for his valuable assistance and patient guidance during the development of this work. His continues encouragement and time he devoted most generously on consultation are greatly appreciated.

The author also would like to express his gratitude and thanks to Prof. A. Ray, for his assistance.

Credits would not be complete without mentioning the assistance and co-operation given by Mr. K. Evans.

The author never forgets his friends in the research group, specially Dr. Asil Hassan, for their help in completing the general requirements for this thesis.

Abstract

The choice of the modulation format is the principle factor in realising a high-performance bandwidth efficient communication system at an acceptable cost and complexity. Pulse time modulation technique represents an attractive alternative to purely digital or purely analogue modulation schemes which has received considerable attention over the years. But very little work has been reported on pulse slope modulation. In this work a pulse slope modulation introduced and full waveform characteristics is given. A simple novel receiver has been proposed, which is based on converting the PSM waveform into a PAM waveform by sampling the received PSM signal at the rise time interval. This design eliminates the use of a differentiator and a voltage slicer adopted in the classical demodulation technique, and it offers simplicity and improved noise performance. A new signal-to-noise formula has been presented for the first time thus enabling users to predict the system noise performance. Experimental results have shown excellent agreement to within ± 1 dB with theoretical predictions using the new formula. Results obtained show the potential of PSM in terms of simplicity and better noise performance compared to its counter part pulse amplitude modulation.

Although PTM has many advantages over analogue and digital schemes when employed as a single channel system, it becomes a challenge when multiplexing is involved. Isochronous PTM schemes are suitable while the anisochronous schemes are not. One solution to overcome this problem is to adopt a hybrid or compound modulation technique, where both isochronous and anisochronous schemes can be combined. Compound frequency and width modulation (CPFWM) is one such a scheme which offers bandwidth efficiency, simplicity and low cost over the more commonly used multiplexed techniques. Detailed investigation of CPFWM has been given and in an expression for its spectrum has been developed. The results obtained have been clarified practically and by means of computer simulation to within ± 1 dB.

In CPFWM, cross talk in the PFM and PWM channels are due to width modulation and frequency modulation, respectively. The main cause of cross talk is the carryover energy from one edge to the next edge. This effect is studied and the results obtained for the cross talk are compared with the predicted data showing an agreement to within ± 1 dB. Results were also compared with time division multiplexed pulse position modulation, showing comparable performance and under certain conditions CPFWM offering better performance.

Noise performance of PFM and PWM channels has been theoretically and experimentally investigated. It has been shown that PFM is superior to PWM over a wide range of modulation indices and pulse characteristics. When both channels are identical in bandwidth and modulation conditions, PFM offers a 7 dB improvement compared to PWM channel. The noise performance of CPFWM system is also compared with digital and analogue modulation schemes. For 25 dB CNR, CPFWM offers a 40 dB SNR which is 20 dB higher than amplitude modulation, 17 dB lower than PCM system. At CNR > 35 dB its performance approaches that of PCM system. Thus showing the potential of the scheme.

List of main symbols

$\alpha(t)$	instantaneous amplitude of the rising edge of the PSM waveform
β	frequency modulation index in PFM and SWFM schemes.
$\delta_1(t)$, $\delta_2(t)$	Delta functions
$\Delta\phi$	maximum deviation in phase (position)
Δf	maximum frequency deviation
$\delta\tau$	change in CPFWM pulse width due to the fall edge of the ramp
δT	edge time jitter in CPFWM waveform
$\Delta\tau$	peak-to-peak deviation in pulse width.
$\Delta\omega$	maximum angular frequency deviation
σ_o^2	edge jitter power
τ	pulse width
τ_g	pulse width of the regenerated PFM pulses at the CPFWM receiver
τ_o	free running pulse width of the CPFWM waveform.
ω_o	angular frequency of the carrier ($\omega_o=2\pi f_o$)
ω_2	angular frequency of the second modulating signal ($\omega_2=2\pi f_2$)
ω_1	angular frequency of the first modulating signal ($\omega_1=2\pi f_1$)
ω_m	angular frequency of the modulating signal ($\omega_m=2\pi f_m$)
ω_o	pulse free running angular frequency ($\omega_o=2\pi f_o$)
A	amplitude of the pulse
B	transmission bandwidth
B_n	noise bandwidth of the PSM receiver
C	capacitor value in PSM modulator

CNR	carrier-to-noise ratio
CT_{FW}	cross-talk from PFM to PWM channel in CPFWM system
CT_{WF}	cross-talk from PWM to PFM channel in CPFWM system
D	pulse duty cycle
$erf(.)$	error function of the enclosed quantity
f	frequency
f_1	frequency of the first modulating signal (in CPFWM system).
f_2	frequency of the second modulating signal (in CPFWM system)..
f_m	frequency of the modulating signal
f_o	pulse free running frequency
$i(t)$	Charging current through capacitor in PSM modulator
I_o	Bias current
$J_n(.)$	Bessel functions of the first kind and order n.
k	VCCS constant (A/V)
k_f	frequency modulator constant (Hz/V)
k_w	PWM modulator constant (s/V)
M	modulation index of PWM scheme
m	modulation index of, PSM, AM and pure analogue systems
M_f	modulation index of PIM waveform.
M_p	modulation index of PPM waveform.
$n(t)$	added noise voltage
n_q	number of the quantisation levels in PCM system
P	instantaneous power of the PSM waveform.
P_o	average power of the PSM waveform

$s(t)$	the instantaneous pulse slope of the PSM waveform
s_{\max}	maximum pulse slope of the PSM waveform.
s_{\min}	minimum pulse slope of PSM waveform.
SNR	signal-to-noise ratio
s_o	pulse slope when modulating signal is off.
s_r	slope of the ramp voltage
$si(\cdot)$	$si(x) \equiv \int_{-\pi}^{\pi} \frac{\sin(x)}{x} dx$
T	PSM pulse ON time
t	time
T_o	the period ($T_o=1/f_o$)
$T_{P_{\text{PWM}}}$	maximum deviation in width in CPFWM waveform.
t_r	instantaneous rise time of the PSM pulse
t_R	rise time of CPFWM pulse ($B=0.5/t_R$)
t_{rav}	average rise time of the PSM waveform
t_{max}	maximum rise time in PSM waveform
t_{min}	minimum rise time of the PSM waveform
t_{ro}	rise time of the PSM waveform when modulating signal is of
T_s	time shift of the sampling pulses
$v(t)$	PTM pulse voltage
$\dot{v}(t)$	$\dot{v}(t) \equiv \frac{dv(t)}{dt}$, slope of PTM pulse.
$v_1(t)$	amplitude of the first modulating signal

$v_2(t)$	amplitude of the second modulating signal
$v_m(t)$	amplitude of the modulating signal
$x(t_0)$	edge displacement in PTM schemes, due to noise.
AM	amplitude modulation
CPFWM	compound pulse frequency width modulation
CPIWM	compound pulse interval with modulation
CPTM	compound pulse frequency modulation
FDM	frequency division multiplexing
FM	frequency modulation
MIPTM	multiplexed isochronous PTM
PAM	pulse amplitude modulation
PCM	pulse code modulation
PFM	pulse frequency modulation
PIM	pulse interval modulation
PIWM	pulse interval width modulation
PPM	pulse position modulation
PSM	pulse slope modulation
PTM	pulse time modulation
PWM	pulse width modulation
SWFM	squarewave frequency modulation
TDM	Time division multiplexing
WDM	wavelength division multiplexing

CONTENTS

Declaration	III
Acknowledgement	IV
Abstract	V
List of main symbols	VI
1. Introduction	1
2. Modulation Techniques for Wideband Signal Transmission	
2.1 Introduction	7
2.2 Pure analogue modulation	8
2.3 Digital modulation	11
2.4 Pulse analogue modulation	13
2.5 PTM schemes	16
2.5.1 pulse width modulation	16
2.5.2 pulse position modulation	21
2.5.3 pulse interval modulation	24
2.5.4 pulse interval width modulation	27
2.5.5 pulse frequency modulation	31
2.5.6 squarewave frequency modulation	33
2.5.7 digital PTM schemes	36
2.6 Noise performance of PTM systems	37
2.7 Non-linear distortion of PTM systems	44

3. The Pulse Slope Modulation Technique

3.1 Introduction	48
3.2 PSM generation	49
3.3 PSM demodulation	57
3.4 Power relations of PSM pulses	62
3.4.1 trapezoidal PSM	62
3.4.2 triangular PSM	67
3.5 Frequency spectrum of the PSM signal	68
3.6 Noise performance of the PSM signal	71
3.7 System implementation and results	80
3.7.1 PSM transmitter	80
3.7.2 PSM receiver	81
3.7.3 experimental results	81

4. Multiplexing and Compound Modulation Techniques

4.1 Introduction	95
4.2 Multiplexing techniques for optical fibre systems	96
4.2.1 time division multiplexing	96
4.2.2 frequency division multiplexing	97
4.2.3 wavelength division multiplexing	99
4.2.4 subcarrier multiplexing	101
4.2.5 multiplexed isochronous PTM	103
4.3 Compound pulse time modulation	108
4.3.1 compound pulse interval and width modulation	111

4.3.2	pulsed frequency and width modulation	114
4.3.3	compound pulse frequency and width modulation	124
5. Compound Pulse Frequency and Width Modulation		
5.1	Introduction	128
5.2	CPFWM modulation and demodulation	129
5.2.1	CPFWM Modulator	129
5.2.2	CPFWM demodulator	139
5.3	Computer simulation of CPFWM system	142
5.3.1	simulation of the CPFWM modulator	143
5.3.2	simulation of the CPFWM receiver	144
5.4	Experimental investigation of the CPFWM system	150
5.4.1	CPFWM modulator	150
5.4.2	CPFWM demodulator	154
5.4.3	Results	157
6. Frequency spectrum of the CPFWM waveform		
6.1	Introduction	170
6.2	Theoretical analysis of the CPFWM modulation spectrum	171
6.3	Experimental and computer simulation results	180
7. Cross-talk and Noise Performance Analysis		
7.1	Introduction	196
7.2	Cross-talk performance in CPFWM systems	197

7.2.1 Cross-talk from PWM signal to PFM signal	200
7.2.2 Cross-talk from PFM signal to PWM signal	215
7.3 Noise Performance of the CPFWM system	235
7.3.1 noise performance of the PFM channel	237
7.3.2 noise performance of the PWM channel	241
8. Conclusions	255
References	262
Appendix I	275
Appendix II	278
Appendix III	283

Chapter One

Introduction

In the past decade there has been a rapid increase in the number of applications of broadband transmission and local area networks for instrumentation and communication systems. In these systems, high speed data and wideband video and voice signals are usually transmitted over short to moderate distances. Diverse services such as teleconferencing, remote monitoring, community antenna television (CATV) networks, TV distribution within schools, hospital etc., along with high speed graphics require wideband and cost effective communication links. In these circumstances, a wideband, high quality, and reliable transmission system is required both in temporary and permanent system installations. Traditionally, coaxial cable has been used as transmission media for wideband systems over short distances and microwave links have been used to cover longer distances [1-5].

However, coaxial transmission is a very limited medium, and suffers from many problems. Depending on the diameter of the coaxial cable, the length of a cable link ranges from few hundred meters to two kilometers. To satisfy the stringent requirements for freedom from interference these cables are usually fitted with special shielding. Thus, they are bulky, heavy and difficult to handle which is a considerable disadvantage in temporary installations. Furthermore, the transmission parameters are temperature and humidity dependent which makes system adjustment always

necessary. Special earthing facilities may also be required in order to protect users from lightning [5, 6].

In case of microwave links, line-of-sight propagation is required between transmitter and receiver. The frequency of operation and polarization should be carefully chosen to avoid interference with other users. If several channels are to be operated in parallel, the required bandwidth is considerably increased. Unfavorable topography or atmospheric conditions can degrade transmission [7].

However, by introducing optical fiber technology, it would be possible to create a transmission system that could outperform coaxial cable and microwave systems and solve all problems associated with them, in both temporary and permanent installations. Therefore, for wideband transmission systems, it seems that optical fiber technology is an attractive and nearly ideal transmission medium because of its wide bandwidth and very low attenuation (<0.1 dB/km). This is in addition to its very small physical size, low weight, flexibility, and immunity against electromagnetic interference. Optical fibre systems have also the property of operating in the multi-gigabits/second region over a very long distance as recently demonstrated [8]. Furthermore, gains may be realised with the advent of wavelength division multiplexing, optical amplifiers, coherent optics and soliton optical communications [9-13].

In all of the above systems, however, several possible methods have been considered for realising optical transmission. These are: direct intensity modulation by the baseband signal or analogue radio frequency (RF) signal, optical intensity modulation after converting the baseband signal into a digital signal such as pulse code modulation (PCM), and finally optical intensity modulation after converting the baseband signal into pulse analogue signal. The careful choice of modulation format is of prime

importance and may need to be looked at from the point of cost, performance and system complexity [9, 10].

Purely analogue transmission is based on the modulation of a light source driving current directly by the information signal or by an intermediate electrical carrier modulated by the information signal. This kind of transmission has the merits of simplicity, bandwidth efficiency, and reasonably low cost [14, 15]. However, the major limitation of this method is the source linearity requirement [15-18]. This requirement is such that, for light emitting diode (LED) implementations, the dynamic range is usually insufficient for realistic application, whereas injection laser sources require very precise biasing and the optical modulation depth is limited by the threshold current [15-17]. In addition to that, pure analogue modulation can not provide the required signal-to-noise ratio for reliable and efficient transmission. This is besides, a significant amplitude and phase distortion which may be experienced due to the modal noise [18].

On the other hand, digital transmission over optical fibre has been proved to be well suited because of their high performance and the simplicity of integration with digital network. Unlike analogue transmission, the digital technique does not suffer from the source linearity. It is also free from deterioration of the quality by relay transmission, making the long-distance transmission feasible. However, the data rate required for digital wideband transmission is very high. Due to the high cost and the complexity of high speed digital transmission the application of a digital scheme to wideband signals is still limited only to the long haul transmission [19]. Therefore, especially for short length links, the analogue transmission is preferable [19].

An alternative approach that occupies an intermediate position between purely digital and purely analogue form is the pulse time modulation (PTM) scheme. This scheme has the features that the performance is less affected by the non-linear distortion of the light

source and allows routing through logic circuits and switching nodes in a network. PTM scheme requires no coding and can be realised by a simple circuit structure. Moreover, it also offers much improved signal-to-noise ratio performance compared with the purely analogue scheme with very low bandwidth overhead when compared with digital schemes. In effect, PTM has the ability to trade-off performance with bandwidth overhead, which is a particularly exploitable feature in fibre systems [20, 21]. For example, in short distance local area networks (LANs) it is most likely to use multimode or monomode fibre with a dispersive optical source, all of which impose a significant bandwidth limitation in optical channel. In these applications low-speed optical sources such as LEDs can be used, while still achieving the required signal-to-noise ratio. In contrast, the available bandwidth on the long distance terrestrial and undersea routes may be many orders of magnitude broader where optical amplification and soliton techniques are employed [13]. This additional bandwidth can be readily exploited by PTM to improve signal-to-noise ratio performance. The ability to exchange signal-to-noise performance against bandwidth extension is a property of PTM modulation techniques and is of increasing importance in high-speed networks [20].

Although the basic framework of research into PTM techniques was first reported in the late 40s' [21-25], it is only recently that a revival of interest has been experienced with the development of fibre transmission systems. The development of the different types of PTMs is basically based on the variation of the particular characteristics of a train of pulses. Consequently, a variety of pulse modulation schemes was developed. In pulse width modulation (PWM), sometimes referred as pulse duration modulation (PDM), the width of the pulse train within a predetermined time frame is changed according to the sampled value of the modulating signal. Pulse position modulation (PPM) may be considered as differentiated PWM and carries information by virtue of

the continuously variable position of a narrow pulse within a fixed time frame. These modulation schemes will be considered in later chapters.

Unlike all the above mentioned PTMs, pulse slope modulation (PSM) is obtained by varying the rise-time of the pulses so that the slope of the rising edge is determined by the amplitude of the modulating signal. Although PSM was first introduced for line circuits in early 50s, no further work was done until recently where PSM has been used for transmitting analogue signals by optical fibres over moderate distances [26-30]. PSM systems have the advantages of simplicity, bandwidth efficiency, very low cost and comparable performance with a number of other PTMs. PSM is very simple to multiplex which is considered as an advantage over most of the PTM techniques where multiplexing is not that straight forward. In the next chapter, full characterisation of the PSM system is given, together with a novel design for the receiver. The noise performance of the PSM system has been treated in detail, and the practical and theoretical results are also compared.

Despite the fact the PTM techniques save transmission bandwidth and are less affected by the non-linearity of the optical source, which make them attractive for many wideband applications, PTMs have a demerit in that the multiplexing is not easy. This is because the information is carried on one of the pulse characteristics, such as the width or position, which makes the time division multiplexing (TDM) difficult. However, although in principle frequency division multiplexing (FDM) is possible, because of the nature of their frequency spectrum, which is spread over a wide range, PTMs are difficult to multiplex in the frequency domain. Very little work has been undertaken on pulse time multiplexing. The usual method for transmitting several signals is based on a FDM/PTM approach. An alternative method of multiplexing PTM signals is to implement either the FDM or the TDM techniques within the PTM framework. In contrast to FDM and TDM, an alternative approach based on combining

different PTM schemes has been recently developed. This type of multiplexing method, known as compound pulse time modulation (CPTM) or some times as hybrid pulse time modulation [31, 32], is accomplished by a sequence of cascade PTM modules, where the modulated PTM signal of the first module is used as a reference signal for the second modulator. The advantage of this technique is that channel synchronisation is not necessary which makes it more attractive than TDM, and the whole system can be realised by simple circuit structure. Also CPTMs have very effective bandwidth utilisation, and each channel can be multiplexed and demultiplexed without the need for modulating or demodulating the other channel. This means that the cross-talk is very low in CPTMs. However, although that some CPTM schemes have been reported but very little work has been carried out on the theoretical analysis of the scheme.

In the following chapters the theory of CPTM techniques is investigated in detail. Both theoretical and experimental results are presented. The different methods of generation, and demodulation, have also been considered. Complete characterisation and implementation of one type of the CPTM, namely, compound frequency width modulation is studied in detail.

Chapter Two

Modulation Techniques for Wideband Signal Transmission

2.1 Introduction

Fibre optic transmission systems offer a unique set of solutions (and problems) to the monumental task of moving mountains of information from one location to another. However, like any form of communication, the signal to be transmitted must be encoded onto the carrier at the source (transmitter) and decoded from the carrier at the destination (receiver). When the carrier is a light wave, signal encoding is physically done either through direct modulation or external modulation of the light source. Within this modulation method exist a variety of signal encoding schemes that can be classified as either analogue or digital. The type of modulation and encoding for the fibre optic transmitter depends on a number of factors, but some light sources are better suited for certain schemes than others.

In this chapter the different modulation techniques are discussed and compared in terms of cost and performance. Emphasis will be on pulse analogue modulation which, as will be seen, is the best compromise in terms of cost and performance.

2.2 Pure analogue modulation

This is the simplest form of transmission, which is based on modulating the amplitude or the phase/frequency of the carrier in electrical transmission. However, in optical transmission, analogue modulation refers to intensity modulation which is based on the modulation of the driving current of the light source directly by the information signal or by an intermediate electrical carrier modulated by the information signal. The basic structure of an analogue optical fibre transmission system is shown in Fig. 2.1. At the transmitting end the baseband information signal is used to modulate the driving current of an optical source which will determine the optical power. At the receiving end optical signal is converted back into electrical signal through an optical receiver. A low-pass filter is employed to recover the information before being amplified.

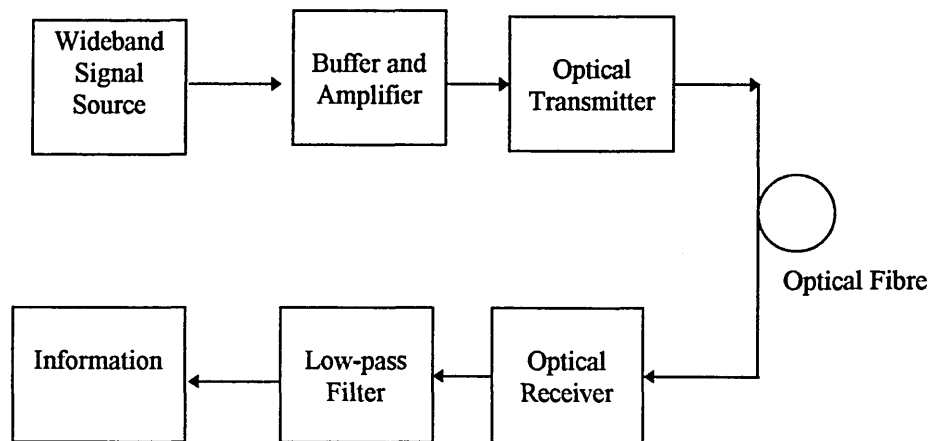


Fig. 2.1 Analogue optical fibre transmission system.

Consider an optical transmission system; The modulation index for analogue intensity modulation is defined as the ratio of the peak modulation current to the D. C. bias current of the optical source as follows [9];

$$m = \frac{I_p}{I_o} \quad (2.1)$$

where I_p is the peak current, I_o is the bias current.

The required optical transmission bandwidth is the same as the baseband signal bandwidth which means that this modulation technique has the best bandwidth efficiency compared to the digital schemes. However, this system suffers from poor noise performance and non-linearity problems. The system linearity is usually determined by the optical source and some times by the optical receiver. The more linear, surface emitting double hetrostructure LED's typically have a total harmonic distortion about 45 dB below the signal level for a modulation index of 0.7. The harmonic distortion decreases as the modulation index is reduced, but at the expense of reduced signal power output and noise performance. Most often an equalisation circuit is needed at both the receiving and the transmitting ends to minimise the non-linear distortion [9, 16, 33 , 34].

At the optical receiver, in general, there are several noise sources that contribute to the system noise performance. These are; thermal noise, shot noise, dark current noise and the modal noise which will be present when multimode fibre is used. An expression for the signal-to-noise ratio (*SNR*) performance may be given as [9];

$$\begin{aligned} SNR &= \frac{[R_o G P_o m / (1+m)]^2}{[2eG^2 (I_d + R_o P_o) + \langle I_s \rangle^2 + (R_o G P_o)^2 (MN + RIN)] f_s} \\ &= m^2 / (1+m)^2 CNR \end{aligned} \quad (2.2)$$

where, e is the electron charge, P_o is the peak received optical power, R_o is the responsivity of the optical detector, I_d is the dark current, $\langle I_s \rangle$ is the receiver equivalent noise current, G is the avalanche gain (which is equal to one for the PIN diode), f_s is the baseband signal bandwidth, MN is the modal noise, RIN is the relative intensity noise which exists when laser diode is used as optical source, m is the modulation index, and CNR is the carrier-to-noise ratio. Equation 2.2 is analogous to that of conventional AM electrical transmission.

Equation 2.2 is plotted in Fig. 2.2 which shows that analogue modulation has no inherent SNR improvement over CNR . The best improvement might be obtained at maximum modulation index ($m=1$), in which SNR is 3 dB less than CNR .

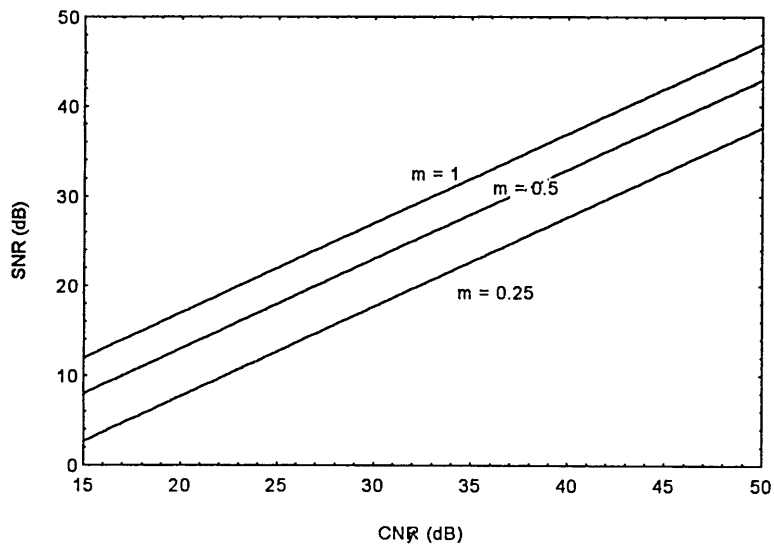


Fig. 2.2 Output SNR versus input CNR for analogue modulation transmission system.

2.3 Digital modulation

A digital wideband transmission system is shown in Fig 2.3. In this system the analogue baseband signal is first converted into digital format by an analogue to digital converter (ADC). The output is then changed into a binary data stream using a coder. In general, the sampling rate should be at least equal to the Nyquist rate, i.e. twice the bandwidth of the baseband. Each sample is then represented by a code, in the case of pulse code modulation (PCM), of n -bit length. The transmission bit rate required for such a system is very high, as an example a baseband signal of 27 MHz bandwidth will require a data rate of 550 Mbits/s at Nyquist sampling rate and 10 bit per sample code word. This indicates that digital transmission requires a very wide channel bandwidth compared to analogue systems, thus making it bandwidth inefficient system.

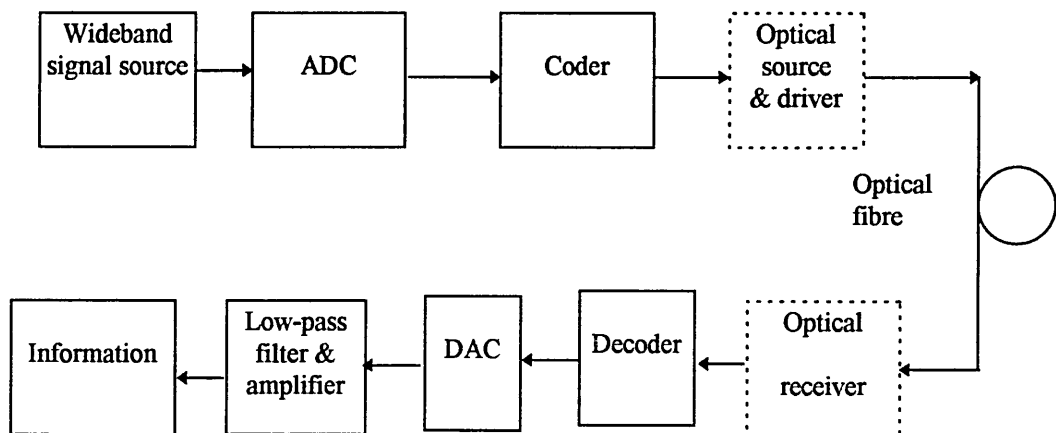


Fig. 2.3 Typical digital transmission system block diagram.

At the receiving end, the optical signal is first converted back into electrical form before being decoded by a decoder. The original information signal is then recovered by a digital to analogue converter (DAC) followed by a low-pass filtering. However,

where non optical transmission is employed, the same demodulation technique will apply, and only the electronic parts of the demodulator will be used.

The most important advantages of digital transmission are the high signal-to-noise performance and improved system linearity which to great extent is independent of transmission channel quality.

In PCM system, the noise level at the output of the receiver is mainly determined by the quantization noise at the encoder. The output SNR in terms of the input CNR is given as [35];

$$SNR = \frac{3n_q^2}{1 + 4n_q^2 P_e} \quad (2.3)$$

and the probability of error is;

$$P_e = erf(\sqrt{CNR}) \quad (2.4)$$

where, P_e is the error rate, n_q is the number of quantisation levels, and $erf(.)$ is the error function of the enclosed quantity. Figure 2.4 shows the noise performance of a digital system with $n_q = 16$ together with an analogue system with 100% modulation index. The digital system offers an SNR of 55 dB at CNR of 20 dB compared to 17 dB obtained in an analogue system. This shows the inherent signal-to-noise ratio performance improvement that digital systems have. Increasing the number of quantisation levels can improve SNR and reduce distortion but at an expense of the increased system bandwidth [9, 35]. A variety of coding and bandwidth compression techniques are being investigated to reduce the bit rate required for digital transmission.

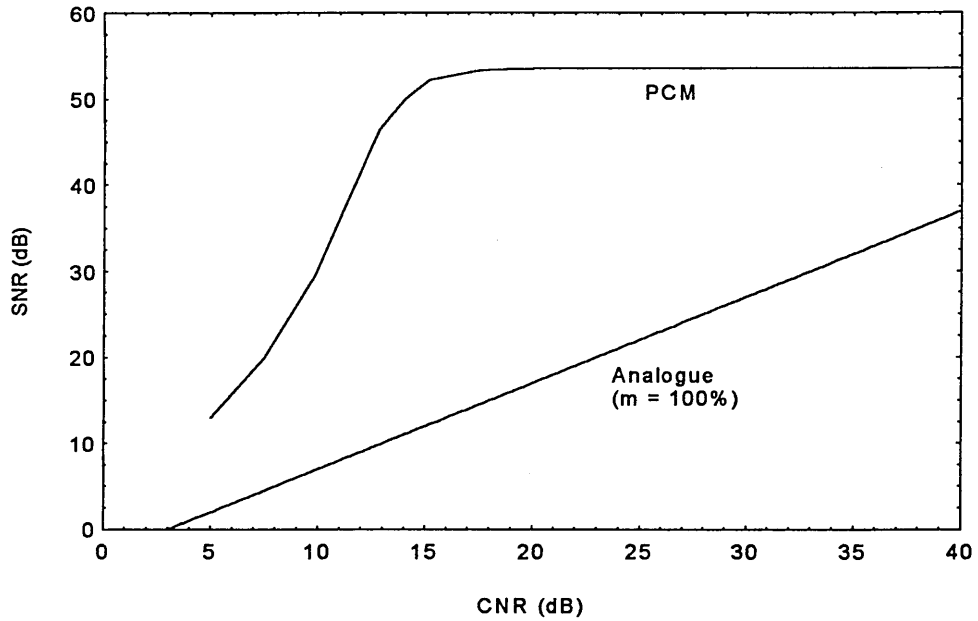


Fig. 2.4 Output *SNR* versus *CNR* for digital and analogue transmission system.

2.4 Pulse analogue modulation

Pulse analogue techniques are based on modulation of light source driving current by intermediate electrical pulses generator modulated by the information signal, as shown in Fig. 2.5. These techniques have the features that the overall system performance is less affected by the light source non-linearity and they have reasonably simple circuitry. This is in addition to having much improved *SNR* performance when compared with purely analogue, and low bandwidth when compared with digital modulation techniques. In effect, pulse analogue schemes have the ability to trade-off performance with bandwidth, which is a particular feature in fibre systems [1, 9]. For example, in short distance local area networks (LANs) it is most likely that multimode or single mode fibre with a dispersive optical carrier will be used, all of which impose a significant bandwidth limitation on the optical channel. In this circumstance, low-speed optical sources such as light emitting diodes (LEDs) may be used, while still achieving

the required signal-to-noise ratio. In contrast, the available bandwidth on long distance terrestrial and undersea routes may be many orders of magnitude broader where optical amplification and soliton techniques are employed. This additional bandwidth can be readily exploited by pulse analogue modulation to improve performance and signal-to-noise ratio [1, 9, 13, 20].

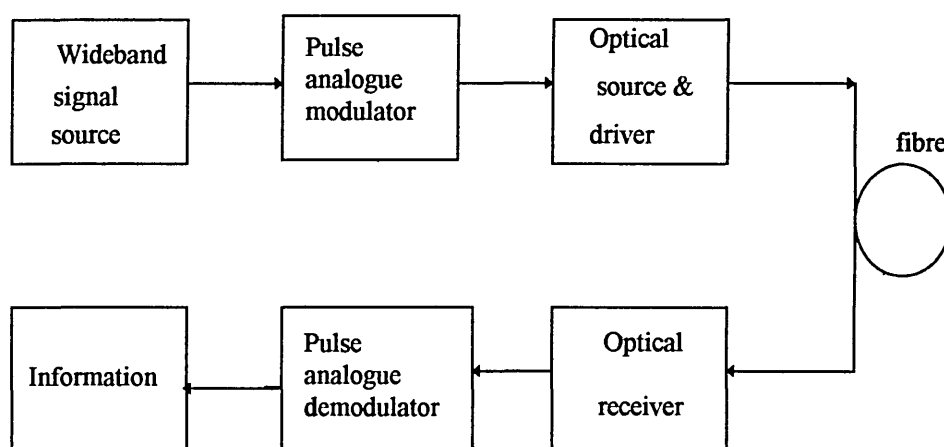


Fig. 2.5 Pulse analogue modulation system.

Although the basic pulse analogue schemes were first reported in the late 40s [21-25], it is only recently that a revival of interest has been experienced with the development of fibre transmission systems. The development of the different types of pulse analogue modulation is based on the variation of particular characteristics of a train of pulses as illustrated in Fig. 2.6. In general, pulse analogue modulation can be divided into pulse time (PTM) and pulse shape modulation. The common feature of all PTM techniques is that the modulated signals are all pulses with amplitude switching between two different levels (zero and one). This means logic circuits can be used to process these pulses. PTMs are divided into two types, namely; isochronous and

anisochronous [20]. In the former category the modulating signal changes the position or the width of the pulses, but maintains a constant sampling frequency, as in pulse width modulation (PWM) and pulse position modulation (PPM). In contrast, in anisochronous methods the frequency of the pulse train varies with the amplitude of the modulating signal at that particular instant, thus has no fixed sampling frequency. PTM schemes of this type are; pulse frequency modulation (PFM), squarewave FM (SWFM), pulse interval modulation (PIM) and pulse interval and width modulation (PIWM), see Fig. 2.6.

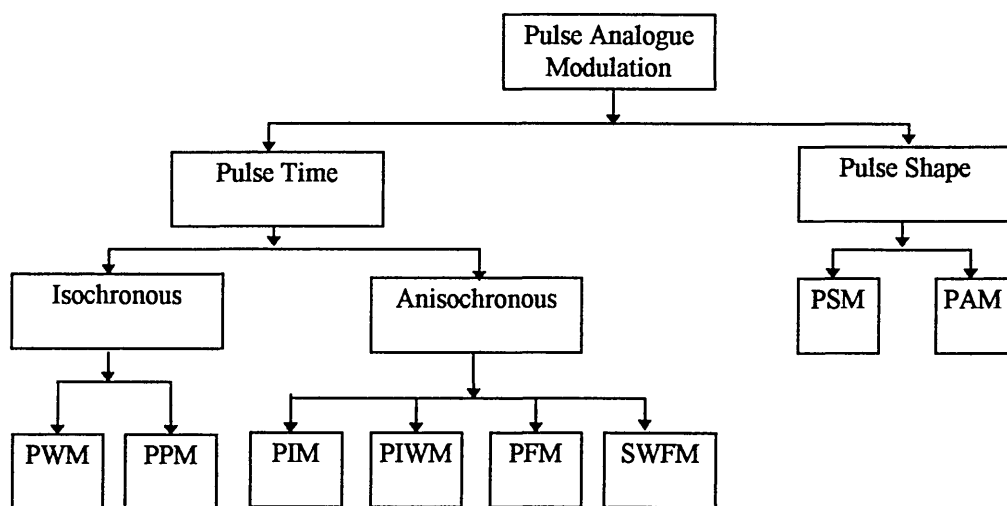


Fig. 2.6 Pulse analogue modulation tree.

On the other hand in pulse shape modulation the modulating signal changes the shape, (either the amplitude or the slope), of the pulses. In pulse slope modulation (PSM) technique the rise time of the carrier pulse is altered according to the information signal. In contrast, in pulse amplitude modulation (PAM) the amplitude of the pulse is varied with the information signal. Although, the PSM technique was discovered in the early 50s', no further work was reported until recently when it has been applied for analogue optical transmission over moderate distances [30].

In order to evaluate the merits of each individual PTM scheme, brief descriptions of several PTM techniques are given in the following sections. The spectral expressions, noise performance and methods of generation and detection will also be presented.

2.5 PTM schemes

It has been mentioned above that there are several types of PTM techniques. All are based on the variation of particular characteristics of a train of pulses, such as width of the pulse, the interval, the frequency of the train of pulses, ... etc. In this section, different PTM techniques are considered, the generation, detection, the spectral analysis, and other features of most PTMs will also be explained. However, pulse slope modulation will be considered in detail in the next chapter.

2.5.1 pulse width modulation

In this technique, the width of the pulses in the carrier is varied according to the amplitude of the modulating signal, as illustrated in Fig. 2.7. Two different types of PWM may be generated; leading (or trailing) and double edge modulated PWM. The leading (or trailing) edge modulated PWM can be generated when the input signal is compared with a linear ramp waveform. However, double edge PWM can be generated by the comparison of the input signal with a triangular signal. In both cases, the PWM could either be naturally or uniformly sampled. The naturally sampled PWM is generated when the comparison, with the ramp or triangular signal, is performed directly at the comparator, whereas uniformly sampled the input signal is routed first through a sample-and-hold circuit so that the input samples are taken at evenly spaced intervals rather than at varying intervals dependent on the signal amplitude, see Fig. 2.7 [36-40].

For all types of PWM the modulation index (M) may be defined such that maximum modulation occurs ($M=1$) when the peak-to-peak amplitude of the input signal is equal to the ramp amplitude. Therefore the modulation index can be expressed as;

$$M = \frac{\Delta\tau}{T_o} \quad (2.5)$$

where, $\Delta\tau$ is the peak-to-peak deviation of the pulse width, and T_o is the period, see Fig. 2.7.

The frequency spectrum of the PWM has been studied by several authors using the Fourier series expansion technique. Black [41], Bennett [42] and Stuart [43] have studied the PWM spectrum signal and they have shown that a trailing edge modulated naturally sampled PWM waveform with unity unmodulated mark/space ratio may be expressed as;

$$v(t) = \frac{1}{2} + \frac{M}{2} \sin \omega_m t \sum_{n=1}^{\infty} \frac{\sin(n\omega_o t)}{n\pi} - \sum_{n=1}^{\infty} \frac{J_o(n\pi M)}{n\pi} \sin(n\omega_o t - n\pi) + \sum_{n=1}^{\infty} \sum_{k=1}^{\infty} \frac{J_k(n\pi M)}{n\pi} \sin[(n\omega_o + k\omega_m)t - n\pi] \quad (2.6)$$

where ω_m and ω_o are the modulating signal and carrier frequencies, respectively, $J_k(x)$ are Bessel functions of the first kind and order of k . The second term in equation 2.6 represents the baseband component, while the combined effect of the third and the fourth terms is to produce components at the carrier frequency and its harmonics. When M is very small ($M \rightarrow 0$) the odd harmonics become dominant, whereas, the even harmonics become more distinguishable as M increased. The fifth term in equation 2.6 represents the sidetone structures set around the carrier frequency and all its harmonics and separated by a frequency equal to the modulating signal frequency. It is clear from equation 2.6 that the frequency of sampling (carrier) component is not

affected by the value of the modulation index and it never falls to zero value under any condition. Therefore, PWM can be classified as an isochronous PTM technique. A typical frequency spectrum of a singleton naturally sampled PWM is shown in Fig. 2.8.

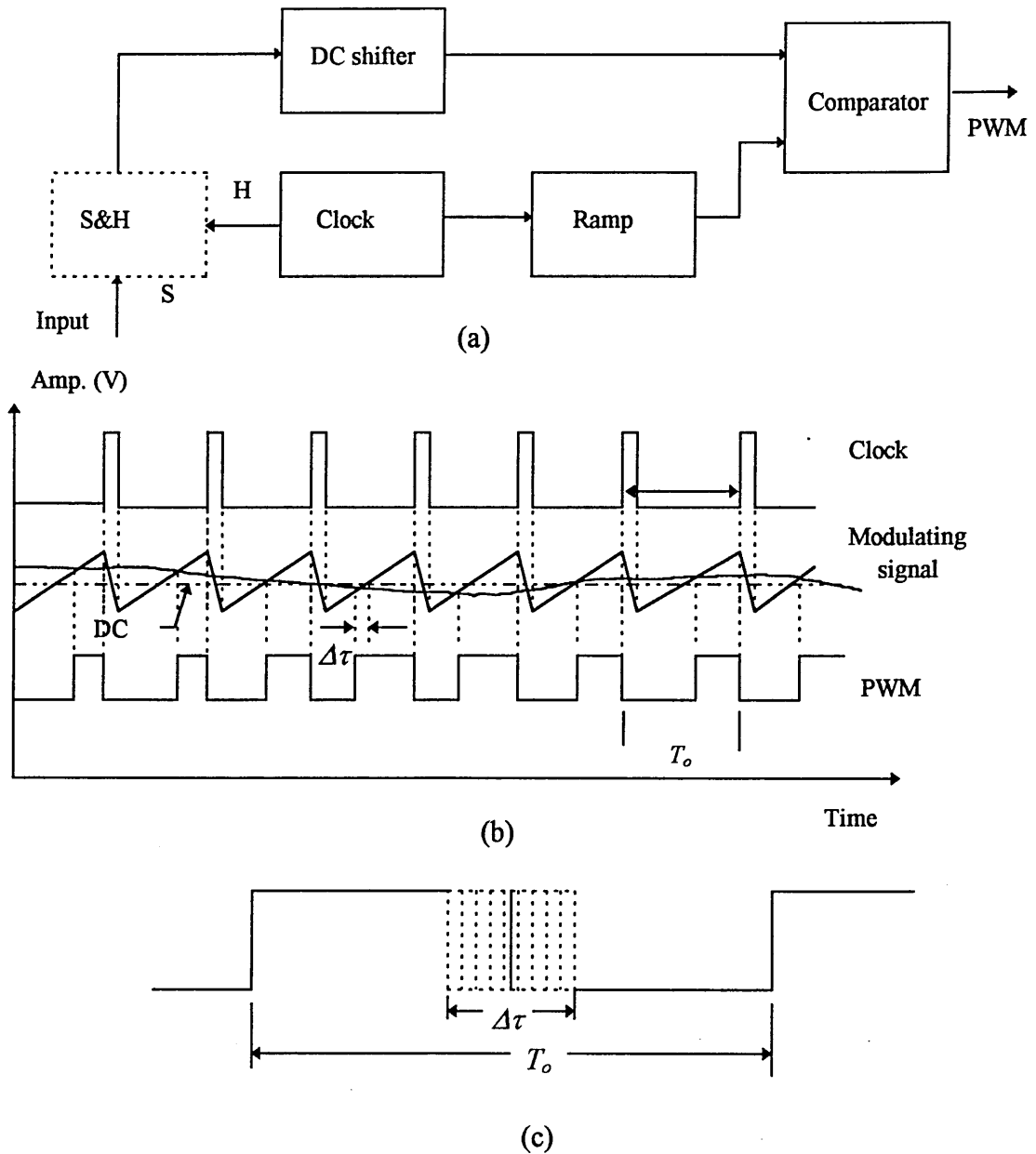


Fig. 2.7 PWM generation: (a) modulator (for uniformly sampled the dotted block should be included, and for double edge modulation the ramp should be replaced by a triangular waveform generator), (b) waveforms and (c) a single pulse.

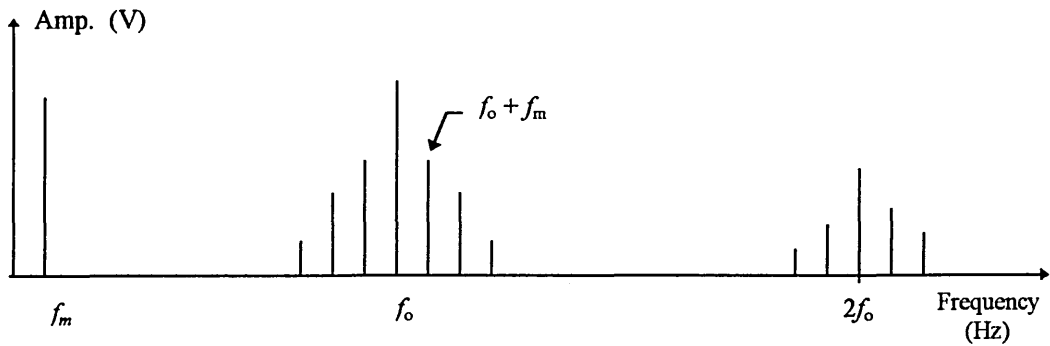


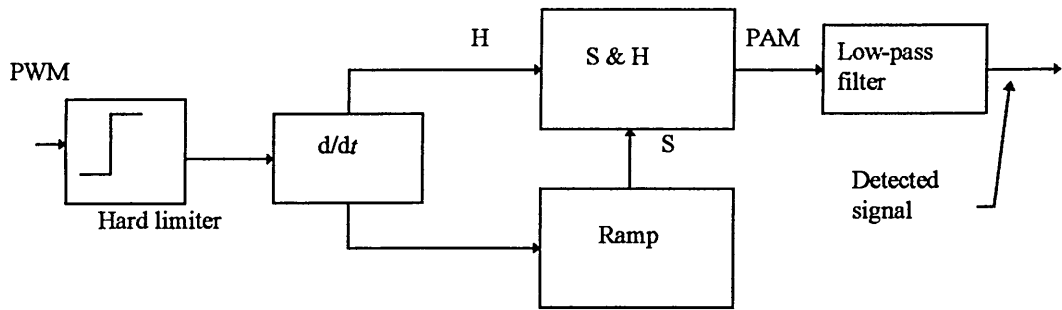
Fig. 2.8 Frequency spectrum for single tone PWM waveform (naturally sampled).

The spectrum of the uniform sampled PWM is very similar to the naturally sampled PWM, except that the baseband now contains in addition a diminishing set of harmonic components, influenced not just by the modulation index, but also by the ratio between the carrier and modulating signal frequencies.

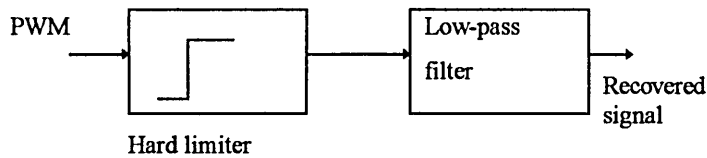
The basic modulation formula is accurate in describing and calculating the structure of the PWM spectral modulation components. However, recent work has highlighted the inability of the traditional formula, based on the double Fourier series due to Black [41], to predict the complex PWM sidetone structure resulting from two or more independent input signals. This is because the original method of derivation was based exclusively on the use of a single sinusoidal input. Nevertheless, Wilson et al [44, 45] have derived more accurate formula to describe the spectral structure of multitone PWM based on viewing the modulated squarewave as a waveform composed of positive and negative staircases, rather than the original double Fourier series approach.

The detection process for naturally sampled PWM can be adapted by threshold detection followed by low-pass filtering to recover the baseband components directly,

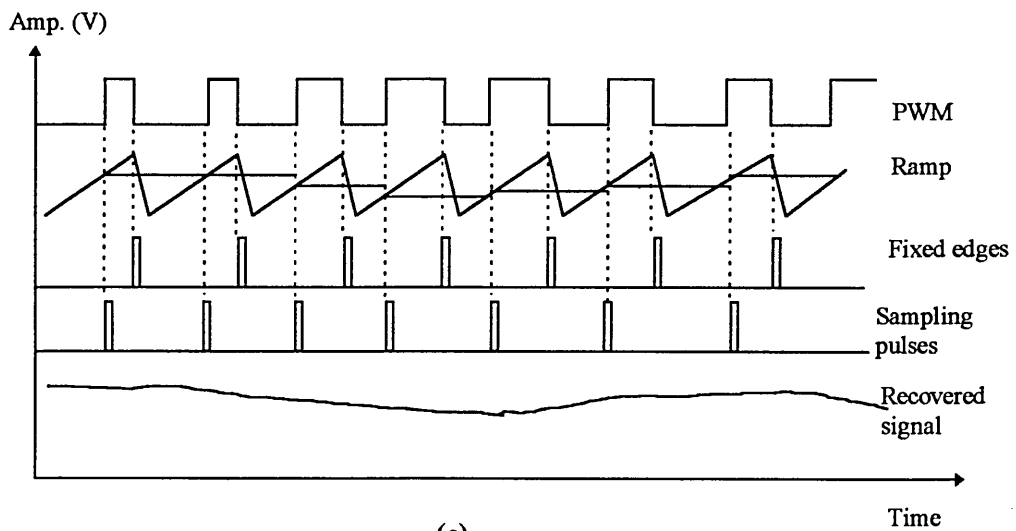
whereas in uniformly sampled PWM, the received signal is first converted into pulse amplitude modulation (PAM) before low-pass filtering, see Fig. 2.9. Despite the additional complexity, uniformly sampled PWM has the advantage of employing higher modulation indices than naturally sampled PWMs thus resulting in an improved signal-to-noise ratio performance [46].



(a)



(b)



(c)

Fig. 2.9 PWM demodulator: (a) uniformly sampled, (b) naturally sampled and (c) waveforms.

However, PWM suffers from a number of problems, such as non-linearity of the ramp generators, both at transmitting and receiving ends, especially when the sampling frequency is high. This of course introduces harmonic distortion of the frequency spectrum and hence distortion. Like most PTMs, as sampling frequency reduces the lower sidetones around the clock frequency will enter the baseband region, thus resulting in non-linear distortion at the output of the receiver. The amount of distortion is proportional to the modulation index and it can be tolerated if PWM is operated at $M < 20\%$.

2.5.2 pulse position modulation

In PWM there is always a wasted portion of transmitted power that conveys no information, and this strongly depends on the maximum level of modulation that may be employed. To save power and increase performance, the leading (or trailing) edge PWM signal can be differentiated to generate a constant width pulse train. The position of those pulses is directly proportional to the modulating signal. This scheme is called pulse position modulation (PPM), see Fig. 2.10. PPM is attractive for switching laser diodes where low average power and high peak power is of prime importance [1, 9]. A typical naturally sampled PPM modulator is very similar to a PWM and consists of a comparator detecting equivalence between the modulating input and a linear ramp, followed by a monostable or other pulse generating circuit.

Employing similar notation as in PWM, the naturally sampled PPM modulation spectrum may be represented by [47];

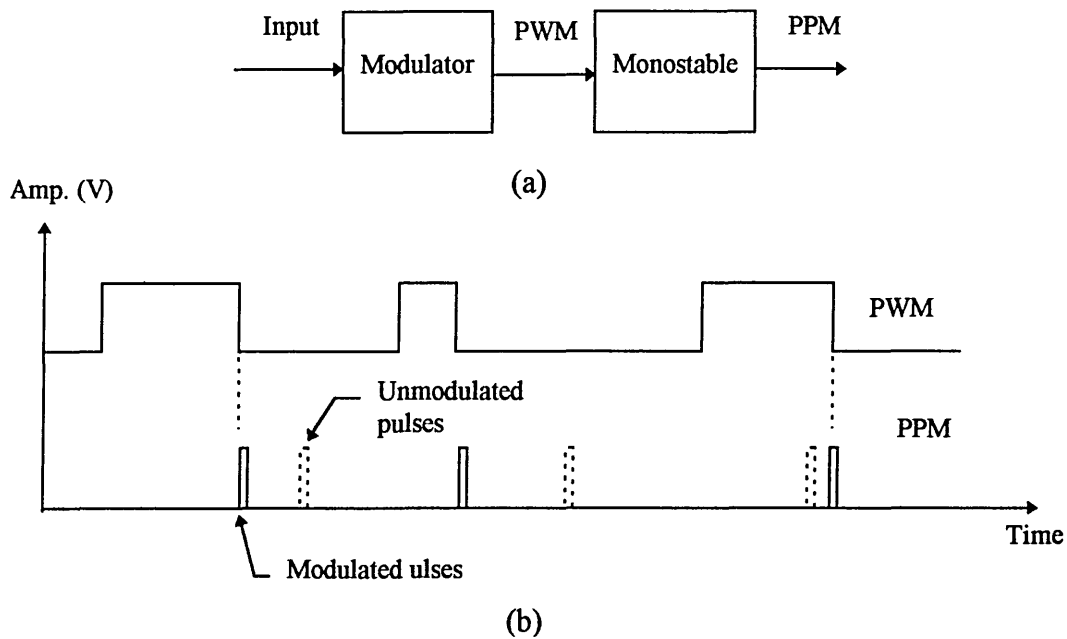


Fig. 2.10 PPM modulator: (a) block diagram and (b) waveforms.

$$\begin{aligned}
 v(t) = & \frac{\omega_o \tau}{2\pi} + M_p \cos(\omega_m t) \sin(\omega_m \tau / 2) \\
 & + \frac{1}{\pi} \sum_{k=-\infty}^{\infty} \sum_{n=1}^{\infty} J_k(n\pi M_p) \frac{\sin[(n\omega_o + k\omega_m)\tau / 2]}{k} \times \cos[(n\omega_o + k\omega_m)t]
 \end{aligned}
 \tag{2.7}$$

where τ represents the width of the PPM pulses, and M_p is the modulation index.

The spectral components generated at the sampling frequency and all its harmonics along with groups of sidetones are given by the third term of equation 2.7. It is clear from the equation that modulation sidetones centred around the sampling frequency and all its harmonics are influenced both by the carrier pulse width and the frequency of the modulating signal. If the pulse width is increased the overall sampling frequency harmonic profile is modified by a sinc(.) function and eventually becomes similar to that of the PWM. This has little effect in practice, as, in general, only low order carrier harmonics are retained in most transmission applications.

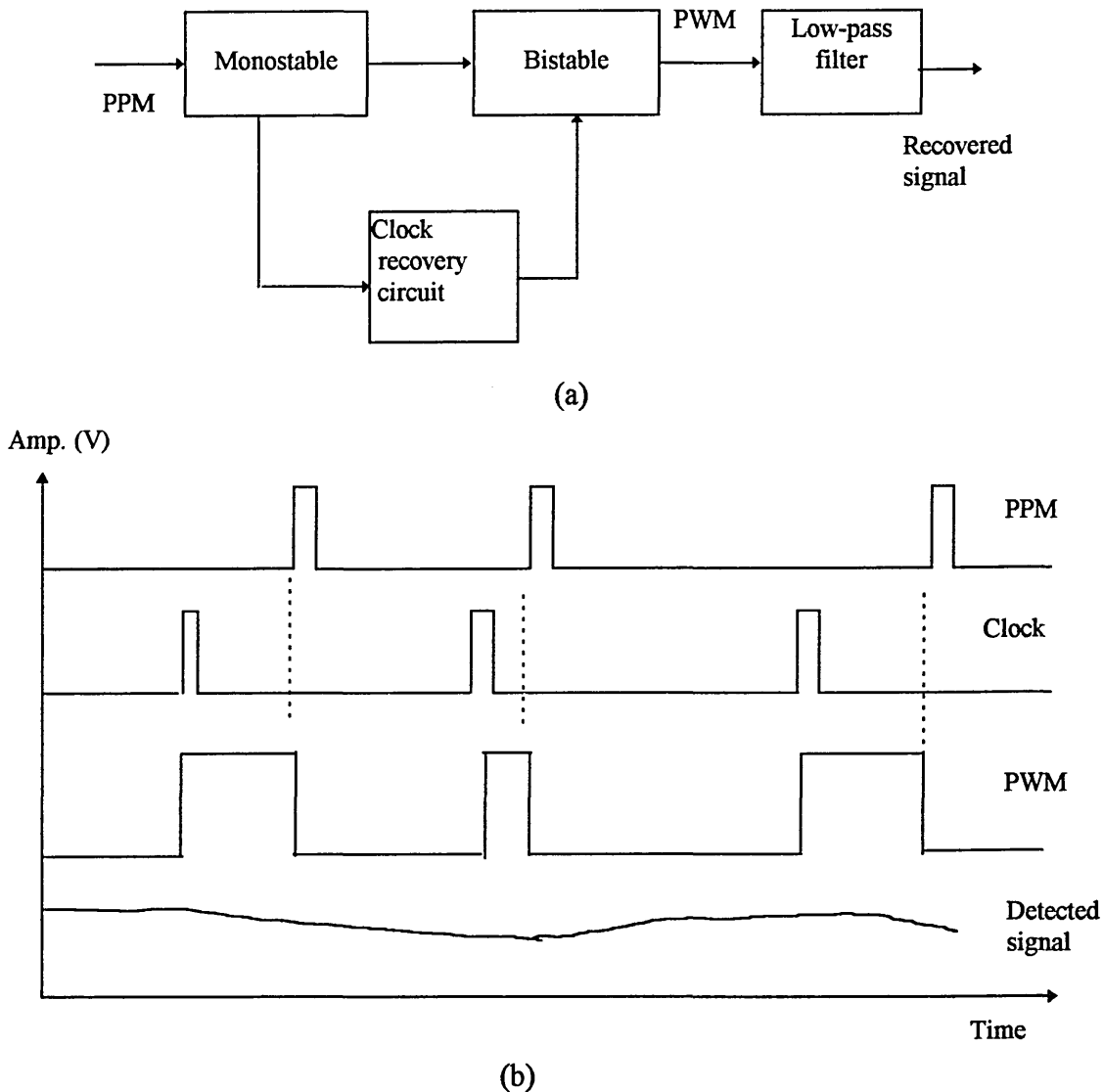


Fig. 2.11 PPM demodulator: (a) block diagram and (b) waveforms.

The second term of equation 2.7 gives the baseband component which represents a differentiated version of the modulating signal. The amplitude of the baseband component depends on both the pulse width and the frequency of the modulating signal. Demodulation of the PPM is carried out by converting into PWM format followed by low-pass filtering to recover the message signal [1]. A clock recovery circuit is employed to recover the reference signal (i.e. carrier component) so that PPM to PWM conversion can take place, Fig. 2.11.

2.5.3 pulse interval modulation

In this PTM modulation scheme, the interval between adjacent constant duration pulses is determined by the amplitude of the modulating signal. This is an anisochronous technique where the duration of each sampling episode is determined by the modulating signal. Therefore, it does not have a fixed clock interval. The pulse interval modulation (PIM) waveform can be generated when a comparator and ramp generator are connected as a feedback loop to reset as equivalence between the ramp and the DC shifted signal is detected, see Fig 2.12. The addition of the DC voltage to the modulating signal is necessary to ensure the existence of a sufficient headroom for the ramp to sample the most negative input swings under all conditions. In the case of uniformly sampled PIM a sample and hold is inserted at the input stage, while in the case of naturally sampled PIM it is omitted. In the case when the modulating signal is absent, the PIM modulator output is a series of uniformly spaced narrow pulses at a constant free-running frequency. The modulation index M_I ($0 < M_I < 1$) can be defined in this context as the peak-to-peak modulating signal swing divided by twice the DC level. Operation at very high levels of modulation index should be avoided since the negative swing of the shifted modulating signal tends to zero hence results in a rapid increase in the instantaneous pulse interval [48, 49].

The spectrum of the PIM modulation has been studied by several authors, and it may be represented by [50, 51];

$$v(t) = \left[\frac{\omega_o}{2\pi} \sum_{p=0}^{\infty} M_I^p \cos^p \omega_m t \right] \left\{ 1 + 2 \sum_{k=\pm 1}^{\infty} \sum_{n=-\infty}^{\infty} \sum_{q=-\infty}^{\infty} J_n(kB_1) J_q(kB_2) \right. \\ \left. \times \cos[(kA_o \omega_o + (n + 2q) \omega_m) t] \right\} \quad (2.8)$$

where

$$A_n = \sum_{r=0}^{\infty} (M_I / 2)^{2r} \frac{(n+2r)!}{(n+r)!r!}, \quad n \text{ is an integer; } n = 0, 1, 2 \quad (2.9)$$

and

$$B_k = \frac{2\omega_0}{k\omega_m} (M_I / 2)^k A_k, \quad k \text{ is an integer; } k = 1, 2 \quad (2.10)$$

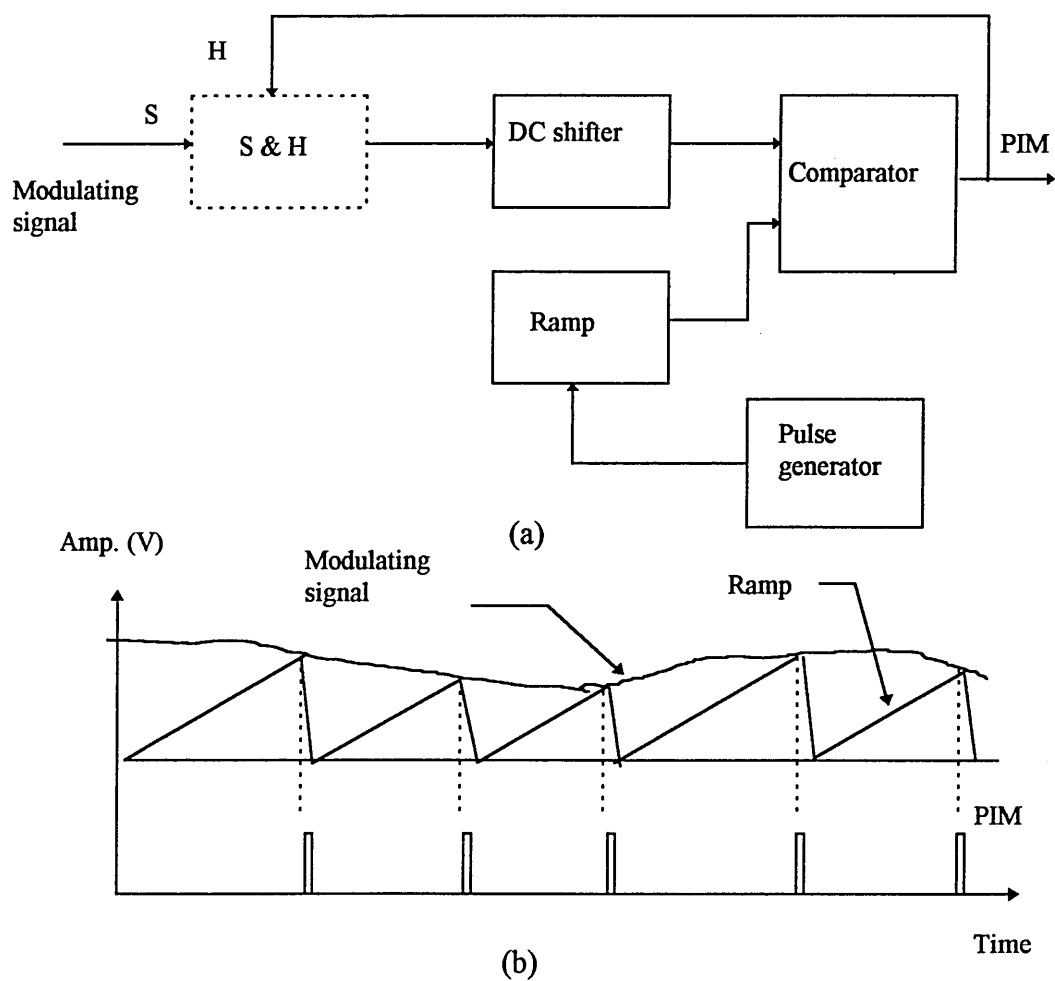


Fig 2.12 PIM modulator: (a) block diagram and (b) waveforms.

The spectral profile of PIM waveform, see Fig. 2.13, can be studied by considering equation 2.8. It can be seen from this equation that the sidetone spectral profiles around the modulated sampling frequency and its harmonics are somewhat asymmetrical and depend strongly on the modulation index. It can, also, be seen that in addition to the baseband component there is a series of baseband harmonics. Unlike PPM, the magnitude of the baseband components of PIM modulation is not influenced by the input frequency, as it is mainly determined by the modulation depth and the free running sampling frequency. Furthermore, the value of the sampling frequency is function of the modulation index, and with the increase in the modulation depth the average sampling frequency increases from its free running value [1].

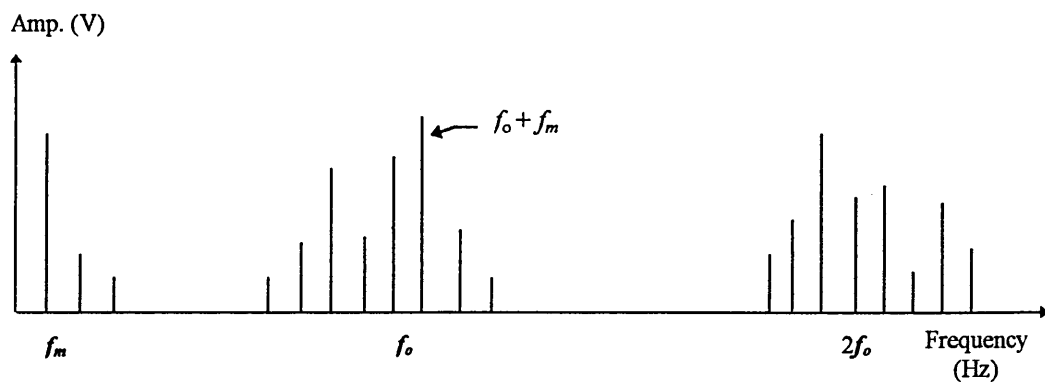


Fig. 2.13 Frequency spectrum for single tone PIM.

At low modulation indices, PIM demodulation may be achieved simply by employing low-pass filtering. However, a more general approach, applicable to the full modulation range, uses the PIM pulses to initiate a voltage ramp whose maximum values constitute sampled modulating waveform, see Fig. 2.14. Finally, a low-pass filter, or a combination of sample and hold followed by a low-pass filter in case of uniformly sampled PIM may be used to recover the modulating signal.

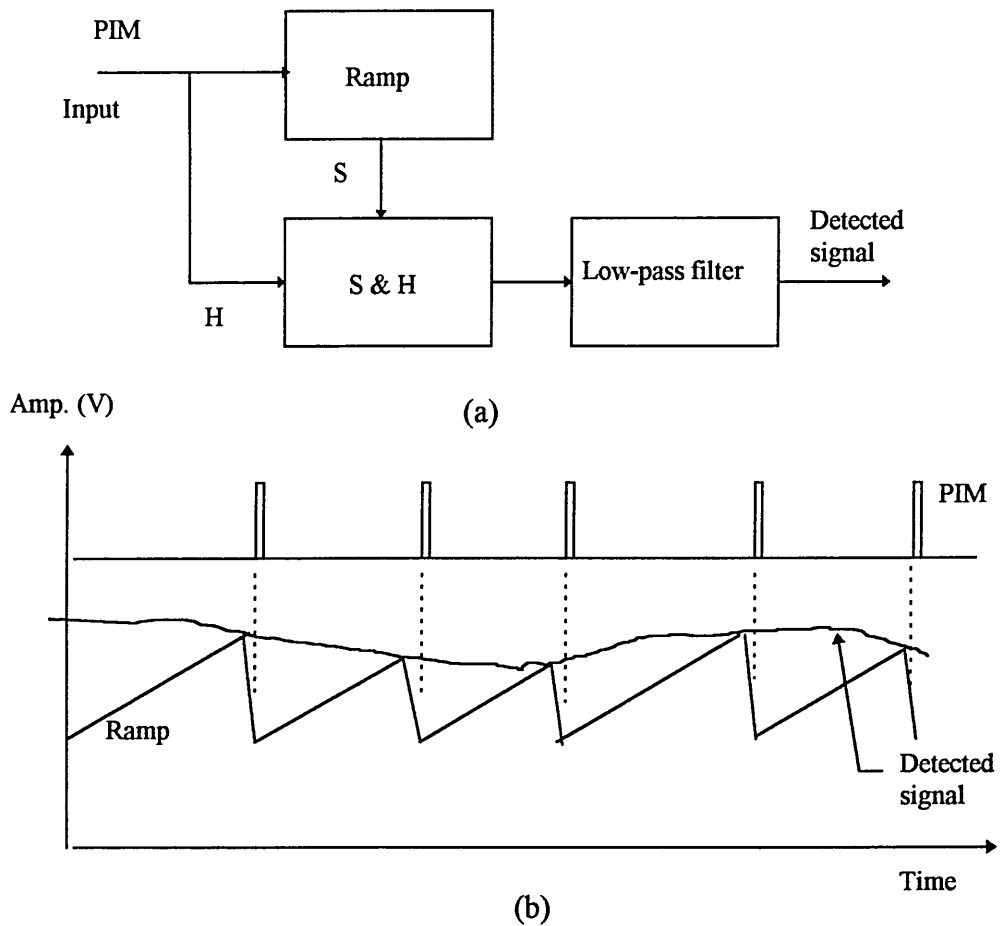


Fig. 2.14 PIM demodulator: (a) block diagram and (b) waveforms.

2. 5. 4 pulse interval width modulation

Pulse interval and width modulation (PIWM) is derived directly from PIM by passing the PIM pulses through a bistable to produce a waveform in which both mark and space convey information. Both uniform and natural sampling may be employed in the PIWM modulator which is identical to that of the PIM modulator except for the addition of a bistable at the output stage [52-54] see Fig. 2.15.

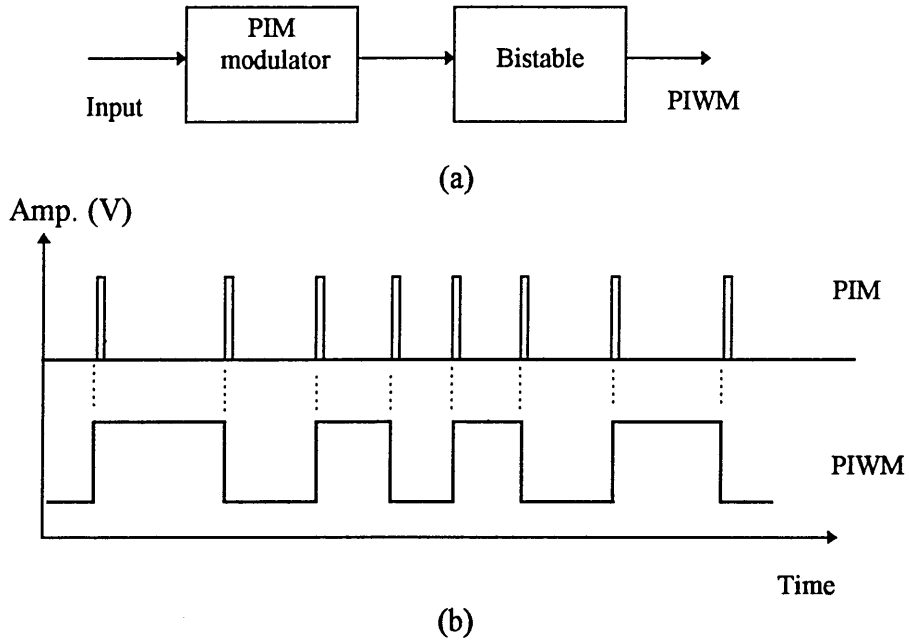


Fig.2.15 PIWM modulator: (a) block diagram and (b) waveforms.

The spectrum of the PIWM modulation can be studied by adopting an expansion based on multiple phase angles (a general method used by several authors). Thereby, a general PIWM spectral expression is given by [55, 56];

$$v(t) = \frac{1}{2} \left[1 + \sum_{k=1}^{\infty} \sum_{p=-\infty}^{\infty} \sum_{q=-\infty}^{\infty} \frac{J_p(kB_1)J_q(kB_2)}{k\pi/2} \sin(kp/2) \cos[(kA_o\omega_o + (p+2q)\omega_m)t] \right] \quad (2.11)$$

where A_o , B_j are defined in equations 2.9 and 2.10. Equation 2.11 is a close approximation based on the fact that both B_j and $J_p(kB_j)$ diminish very rapidly for $j > 2$. It might be concluded from equation 2.11 that the PIWM modulation spectral profile is asymmetrical and does not have a baseband component. As in PIM, the average sampling frequency ($A_o\omega_o$) strongly depend on the modulation index M_{IW} . For values of

M_{IW} less than 50% A_o may be approximated by $1 + M_{IW}^2/2$. For example if $M_{IW} = 0.3$, $A_o = 1.045$. This means that the total shift in the sampling frequency is + 4.5%. It can be also noticed that there are strong spectral components generated around the modulated sampling frequency and all its odd harmonics, surrounded by a diminishing series of sidetones separated by a frequency equal to $(p+2q)$ times the modulating frequency (not by the modulating frequency only, as is the usual case) see Fig. 2.16. The profile of these sidebands changes considerably with the modulation depth and the sampling ratio (ω_o/ω_m).

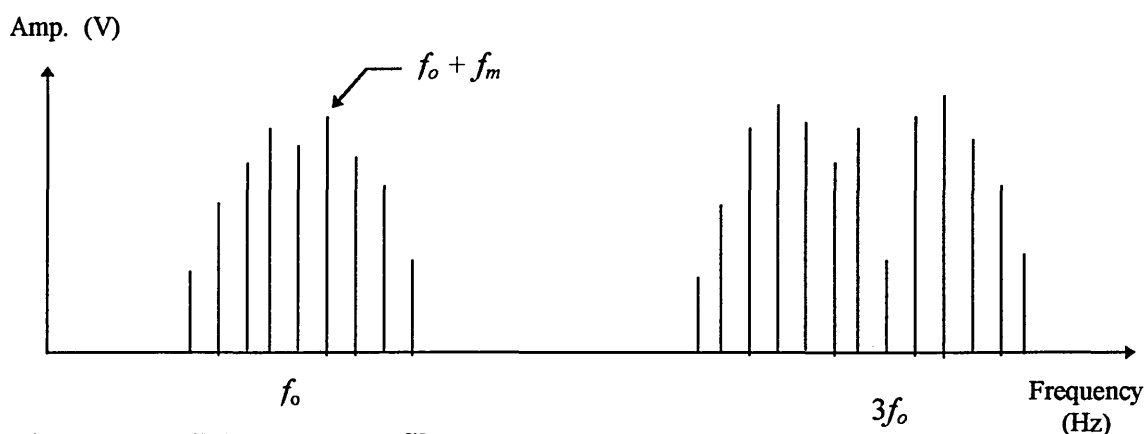


Fig. 2.16 PIWM spectral profile.

In order to satisfy the sampling theory requirements, for PIM the minimum permitted ratio of sampling frequency to modulating signal frequency is 2:1. Since PIWM is generated by passing the PIM pulse train through a bistable which divides the frequency by 2, the ratio of sampling frequency to modulating frequency is reduced to unity for PIWM. This does not violate sampling theory as information will be carried by both the width and the interval of the pulses (i.e. in both rising and falling edges of the pulses).

2.5.5. pulse frequency modulation

In pulse frequency modulation the instantaneous frequency of a train of narrow pulses is determined by the magnitude of the modulating signal. PFM generation can be simply implemented by a voltage controlled multivibrator (VCM) followed by a circuit, such as monostable, to generate low duty cycle pulses, see Fig 2.18. For carrier frequencies of 20 MHz to 30 MHz standard TTL logic VCM are suitable, whereas above this frequency ECL devices are necessary [17, 57-61].

The spectrum of single tone PFM modulation may be represented as [1];

$$v(t) = \frac{\omega_o \tau}{2\pi} \left\{ 1 + \frac{2\beta}{\omega_o \tau} \sin(\omega_m \tau / 2) \cos(\omega_m t - \omega_m \tau / 2) \right. \\ \left. + 2 \sum_{n=1}^{\infty} \sum_{k=-\infty}^{\infty} J_k(n\beta) \frac{\sin(n\omega_o + k\omega_m)\tau / 2}{n\omega_o \tau / 2} \cos[(n\omega_o + k\omega_m)t - k\omega_m \tau / 2] \right\} \quad (2.12)$$

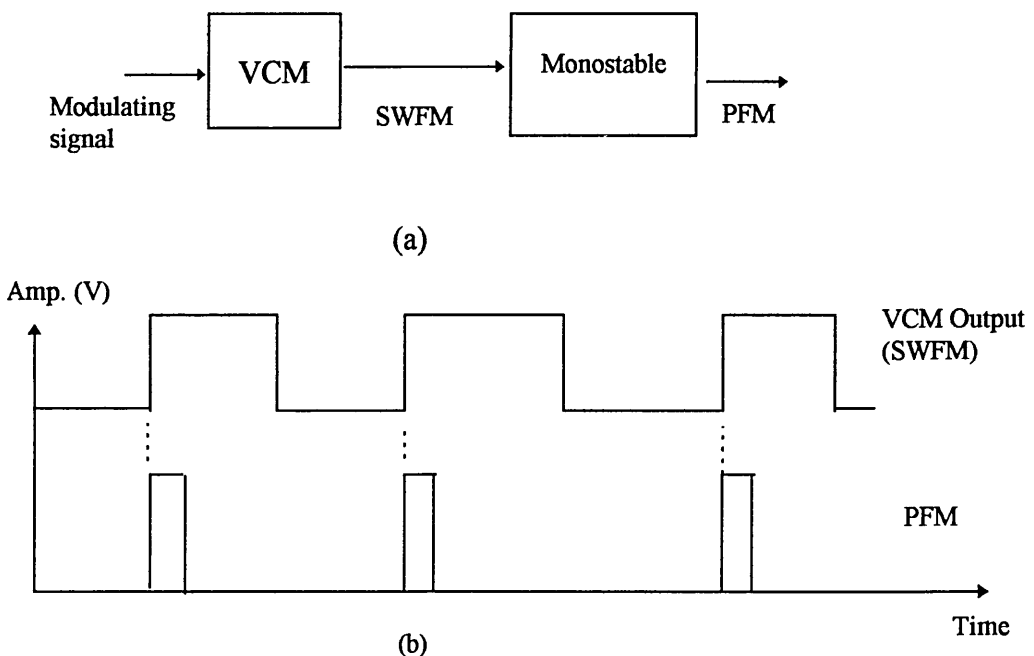


Fig. 2.18 PFM modulator: (a) block diagram and (b) waveforms.

where β is the modulation index, defined as $\Delta\omega/\omega_m$, which may have values greater than unity, $\Delta\omega$ is the frequency deviation, as in conventional frequency modulation, τ is pulse width, and J_k are Bessel functions of the first kind and order k .

Clearly, the PFM spectrum consists of a baseband component which represents the modulating signal, along with sidetones around the carrier and all its harmonics, see Fig. 2.19. The sidetone pattern is slightly asymmetrical, with the upper sidetones being stronger than lower sidetones. The number of sidetones appearing around the carrier and its harmonics and their amplitude is mainly determined by the modulation depth β which depends on both the modulating signal level and the frequency and the carrier frequency. Since the effective modulation index for any carrier harmonic is proportional to the harmonic number, sidetone overlapping is always expected around the harmonics of high order. PFM can be classified as anisochronous PTM technique as the carrier frequency component in the modulation spectrum will vanish when $\beta = 2.405$, as in the conventional FM system.

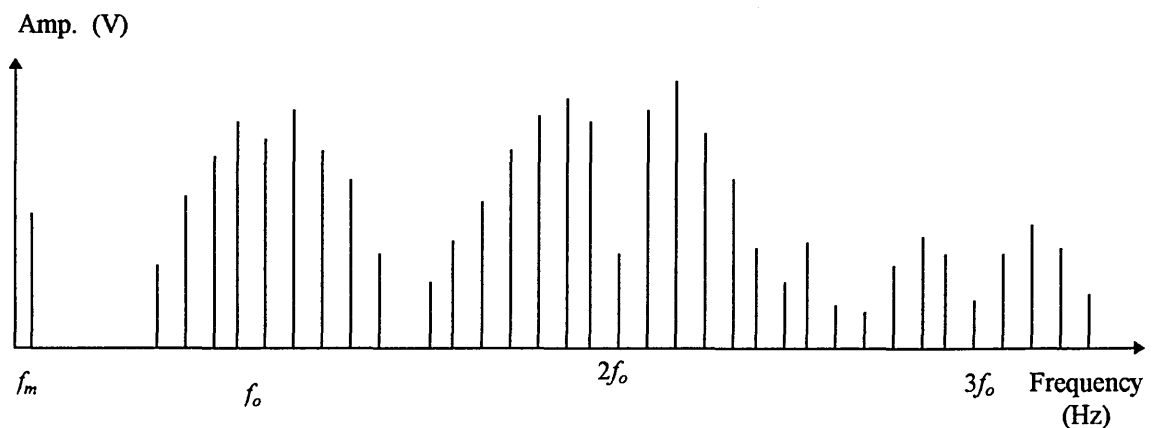


Fig. 2.19 Frequency spectrum of a PFM signal.

Demodulation of PFM is usually achieved by threshold detection and monostable to produce equal length pulses, followed by low-pass filtering to directly recover the baseband signal component from the PFM spectrum, see Fig 2.20.

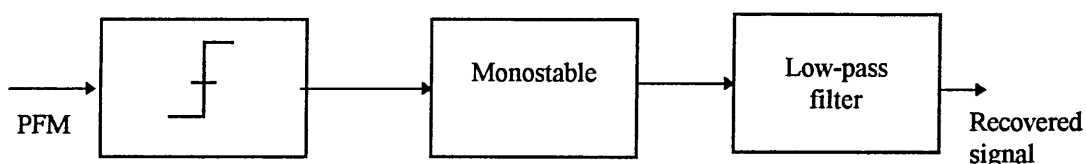


Fig. 2.20 PFM demodulator.

2. 5. 6. squarewave frequency modulation

Squarewave frequency modulation is an anisochronous PTM technique, closely related to the PFM and conventional frequency modulation (FM) consisting of a series of square waves edge transition occurring at the zero crossing points of conventional FM, see Fig. 2.18 (b) [61-64]. The simplest method of SWFM generation is performed by passing the conventional FM signal through a zero crossing detector or by employing a VCM, see Fig. 2.18 (a). The modulation spectrum of the SWFM with a single tone input frequency ω_m , and unity pulse amplitude, may be expressed as [61];

$$v(t) = D \sum_{n=-\infty}^{\infty} \sin c(\pi n D) \sum_{k=-\infty}^{\infty} J_k(n\beta) \exp[j(n\omega_o + k\omega_m)t] \quad (2.13)$$

where D is the duty cycle, β is the modulation index. The modulation spectrum is composed of an FM-like spectrum at the carrier frequency with slightly modified forms

at all odd harmonics, see Fig. 2.21. When the carrier wave is a perfect squarewave with 50% duty cycle ($D = 0.5$) there is no baseband component. However, departure from an accurate 50% duty cycle will result in the appearance of a baseband component as well as the FM sidetones at even harmonics of the carrier frequency. Extreme asymmetry in the carrier duty cycle produces a modulation spectrum very similar to that of the PFM where the relative power of the higher order terms increases with decreasing the pulse width. This indicates that PFM transmission requires a wider bandwidth than the SWFM to achieve the same signal-to-noise performance.

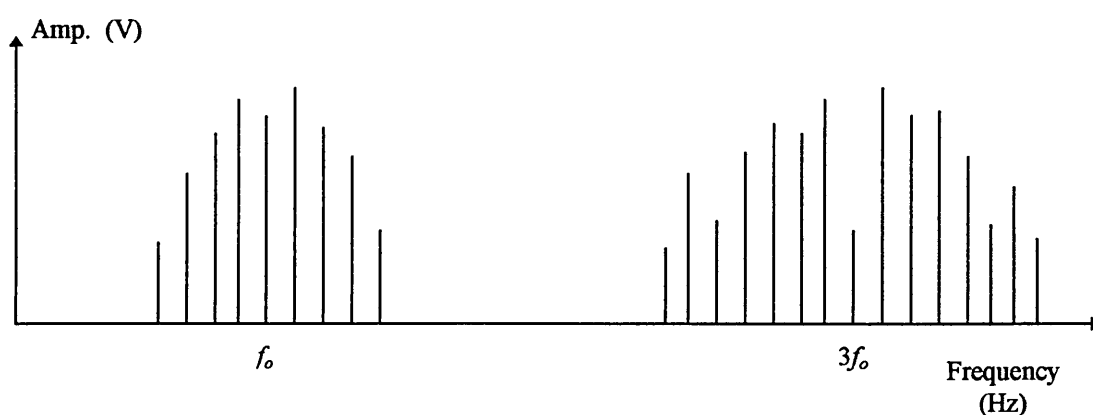


Fig. 2.21 SWFM spectrum ($D = 0.5$).

Demodulation can be performed by using a phase locked loop (PLL), as in ordinary FM demodulation, locked to the carrier or its harmonics. This method suffers from limited linearity and noise performance. There exists an alternative demodulating scheme based on edge detection techniques for converting SWFM into a PFM pulse train, see Fig. 2.22. In this method either the leading or the trailing (or preferably both) edges of SWFM are used to reconstruct the associated PFM signal, as this contains a baseband component that can then be extracted by simply employing a low-pass filter

[61]. A monostable is used to ensure a constant pulse width before passing the PFM pulses through the low-pass filter.

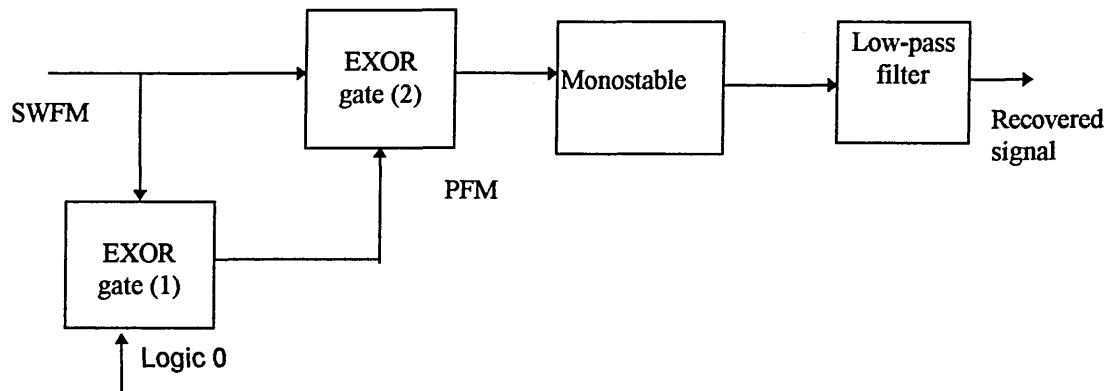


Fig. 2.22 Block diagram of the double edge SWFM detection.

In the single-edge pulse regeneration method, the spectrum of the reconstructed PFM pulses has sideband structures around every harmonic of the carrier frequency along with the desired baseband component. In contrast, in double edge detection, only even harmonics of the carrier frequency are present. This suggests that the double-edge detection has greater spectral efficiency via a lower bandwidth overhead penalty by lowering the minimum SWFM carrier frequency necessary for any particular maximum modulation frequency. In addition there is also a doubling in the modulation index of the reconstructed PFM, which results in improved signal-to-noise ratio compared to single edge detection method, see Fig. 2.23 for waveforms [61].

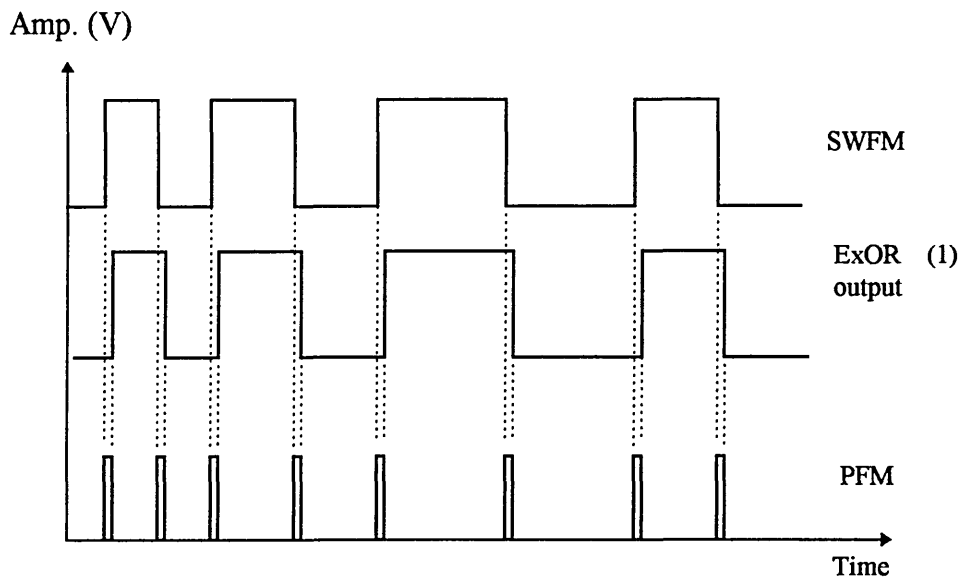


Fig. 2.23 Double edge SWFM detection waveforms.

2.5.7 digital PTM schemes

Digital PTM schemes are relatively new techniques which generally show a high degree of efficiency in optical and deep space communications [56]. The PTM technique that has received most attention so far in this category is digital PPM. In this technique, the message signal is first digitally encoded as in a PCM system. The encoded signal is then further encoded by replacing packets of typically up to 16 bits with a single PPM pulse whose position within the frame interval is determined uniquely by the code sequence of the associated packet, see Fig. 2. 24. Digital PPM has the advantages of improved receiver sensitivity, lower transmission rate in the optical channel, when compared with digital modulation schemes, and the normal trade-off with bandwidth. This modulation scheme is suitable for deep space communications where economy of transmission over vast distance is vital [65]. However, digital PPM has poor clock recovery characteristics, unless a framing pulse is used to mark the beginning of each encoded sequence; but this will increase the duty cycle and hence degrade the overall

performance of the system [66]. Digital PIM (a modified form of PPM, Fig. 2.24), which offers solution to these problems. In digital PIM, the data sequence is coded such that it is represented by the time interval between the previous and the present pulses. Therefore, unlike PPM, where the frame width is constant, the PIM frame varies in width according to the data encoded. To date only limited work have been performed on digital PTMs [66].

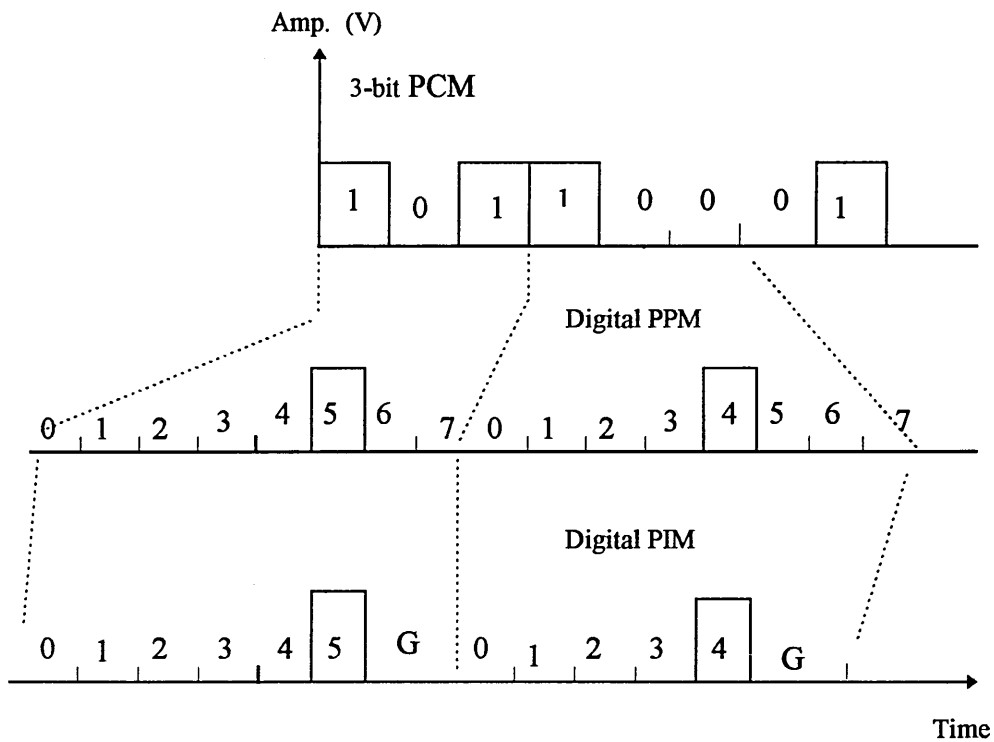


Fig. 2.24 Digital PTMs.

2.6 Noise performance of PTM systems

At the receiver all PTMs techniques employ pulse regeneration (or threshold detection) technique before signal detection. This is usually realised by a level detector, with threshold level set at half of the pulse height. The basic demodulation techniques

of a number of PTM schemes are shown in Fig. 2.25. The PWM waveform is demodulated by extracting the message signal by simple low-pass filtering. However, PPM, PFM and SWFM waveforms are demodulated using a monostable to generate constant width pulses followed by low-pass filtering, whereas PIM and PIWM are detected by a time-to-voltage conversion (i.e. sample and hold a ramp signal as explained earlier) followed by low-pass filtering, see Fig. 2.25. As a result the noise analysis of most of the PTMs are very similar. The noise added to the signal affects the threshold crossing and displaces the pulses at the monostable output from their regular position or affects the pulse duration in the case of PWM, causing a noise voltage superimposed at the output signal [67-73].

A noise voltage $n(t)$ added to $v(t)$ displaces the threshold from t_o to $t_o + x(t_o)$, see Fig. 2.26. If the noise level is low, then the displacement $x(t_o)$ can be approximated by;

$$x(t_o) = \left| \frac{n(t_o)}{\dot{v}(t_o)} \right| \quad (2.14)$$

where $\dot{v}(t_o)$ is the gradient of PTM pulses at t_o . When edge jitter is small (i.e. high input carrier-to-noise ratio) the edge jitter power can approximately be given as;

$$\sigma^2 = \langle x^2(t) \rangle = \frac{\overline{n(t_o)^2}}{\left| \dot{v}(t_o) \right|^2} \quad (2.15)$$

where, $\langle \rangle$ denotes time average of the enclosed quantity.

When a threshold crossing is displaced by $x(t_o)$ the effect on the pulses entering the low-pass filter can be represented as in Fig. 2.27. In this figure, PPM, PFM and PWM have been considered. SWFM can be looked at as a special case of PFM, (i.e. a PFM

with pulse width equal to half of the pulse period); however, PIWM and PIM will be considered later. It is indicated that the pulses affected by the noise can be considered as sum of the uncorrupted signal and a pulse with added edge noise $y(t)$.

The edge noise power spectral density $N(f)$ can be determined by the Fourier transformation of the autocorrelation function of pulse train $y(t)$. The noise power can then be evaluated as by integrating $N(f)$ over the baseband bandwidth. Finally, the output signal-to-noise ratio (SNR) can then be calculated by dividing the signal power by the noise power. This leads to;

$$SNR = \frac{S}{\int_{f_s} N(f)df} \quad (2.16)$$

The signal-to-noise ratio for all PTMs can be calculated using equation 2.16. However, in order to compare the noise performance of different PTM schemes, let us consider the case when the transmission system has a low-pass characteristic of first order, with bandwidth of B Hz. The formulae for SNR in different PTM schemes are given in Table 2.1, and the detailed analysis is given in Ref. [60].

The above analysis is applicable for PFM, PPM and PWM receivers. However, in PIM and PIWM receiver the detection technique is different and therefore they will be treated separately. In basic PIM and PIWM receivers, a time-to-voltage conversion technique is used to extract the message, see Fig. 2.25. This means that the reconstructed pulses are used to sample a ramp waveform of constant slope. Due to the existence of noise, the sample pulses will be time shifted by $x(t_o)$, see Fig. 2.28. Thus the noise at the low-pass filter input can be evaluated as [74, 75];

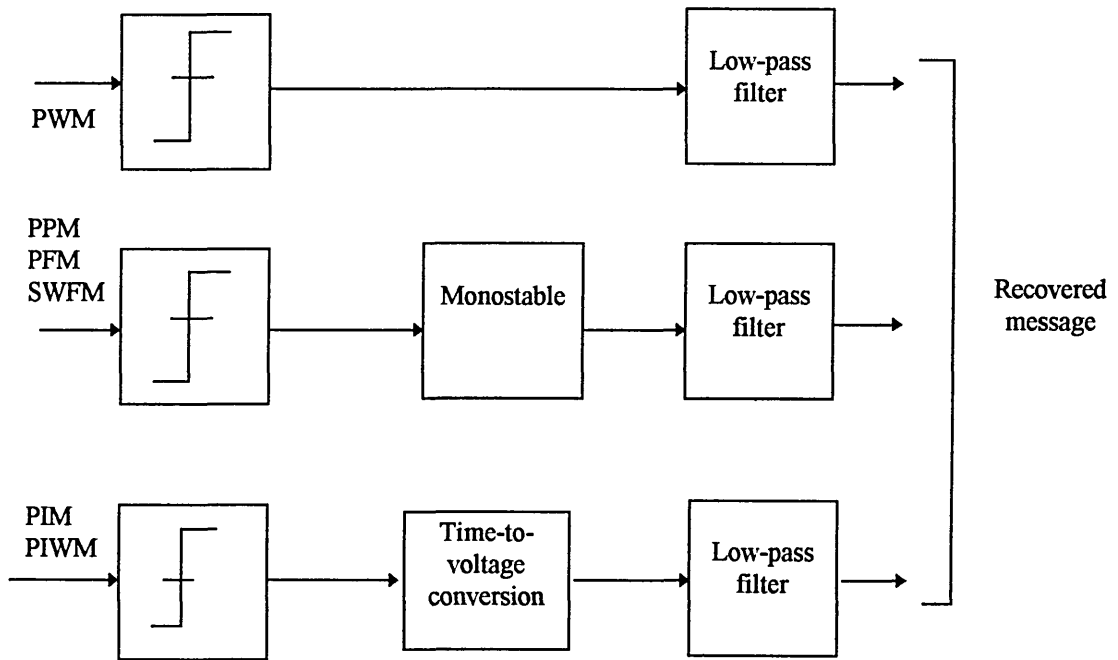


Fig. 2.25 The basic PTM demodulation techniques.

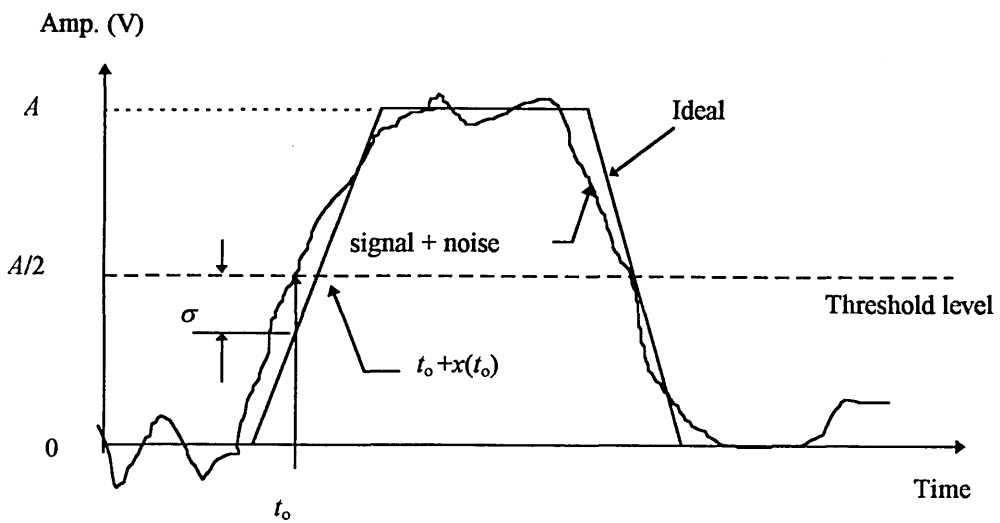


Fig. 2.26 General PTM waveform with noise.

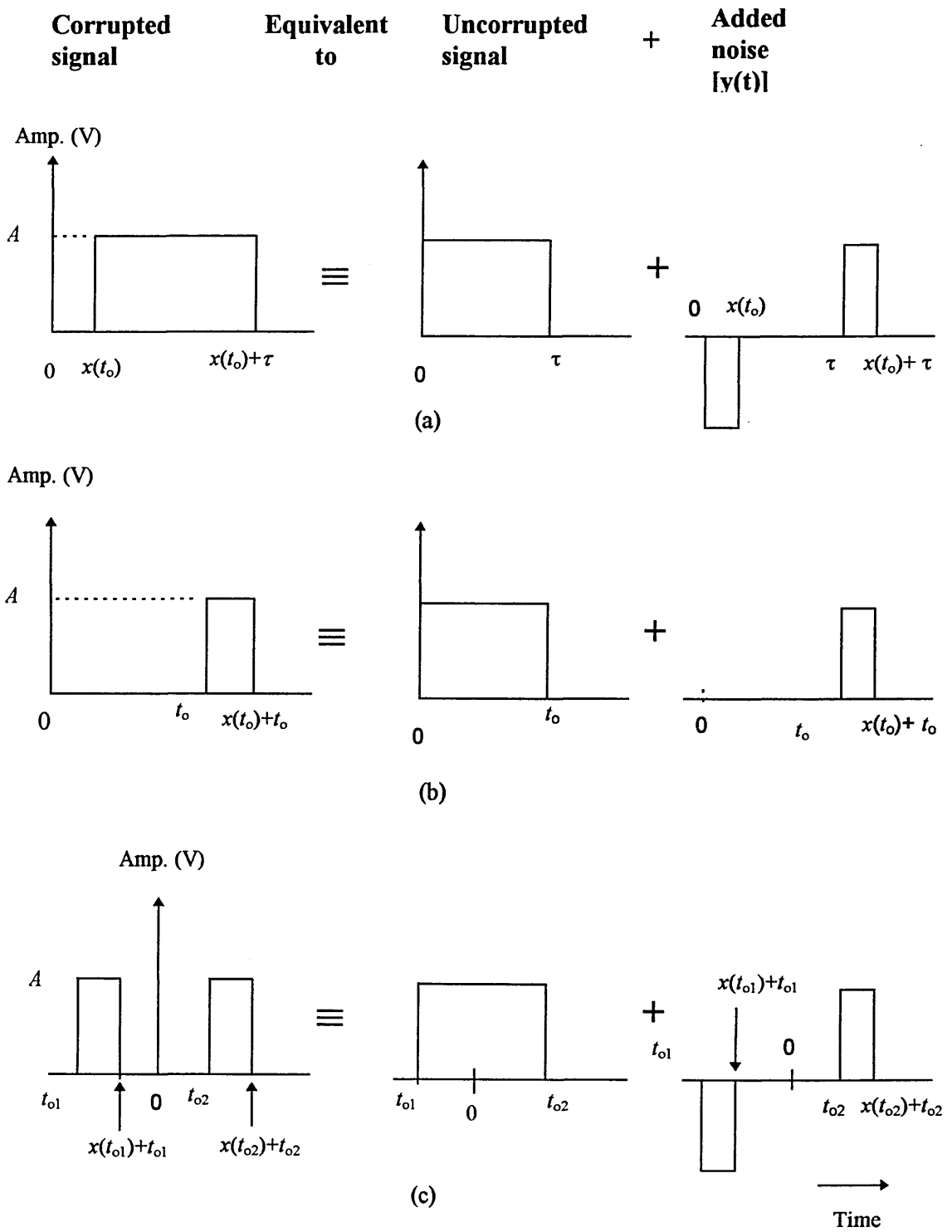


Fig. 2.27 Pulses at the input of the low-pass filter: (a) PWM, (b) PPM and (c) PFM.

$$n(t) = \left. \frac{k}{v(t)} \right|_{at t=t_o} [n(t_o) - n(t_o - T_o)] \quad (2.17)$$

where k is the time to voltage conversion factor of the demodulator. Following the same technique explained above, i.e. evaluating the noise spectral density function then the noise power, the expressions for SNR of PIM and PIWM systems can be evaluated.

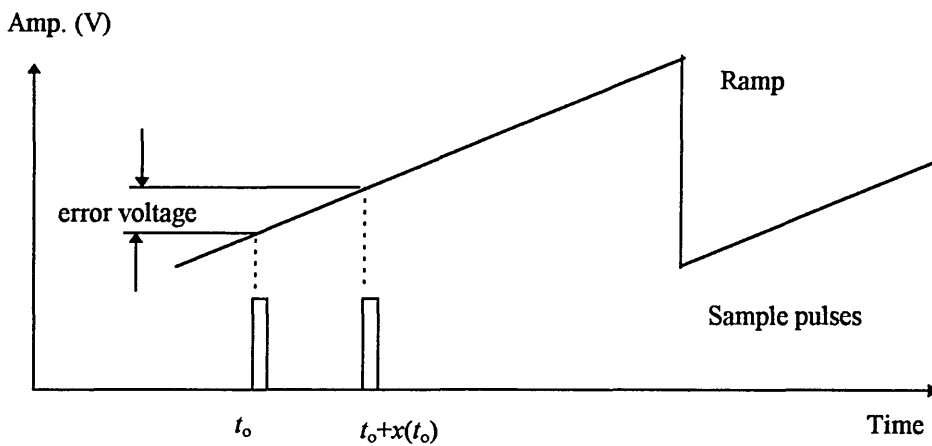


Fig. 2.28. Time-to-voltage conversion technique.

Scheme	SNR	Scheme	SNR
PWM	$\frac{(\pi MB)^2}{8f_o^2} CNR$	SWFM	$\frac{3\beta^2 B^2}{2f_o^2} CNR$
PPM	$\frac{(\pi MB)^2}{4f_o^2} CNR$	PIM	$\frac{(\pi M_I B)^2}{2f_m f_o} CNR$
PFM	$\frac{3\beta^2 B^2}{4f_o^2} CNR$	PIWM	$\frac{(\pi M_{IW} B)^2}{4f_m f_o} CNR$

Table 2.1 Noise performance of some PTM schemes [1, 61, 72, 73].

A summary of SNR expressions for PIM and PIWM systems is also given in Table 2.1. The carrier-to-noise ratio (CNR) is calculated as the ratio between the input pulse train power and the input noise power. It must be mentioned that all the above analysis is applicable only when the systems are working well above the threshold level. Finally, a comparative study for the noise performance of the PTM schemes has been given in Fig. 2.29, for sampling frequency of 2.5. As a benchmark the behaviour of 8-bit PCM as well as pure analogue modulation system are also shown. SWFM demonstrates the best performance among all PTMs. It offers about 3 dB superiority over PFM, and better than PCM noise performance for CNR of 37 dB and above. SWFM and PFM compare favourably with PCM performance except at low CNR and may be expected to find applications over longer distance than other PTMs.

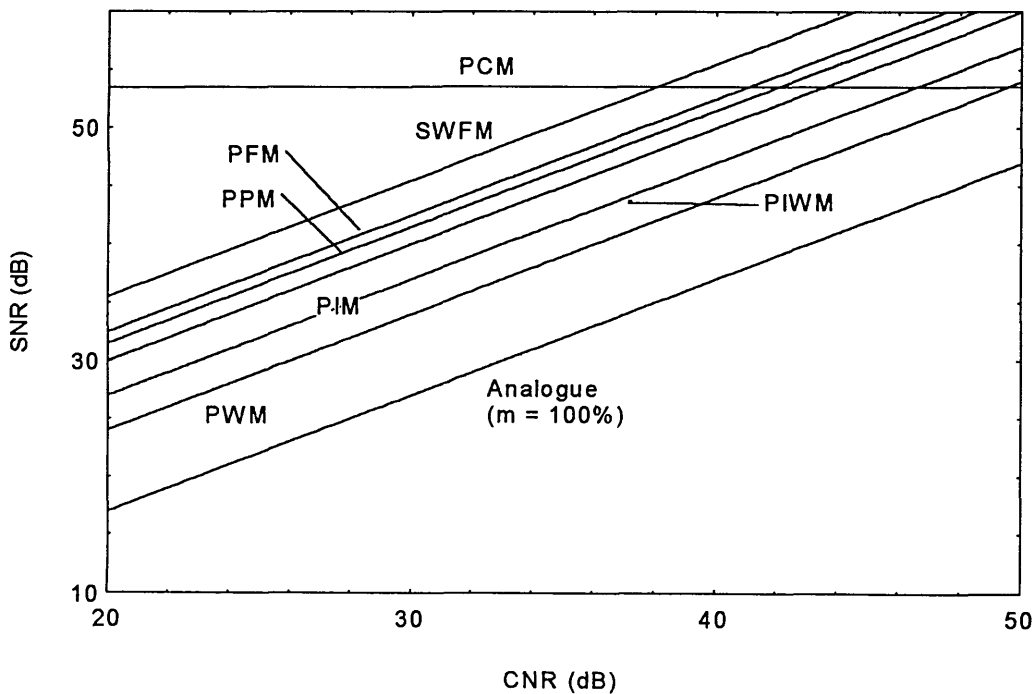


Fig. 2.29 Theoretical noise performance of different modulation schemes.

PPM and PWM have both been widely used in optical fibre applications and are far easier to multiplex in time domain than anisochronous format. PPM is marginally superior to PWM but relatively more complex to implement due to the need for clock recovery and synchronisation. PIM and PIWM show performances between those of PWM and SWFM. All PTMs show noise performance much better than analogue modulation.

2.7 Non-linear distortion of PTM systems

The suitability of a particular modulation technique for transmission of wideband signals can be evaluated by its ability to produce low distortion at low sampling ratio with a high signal-to-noise ratio. From the spectral overlapping between the modulating signal and the carrier fundamental lower sideband structure, it is possible to predict the minimum carrier frequency for each of the PTM schemes [1].

All the PTM schemes have a very similar spectral modulation structure with sidetones appearing around the carrier frequency and its harmonics. However, there are a particular differences between techniques concerning the presence of a baseband component and detailed behaviour of the carrier frequency lower sideband profile which will determine the minimum sampling ratio for a given distortion behaviour.

From the spectral equations of the different PTMs techniques it is possible to calculate the ratio of the recovered signal modulation level A_m to sidetone amplitude A_k (A_m/A_k). k is the sidetone number which enters the baseband region. Table 2.2 summarises these ratios for different PTM schemes [1, 46]. Figures 2.30 and 2.31 show the non-linear distortion in a number of PTM schemes, where the minimum

required sampling ratio is plotted for two values of distortion performance levels as a function of modulation index. Figure 2.30 illustrates that for sampling ratio of 4, to achieve non-linear distortion of 1% (-40dB), the modulation index should not exceed 15%. Increasing the sampling ratio to 6, the modulation index required for the same non-linear distortion performance (i.e. -40 dB) will increase to 70 %. This clearly indicates that, PWM and PPM should be operated with sampling ratio above 6 if low nonlinear distortion performance is required.

A comparison between PFM and SWFM is drawn in Fig. 2.31. SWFM is clearly markedly superior to PFM achieving theoretical distortion levels due to sidetone incursion of better than -60 dB under modulation conditions where PFM can only achieve -30 dB. In turn PFM is superior to PWM under similar modulation conditions.

PTM Scheme	A_m/A_k
PWM	$\frac{\pi m}{2J_k(\pi M)}$
PPM	$\frac{\pi m}{2J_k(\pi M_p)}$
PFM	$\frac{\pi \Delta f \tau}{\sin[\pi(f_o + kf_m)]J_k(\beta)}$
SWFM	$\frac{2\pi \Delta f \tau}{\sin[\pi(2f_o + kf_m)]J_k(2\beta)}$

Table 2.2 The A_m/A_k ratio for some PTMs [1, 46].

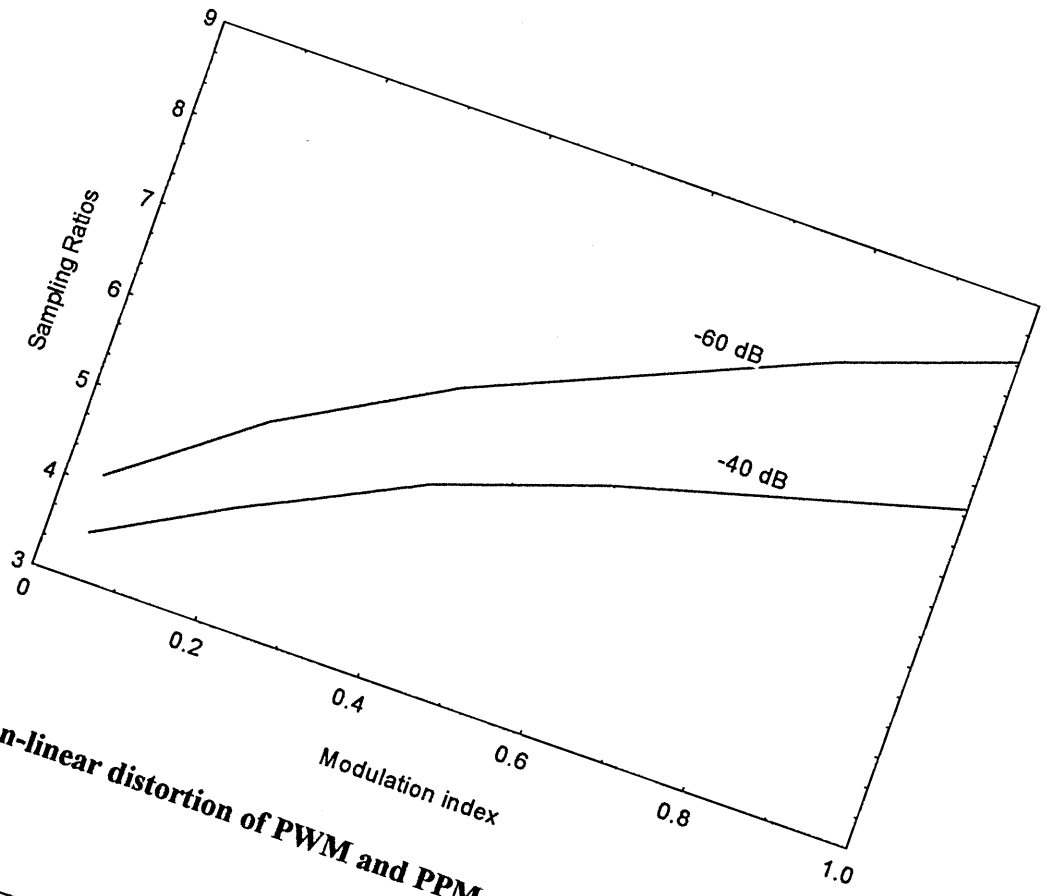


Fig. 2.30 Non-linear distortion of PWM and PPM.

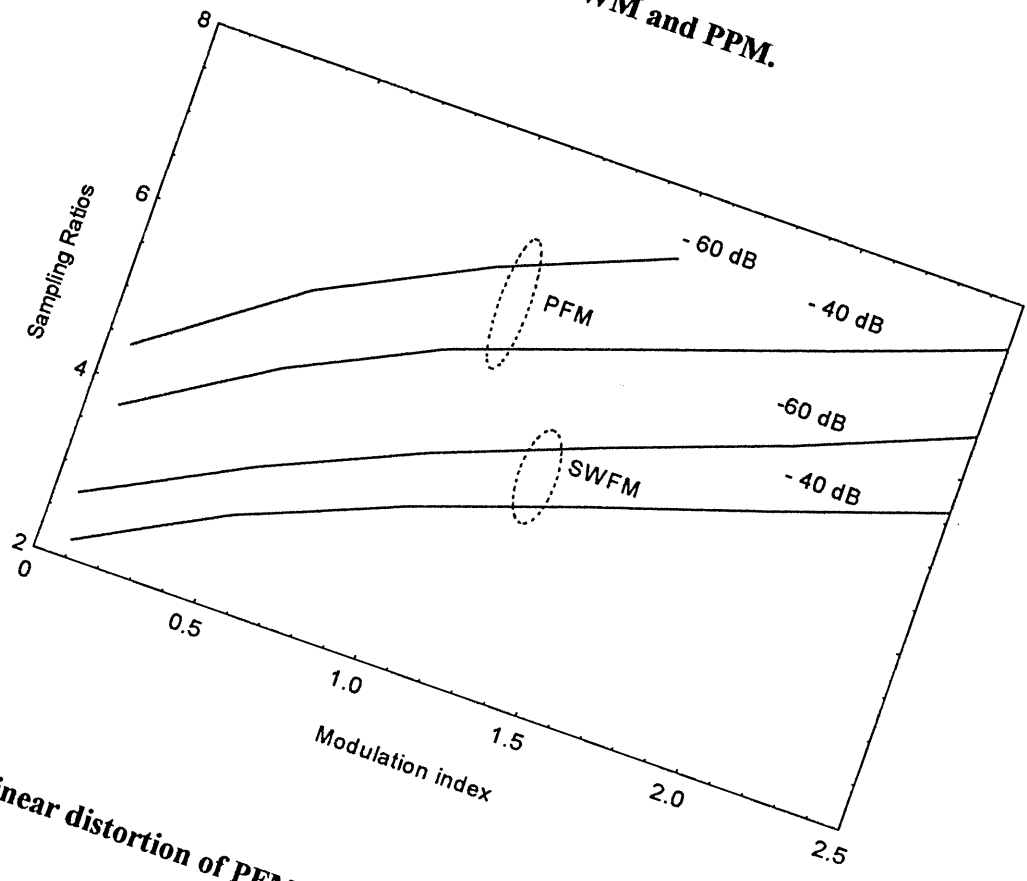


Fig. 2.31 Non-linear distortion of PFM, and SWFM.

To conclude, the potential of the different PTM techniques may be explored by considering their spectral occupancy, distortion and signal-to-noise ratio. The choice of a suitable modulation technique for transmission of a given signal depends on its ability to produce high signal-to-noise ratio and low distortion, at low sampling ratio. The minimum carrier frequency (sampling ratio) may be predicted from the spectral overlap between the modulating signal and the carrier fundamental lower sidetone structure. The ratio of recovered signal level to sidetone amplitude gives a clear indication of the non-linear distortion behaviour of the PTM scheme. In general, these techniques have different characteristics and trade-off, but they have a very similar spectrum.

Another important factor which should be considered when selecting a suitable modulation scheme is the interaction between the noise performance and the received pulse edge rise time, as dictated by the transmission channel bandwidth. The unweighted improvement factor, given by signal to noise ratio minus carrier to noise ratio, expressed in dBs, varies above the threshold as the square of the ratio of transmission channel bandwidth to carrier frequency. The constant of proportionality is slightly different for each of the PTM techniques [1, 9].

In this chapter, a brief discussion on the most of the PTMs techniques has been presented. The pulse slope modulation technique will be covered extensively in the next chapter.

Chapter Three

The Pulse Slope Modulation Technique

3.1 Introduction

The development of different types of pulse modulation is based on the variation of a particular characteristics of a constant amplitude pulse train. For instance, PWM is generated by varying the width of the carrier pulse, while the PFM is obtained by varying the frequency of the pulses, and so on. However, it is also possible to modulate the rise or fall times (or both) thus producing pulse slope modulation (PSM) signals.

PSM was first introduced for line transmission of low frequency signals (audio frequency band) in 1950s, by Kruse [26], and Das [27]. Early work reported suggested that the technique has improved overall system performance such as; signal-to-noise ratio, bandwidth utility, and multiplexing capability compared with PAM, and has similar performance to PPM and PWM. Despite the proven experimental success, PSM has not been developed to the extent that other PTMs have. No further work was done until recently where PSM has been used for transmitting analogue signals using optical fibres over a moderate length link [30]. Probably the reason for not using PSM over this long period is because the other PTM techniques were well developed and applied in many systems at the time when was PSM invented.

In this chapter, PSM modulation technique is studied in detail. The mathematical characterisation of the different types of the PSM waveforms is given and generation and detection techniques of the PSM signals are investigated in detail. Furthermore, a new technique for the PSM demodulation is proposed, which has the advantages of simplicity, reduced hardware and improved noise performance over the traditional method of PSM detection. The noise performance of the proposed PSM receiver system is studied, and both results from theoretical and practical results are compared.

3.2 PSM generation

It is known that on integration of a step function, the slope of the resulting function is dependent on the amplitude of the step function and the constant of integration. Further, on differentiation of a ramp function the magnitude of the step function generated depends on the slope of the original function.

In principle, PSM signals can be generated by using a rectangular pulse as a gating pulse for a constant current charging circuit, see Fig. 3.1. The modulating signal $v_m(t)$ varies the charging current (I) via a voltage controlled current source (VCCS) and hence the slope of the output pulse. The output voltage across the capacitor is a ramp waveform with a slope determined by the current and the capacitor value. A voltage clipper can be added to remove the parasitic amplitude modulation that might be present in the waveform [27], and the resulting waveform generated is the trapezoidal shaped PSM signal, see Fig. 3.1.b and c. However, if the charging capacitor is discharged at the moment when the output ramp is equal to a threshold value (A) then a triangular wave form is generated. This can be realised by an extra switching circuit to control the discharge (see Fig. 3.1.d and e). In general, both types of the PSM signal have very similar properties, but the trapezoidal PSM is easier to generate.

The mathematical analyses of both the trapezoidal PSM and the triangular PSM waveforms are very similar. The triangular PSM waveform can be treated as special case of the trapezoidal waveform as the later is more general waveform. Later both types of PSM waveform will be treated independently to show the differences between them, but, at this stage the analysis is true for both types of PSM waveform.

When a modulating signal $v_m(t)$ exists, the charging current through the capacitor can be given as;

$$i(t) = I_o [1 + kv_m(t)] \quad (3.1)$$

where, $i(t)$ is the charging current, I_o is the output current when modulation is absent, k is a constant which represents the sensitivity of VCCS, and $v_m(t)$ is the modulating signal. The voltage across the capacitor C is;

$$v_o(t) = \frac{I_o}{C} [1 + kv_m(t)]t \quad (3.2)$$

and the slope is given as;

$$\begin{aligned} s(t) &= \frac{dv_o}{dt} \\ &= \frac{I_o}{C} [1 + kv_m(t)] \end{aligned} \quad (3.3)$$

However, the slope can also be given as, see Fig. 3.1;

$$s(t) = \frac{A}{t_r} \quad (3.4)$$

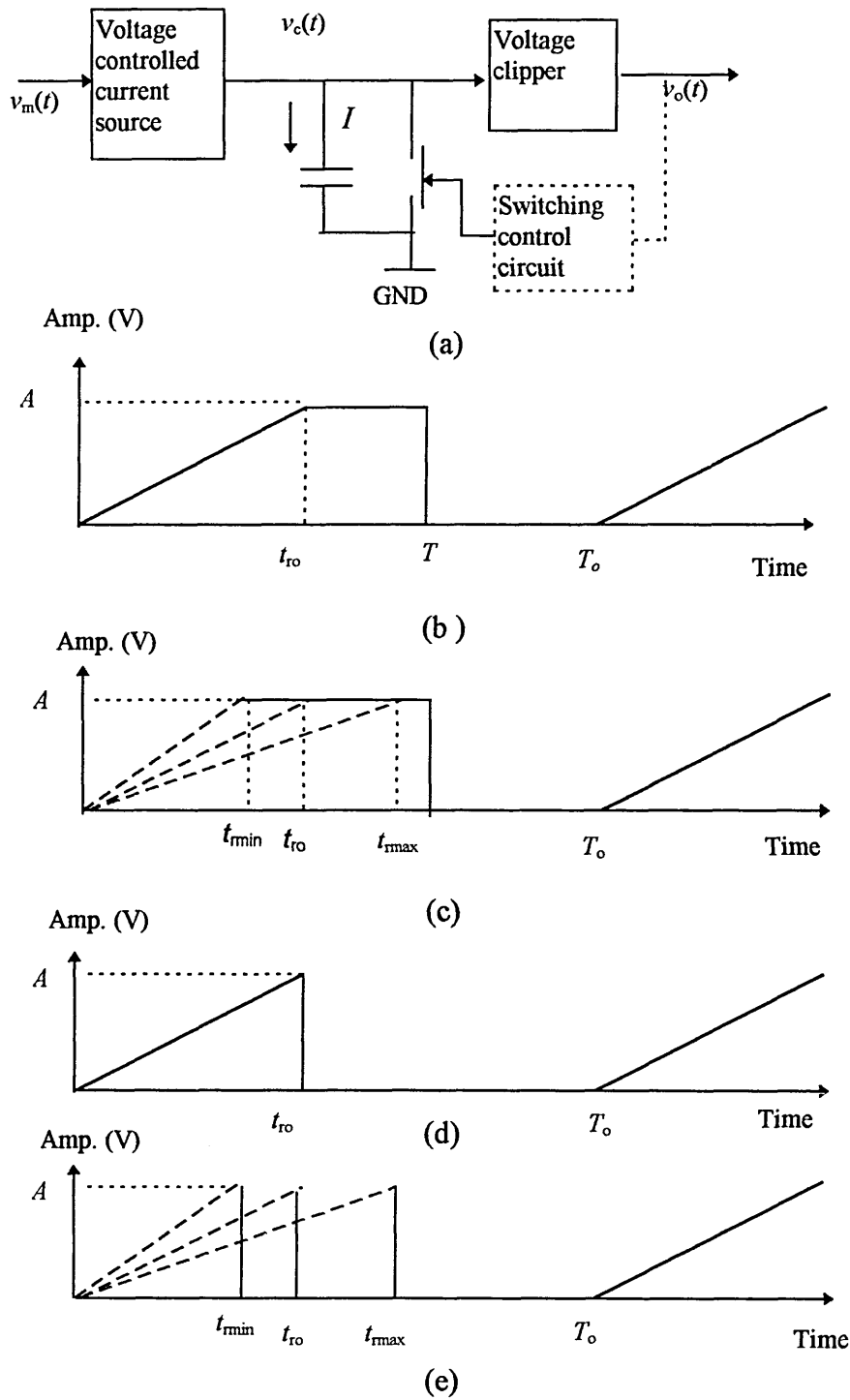


Fig. 3.1 (a) PSM modulator (for triangular PSM control circuit shown dotted is used), (b) trapezoidal PSM waveform in the absence of modulation (c) trapezoidal PSM waveform when modulation is exist (d) triangular PSM waveform in the absence of modulation and (e) triangular PSM when modulation is exist.

where t_r is a specific pulse rise time of the output waveform, and A is the amplitude of the output waveform. However, when the modulation is absent, the slope of the capacitor voltage is simply given as;

$$s_o = \frac{I_o}{C} = \frac{A}{t_{ro}} \quad (3.5)$$

where, t_{ro} is the value of t_r for no modulation, (see Fig 3.1). From equation 3.3, the maximum and minimum slopes of the output voltage can be given as;

$$s_{\max} = \frac{A}{t_{r\min}}, \quad \text{and} \quad s_{\min} = \frac{A}{t_{r\max}} \quad (3.6)$$

where, $t_{r\max}$ and $t_{r\min}$ are the maximum and the minimum values of t_r , see Fig 3.1.

Therefore, the modulation index can be defined as [27-30];

$$m = \frac{s_{\max} - s_{\min}}{s_{\max} + s_{\min}} \quad (3.7)$$

Substituting equation 3.6 into equation 3.7, the modulation index can be rewritten in terms of the rise times as;

$$m = \frac{t_{r\max} - t_{r\min}}{t_{r\max} + t_{r\min}} \quad (3.8)$$

If we assume $v_m(t)$ is symmetrical and has zero average (i.e. no DC component), so that $|v_m(t)| \leq 1$, in this case the maximum and minimum values of $v_m(t)$ will be +1 and -1, respectively. Therefore, the maximum and minimum values of the slope can be calculated from equation 3.6 as, respectively;

$$s_{\max} = \frac{I_o}{C} [1 + k] \quad (3.9)$$

and,

$$s_{\min} = \frac{I_o}{C}[1 - k] \quad (3.10)$$

Substituting equations 3.9 and 3.10 into equation 3.7 gives;

$$k = m \quad (3.11)$$

This leads to;

$$s(t) = \frac{A}{t_{ro}}[1 + mv_m(t)] = \frac{A}{t_r} \quad (3.12)$$

or simply,

$$t_r = \frac{t_{ro}}{[1 + mv_m(t)]} \quad (3.13)$$

Substituting the minimum and the maximum values of $v_m(t)$, i.e. -1 and +1, in equation 3.13, the maximum and the minimum rise time can be evaluated, respectively, as;

$$t_{r\max} = \frac{t_{ro}}{1 - m} \quad (3.14)$$

$$t_{r\min} = \frac{t_{ro}}{1 + m} \quad (3.15)$$

The values $t_{r\max}$ and $t_{r\min}$ are asymmetrical with respect to t_{ro} , see Fig 3.2. This non-symmetry can be seen when examining the values $(t_{r\max} - t_{ro})$ and $(t_{ro} - t_{r\min})$. Using equations 3.14 and 3.15 the following can be obtained;

$$t_{r\max} - t_{ro} = \frac{m}{1-m} t_{ro} \quad (3.16)$$

and

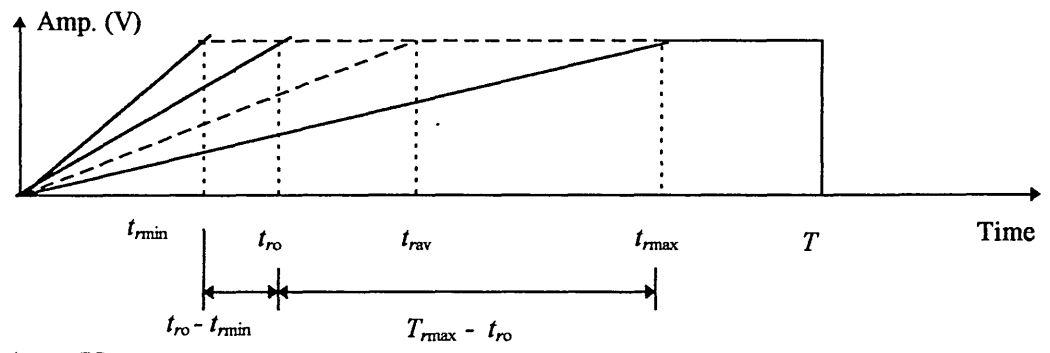
$$t_{ro} - t_{r\min} = \frac{m}{1+m} t_{ro} \quad (3.17)$$

However, the average value t_{rav} , see Fig 3.2, can be evaluated as;

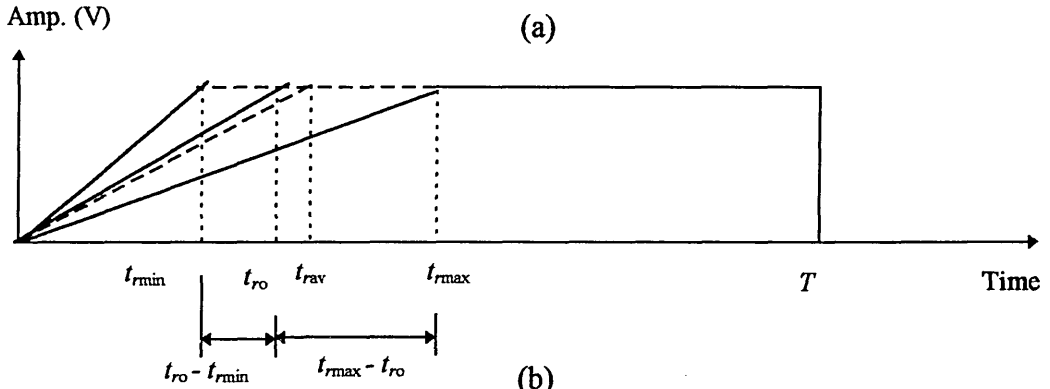
$$\begin{aligned} t_{rav} &= \frac{t_{r\max} + t_{r\min}}{2} \\ &= \frac{1}{(1+m)(1-m)} t_{ro} \end{aligned} \quad (3.18)$$

Equations 3.16-3.18 have been plotted (Fig. 3.3) as normalised values with respect to t_{ro} . When the modulation index is very small the values $(t_{r\max} - t_{ro})$ are comparable with $(t_{ro} - t_{r\min})$, and t_{rav} is nearly equal to t_{ro} . Thus the variation in the rise time due to the existence of modulation is almost symmetrical with respect to t_{ro} . As the value of m increases, $(t_{r\max} - t_{ro})$ increases much faster than $(t_{ro} - t_{r\min})$, which means that the variation in the rise time due to the existence of modulation is asymmetrical with respect to the unmodulated rise time t_{ro} , and t_{rav} is mainly determined by $(t_{r\max} - t_{ro})$.

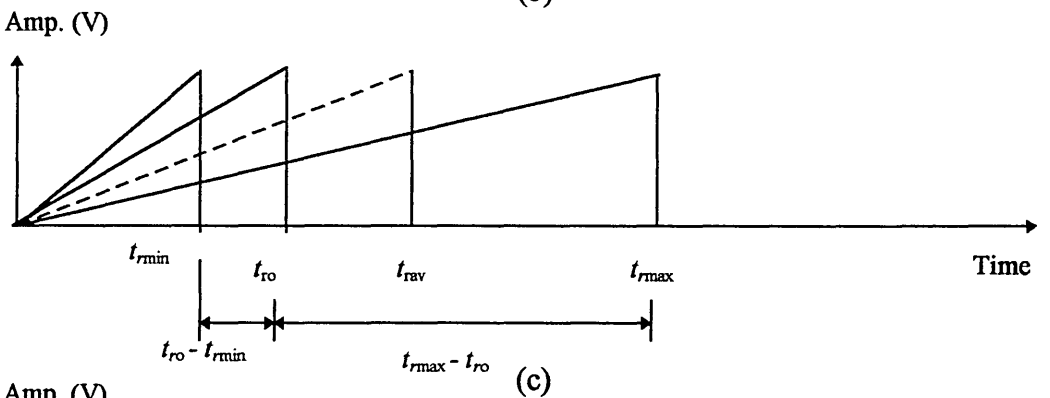
The above analysis is valid for both trapezoidal and the triangular PSM waveforms. However, the maximum modulation index (m_c) that can be achieved without distorting the output waveform depends on the type of PSM. In order to evaluate m_c for both PSM waveforms, the two types of PSM waveforms are treated separately;



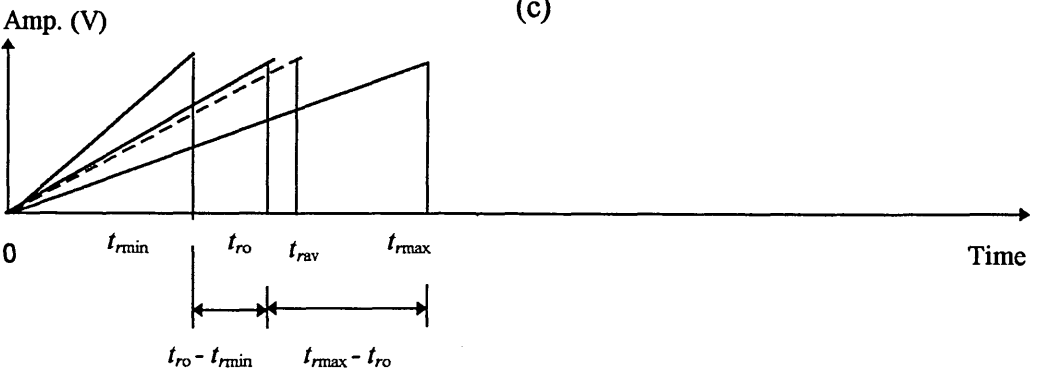
(a)



(b)



(c)



(d)

Fig. 3.2 PSM waveform: (a) trapezoidal PSM with high modulation depth, (b) trapezoidal PSM with low modulation depth, (c) triangular PSM with high modulation depth and (d) triangular PSM with low modulation depth.

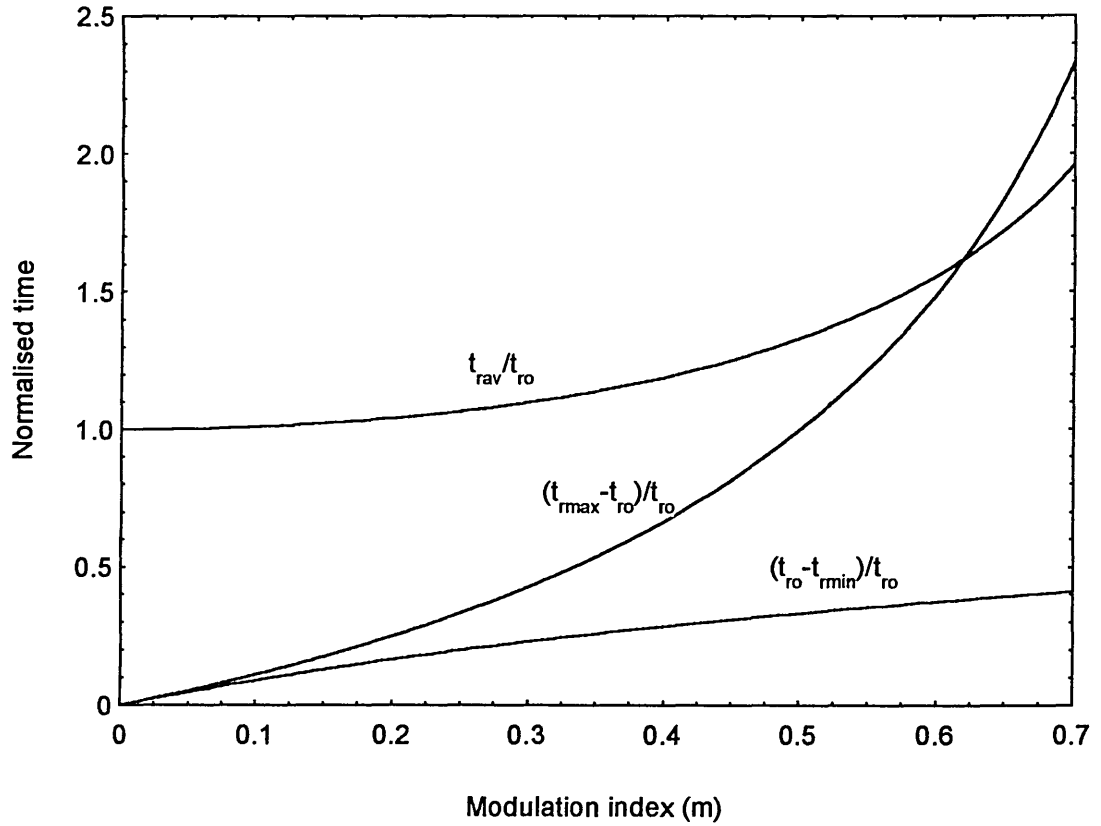


Fig. 3.3 Normalised $(t_{rmax}-t_{ro})$, $(t_{ro}-t_{rmin})$, and t_{rav} versus modulation index m .

I. The trapezoidal PSM waveform: In this type of PSM, the maximum modulation index that can be achieved without distorting the output waveform is when

$$t_{rmax} = T \text{ where } T \text{ is defined in Fig. 3.2, and } t_{rmin} = \frac{t_{ro}}{1-m_c}, \text{ i.e when } v_{min} = -1.$$

Substituting these values into equation 3.8, the maximum modulation index can be evaluated as;

$$m_c = 1 - \frac{t_{ro}}{T} \tag{3.19}$$

II. The triangular PSM waveform: The triangular PSM waveform can be treated as trapezoidal PSM with $T = T_o$ (where T_o is the period). Therefore, from equation. 3.19

the maximum modulation index which can be achieved for the triangular PSM without distorting the output waveform is;

$$m_c = 1 - \frac{t_{ro}}{T_o} \quad (3.20)$$

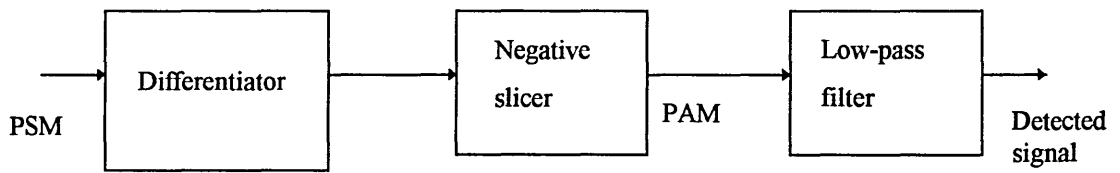
Since $T < T_o$, by comparing equations 3.19 and 3.20, it can be concluded that triangular PSM has a wider range of modulation index without distortion than the trapezoidal PSM.

3.3 PSM demodulation

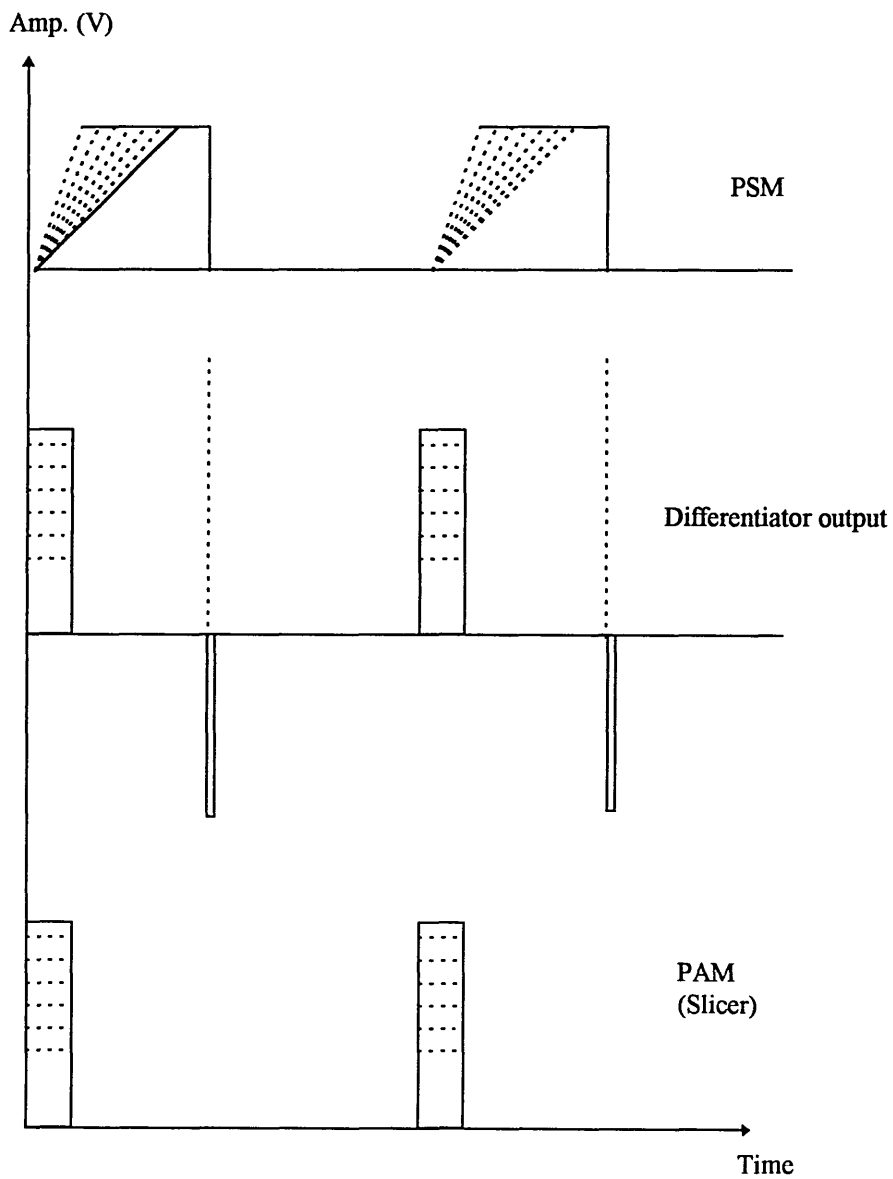
The basic principle of PSM demodulation is to convert the PSM into PAM and extract the message using a low pass filter. There exists an alternative demodulation method which is based on a differentiator followed by a negative slicer, to eliminate any negative spikes. The output of the slicer is the required PAM signal from which the message can be extracted by using a low-pass filter, see Fig. 3.4 [28]. The amplitude of the PAM signal can be determined by differentiating equation 3.2 and substituting equations 3.5 and 3.11 into the result. This leads to;

$$V_{\text{PAM}}(t) = \frac{A}{t_{ro}} [1 + mv_m(t)] \quad (3.21)$$

where, V_{PAM} is the amplitude of the PAM waveform. Further improvement in the noise performance can be achieved by incorporating a sample and hold circuit prior to low pass filtering, see Fig. 3.5.



(a)



(b)

Fig. 3.4 PSM demodulator: (a) block diagram and (b) waveforms.

Because of its transfer function, the differentiator has a negative contribution to the noise performance of the receiver. As a result of this project an alternative demodulator scheme has been suggested where the PSM signal is directly sampled at the rising edge to generate the PAM, see Fig. 3.6. This technique eliminates the use of the differentiator and the negative slicer, and hence improves the noise performance of the receiver as well as reducing cost and complexity. Furthermore, this technique can be applied for both types of the PSM signals, the trapezoidal and the triangular. However, synchronisation of the sampling pulses and the PSM is essential and this is achieved by generating the sampling pulses from the falling edge of the PSM signal. In trapezoidal PSM, the sampling pulses can be generated by using monostables in order to produce a narrow pulse train which can be shifted in time, see Fig. 3.7. The time shift (T_s) is determine by the width of the first monostable output which can be made variable.

In general, in order to minimise the output signal distortion it is essential to chose $T_s < t_{rmin}$. In triangular PSM synchronisation may be achieved by using a phase-lock loop techniques.

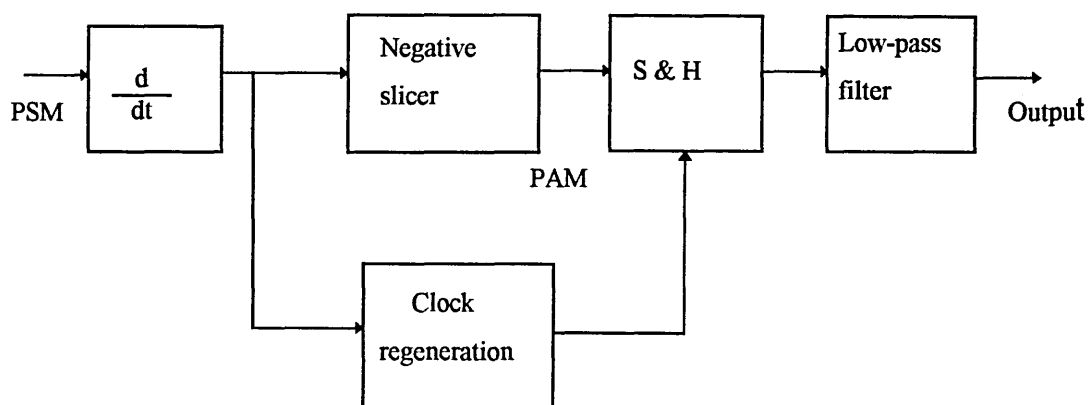


Fig. 3.5 PSM demodulator using sample and hold.

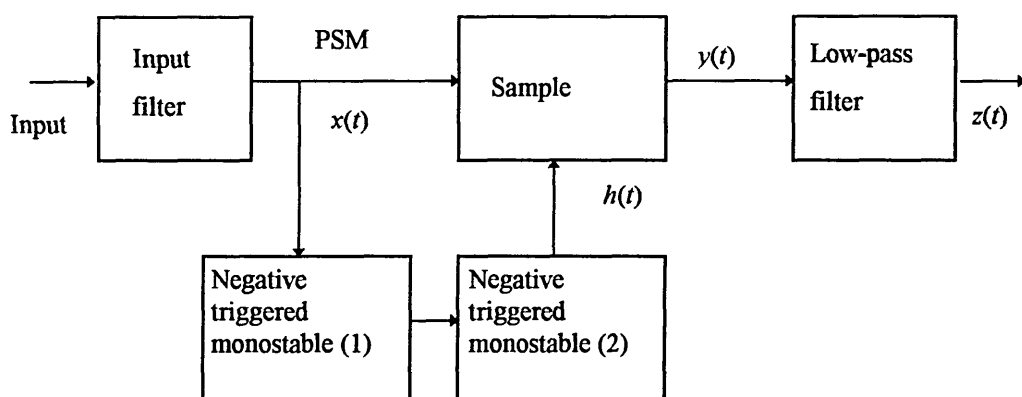


Fig. 3.6 Block diagram of the proposed PSM demodulator.

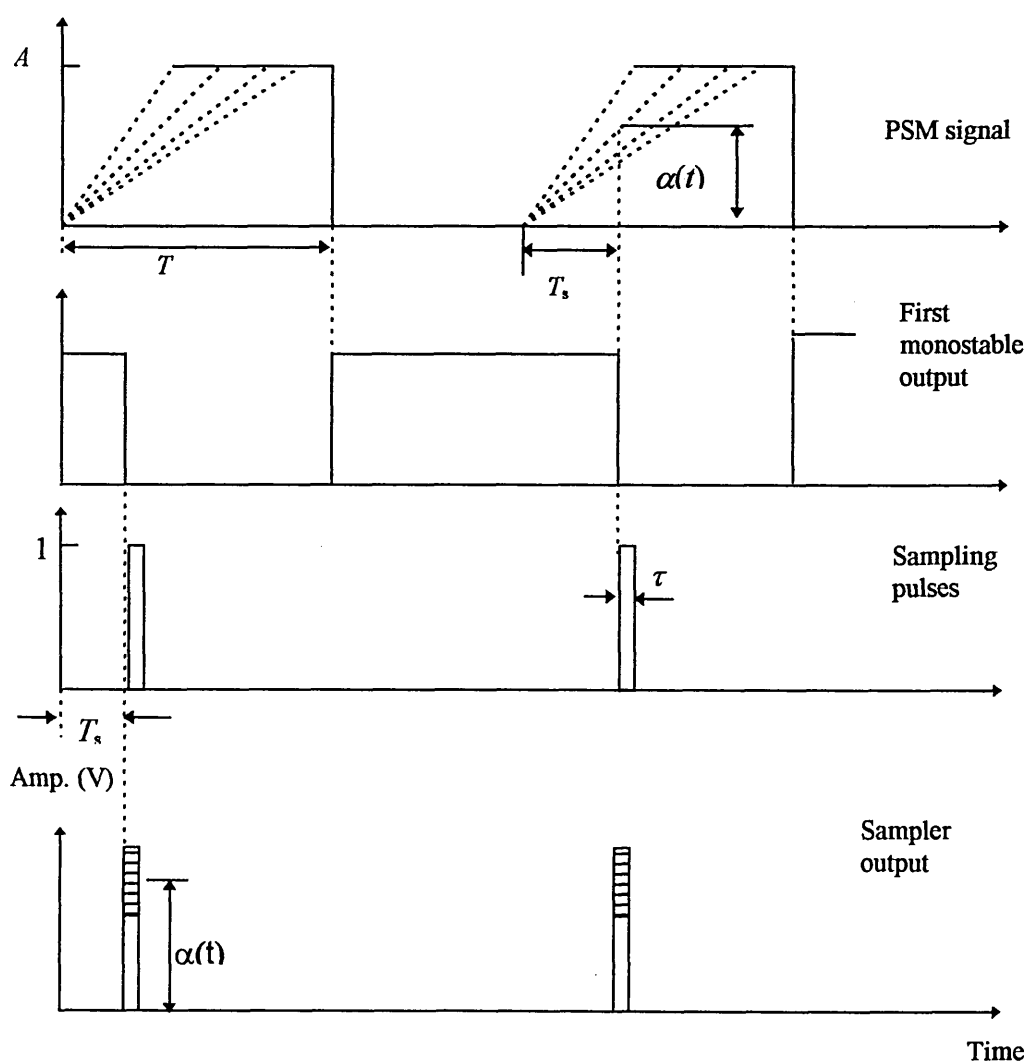


Fig. 3.7 Timing diagram of the proposed PSM demodulator.

Assuming that the sampling pulses have unity amplitude, then from Fig. 3.7 it can be shown that the slope of the PSM signal can be recalculated as;

$$s(t) = \frac{\alpha(t)}{T_s} \quad (3.22)$$

where $\alpha(t)$ is the instantaneous amplitude of the rising edge of the PSM waveform. Substituting equation 3.12 into 3.22, the instantaneous amplitude $\alpha(t)$ can be found as;

$$\alpha(t) = T_s \frac{A}{t_{ro}} [1 + m v_m(t)] \quad (3.23)$$

As the sampling pulses have unity amplitude, the above value of $\alpha(t)$ will represent the envelope of the PAM signal at the sampler output, otherwise amplitude scaling must be introduced. It is clear that the envelope is linearly dependent on the message signal $v_m(t)$. Finally, the detected signal at the output of the low pass filter can be shown to be;

$$z(t) = \frac{A \tau T_s}{T_o t_{ro}} m v_m(t) + \frac{A \tau T_s}{T_o t_{ro}} \quad (3.24)$$

where T is the period of the PSM signal. The first term in equation 3.24 represents the detected signal and the second term represents the DC component which can be eliminated by capacitive coupling. Note that the strength of the detected signal is proportional to the time shift (T_s), the unmodulated slope (A/t_{ro}) and the width of the sampling pulses.

3.4 Power relations of PSM pulses

Unlike rectangular pulses, the power relations in PSM are more complex due to the slope of the transmitted pulses. Here we will consider both trapezoidal and triangular PSM signals.

3.4.1 trapezoidal PSM

Figure 3. 8 shows a trapezoidal PSM pulse which can be represented as;

$$v(t) = \begin{cases} \frac{At}{t_r} & 0 \leq t \leq t_r \\ A & t_r < t < T \\ 0 & T < t < T_o \end{cases} \quad (3.25)$$

where t_r is the rise time of the PSM pulse, in the absence of the slope modulation $t_r = t_{ro}$. The total energy in a pulse can be obtained from equation 3.26;

$$E = A^2 \left(T - \frac{2}{3} t_r \right) \quad (3.26)$$

The instantaneous power delivered to 1 Ω resistor can be shown to be;

$$P = \frac{A^2}{T_o} \left[T - \frac{2}{3} t_r \right] \quad (3.27)$$

and the average transmitted power is;

$$P_o = \frac{A^2}{T_o} \left(T - \frac{2}{3} t_r \right) \quad (3.28)$$

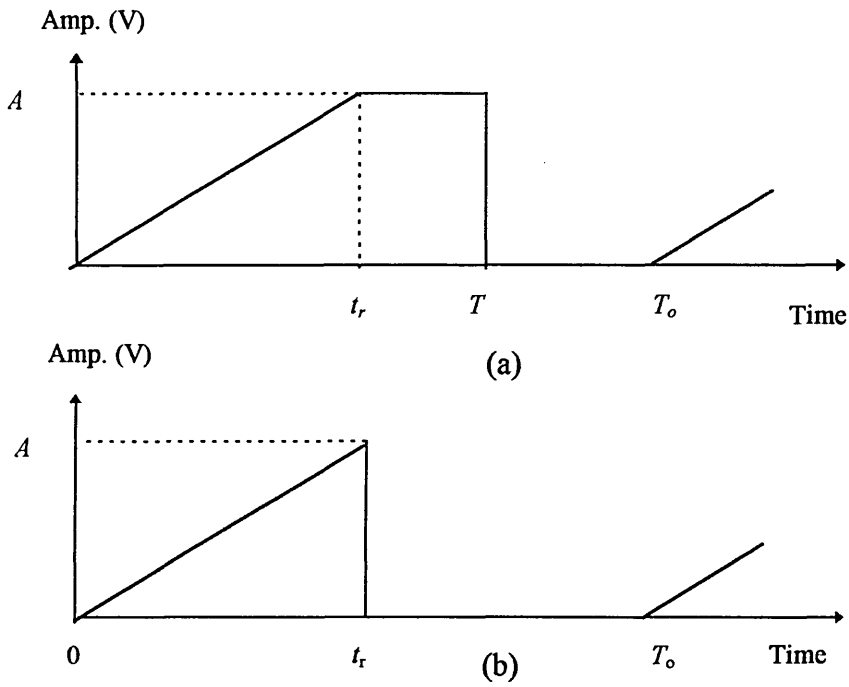


Fig. 3.8 PSM pulses waveforms: (a) trapezoidal and (b) triangular.

where $\langle \cdot \rangle$ denotes time averaging for the enclosed quantity. Equation 3.28 is a general equation which is true both when slope modulation is present or absent, and is plotted in Fig. 3.9 as a function of the normalised average rise time ($\langle t_r \rangle / T_o$). It is clear that the average power decreases when the average rise time increases. This is because the shape of the pulse becomes closer to a triangular. In the absence of slope modulation, i.e. $\langle t_r \rangle = t_{ro}$, equation 3.28 is reduced to;

$$P_{oun} = \frac{A^2}{T_o} \left(T - \frac{2}{3} t_{ro} \right) \quad (3.29)$$

In the case of pulse modulation, the value of t_r , as given in equation 3.13, is $t_r = \frac{t_{ro}}{1 + m v_m(t)}$, but, t_r will have discrete values depending on the phase relation between the sampling pulse and the modulating signal voltage. Therefore, equation 3.28 can be rewritten as;

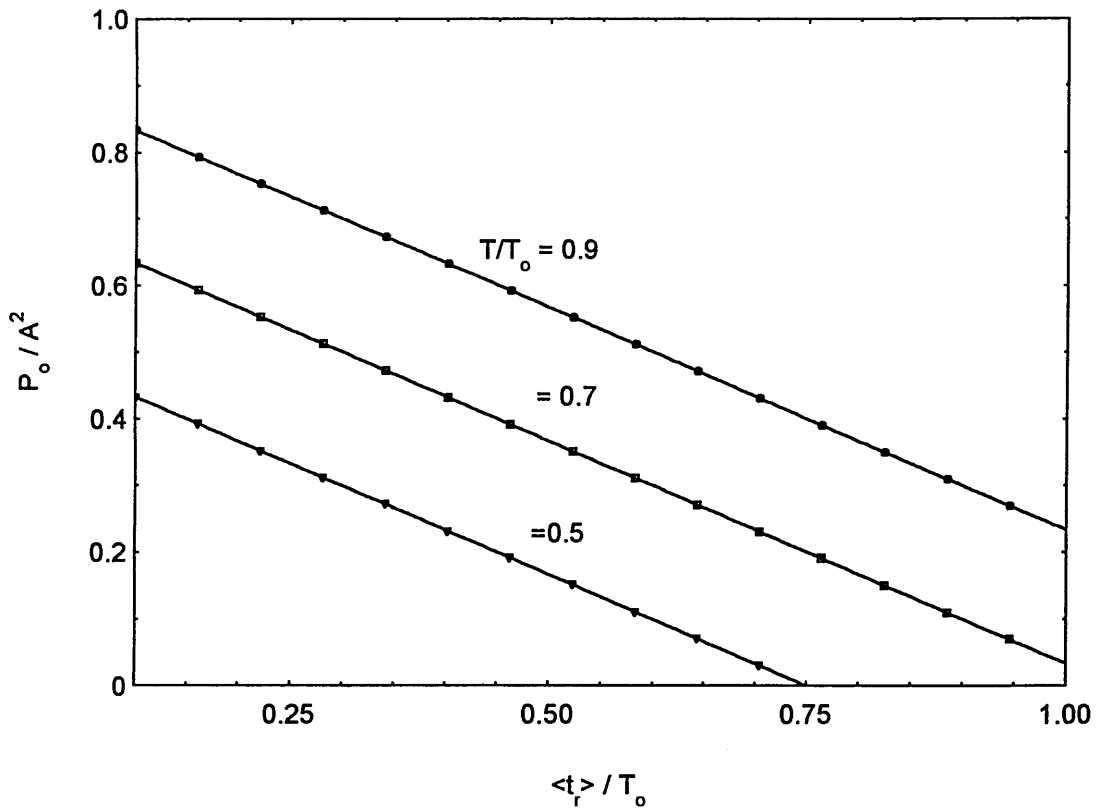


Fig. 3.9 Normalised average power of trapezoidal PSM as a function of the normalised rise time.

$$P_o = \frac{A^2}{T_o} T \left[1 - \frac{2}{3T_o} \frac{1}{N} \sum_{n=1}^N t_m \right] \quad (3.30)$$

where t_m are the instantaneous discrete values of t_r and N is an integer. Substituting equation 3.13 into 3.30 the average power can be written in terms of the modulating signal values as;

$$P_o = \frac{A^2}{T_o} T \left[1 - \frac{2}{3T_o} \frac{1}{N} \sum_{n=1}^N \frac{t_{ro}}{1 + mv_m(t_n)} \right] \quad (3.31)$$

where t_n is the sampling time at which the discrete values of the rise time exists. When N is a large integer, which is true when the sampling ratio is relatively high, the summation in equation 3.31 can be approximated to;

$$\xi(m) = \frac{1}{N} \sum_{n=1}^N \frac{1}{1 + mv_m(t_n)} \approx \lim_{\Delta T \rightarrow \infty} \frac{1}{T_o} \int_0^{\Delta T} \frac{dt}{1 + mv_m(t)} \quad (3.32)$$

where ΔT is the time interval (in case of periodic signal ΔT represents the period). For a unity amplitude sinusoidal signal it can be shown that [76, 77];

$$\xi(m) = \frac{1}{\sqrt{1 - m^2}} \quad (3.33)$$

Finally, substituting equations 3.33 and 3.32 into 3.31 the average transmitted power can be given as;

$$P_o = \frac{A^2}{T_o} T \left[1 - \frac{2t_{ro}}{3T_o} \xi(m) \right] \quad (3.34)$$

Substituting equation 3.19 into 3.34, the average power at the maximum modulation index m_c can be evaluated as

$$P_{oc} = \frac{A^2}{T_o} T \left[1 - \frac{2}{3} (1 - m_c) \xi(m_c) \right] \quad (3.35)$$

The above equation represents the upper limit beyond which the PSM waveform will be distorted. Equations 3.34 and 3.35 have been plotted against modulation index for different values of T/T_o and t_{ro}/T_o , see Figs. 3.10 and 3.11. It can be seen that the power decreases as the modulation index increases. This is because that as the modulation index increases, the average rise time increases, as explained in the last section, which leads to a decrease in the power.

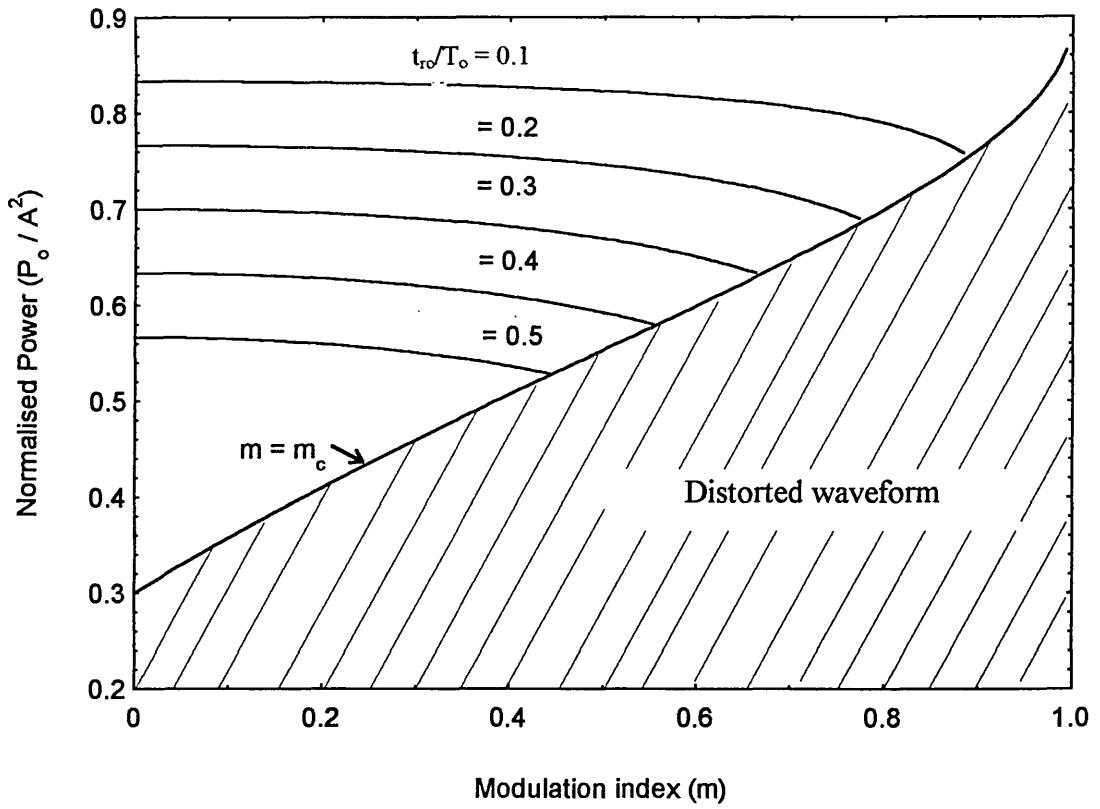


Fig. 3.10 Normalised average power of trapezoidal PSM signal ($T/T_o = 0.9$)

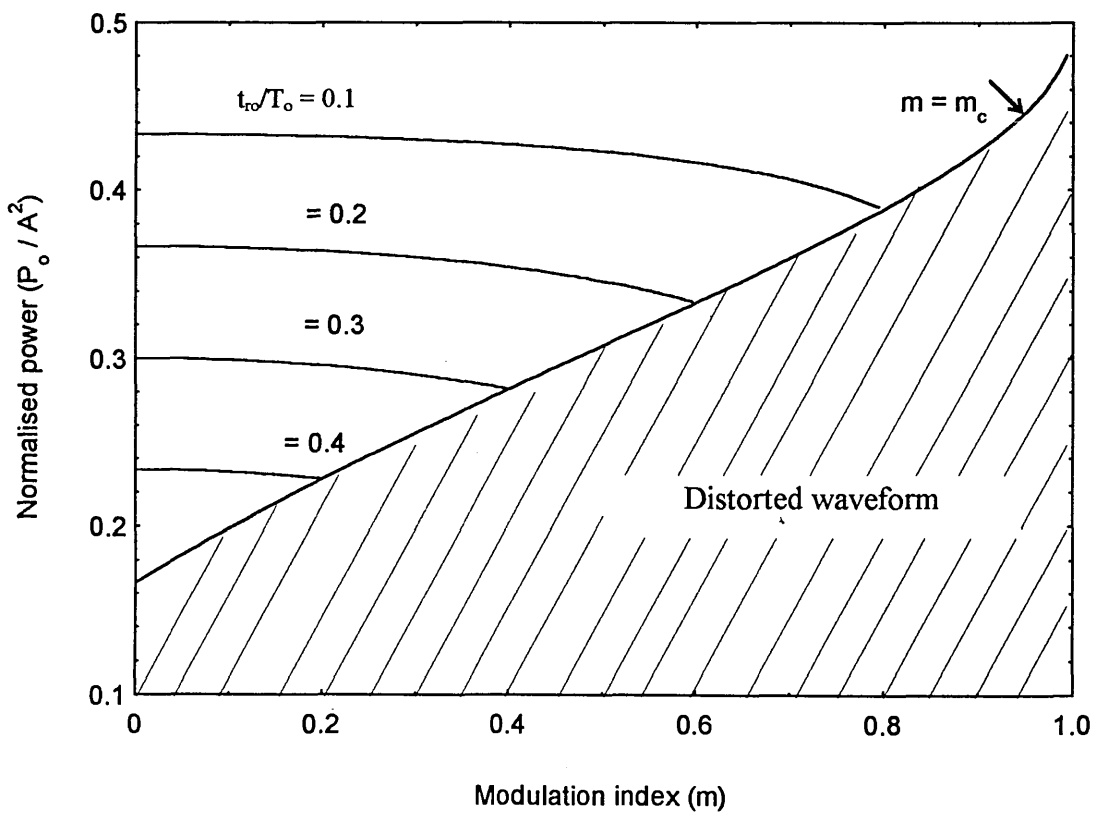


Fig. 3.11 Normalised average power of trapezoidal PSM signal ($T/T_o = 0.5$).

3.4.2 triangular PSM

This is illustrated in Fig. 3.8.b and may be expressed as;

$$v(t) = \begin{cases} At / t_r & 0 \leq t \leq t_r \\ 0 & t_r < t < T_o \end{cases} \quad (3.36)$$

Comparing equation 3.36 with equation 3.25, it is clear that triangular PSM pulses can be considered as trapezoidal PSM with $T = t_r$. Therefore, the average transmitted power can be obtained as;

$$P_o = \frac{A^2}{3T_o} \langle t_r \rangle \quad (3.37)$$

Equation 3.37 shows the relation between the average rise time and the transmitted power. Unlike the trapezoidal PSM, the average power of triangular PSM increases with increasing average rise time. Following the same procedure used in deriving the power relations of the trapezoidal PSM, the average power per second for the triangular waveform can be found as;

$$P_o = \frac{A^2}{3T_o} t_{ro} \xi(m) \quad (3.38)$$

The average PSM waveform power when the modulation index is maximum can be obtained by substituting equation 3.20 into 3.38. this gives;

$$P_{oc} = \frac{A^2}{3} (1 - m_c) \xi(m_c) \quad (3.39)$$

Equations 3.38 and 3.39 have been plotted as a function of the modulation index m for different values of t_{ro}/T_o , and shown in Fig 3.12. Unlike the trapezoidal PSM, the average transmitted power of the triangular PSM increases as the modulation index increases. This is because the average rise time increases as the modulation index increases, and consequently the average power increases, as it can be seen from equation 3.37.

A comparison between the power relations of triangular PSM and trapezoidal PSM is shown in Fig. 3.13 which demonstrates results as expected. With small values of t_r , triangular PSM needs less power than trapezoidal for the same value of modulation index. However, as T/T_o decreases, the trapezoidal PSM approaches the triangular behaviour. It can also be seen that the maximum modulation indices in both types of PSM are different, triangular PSM shows wider range for less transmitted power.

3.5 Frequency spectrum of the PSM signal

The frequency spectrum of the PSM signal has been studied by several authors [29, 78-80]. Different analytical approaches have been tried for both trapezoidal and the triangular PSM waveforms. The method reported by Das [29] is based on expanding the unmodulated trapezoidal pulse in a Fourier series and the effect of modulation on the rise time was introduced on the series in order to produce a more general Fourier series expression which is given by the following equation [29];

$$v(t) = A \frac{T}{T_o} + \frac{At_{ro}}{2T_o[1+m \sin \omega_m t]} + \frac{2A}{T_o} \sum_{n=1}^{\infty} \left[\frac{\sin n\omega_o(T-t)}{n\omega_o} \right] + \frac{2A}{T_o} \sum_{n=1}^{\infty} \frac{1+m \sin \omega_m t}{n^2 \omega_o^2 t_{ro}} [\cos n\omega_o \{t - \frac{t_{ro}}{1+m \sin \omega_m t}\} - \cos n\omega_o t] \quad (3.40)$$

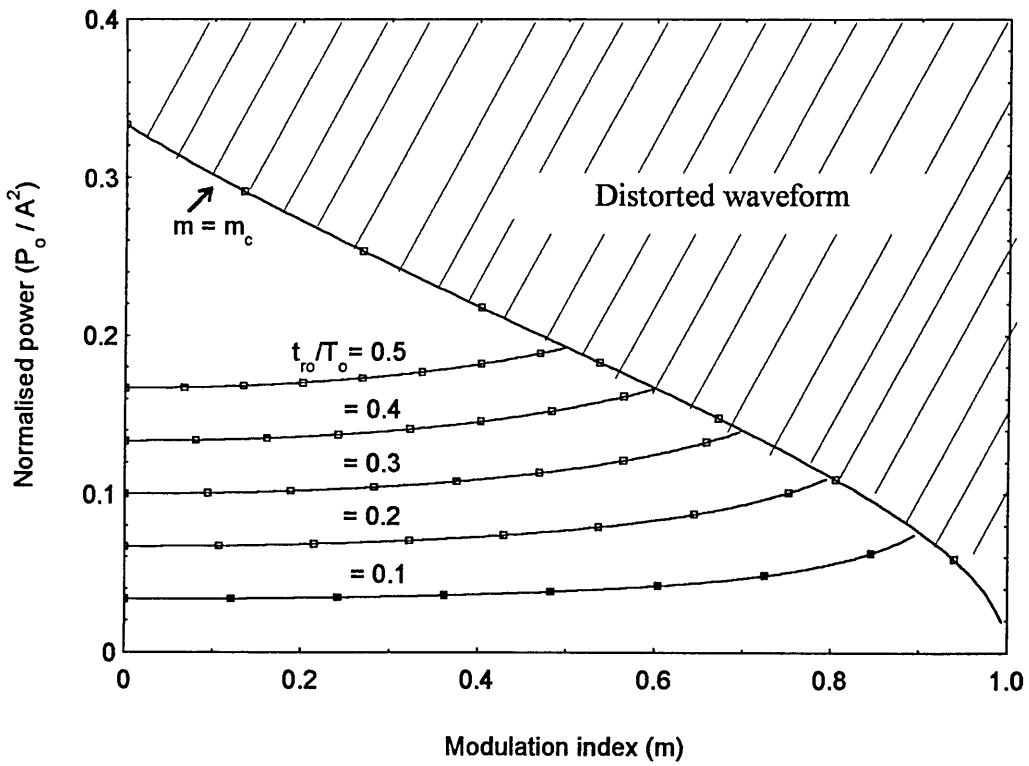


Fig. 3.12 Normalised average power for triangular PSM waveforms.

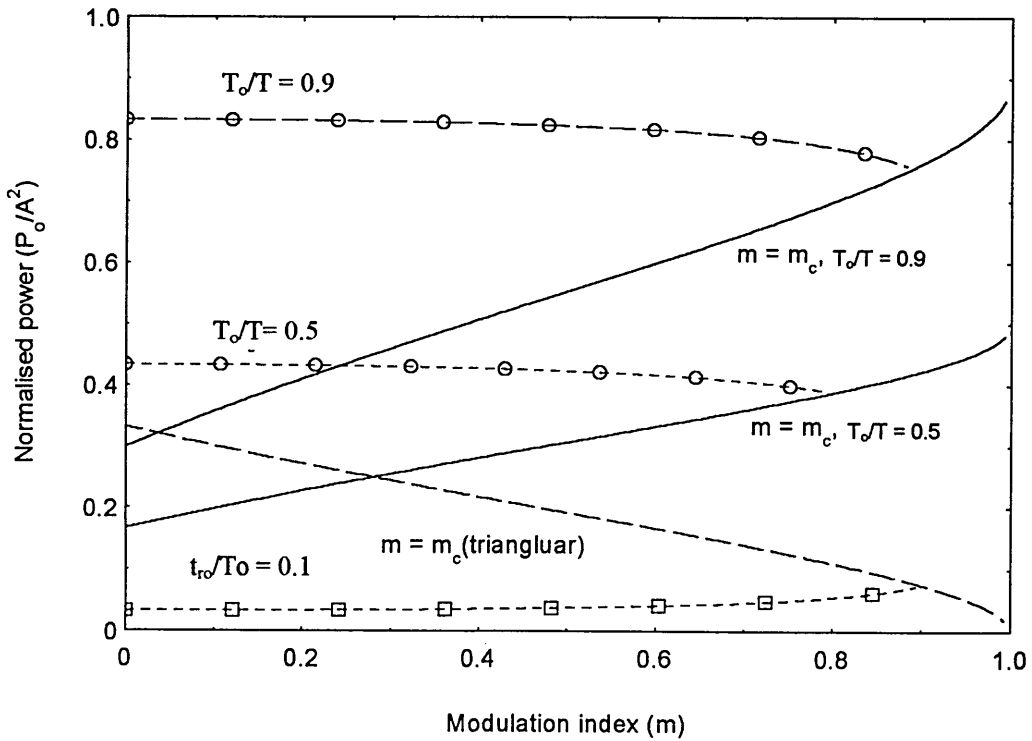


Fig. 3.13 Normalised transmitted power for both types of PSM pulses ($t_{ro}/T_o = 0.1$,

□ triangular PSM, ○ Trapezoidal PSM).

where ω_o is the carrier frequency and n is an integer index. Inspection of equation 3.40 shows the presence of a DC component (first term), as well as many different frequencies. These include the baseband component (second term), carrier components and a set of sidetone set around the carrier components separated by the modulating frequency (ω_m) (last term), see Fig. 3.14. The amplitude of these components is inversely proportional to square of that of the harmonics of the carrier frequency and their order ($n\omega_o$). The baseband component is inversely proportional to the message signal ω_m and simple low-pass filtering of the PSM waveform at the receiver will not generate the required message signal. The modulation spectrum of the triangular PSM waveform can be simplified when assuming small modulation index so that [79, 80];

$$\frac{1}{1 + m \sin \omega_m t} \cong 1 - m \sin \omega_m t \quad (3.41)$$

The Fourier series expansion for the trailing edge variable slope PSM wave is given as;

$$\begin{aligned} v(t) = & \frac{t_{ro}}{2T_o} - \frac{t_{ro}}{2T_o} m \sin \omega_m t + \sum_{n=1}^{\infty} \frac{1}{n^2 \omega_o^2 t_{ro} T_o} \{ [H - J_o \sin H + J_1 m \cos H] \sin n\omega_o t \\ & + [1 - J_o \cos H - J_1 m \sin H] \cos n\omega_o t \\ & + [-\frac{1}{2}m + J_1 \sin H - \frac{1}{2}(J_2 - J_o)m \cos H] \sin(n\omega_o - \omega_m)t \\ & + [J_1 \cos H + \frac{1}{2}(J_2 - J_o)m \sin H] \cos(n\omega_o - \omega_m)t \\ & + [\frac{1}{2}m - J_1 \sin H + \frac{1}{2}(J_2 - J_o)m \cos H] \sin(n\omega_o + \omega_m)t \\ & + [-J_1 \cos H + \frac{1}{2}(J_2 - J_o)m \sin H] \cos(n\omega_o + \omega_m)t \\ & + [-J_2 \sin H + \frac{1}{2}(J_3 - J_1)m \cos H] \sin(n\omega_o - 2\omega_m)t \\ & + [-J_2 \cos H + \frac{1}{2}(J_3 - J_1)m \sin H] \cos(n\omega_o - 2\omega_m)t \\ & + [-J_2 \sin H + \frac{1}{2}(J_3 - J_1)m \cos H] \sin(n\omega_o + 2\omega_m)t \\ & + [-J_2 \cos H + \frac{1}{2}(J_3 - J_1)m \sin H] \cos(n\omega_o + 2\omega_m)t \\ & + \dots \} \end{aligned} \quad (3.43)$$

where, $H = n\omega_o t_{ro}$, and $J_k = J_k(Hm)$, $k = 1, 2, \dots$ are the Bessel functions of the first kind and order k . In the above equation the first and second terms represent the DC and baseband components respectively. The pulse repetition frequency ω_o and its harmonics are represented by the third and the fourth terms. the remaining terms represent the sidetones around ω_o and its harmonics, see Fig. 3.14. All spectral analysis has been carried out for the case when m is small. However, the modulation spectrum of the triangular PSM waveform is very similar to that for trapezoidal PSM.

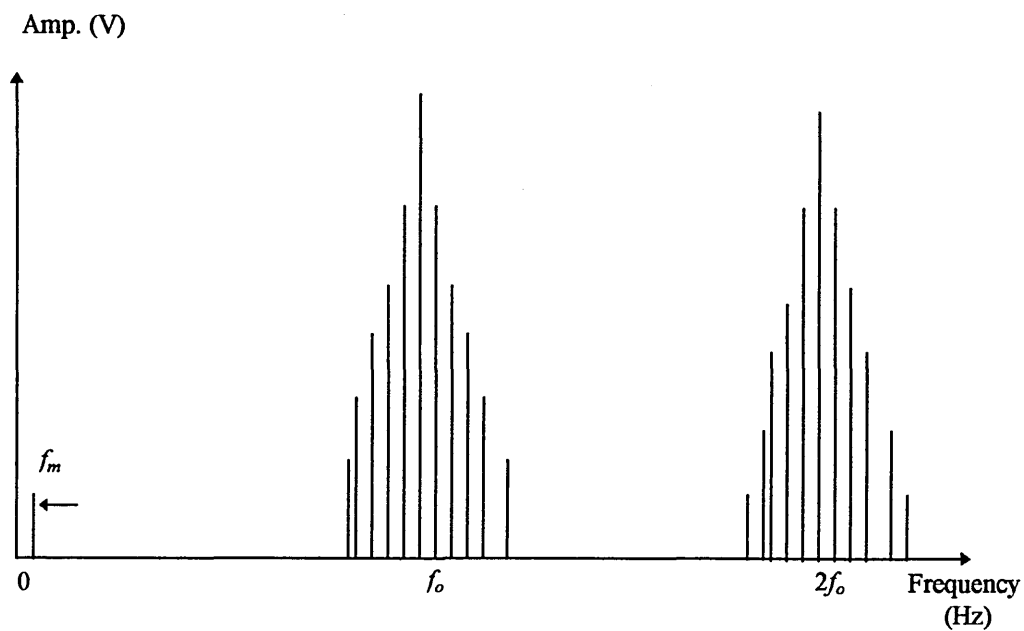


Fig. 3.14 Single tone modulation spectrum of triangular PSM waveform.

3.6 Noise performance of the PSM signal

Unlike PTMs PSM demodulation does not employ threshold detection as the information is carried by the shape of the pulse. Therefore, in case of optical transmission of PSM pulses, intensity modulation should be used where the PSM pulses directly modulate the intensity of an optical source, see Fig 3.15. An optical fibre is then

used as a transmission medium. At the receiving end, the optical signal is converted into an electrical signal by an optical receiver and then passed to a PSM demodulator. No pulse regeneration before demodulation will be employed as this process will distort the information contained by the slope of the pulse and make the output signal undetectable. The noise jitter produced by the amplitude to phase conversion at threshold detector, which converts the amplitude noise into noise pulse jitter is not present in PSM systems. The main noise sources in optical PSM transmission are;

- (i) intensity noise of the optical source.
- (ii) mode partition noise.
- (iii) receiver noise caused by optical detection and pre-amplification.

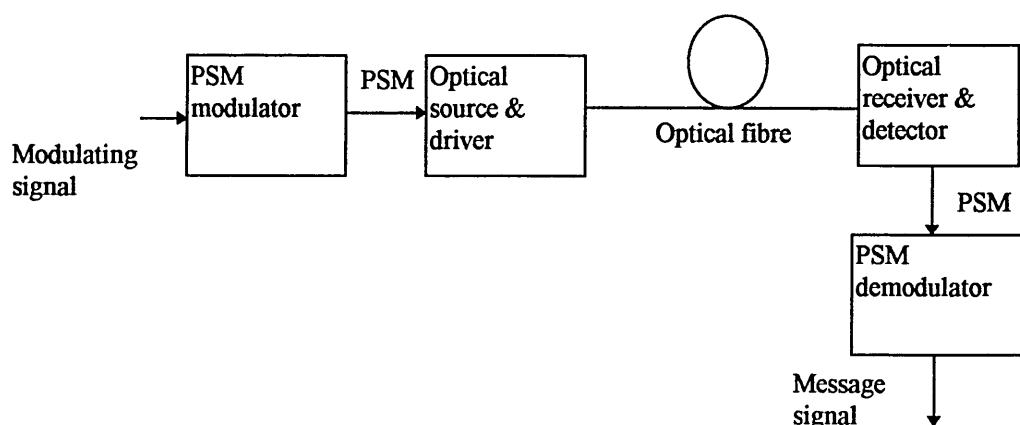


Fig 3.15 PSM optical transmission.

Random fluctuations of the optical source will result in intensity noise. It becomes more significant when a laser diode is used as the optical source. The intensity noise is usually smaller than that generated in other parts of the system, particularly at the receiving end. However, it can increase significantly due to optical reflection back to the laser diode, especially with the longitudinal mode laser type.

Modal noise exists when multimode fibre is used. Each longitude mode of the optical source will split into several waveguide modes when coupled into multimode fibre. At the receiving end, these modes will interfere and form speckle patterns. The pattern is always changing because of the slight change in the fibre properties. Modal noise depends on the material dispersion of the fibre and the optical source spectrum.

The most important amplitude noise in the optical receiver is that generated by shot and thermal noise. This includes photo-diode shot noise and the preamplifier noise with the later usually the dominating factor. The receiver noise is usually a function of frequency, but it can be approximated as white noise.

In this section, the noise performance of a PSM system will be studied. A full mathematical analysis of signal-to-noise ratio of the PSM system will be made. The system has been investigated when white noise is added to the signal. This method has the advantage of simplicity and can be used for both the optical receiver, when optical receiver noise is the dominant factor, and non-optical system.

The main key to the noise reducing property of pulse modulation is the slicing process. Both theory and experiments show that the optimum value of the slicing level is half the peak signal amplitude, taking all types of noise and interference into consideration. Further, for maximum SNR in the output, the thickness of the pulse slice should not exceed a few per cent of the pulse height .

In case of PSM, this cannot be reached, as an appreciable percentage of the pulse height is required to obtain the information back, as the information is carried in the slope of the pulse edge. Das [29] found that the thickness of the slice should be about 20% of the pulse height for efficient differentiation, Fig. 3.16, and with slicing level of 40% of the pulse height the allowable input signal-to-noise ratio is 8 dB for acceptable reception.

All PTMs are expected to have a time shift problem due to the existence of noise. However in PSM it has been seen that the resultant noise due to this time shift is very small as the information is dependent not on the position of the leading edge, as in PWM and PPM, but on the slope.

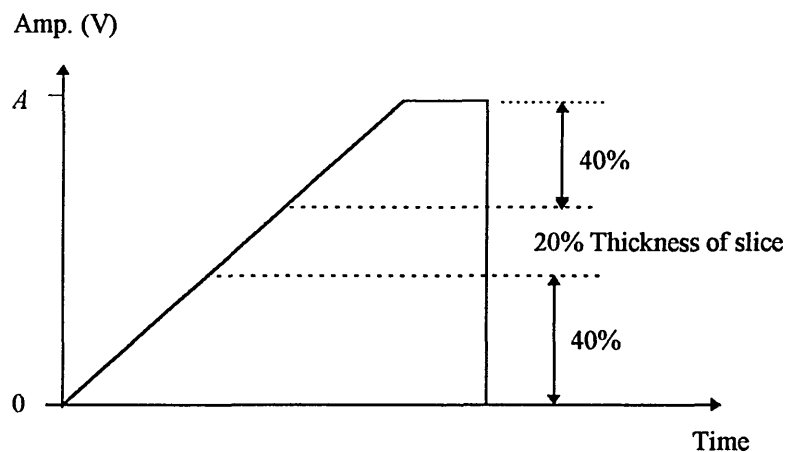


Fig. 3.16 Slicing level of the PSM signal.

Das [29] also studied the case when the noise level is above the slicing level, and spurious pulses are generated. This problem has been overcome by using a narrow gating pulse after the differentiator, so that only the narrow information carrying differentiated pulses, corresponding to the leading edge of the transmitted pulses, are selected and demodulated, see Fig. 3.17. This process improves the performance of the wide pulse system to the level of systems using narrow pulses.

However, in the receiver proposed earlier in this work, the process of noise reduction by slicing and gating is not important, and therefore it can be eliminated. This is because the PSM pulses are sampled at the rising edge and therefore the regions outside the sampling pulses will not pass to the next stage (see Figs. 3.6 and 3.7). The sampling pulses can be made narrow enough to reject most of the noise in the waveform

background. As a result, the same improvement in noise performance can be achieved without using extra processing on the received signal. This is another advantage of the proposed technique of the PSM demodulation.

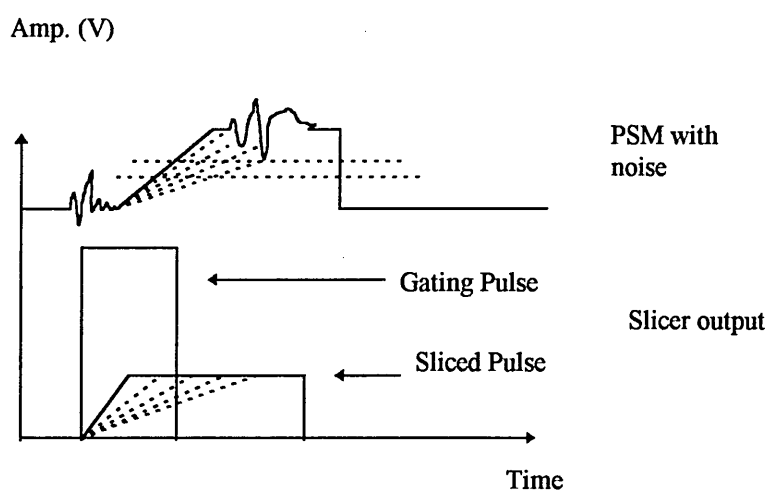


Fig. 3.17 Reduction of noise by slicing and gating.

Although some results have been reported on the noise performance of the PSM in the early papers, no detailed analysis or theoretical analysis for the signal-to-noise ratio were given. As part of this work, a full analysis of the noise performance of the PSM was reported. In this analysis, the proposed receiver shown in Fig. 3.6 has been considered. As mentioned the basic principles of this receiver are based on sampling the PSM signal at the rising edges to generate PAM which then passed through a low pass filter to extract the message. This receiver does not require slicing as the sampling process has the same effect.

Noise analysis can be carried out by assuming that both a PSM signal and white Gaussian noise are applied at the input filter of the receiver shown in Fig. 3.6. This

makes the analysis suitable for both electrical and optical transmission. The output of the sampler due to the PSM and the noise may be expressed as [35];

$$y(t) = \sum_{k=-\infty}^{\infty} \frac{A}{T_o t_{ro}} [1 + m v_m(t)] h(t - T_s - kT_o) + \sum_{k=-\infty}^{\infty} n(t) h(t - T_s - kT_o) \quad (3.42)$$

where $h(t)$ is the shape function of the sampling pulses, and $n(t)$ is the bandlimited input noise with a bandwidth B equal to that of the input filter.

The first term in equation 3.42 represents the amplitude of the modulated pulse train containing the message signal $v_m(t)$ and the second term represents the noise process. The output of the filter due to the signal is given in equation 3.24 which can be rewritten as

$$z_{\text{signal}}(t) = \frac{A \tau T_s}{T_o t_{ro}} m v_m(t) + DC \quad (3.43)$$

The detected message power at the output filter in the absence of noise can be obtained from equation 4.30 after eliminating the DC term which is usually done by capacitive coupling. The average signal power is then given as;

$$S = \left(\frac{\tau T_s}{T_o t_{ro}} A m \right)^2 \overline{v_m^2(t)} \quad (3.44)$$

The bar sign denoting averaging.

When the modulating signal is absent, the pulses at the sampler output (see Fig. 3.18.a) can be mathematically represented by substituting $m = 0$ in equation 3.42. These pulses are very similar to those considered by Jelonek [25], see Fig. 3.18.b. In order to find the power spectral density of the noisy pulses at the sampler output, it is more convenient to consider the pulses in Fig. 3.18-b rather than considering the actual pulse

shape in Fig. 3.18.a. Such an approximation does not introduce significant error as the shape of the two pulses is very similar.

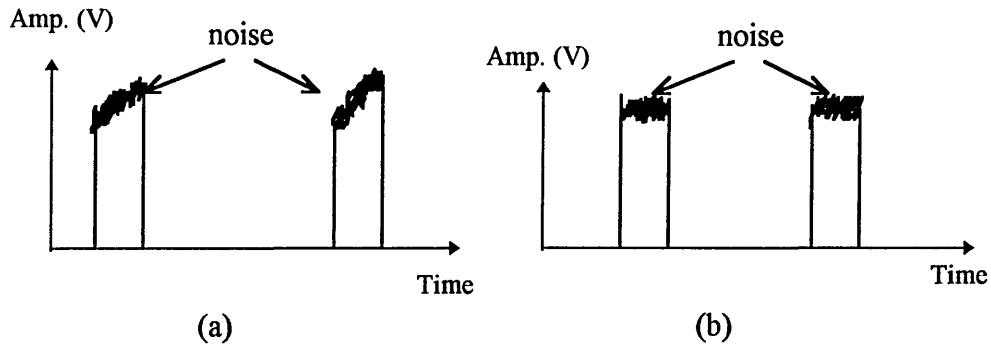


Fig. 3.18 (a) Pulses at the sampler output when modulation is absent and (b) pulses considered by Jelonek [25].

Following the same procedure used by Jelonek [25] the noise power spectral density at the input of the output filter can be given as;

$$P_n(f) = \frac{\overline{2n^2(t)\tau}}{\pi BT_o} \left\{ \text{Si}\pi\left(\frac{B}{2} + f\right)\tau + \text{Si}\pi\left(\frac{B}{2} - f\right)\tau - \frac{\sin^2\left[\pi\left(\frac{B}{2} + f\right)\tau\right]}{4\pi\left(\frac{B}{2} + f\right)\tau} - \frac{\sin^2\left[\pi\left(\frac{B}{2} - f\right)\tau\right]}{4\pi\left(\frac{B}{2} - f\right)\tau} \right\} \quad (3.45)$$

where f is the frequency in Hz. The quantity between brackets (W) has been drawn as a function of the normalised frequency (f/B) for different values of $B\tau$ and displayed in Fig. 3.19. It can be concluded that as $B\tau$ increases the noise spectral density tends to have a rectangular shape (i.e. tends to have the shape of a bandlimited white noise). With $B\tau$ decreasing the spectral density will be more flat and spread over wider

frequency range. For the case when $B\tau \gg 1$ the noise spectral density can be assumed to be a rectangular with falling, and rising edges at $f = |B|$, and an area equal to π . This means that the noise power at the input of the output filter will be given as;

$$N_i = \frac{\overline{n^2(t)}}{BT_o} \tau \quad (3.46)$$

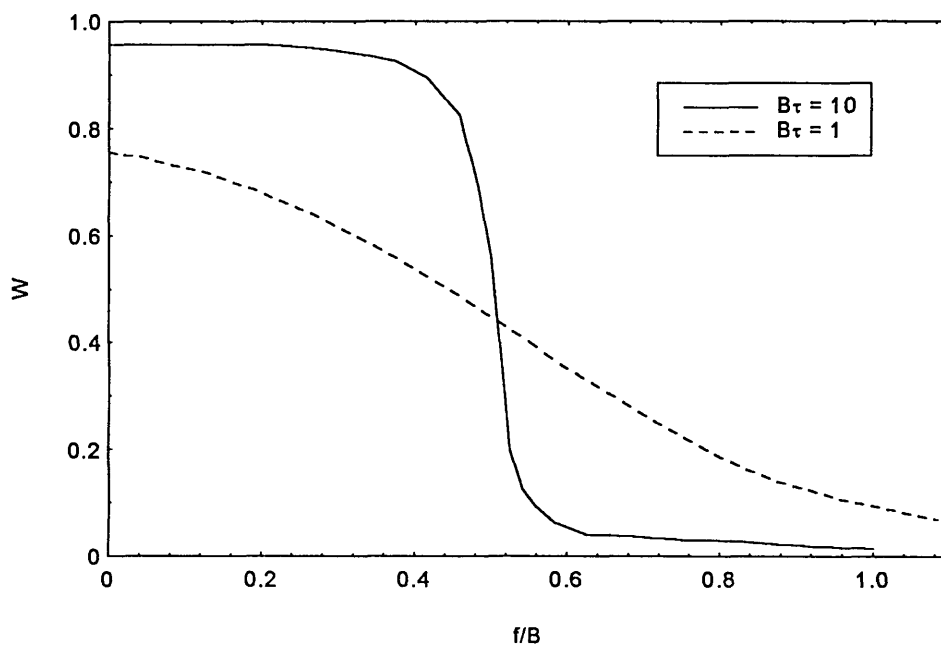


Fig. 3.19 Normalised noise power spectral density of PSM system.

Note that the above equation is true for $B\tau \gg 1$ which is the case for most practical systems, as the transmitted bandwidth usually chosen greater than $(1/\tau)$. Nevertheless, when considering the worst case, when $B = 1/\tau$, the error in the above equation will be less than 25%. Therefore, without losing generality, we can assume that the above equation is valid for $B\tau > 1$. The noise power at the output can be given as;

$$N_o = \frac{\overline{n^2(t)}}{BT_o} B_n \tau \quad (4.47)$$

The output signal-to-noise ratio (*SNR*) can then be obtained by dividing equation 3.44 by 4.47, this leads to;

$$SNR = \left(Am \frac{T_s}{t_{ro}} \right)^2 \frac{B\tau}{B_n T_o} \frac{\overline{v_m^2(t)}}{\overline{n^2(t)}} \quad (3.48)$$

The above equation can be rewritten in terms of the input carrier -to-noise ratio (*CNR*) where,

$$CNR = \frac{P_o}{\overline{n^2(t)}} \quad (3.49)$$

So far the above analysis is general and can be applied to both trapezoidal or triangular PSM. However, when considering the trapezoidal PSM, a formula for the output *SNR* in terms of the *CNR* can be driven if equations 3.34 and 3.49 are substituted into 3.48. This leads to;

$$SNR = \left(m \frac{T_s}{t_{ro}} \right)^2 \frac{B\tau}{B_n T_o} \frac{CNR}{1 - \frac{2t_{ro}}{3T} \xi(m)} \overline{v_m^2(t)} \quad (3.50)$$

If triangular PSM is assumed, a similar formula can be driven when substituting equations 3.38 and 3.49 into 3.48, which gives;

$$SNR = 3 \left(m \frac{T_s}{t_{ro}} \right)^2 \frac{B\tau}{B_n t_{ro}} \frac{CNR}{\xi(m)} \overline{v_m^2(t)} \quad (3.51)$$

The above equations show that the relation between the input *CNR* and the output *SNR* is linear for both the trapezoidal and the triangular PSMs. They also show that the

output SNR is proportional to the square of the modulation index and to the square of the ratio between the time shift and unmodulated rise time. Both have a value less than unity.

3.7 System implementation and results

A practical verification for the PSM system has been undertaken using a purpose built low frequency hardware model of both the receiver and transmitter. The transmitter has been constructed according to the principles discussed earlier in this chapter, whereas the receiver has been constructed according to the proposal in Fig. 3.6. Throughout the development of this work, only trapezoidal PSM has been considered as it is easier to generate and is the more general waveform. The triangular PSM can be driven from the trapezoidal PSM as special case when $T = 0$. Furthermore, the proposed receiver design is applicable for both types of PSM signal, and shows the same performance. A detailed circuit description is given in the next section.

3.7.1 PSM transmitter

The circuit diagram of the PSM modulator is shown in Fig. 3.20. A simple operational amplifier based VCCS is used to provide a charging current of about 2 mA. The DC voltage at V1 (see Fig. 3.20) controls the bias of transistor Q1 and Q2, and the current through Q2 is used as a current source. Any fluctuation in V1 will modulate the current through Q2.

The charging current is passed through a capacitor C , which has been chosen to provide a PSM with slope of $1.33\text{V}/\mu\text{s}$. The FET transistor Q3 is used as a switch to discharge

the capacitor C . The voltage across the capacitor is the required PSM, which is passed through a buffer, and voltage clipped by the diode D1. An external pulse generator (frequency = 45 kHz) is used as a switching signal, as shown in Fig. 3.20. The transmitting media is modelled by a simple RC circuit of bandwidth $B = 870$ kHz. The PSM system is designed to operate with the following specifications; carrier frequency = 45 kHz, $t_{ro} = 6.5$ μ sec, $T_o = 14.6$ msec, $T_s = 3.1$ msec, $B_n = 2.4$ kHz, and $A = 9$ Volts.

3.7.2 PSM receiver

The PSM receiver is based around the diagram shown in Fig. 3. 6 . The circuit diagram of the PSM receiver is shown in Fig 3.21, in which a simple RC circuit followed by an operational amplifier based adder circuit is used to enable the introduction of noise to the PSM pulses. This will simulate the electrical transmission of the PSM signal. The sampling pulses are generated from the unmodulated edge of the PSM waveform using two monostables. A dual monostable TTL integrated circuit (IC1) is used as a clock pulses recoverer to provide the sampling pulses, and a simple FET (Q4) circuit is used as a sampler. The sampler output is then connected to an operational amplifier based low pass filter, see Fig. 3.21.

3.7.3 experimental results

During the experimental investigation, a number of tests were carried out to determine the system performance and verify the theory derived early in this chapter. As indicated, the PSM system were designed with the following specification; carrier frequency 45 kHz, $t_{ro} = 6.5$ μ sec, $T_o = 14.6$ msec, $T_s = 3.1$ msec, $B_n = 2.4$ kHz, and $A = 9$ Volts. A number of photographs of the waveforms at different points on both the receiver and transmitter has been taken and are displayed in Figs.3.22 and 3.23. Figure 3.22 compares the unmodulated and modulated PSM waveforms and show the modulated

PSM waveform at almost maximum possible modulation index. Figure 3.23 shows the waveforms at the receiver side; the received PSM, PAM and the detected signal.

A linearity test has been performed by measuring the characteristics of the modulator, i.e. the relation between the pulse slope (in Volt/ μ sec) and the level of the modulating signal (Volts). The practical results together with the results of linear curve fitting of the practical results are displayed in Fig. 3.24. The curve fitting results have been included to highlight the degree of linearity the modulator achieved over a very wide range of input signal levels. These results have been used to choose the best free running operating point (the DC voltage that should be added to the modulating signal) of the PSM modulator, which is normally in the middle of the linear dynamic range. The dynamic range of the receiver has been measured and is displayed in Fig. 3.25. This figure shows the relationship between the modulation index and the detected signal level.

The noise performance of the PSM was measured using a 1 kHz single tone modulating signal. The measurement has been carried out using true RMS voltmeters in measuring both the noise and the signal level. The noise power was measured when the modulation was absent, and the signal power was measured when the noise was off. The measured results obtained for the output SNR against the CNR for two values of $B\tau$ ($B\tau = 1$ and 2), and at different modulation indices ($m = 0.1, 0.35$ and 0.5). The measured results, together with the predicted results obtained using equation 3.50, are displayed in Fig. 3.26 - 3.28. The noise performance of the AM system is included in these figures in order to compare the noise performance of the PSM system with other standard systems. It can be seen that output SNR increases with the modulation index and $B\tau$, when $B\tau$ is doubled the SNR improves by 3 dB. Figures 3.26 - 3.27 also show that for the same modulation conditions, PSM is clearly superior to the AM modulation scheme. However comparison assessment has been shown for the noise performance of the PSM system under different values of $B\tau$ and m in Fig. 3.29. When the modulation

index increases the SNR increases, as expected. Furthermore, the improvement factor IF , given by SNR minus CNR , expressed in dB for both PSM and AM as a function of the modulation index m , is shown in Fig. 3.30. At 50% modulation index PSM is superior to AM by 8dB. When m increases to 80%, PSM shows 12 dB superiority over AM.

From the above results, it can be concluded that a novel PSM receiver design has been reported and constructed using low frequency hardware. The practical results show that PSM detection by sampling the input signal at the rising edge is a successful method of demodulation which eliminates the differentiator circuit at the input stages of the receiver. It has also been shown that it is possible to eliminate the need for waveform slicing which is usually applied to improve the noise performance. The novel detection technique offers simplicity and improved performance compared to classical receiver design.

Further, a new SNR formula for PSM has been presented for the first time enabling users to predict the system noise performance. Experimental confirmation for the theoretical noise investigation has been shown at different values of modulation indices and transmission bandwidths.

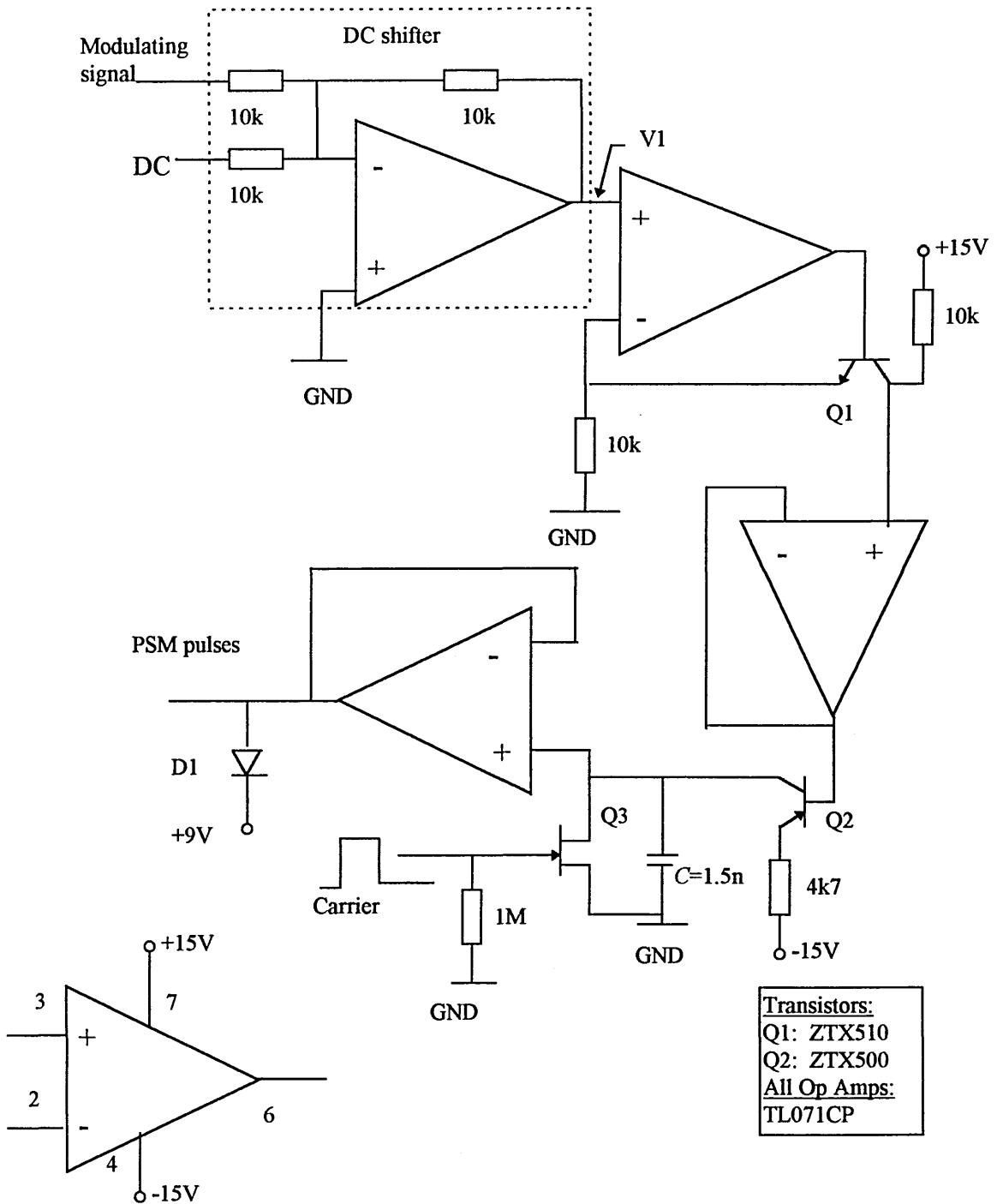


Fig. 3. 20 Circuit diagram of PSM transmitter.

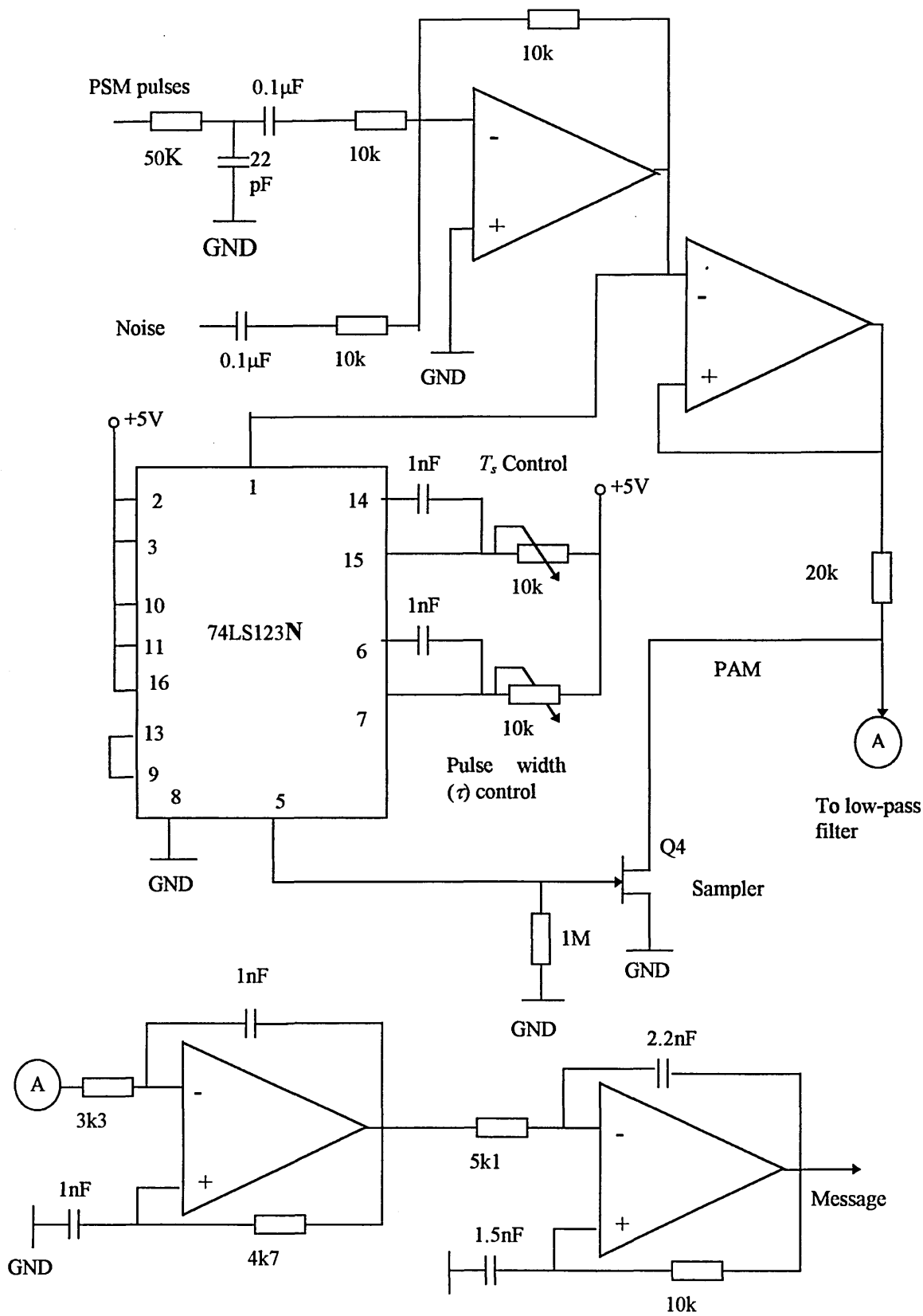
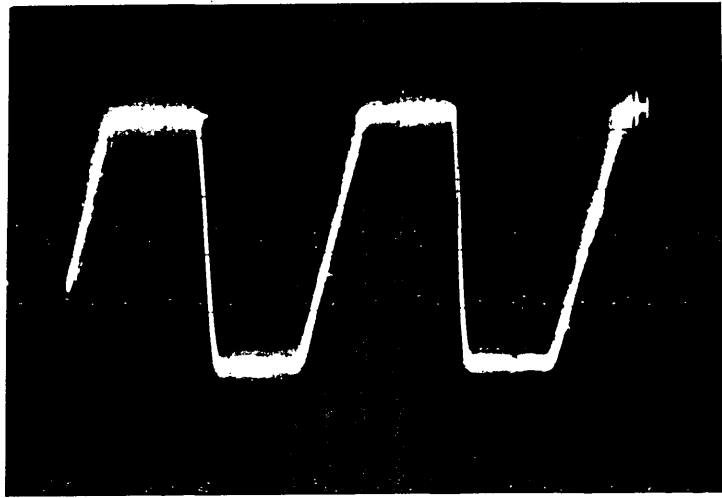
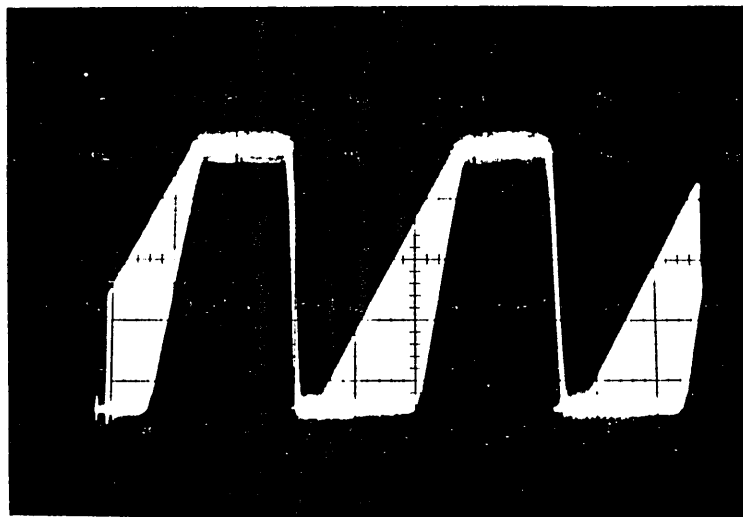


Fig. 3.21 Circuit diagram of PSM receiver (all op. amps are TL071CP).

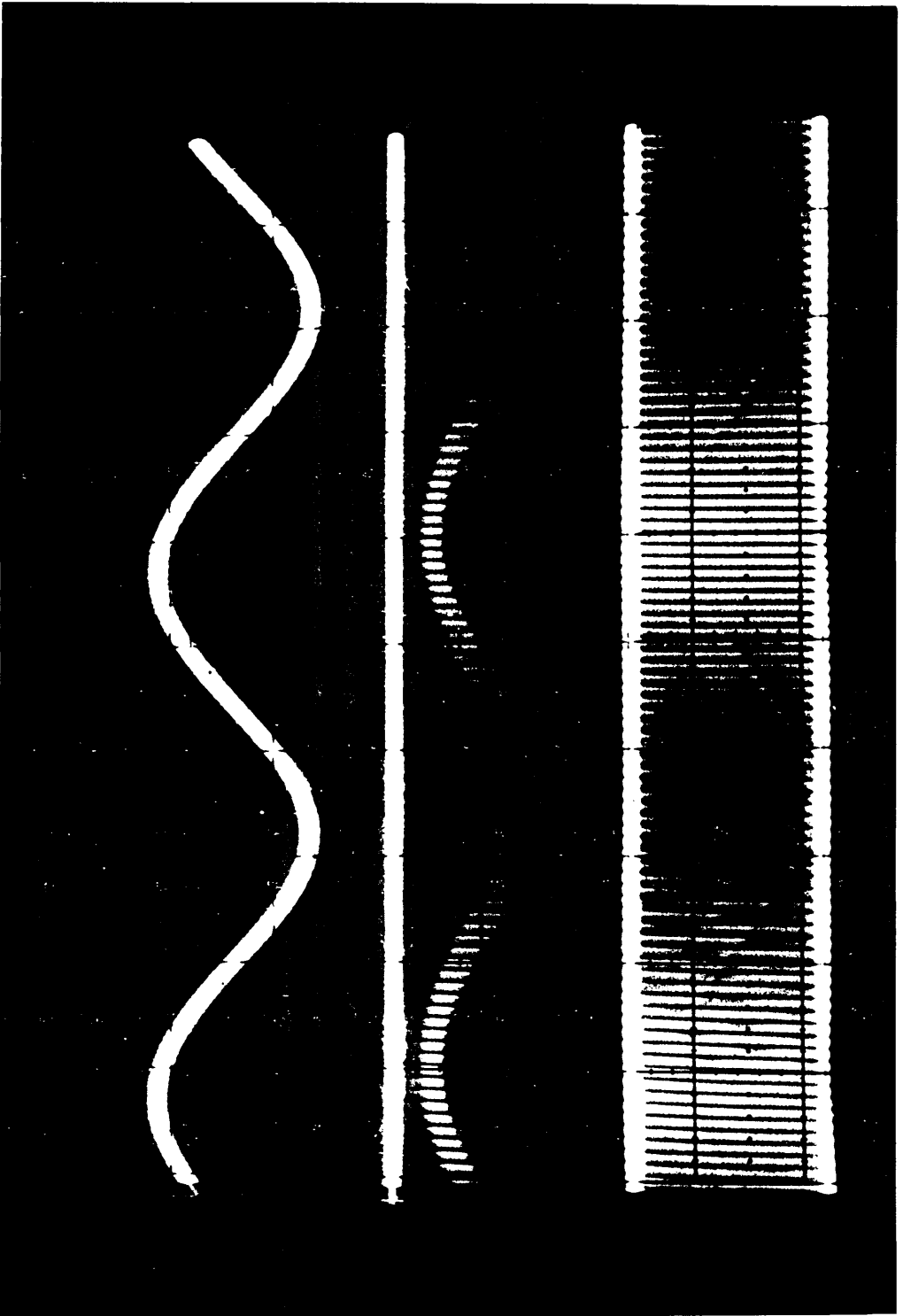


(a)



(b)

Fig. 3.22 PSM waveforms: (a) unmodulated and (b) PSM waveform (scale, 2V/div., 5 msec/div.)



(a) (Scale 5V/div)

(b) (scale 5V/div)

(c) (scale 0.5V/div)

Fig. 3.23 Waveforms at the PSM receiver: (a) PSM (b) PAM and (c) detected signal (Scale 200 msec/div)

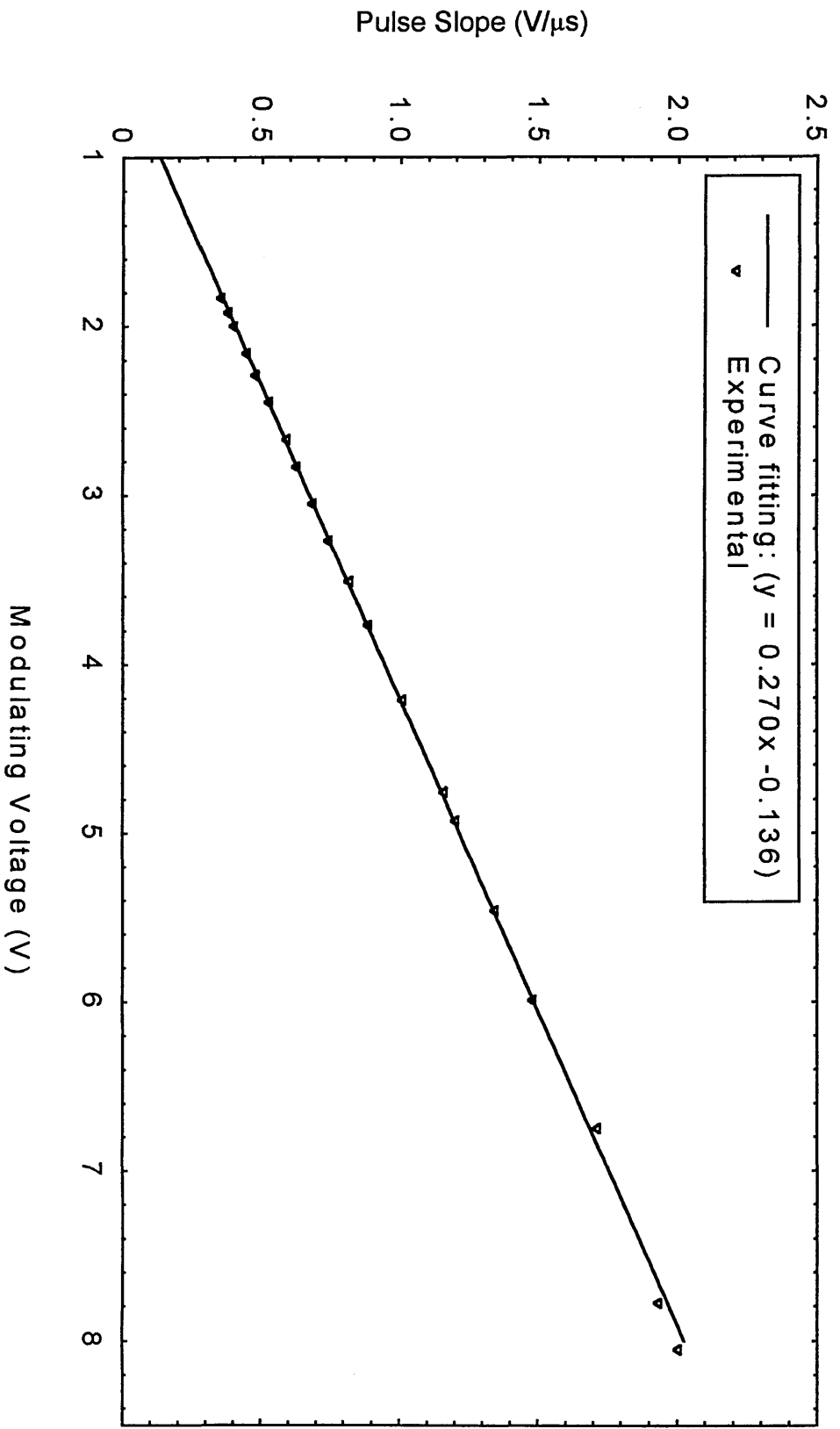


Fig. 3.24 Characteristics of the PSM modulator.

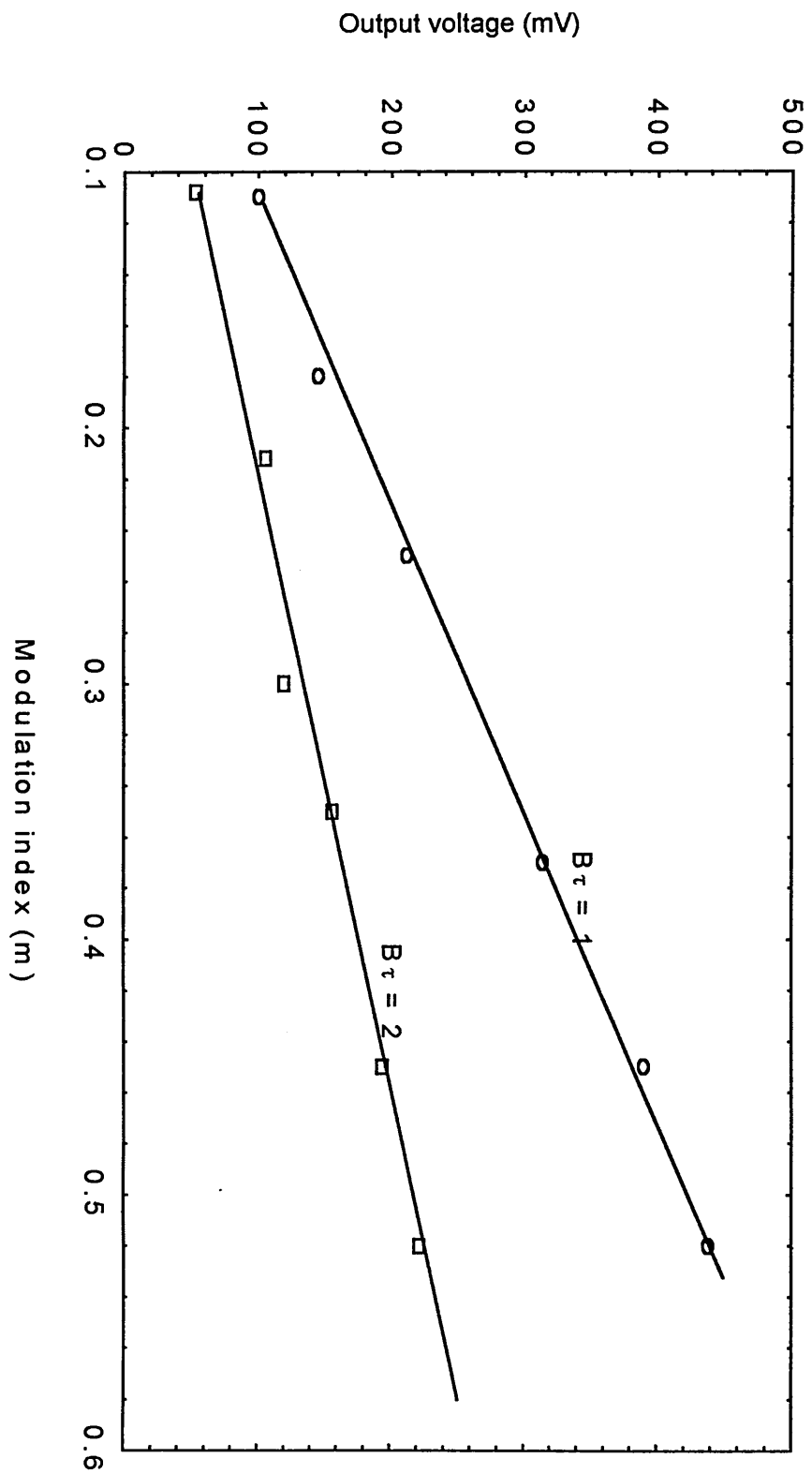


Fig. 3.25 Characteristic of PSM receiver.

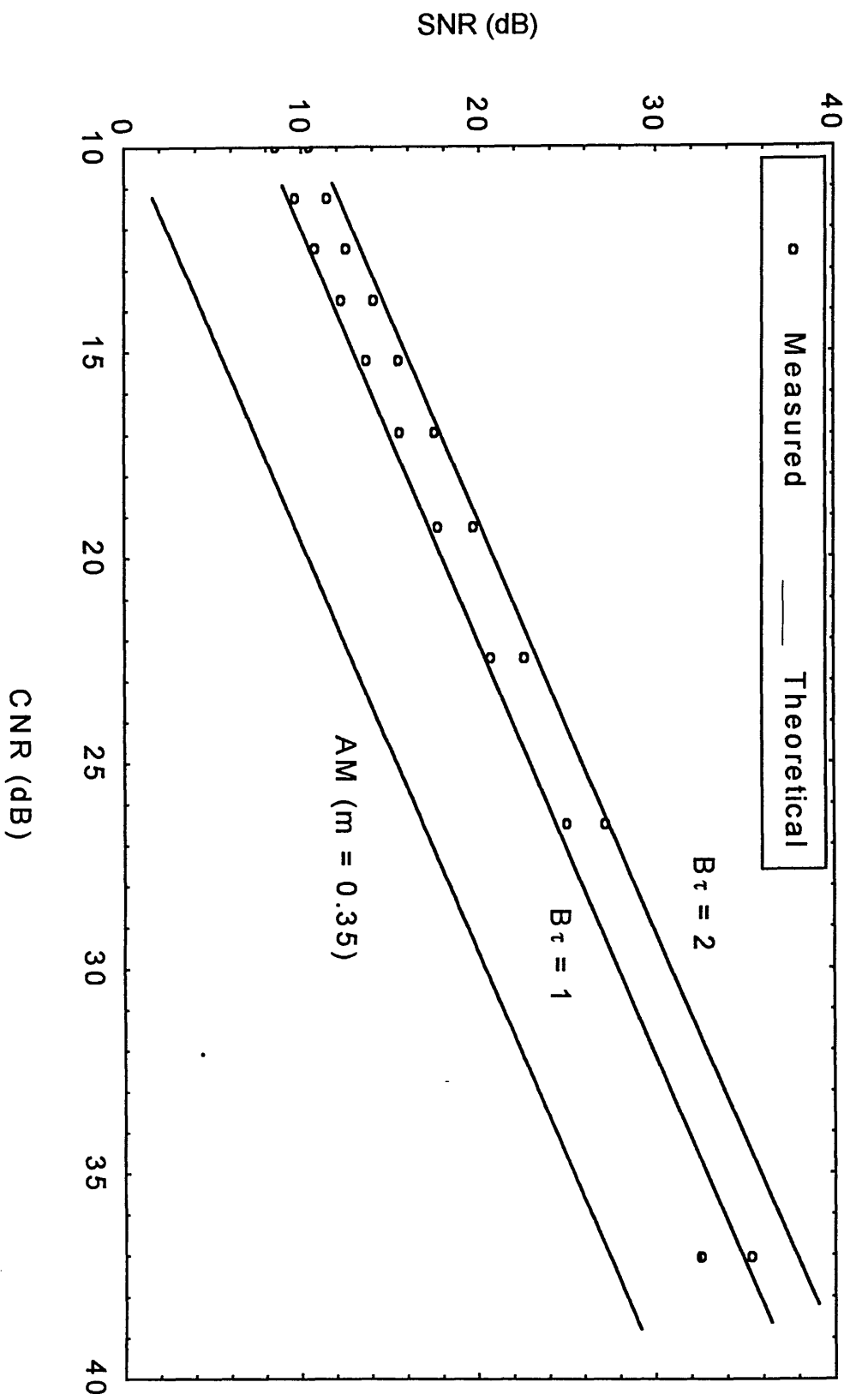


Fig. 3.26 Noise performance of PSM system ($m=0.1$).

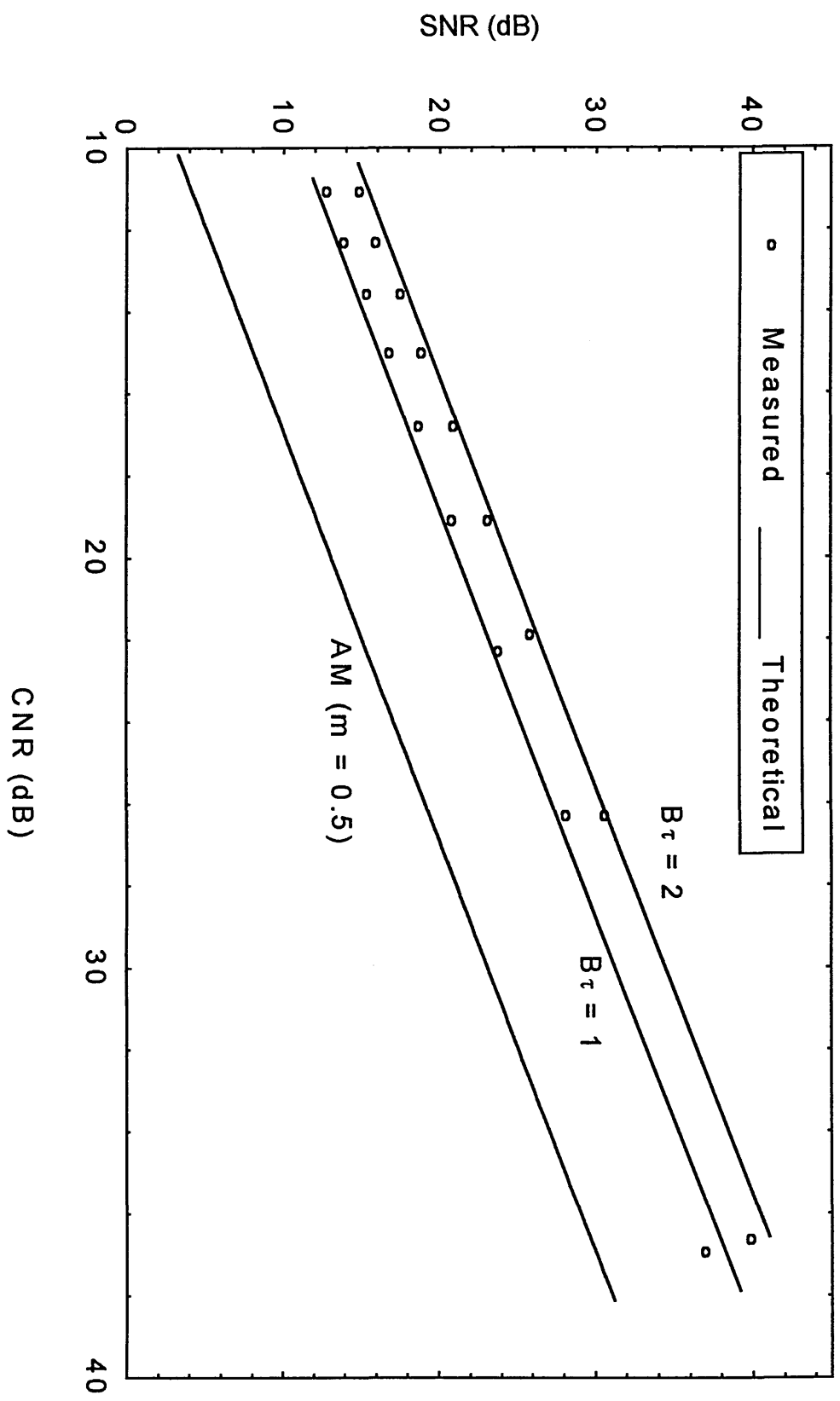


Fig. 3.27 Noise performance of PSM system ($m=0.35$).

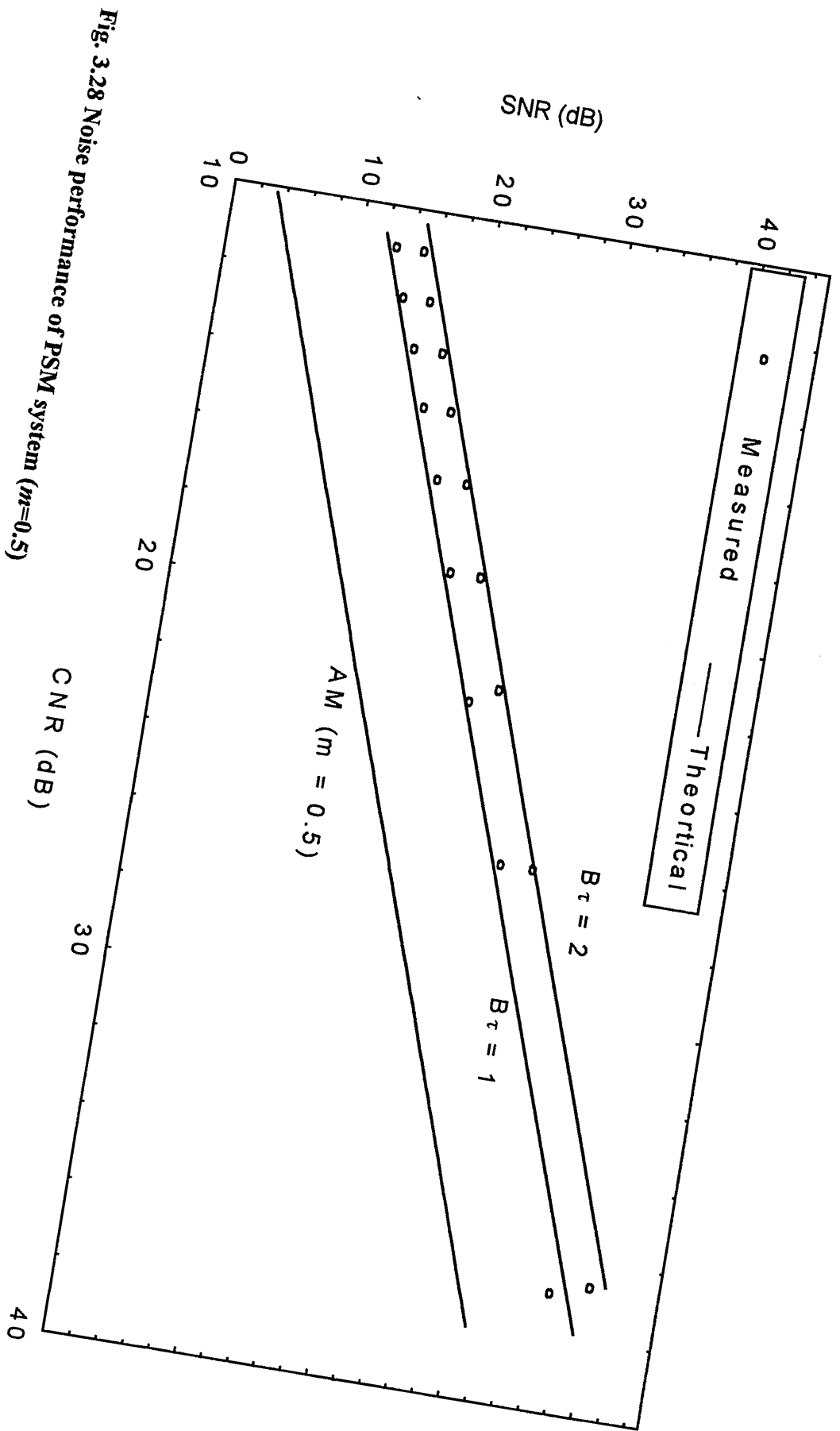


Fig. 3.28 Noise performance of PSM system ($m=0.5$)

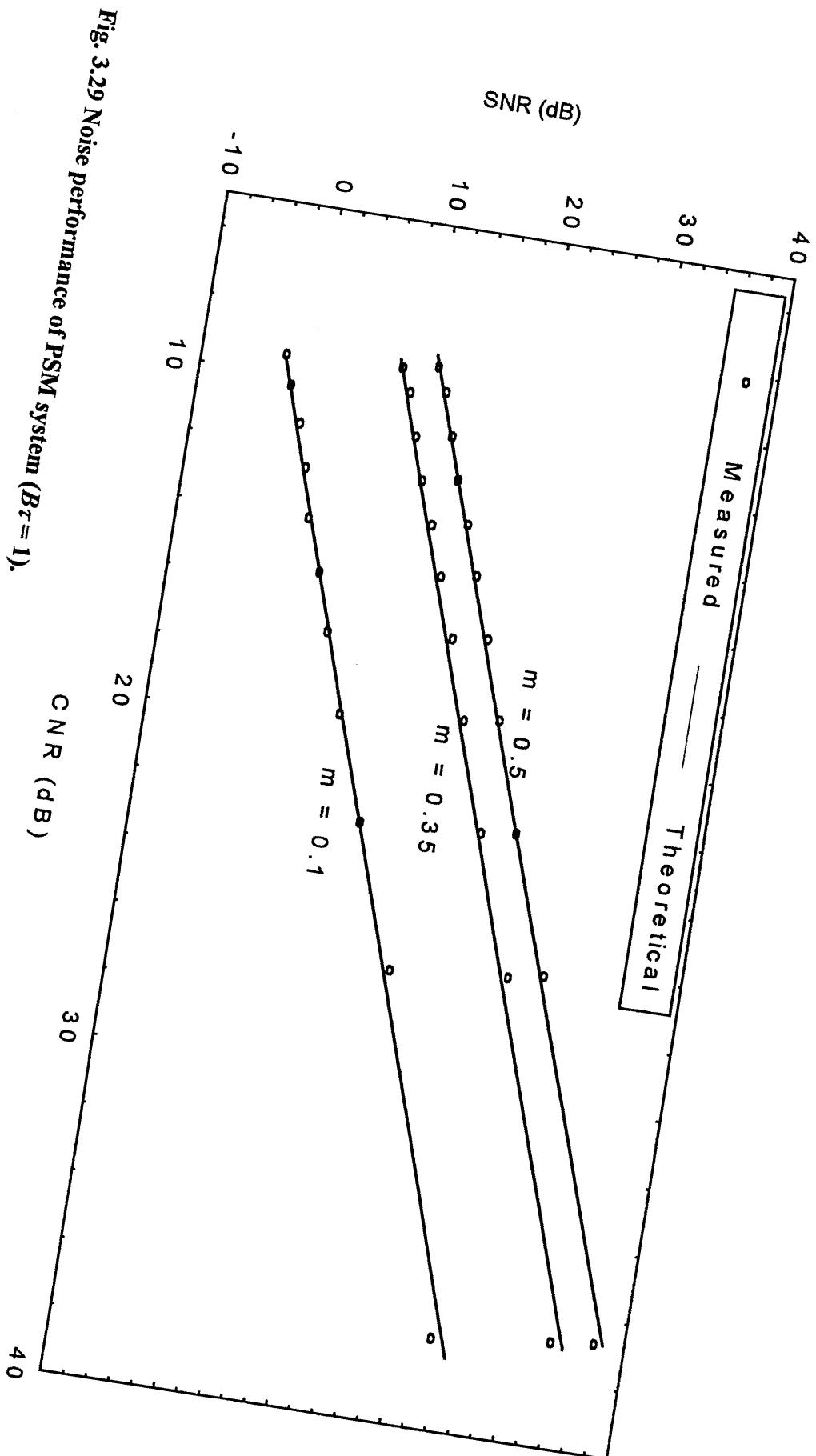


Fig. 3.29 Noise performance of PSM system ($B_T = 1$).

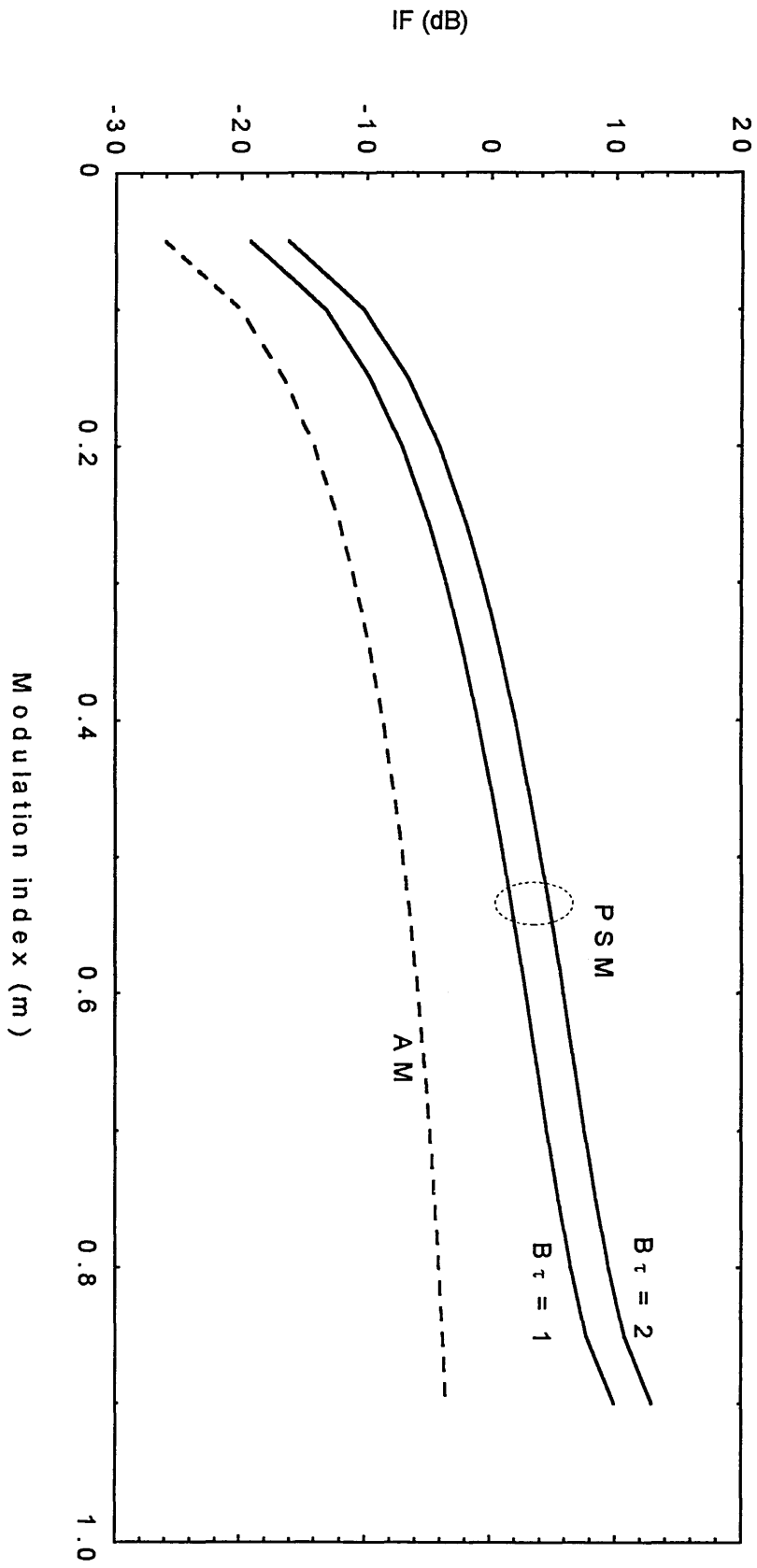


Fig 3.30 Improvement factors for PSM and AM schemes.

Chapter Four

Multiplexing and Compound Modulation Techniques

4.1 Introduction

The benefits of using PTM techniques in optical transmission are that their performance is less affected by the non-linearity associated with the light source, they require less bandwidth, and their hardware implementation is simple and low cost [1]. PTM modulation schemes are attractive for many applications where transmission of wideband signals such as video, audio and high speed data is essential. In order to achieve the required performance a compromise between different factors governing the system implementation and performance is inevitable. Up to now most of the PTM schemes reported are not multiplexed and are based on a single channel or used for transmitting signals already multiplexed.

PTM techniques have the disadvantage that multiplexing is not easy [31, 32], although, basically, both time division multiplexing (TDM) and frequency division multiplexing (FDM) can be implemented within the framework of PTM modulated optical communication systems. TDM is a more suitable multiplexing technique for PTMs because of their digital nature. Other multiplexing techniques such as wavelength division multiplexing and subcarrier multiplexing are also possible [31]. However, there

exists an alternative multiplexing approach based on combining different PTM schemes which overcomes some of the problems in multiplexing PTMs [31, 32]. The scheme is known as hybrid (or compound) PTM and is accomplished by a sequence of cascaded PTM modules, where the modulated PTM of the first module is used as a reference signal for the second modulator. Very little work has been undertaken on pulse time multiplexing, especially on CPTM techniques. In this chapter, different multiplexing techniques for PTMs are considered, with special emphasis on the CPTM techniques.

4.2 Multiplexing techniques for optical fibre systems

Multichannel wideband signal transmission is essential in today's broadband services over optical fibres systems. It is possible to convey these multichannel signals by multiplexing in the time or frequency domain prior to intensity modulation of the optical source. Hence PTM schemes may be extended to multichannel operation by TDM, FDM, WDM, and compound modulation techniques. In this section some of the possible multiplexing techniques are discussed.

4.2.1 time division multiplexing

PTM techniques may be extended to multichannel systems by TDM using narrow pulses from multiple modulators under the control of a common clock as shown in Fig. 4.1. Pulses from individual channels are interleaved and transmitted sequentially, thus enhancing the bandwidth utilisation of a single fibre link [81, 82]. Channel assignment in this method is rigid, and it seems that it is more suitable method for PTMs, because of their digital nature. The major problem with this technique is the difficulty to accommodate channels of different clock rates, and channels with variable clock frequency. Therefore, SWFM, PFM, PIM, and PIWM can not be implemented in

TDM, because they do not have a fixed clock rate. However, when other PTM schemes such as PPM or PWM are implemented, transmission of the clock is essential to maintain synchronisation at the demultiplexing end which complicates the system and requires the implementation of clock recovery techniques. This may be the reason why no work has been done on PPM and PWM.

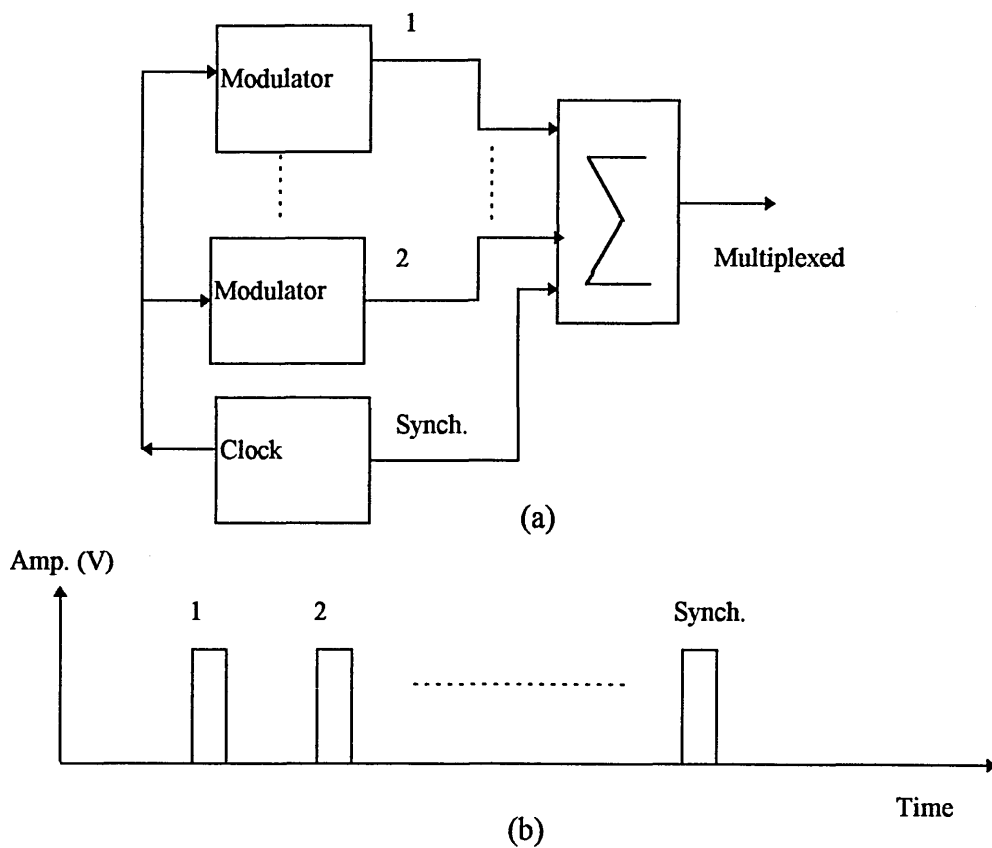


Fig. 4.1 Synchronous TDM: (a) possible block diagram and (b) timing diagram.

4.2.2 frequency division multiplexing

In this technique, different PTM channels are modulated at different subcarrier frequencies, as shown in Fig. 4.2. In theory, FDM is suitable for wideband or

narrowband signals, however, in practice there are a number of limitations to this technique. It is necessary to achieve a high degree of system linearity over a very wide bandwidth in order to reduce cross-talk between channels. In addition, it is necessary to leave adequate frequency separation gaps between channels to avoid spectrum overlapping, and hence non-linear distortion. Consequently, the overall possible number of multiplexed channels will be limited.

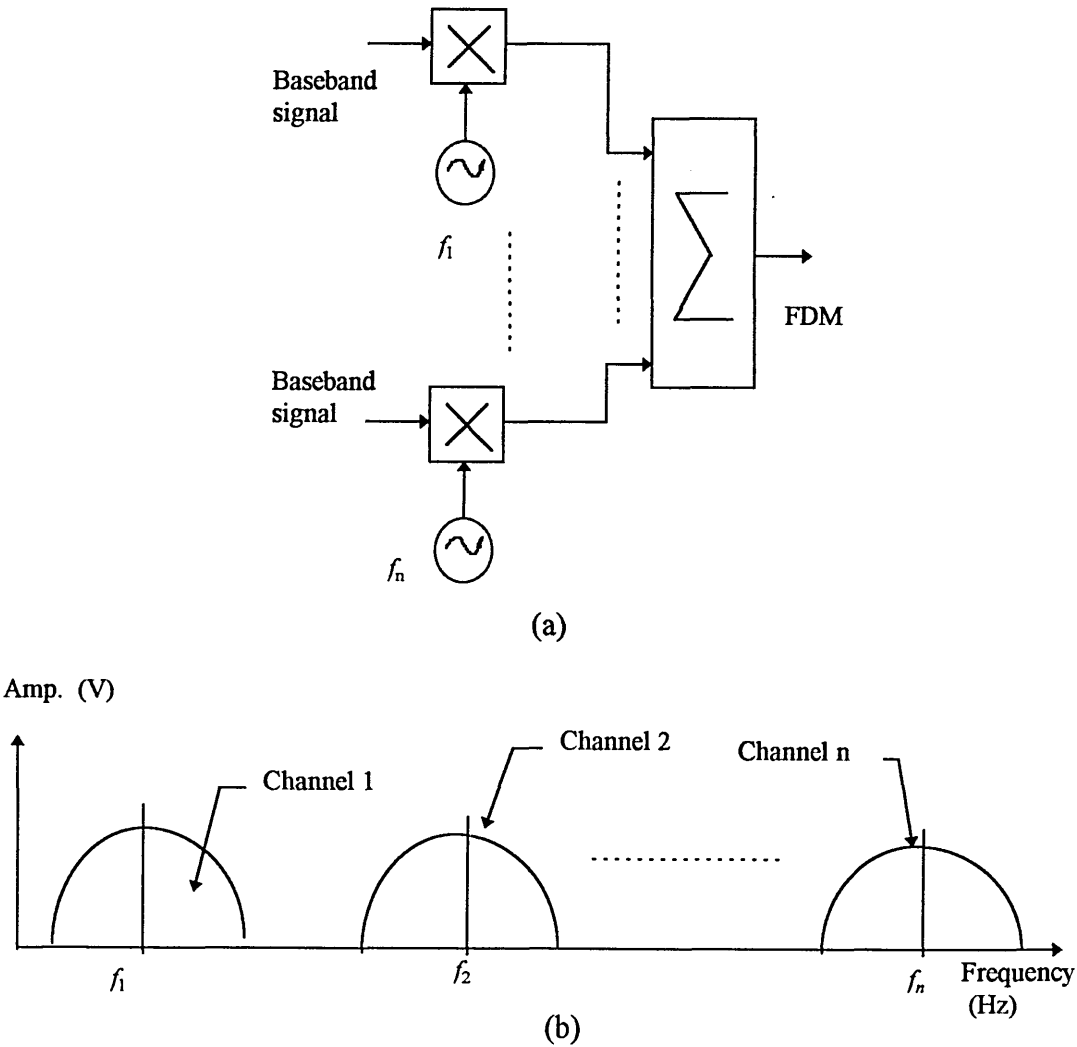


Fig. 4.2 Frequency division multiplexing: (a) block diagram and (b) frequency spectrum.

At the receiving end, channel demultiplexing could be achieved by linear wideband band-pass filters, with a sharp cut off. If coherent demultiplexing is employed, it is essential to employ carrier synchronisation to eliminate frequency and phase errors that occur during transmission and regeneration of the carrier and sub-carrier. Therefore, it could be more useful to multiplex the baseband channels using FDM technique first, afterwards a PTM scheme could be employed to intensity modulate an optical source. This technique has the advantage of multichannel services, and the features of the PTMs [83].

4.2.3 wavelength division multiplexing

In this technique, it is possible to utilise a number of optical sources, each operating at a different wavelength on a single fibre link. Although in spectral terms optical wave division multiplexing (WDM) is analogous to electrical FDM, it has the distinction that each channel effectively has access to the intensity modulated fibre bandwidth. In WDM, the separation and extraction of the multiplexed signal is performed with optical filters [84].

Wavelength division multiplexing technique can be accomplished by using wavelength filtering technique, where, identical LEDs are followed by a number of filters centred at different wavelengths which are used to slice the spectrum for different channels before they are combined together to be transmitted in a single fibre. At the receiving end filters centred at different wavelength are used to recover different channels, as shown in Fig 4.3. The restriction of this method is the power budget for each channel. This is because of the slicing of the LED spectrum which means that the available power of each channel is only a fraction of total LED power [85]. Consequently, it is necessary

to use very sensitive receiver in order to have good signal performance. This restricts the use of this method to low bandwidth systems only.

This technique overcomes certain power budgeting restrictions associated with TDM. When the transmission rate over a particular optical link is doubled using TDM a further 3 to 6 dB of optical power is generally needed at the receiver. However, in the case of WDM, additional losses are incurred by the incorporation of multiplexers and demultiplexers.

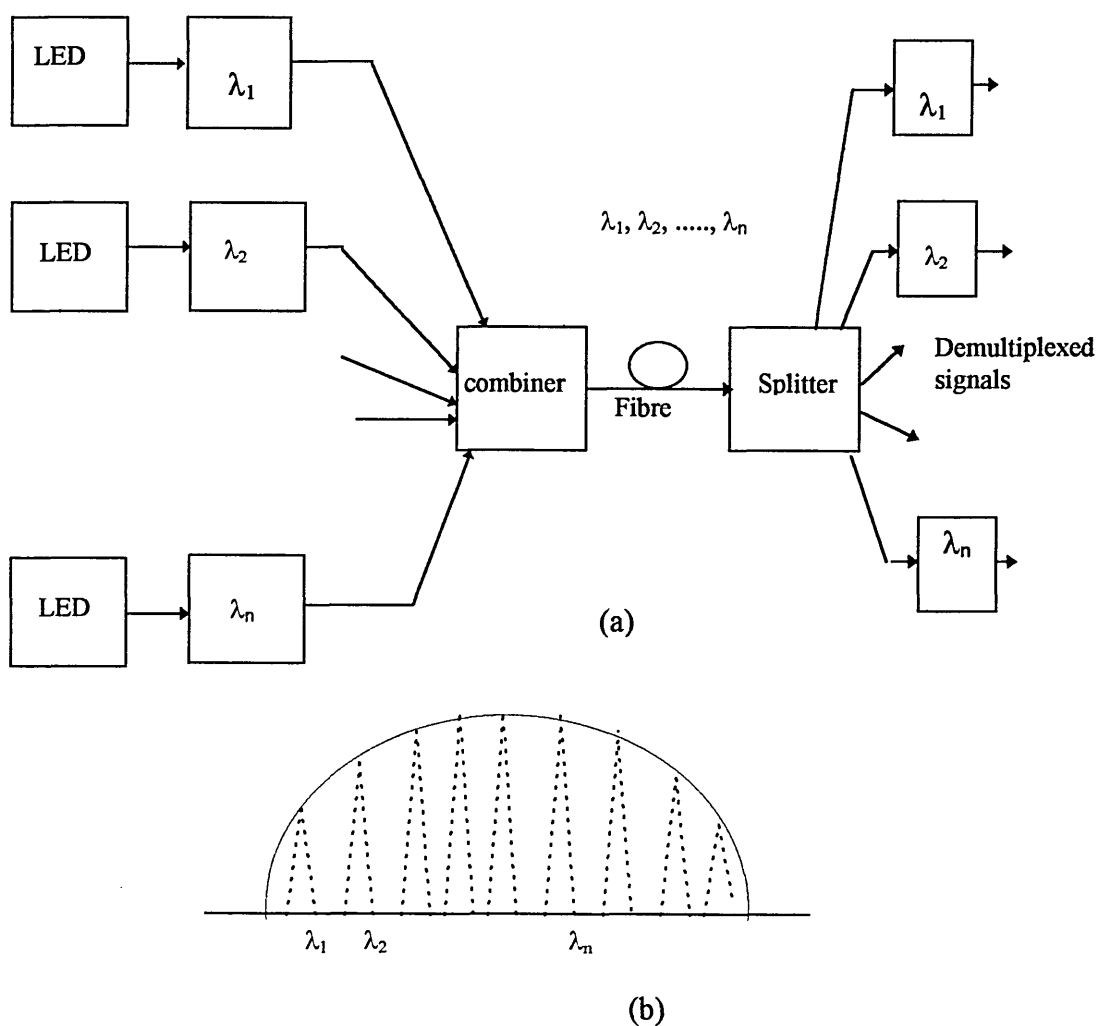


Fig. 4.3 WDM using filtering devices: (a) system block diagram and (b) LED spectrum.

4.2.4 subcarrier multiplexing

This method has been widely used for multichannel wideband signal transmission for video signals. In this technique, each channel is modulated onto a different subcarrier using frequency or amplitude modulation (FM or AM). The combined signal is then used to intensity modulate an optical source [86]. At the receiving side, the optical signal is first converted to an electrical signal using an optical receiver. The electrical signal is then demultiplexed by down conversion and filtering, Fig. 4.4.

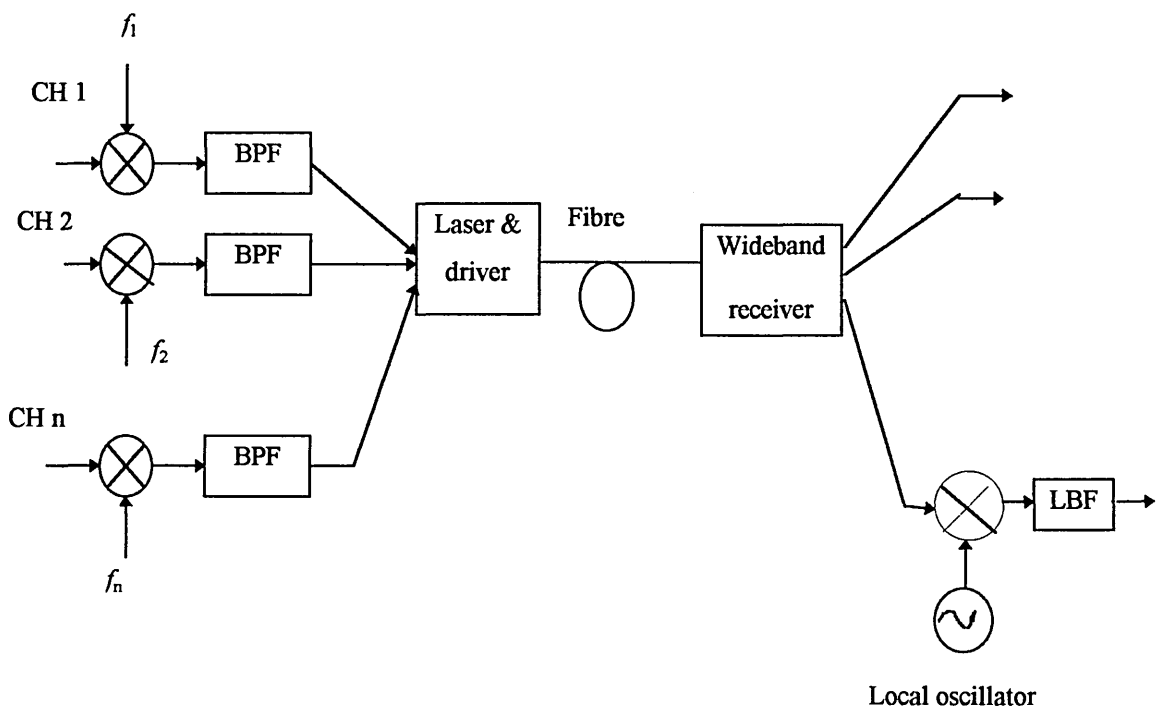


Fig. 4.4 Subcarrier multiplexing.

There are two important factors which should be considered when designing a subcarrier system the system linearity and noise performance. The noise performance of

the system determines the number of channels that can be multiplexed as well as the overall performance of the system. However the system non-linearity is determined by the optical source, and will introduce inter modulation distortion, which will affect the carrier to noise ratio. In general, FM systems are less affected by the non-linearity than AM, and FM systems show better noise performance than AM based systems.

In the above sections three general multiplexing techniques have been discussed. These techniques can be applied to PTM signals. However, despite the digital nature of the PTMs, TDM is the only appropriate method for multiplexing isochronous PTMs, such as PWM and PPM, as they have a fixed frame timing interval. Clock synchronisation, at the receiving and transmitting ends, is essential for both signal generation and detection. Anisochronous PTMs such as PIM, PFM SWFM are problematic to multiplex in the time domain because of their variable timing interval. In this case, FDM may be employed when signals are band pass filtered before multiplexing, but FDM can place several demands on the linearity of the optical transmission system if cross-talk between the channels is to be avoided. When PTM techniques are used, the problem of achieving adequate linearity rests principally with the modulator and demodulator [86]. As a result, the usual method which used to transmit several signals by PTMs is that the frequency multiplexing signals are converted into a PTM.

An alternative approach which solves the problem associated with PTMs multiplexing is recently developed. This method is called compound (some times hybrid) pulse time modulation (CPTM) techniques. which is discussed in more detail in the following sections.

4.2.5 multiplexed isochronous PTM

Multiplexed isochronous pulse time modulation (MIPTM) is different from the systems mentioned above as it is based on multiplexing two PPMs without the need for synchronisation. This system has been recently developed to transmit two multiplexed video signals on optical fibre [87]. The modulator block diagram is shown in Fig. 4.5, in which the rising edge and the falling edge of the clock are used to initiate two ramp generators. Each ramp is compared with one level shifted modulating signal (channel) using two independent voltages. The output of each comparator is a PPM signal which will be used to reset the corresponding ramp generator. These two PPMs are time synchronised as they are driven from the same clock. The two PPMs are used to set and reset a multivibrator which produces the MIPTM signal (Fig. 4.6).

Time division multiplexing for the two PPM signals can also be achieved by passing the PPMs through an OR gate (Fig. 4.5, the dotted lines). Although this kind of multiplexing uses narrow pulse width which makes it very suitable when a laser is used as a light source, it has the drawback of poor channel identification. This means that either reference pulses should be transmitted with the multiplexed signal, or the pulse width of one channel should be made different from that for the second channel.

At the receiver side, (see Figs. 4.7 and 4.8 for waveforms) the two messages are separated by an edge separation technique. Each edge is used to initiate a ramp generator and due to position modulation the ramp output will be amplitude modulated. The envelope of the ramp is the derivative of the message signal and the message signal can then be extracted from the ramp using the sample and hold

technique. This method requires synchronisation of the sample and hold pulses with the incoming signal, followed by low pass filtering. Clock recovery and synchronisation circuits are also necessary for proper detection. Alternatively, the messages might be extracted from the envelope of the ramp generators by low pass filtering followed by integration. Since the integration of wideband signals is usually difficult, more signal distortion at the output is expected with this demodulation technique rather than the sample and hold method.

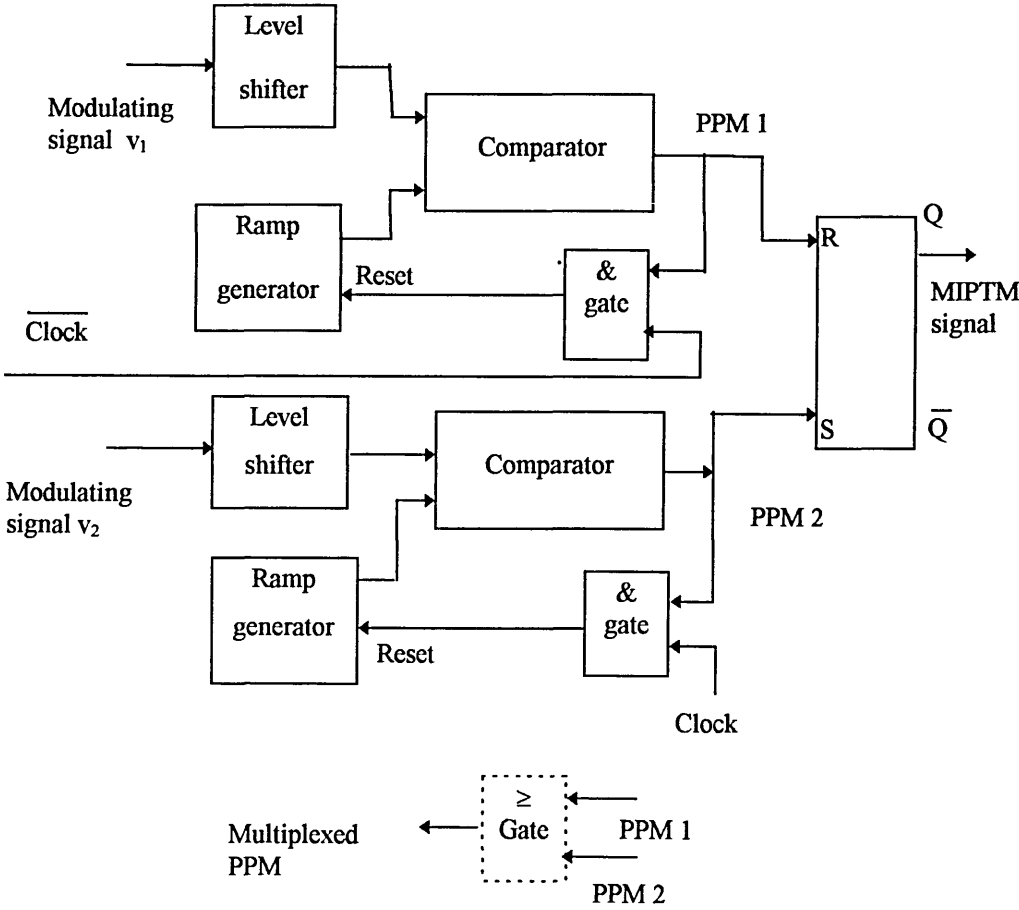


Fig. 4.5 Block diagram of MIPTM system.

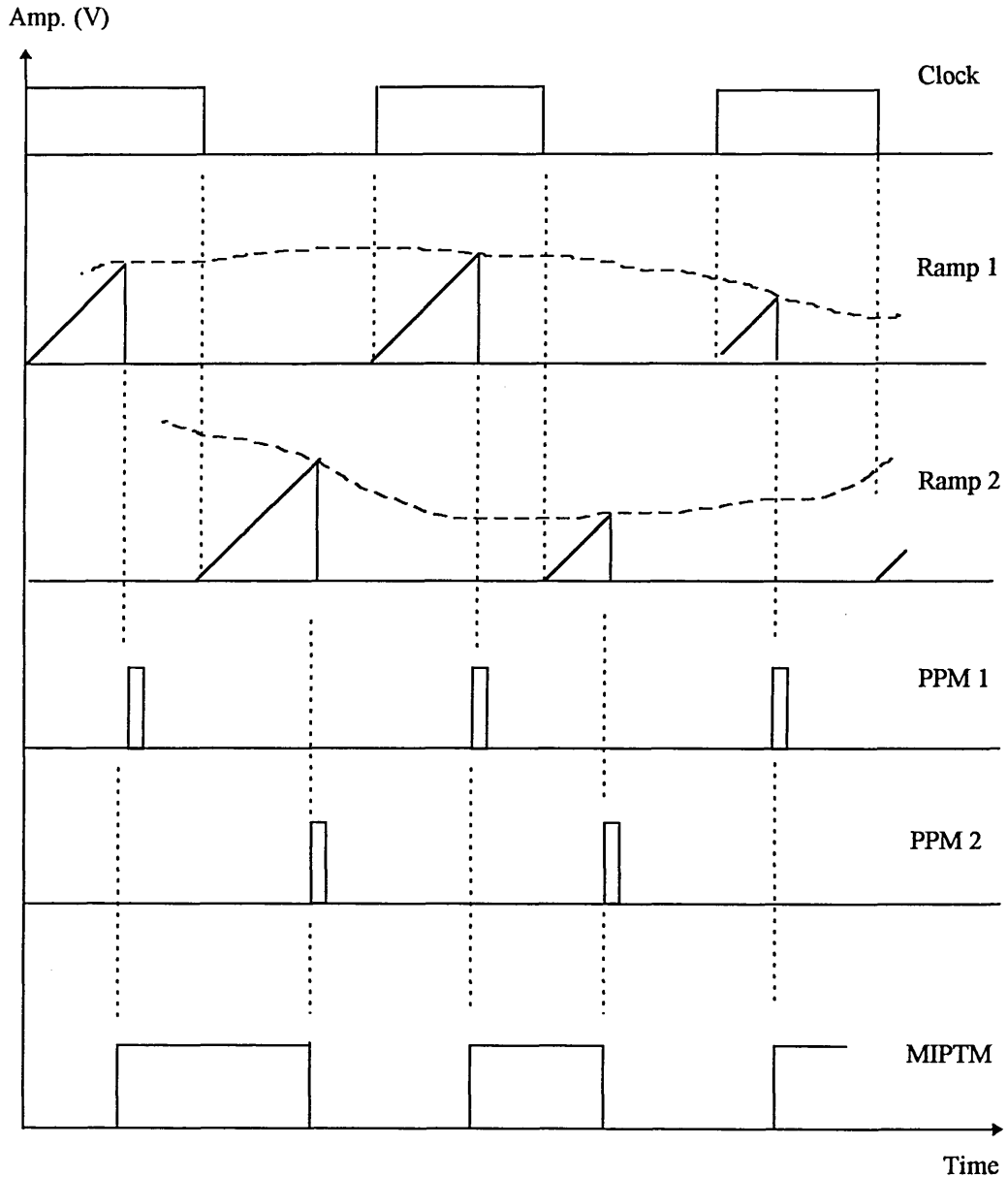


Fig. 4. 6 MIPTM multiplexing waveforms.

The modulation index of each channel can be calculated as the ratio of the pulse deviation of the modulated edge to the maximum available time interval (which is half the period of the clock). Therefore, the modulation index can be given as;

$$m_n = \frac{2\Delta\tau_n}{T} ; n = 1, 2 \text{ (the channel number)} \quad (4.1)$$

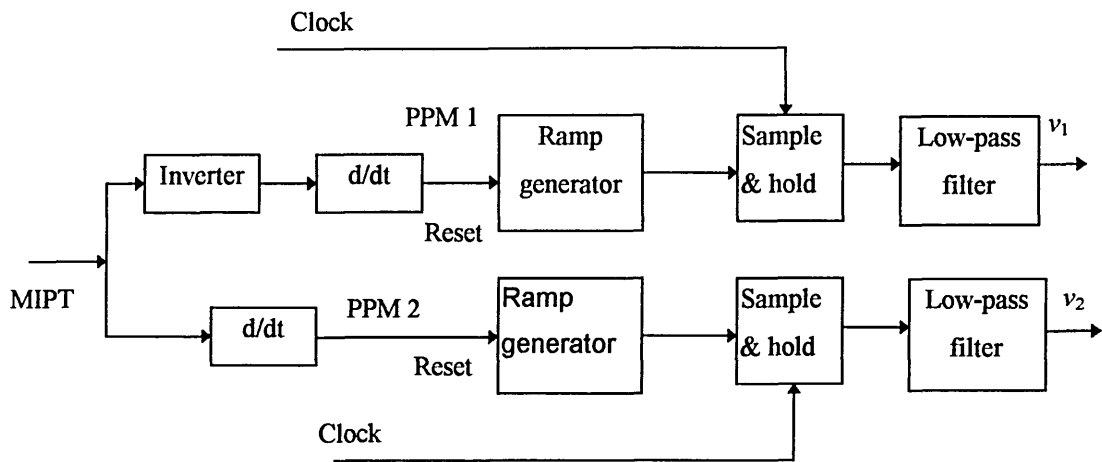


Fig. 4.7 Block diagram of MIPTM receiver.

This system has been used experimentally to transmit two video signal through optical fibre. The results show that this system can provide reasonable cross-talk performance which is in order of -30 dB over a wide range of modulation indices. The non-linear harmonic distortion has also been measured for this system and was in the order of -40 dB over a reasonable range of modulation indices. Very few investigation or measurements have been done on this system. Full characterisation is not available.

However, all the available results indicate that the system can be used to multiplexed wideband signals such as video with reasonable hardware and performance. The main drawback of this system is the requirement of the clock regeneration and synchronisation at the receiving end.

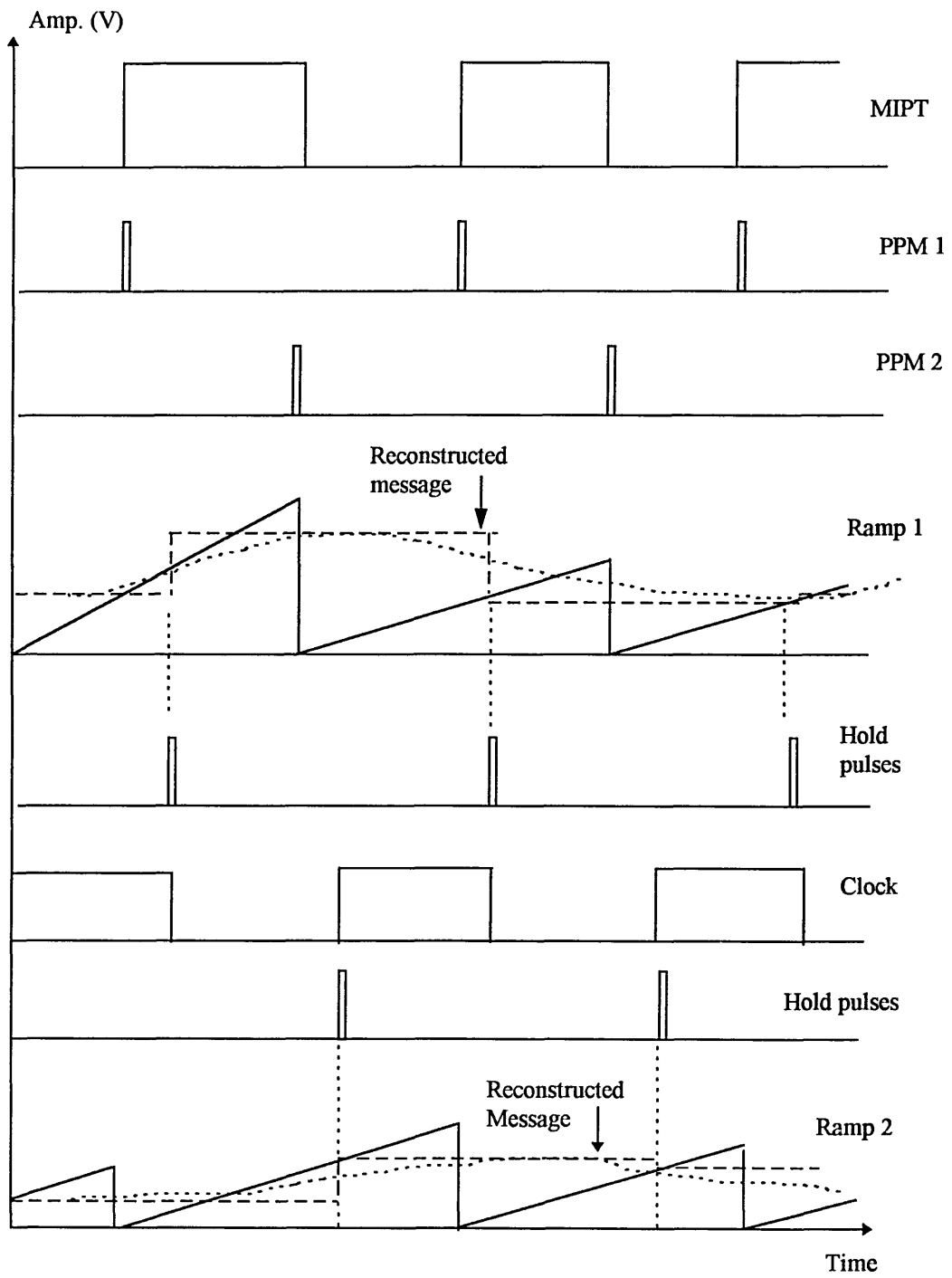


Fig. 4.8 Waveforms of the MIPTM receiver.

4.3 Compound pulse time modulation

Compound pulse time modulation (CPTM) is an alternative approach to TDM and FDM multiplexing schemes. It is based on combining different PTM schemes on the same carrier pulses. CPTM is accomplished by a sequence of cascaded PTM modules, where the modulated PTM signal of the first module is used as a reference signal for the second modulator [31, 32]. Fig. 4.9 lists a number of possible CPTM techniques, not all of these possible schemes have been studied or even tried.

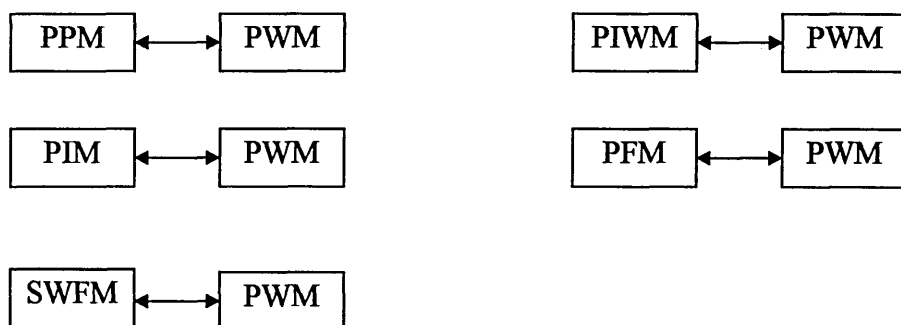


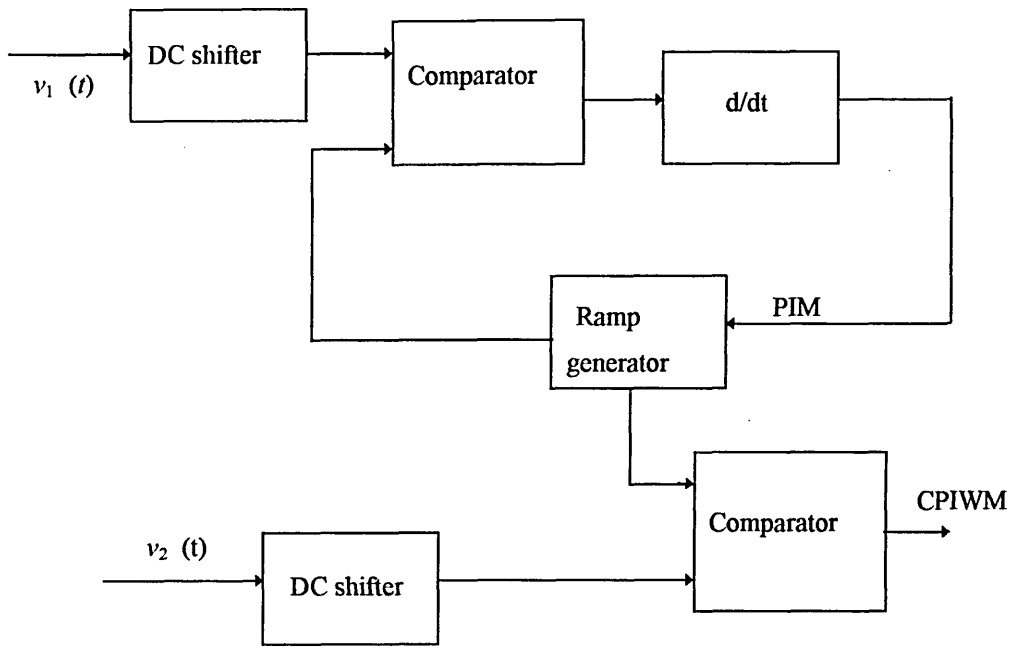
Fig. 4.9 Possible CPTM schemes.

In most CPTM systems, channel synchronisation is not usually necessary making them more attractive than TDM, and also, very effective in utilising transmission bandwidth, as the bandwidth in these systems is approximately equal to the bandwidth of a single channel PTM. Further, using the CPTM technique each channel can be multiplexed and demultiplexed without the need for modulating or demodulating the other channel. This results in very little cross-talk when compared with TDM or FDM, and means that the cross-talk in CPTMs is very low compared with TDM or FDM [31, 32]. Recently,

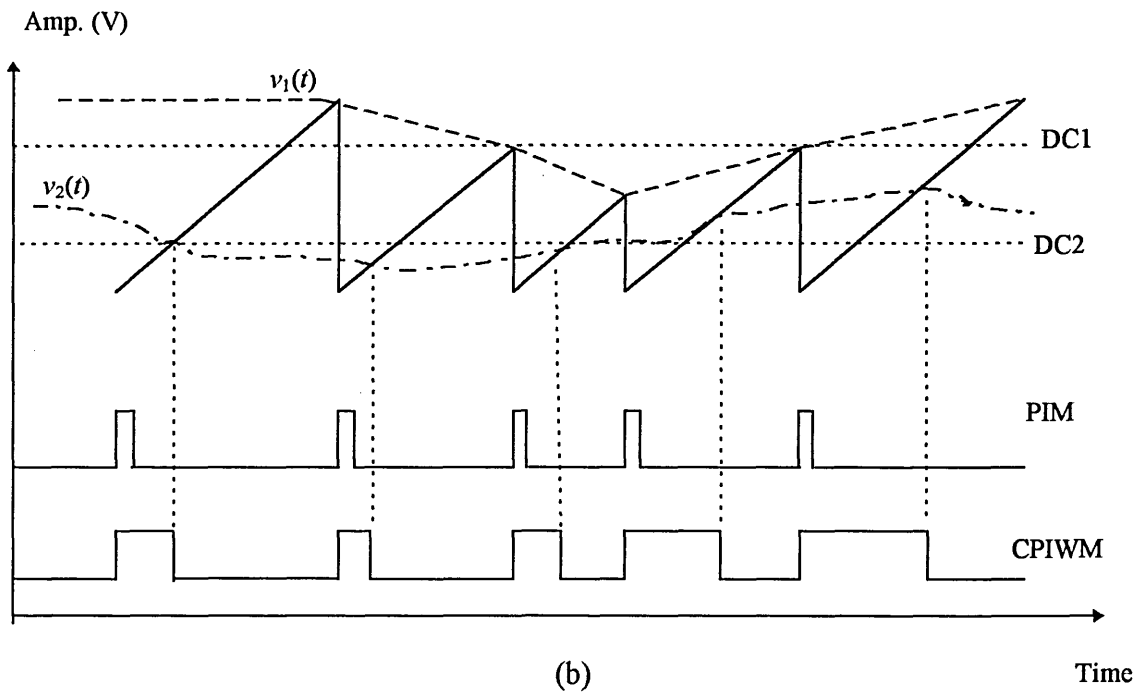
several successful attempts have been made to develop CPTM schemes for transmission of video and data signals; such as the compound pulse interval and width modulation (CPIWM) [88], compound pulse frequency and width modulation (CPFWM) [32]. However, despite the fact that these CPTM schemes have been developed and implemented, very little work has been reported on the theory of these techniques. In this section we will be looking at CPTM from the point of view of modulation, demodulation, spectral characterisation and system performance. The more detailed analysis of the compound pulse frequency and width modulation technique will be considered later in next chapters.

4.3.1 compound pulse interval and width modulation

In this scheme the PIM signal is generated first and is then used as a reference signal for a pulse width modulator. Figure 4.10.a shows a block diagram of the naturally sampled CPIWM transmitter. A comparator and ramp generator are connected as a feedback loop to reset the ramp when equivalence is detected between the DC shifted modulating signal $v_1(t)$, and the ramp. When the modulating signal is absent, the comparator output is a series of uniformly spaced short-duration pulses at a free running frequency determined by both the unmodulated DC level and the ramp slope, Fig. 4.10-b. A pulse generator is used to stretch the PIM pulse train before being input to the ramp generator. The addition of a DC level to the modulating signal is necessary so that there is always headroom for the ramp to sample the most negative input swings. If a sample and hold unit is incorporated and triggered from the comparator output, uniformly sampled PIM generation is possible [88].



(a)



(b)

Fig 4.10 CPIWM transmitter: (a) block diagram and (b) waveforms.

The second modulating signal, $v_2(t)$, is level shifted before being compared to the modulated ramp. The output of this comparator is the desired CPIWM waveform in which both the rising and falling edges convey modulating signals $v_1(t)$ and $v_2(t)$ respectively, see Fig. 4.10-b. The second input channel could be a data signal provided it is first frequency/phase shift modulated before being compared to the modulated ramp signal. CPIWM can be changed to naturally sampled PWM by turning off either of the modulating signals.

CPIWM is anisochronous in nature because the modulated ramp is reset at a point determined by the instantaneous value of the modulating signal and not by the choice of the carrier frequency. The sampling frequency component amplitude is a function of the modulation index and vanishes at a certain values of the modulation index. The minimum permitted ratio of sampling to modulating frequency is 2:1 which is the same as that for PIM [88].

The spectrum of the CPIWM is composed of baseband components and sideband components centred around the sampling signal fundamental and its harmonics. The minimum pulse frequency must be chosen so that the sideband components do not interfere with the baseband component to reduce the non-linear distortion.

The modulation index for the first channel m_1 may be defined as the peak-to-peak modulating signal swing divided by twice the DC level. PIM channel is best operated at modulation index less than 50%, thus giving sufficient headroom for the modulated ramp to sample the second channel, see Fig. 4.11. The minimum required amplitude of the ramp can be determined from the following relation [88];

$$(V_{ramp})_{\min} = \frac{sT_o}{1 + m_1} \quad (4.2)$$

where s is the slope of the ramp and T_o is the period of the unmodulated carrier. The modulation index of the width modulation channel is [88];

$$m_2 = \frac{\Delta\tau}{T_o} \sum_{n=0}^{\infty} m_1^n v_1^n(t) \quad (4.3)$$

where $\Delta\tau$ is the maximum pulse width deviation. Note that when the first modulating signal is absent, the modulation index m_2 becomes;

$$m_2 = \frac{\Delta\tau}{T_o} \quad (4.4)$$

A channel may be operated at a modulation index as high as 70%. however, operating at $m_2 \leq 50\%$ will result in reduced harmonic distortion and interchannel cross-talk [88].

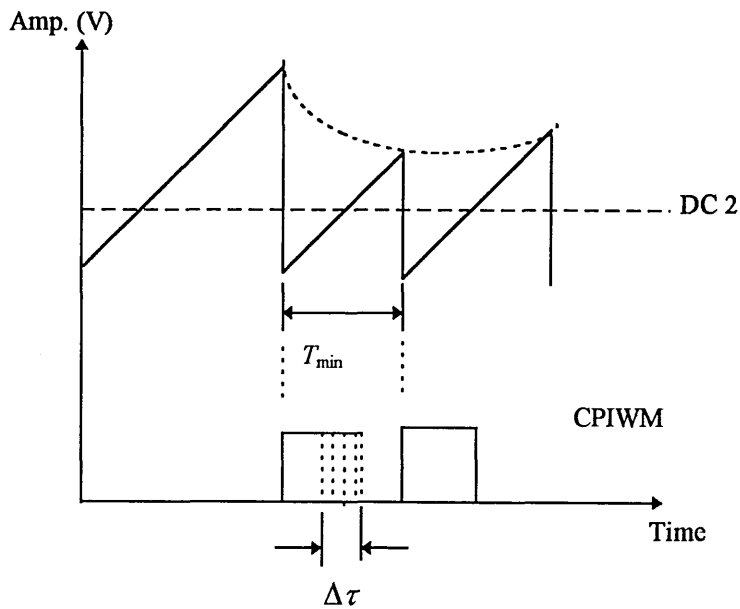


Fig. 4.11 Modulated ramp waveform and CPIWM signal.

At the receiver (see Fig. 4.12), after threshold detection, demultiplexing is carried out by an edge separation technique which converts the CPIWM waveform to a series of short duration pulses by employing differentiators. The pulses are reset and initiate a ramp generator of constant slope, whereas the falling edge pulses are employed to control a sample and hold operation. The modulated ramp signal is then passed through a high order low pass filter in order to recover the first message signal. The output of the sample and hold unit is a pulse amplitude modulated waveform, which is then passed through a low pass filter in order to extract the second message signal.

However, the PAM signal at the output of the sample and hold is affected by the interval modulation of the first channel, thus resulting in cross-talk from the PIM to the PWM channel. This cross-talk may increase with increasing modulation index m_1 . On the other hand, in an ideal system there is no cross-talk on the PIM due to width modulation. However, in practice, due to pulse width being modulated by the $v_2(t)$, the rising edge of the next CPIWM pulse is affected by the falling edge of the preceding pulse due to the waveform distortion, and limited transmission bandwidth. This results in PIM pulses being phase modulated by the second channel, and hence cross-talk from the PWM signal to the PIM channel. In general, the cross-talk in the PWM channel due to PIM signal is lower than that in the PIM channel due to PWM signal [88].

The CPIWM spectral profile is slightly asymmetrical. As the case with PIM and PIWM, shown in Fig. 4.13, it contains baseband components and their harmonics together with a series of diminishing sidetones spaced ω_1 (lowest information frequency) apart around the second input signal frequency ω_2 . Also, present are spectral components generated around the modulated sampling frequency ω_o and its harmonics, surrounded by a diminishing series of sidetones separated from each other by a frequency equal to the modulating frequencies ω_1 and ω_2 . The sidetone corresponding to the sum and the difference between the modulating frequencies have

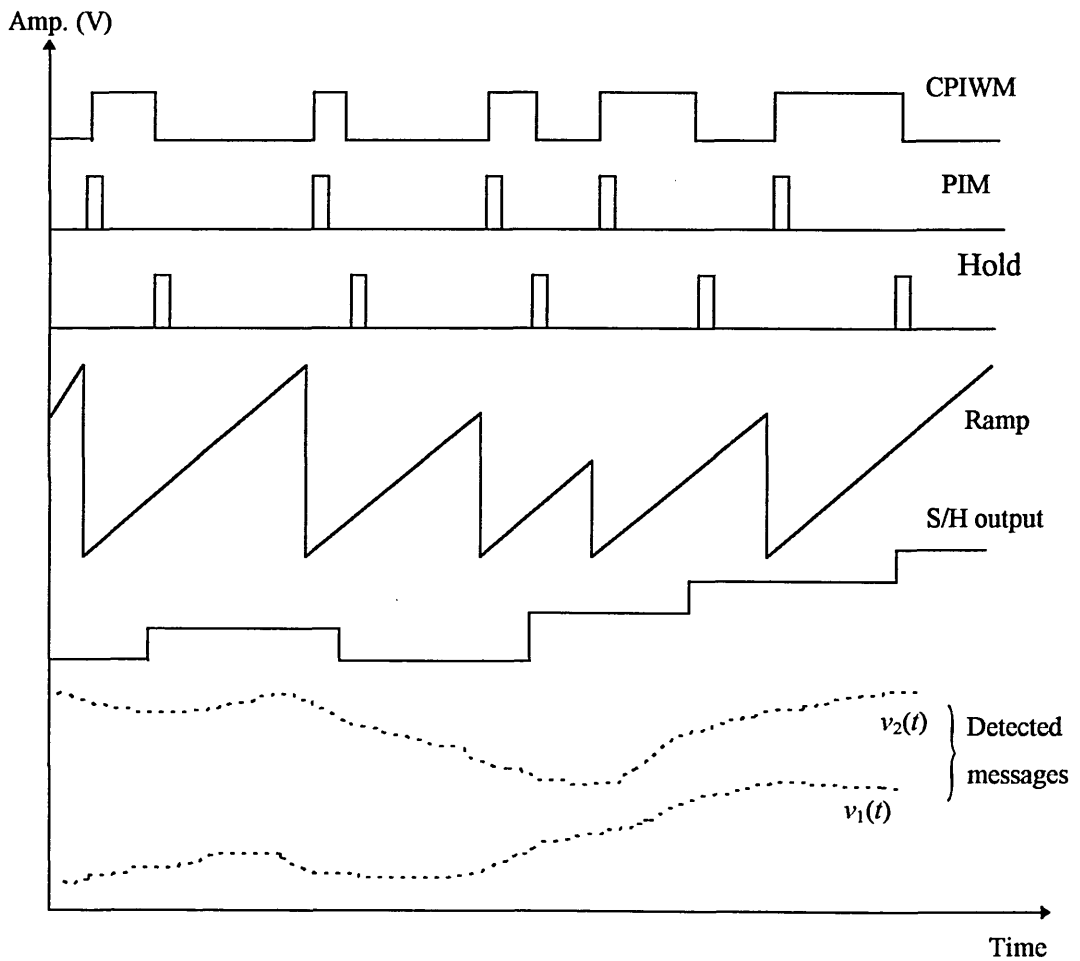
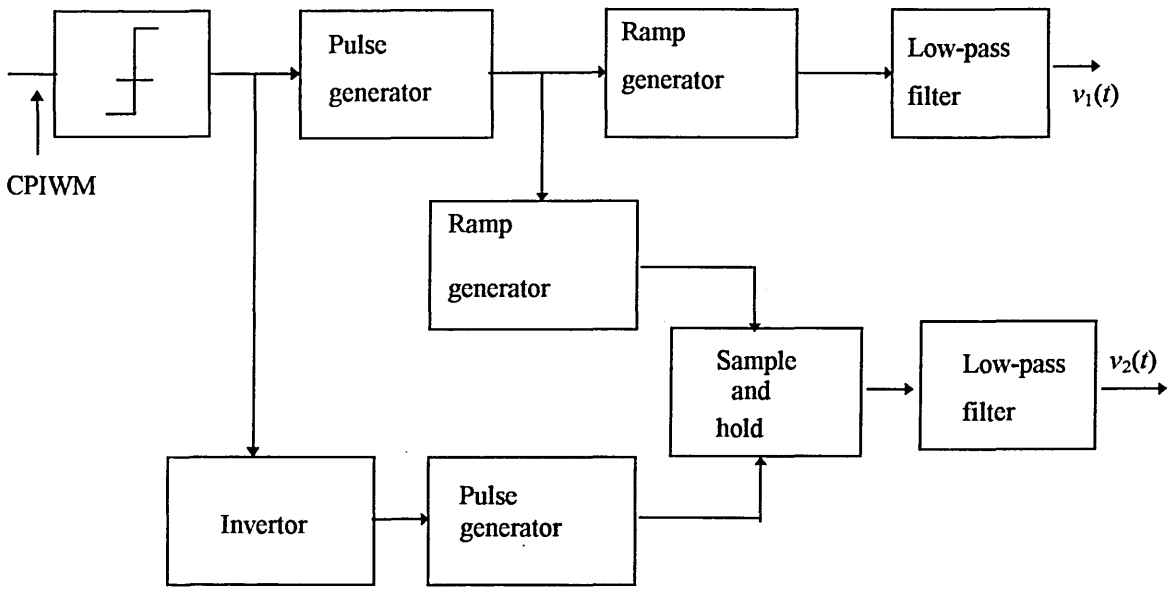
also developed a diminishing series of sub-sidestones spaced ω_1 apart. The sampling frequency component and its harmonics are not constant, but increase from their free-running (unmodulated) values of ω_o , $2\omega_o$, as a function of the modulation index. For CPIWM the minimum sampling frequency to modulating frequency ratio is still 2:1 as in PIM and PWM.

For high signal-to-noise ratio (i.e. low edge jitter) the transmission channel must be capable of carrying CPIM with very little distortion. However, for moderate signal-to-noise ratio, it is possible to reduce the channel bandwidth up to a point where only the low level components and fundamental sampling components are transmitted. The bandwidth saved may be used for transmission of other services.

Like all PTM transmission techniques, the signal performance of the CPIWM is mainly determined by the pulse jitter to amplitude conversion at the threshold detector and the optical receiver. Fig. 4.14 shows that the performance of both channels (the PIM and the PWM) are comparable. Finally, CPIWM also display a noise threshold below which the system noise performance rapidly deteriorates, see Fig. 4.14.

4.3.2 pulsed frequency and width modulation

In this type of multiple modulation technique, a frequency modulated signal is first generated and then used as a reference for the width modulation stage. In effect, a signal which carries two independent channels, one in its frequency and the other in its width, will be generated. There are two possible types of compound frequency and width modulation, namely; pulsed frequency and width modulation and compound pulse frequency and width modulation (CPFWM). The later will be discussed in more detail in the next chapter.



(b)

Fig. 4.12 CPIWM receiver: (a) block diagram and (b) waveforms.

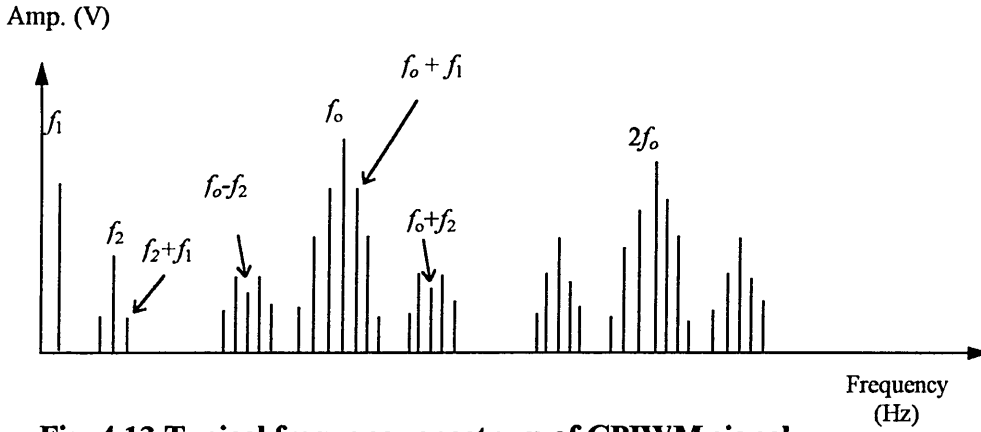


Fig. 4.13 Typical frequency spectrum of CPIWM signal.

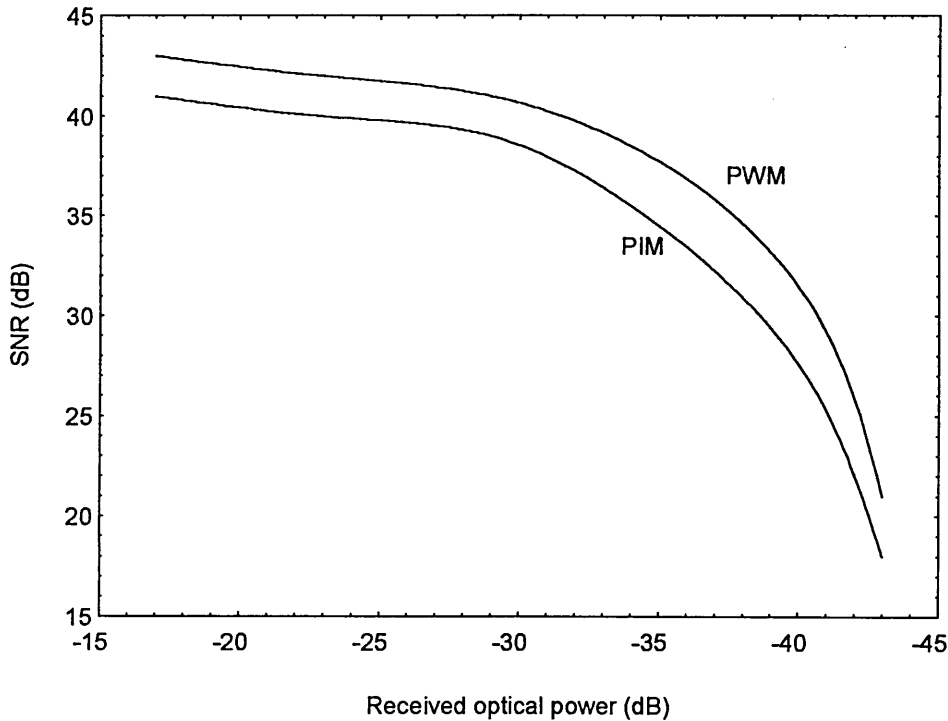


Fig. 4.14 Noise performance of CPIWM system [88].

As mentioned above, the pulsed FWM is a multiple modulation system, where separate information is carried by the frequency and the pulse width. Pulsed FWM was first reported by Tanaka and Okamura [31], where they applied this technique to the optical transmission of video signal and digital audio signal. A block diagram of a pulsed FWM

transmitter is shown in Fig. 4.15. A conventional frequency modulation (FM) signal is first generated which carries the first modulating signal, $v_1(t)$. This FM signal is then compared to the second modulating signal, $v_2(t)$, or to the PSK signal. The output of the comparator is the desired pulsed FWM signal, Fig. 4.15-b shows the signal waveforms. The pulsed FWM has the feature that even if both modulating signals have the same bandwidth, they can be multiplexed or demultiplexed, thus, making it possible to utilise effectively the available transmission channel bandwidth effectively [31].

Another feature is that the second channel can be multiplexed and separated without demodulating the FM signal. this makes the scheme attractive for video distribution systems, providing services independently for video and data or audio.

The frequency spectrum of pulsed FWM is shown in Fig. 4.16. It can be noticed from examining the low frequency components of the pulsed FWM, that the frequency modulation components and the second modulating signal (or PSK signal) are located separately on the frequency axis. Therefore, they can be separated by two band pass filters. The rest of the spectrum is just like that for ordinary PFM.

At the receiving end, the FM and the PWM signals are separated by band pass filters after threshold detection, see Fig. 4.17. The FM signal is first converted into an SWFM signal, and then into PFM pulses of fixed duration. Since the spectrum of the PFM signal contains the baseband component, the information carried in the PFM is extracted by a low pass filter. Finally the second channel (or PSK signal) is passed through a band pass filter (followed by PSK demodulator in case of using PSK signal) in order to recover the information $v_1(t)$.

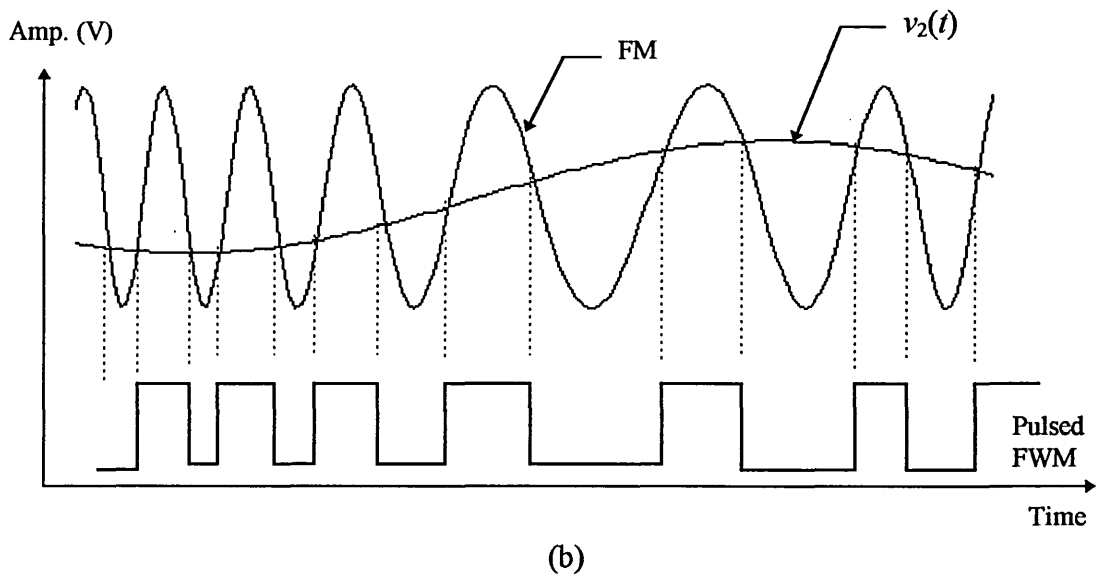
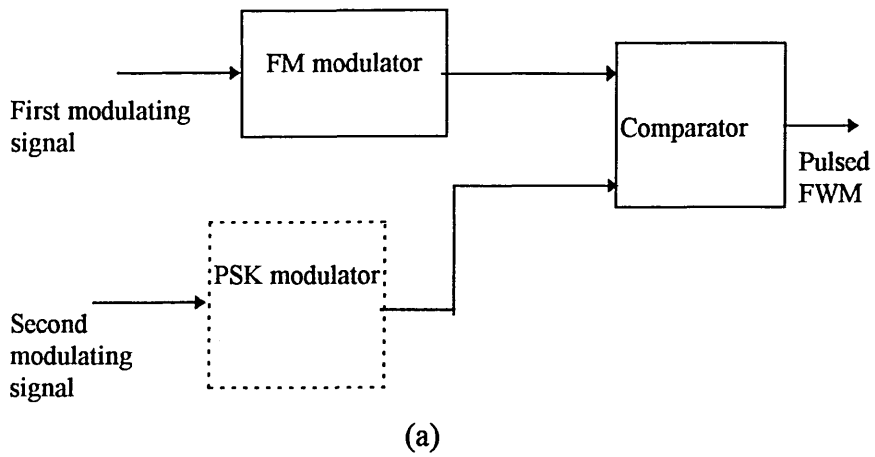


Fig. 4.15 Pulsed FWM transmitter: (a) block diagram and (b) waveforms.

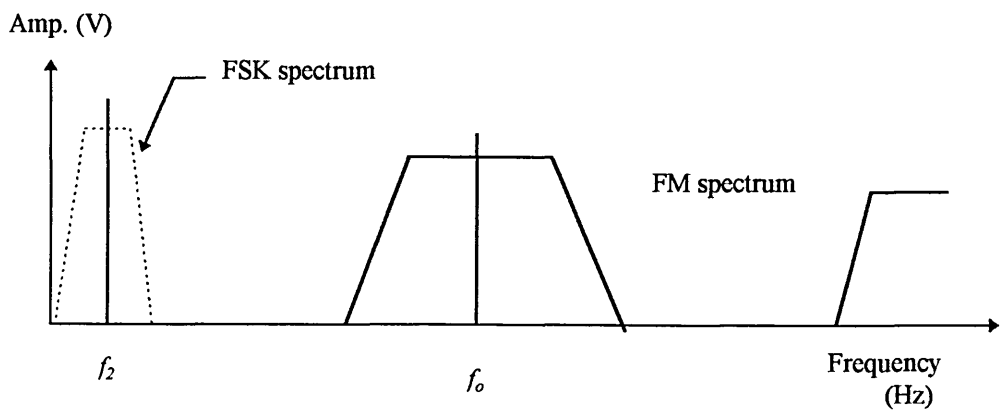


Fig. 4.16 Frequency spectrum of pulsed FWM waveform.

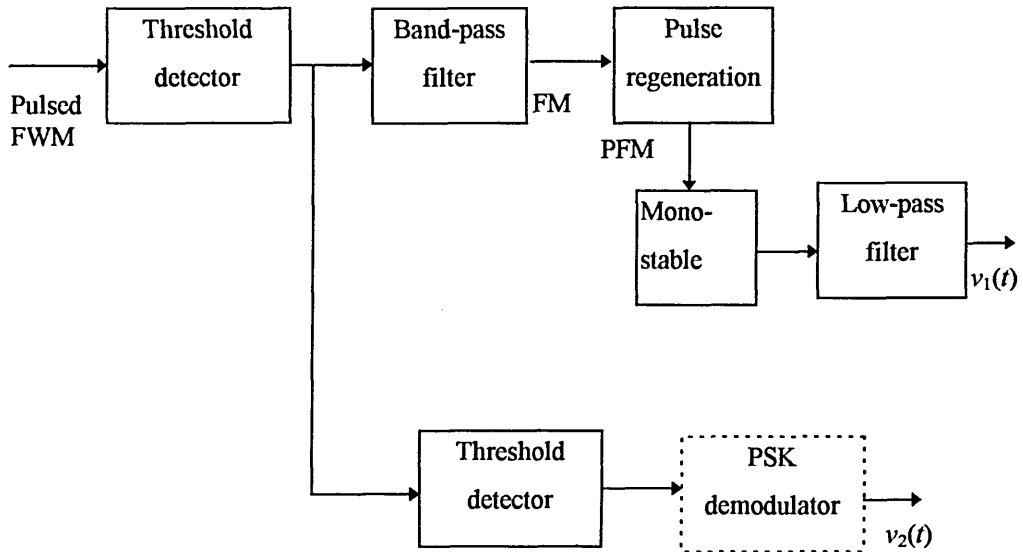


Fig. 4.17 Pulsed FWM receiver.

The cross-talk performance of the pulsed FWM system is studied by Tanaka and Okamura [31]. Like the FDM systems, the main causes of the cross-talk are possible spectrum overlapping between the second modulating signal and the FM signal side bands, and the separation band pass filters' characteristics that passes some components from the other channel. Brief cross-talk analysis is given in this section, however, the detailed mathematical analysis is given in Ref. [31].

The cross-talk analysis is based on finding the frequency components that pass through the stop band of the separation filters in each channel. In order to find that, time domain Fourier series representation of the pulsed FWM signal should be found first. This is given as [31];

$$\begin{aligned}
f(t) &= \sum_{n=-\infty}^{\infty} \{U(t - T_{1,n}) - U(t - T_{2,n})\} \\
&= \sum_{n=-\infty}^{\infty} \{a_n \cos(2\pi f_o t) + b_n \sin(2\pi f_o t)\}
\end{aligned} \tag{4.4}$$

where $U(t)$ is unit step function, $T_{1,n}$ and $T_{2,n}$ are time sequences where the FM signal and the second channel signal intersect, f_c is the free-running frequency, a_n and b_n are the Fourier coefficients. The channel separation (demultiplexing) is achieved by filtering. If the filter used to separate the FM signal has a characteristic $H(f)$, then the signal at the filter output can be written as;

$$f_R(t) = \sum_{n=-N}^N \{a_n \cos(2\pi f_o t) + b_n \sin(2\pi f_o t)\} |H(f)| \tag{4.5}$$

where N is an integer representing the order of the frequency component to be considered, usually N is taken to be 3 or 4, as the higher frequency components will be significantly attenuated by the filter.

The regenerated PFM pulses are obtained by passing the signal from the band pass filter through a zero crossing detector, producing a pulse of constant width whenever $f_R(t) = 0$. The solutions of $f_R(t) = 0$ is usually very complicated and needs numerical analysis, however, this solution will give the regenerated PFM at the receiver. Passing the regenerated pulses through the low pass filter, the interference component from the second modulating signal (or PSK) can be obtained. The cross-talk is evaluated by dividing the interference component by the demodulated FM signal level.

Figure 4.18 shows the cross-talk from the width modulation (second modulating signal) to the FM signal when the mixing ratio (v_2/v_1) is varied. The results shown in this figure were obtained numerically by applying the procedure mentioned above. It can be noticed that when the carrier frequency of the second modulating signal (or PSK signal) increases the cross-talk increases [31].

The cross-talk from FM signal to the second modulating signal (or PSK signal) can be calculated using similar technique. The main cause of the cross-talk from the FM signal are spectrum overlapping and the characteristics of the band pass filter used to separate the second modulating signal (or PSK signal). The components from the FM signal that mix with the second modulating signal can be evaluated from the FM spectrum near the carrier frequency f_o which can be given as;

$$\begin{aligned}
 g(t) &= A \sin[2\pi f_o t + \beta \sin(2\pi f_1 t)] \\
 &= A \sum_{n=-\infty}^{\infty} J_n(n\beta) \cos[2\pi(f_o + n f_1)t + n\pi / 2]
 \end{aligned}
 \tag{4.6}$$

where β is the modulation index of the FM signal. The order of the components that give rise to the interference depend on the ratios f_o / f_1 and f_o / f_2 . In practice, however, the fourth and the following sidebands could be considered as the component that give rise to the interference. This can be evaluated from equation 4.6 by substituting $n = 4$. In this case a cross-talk of -24 dB is obtained, however, if a different order is considered then a different value of cross-talk may be obtained. As a conclusion the sampling ratio should be chosen in order to minimise the cross-talk, although cross-talk between channels are inevitable as is the case in all FDM systems.

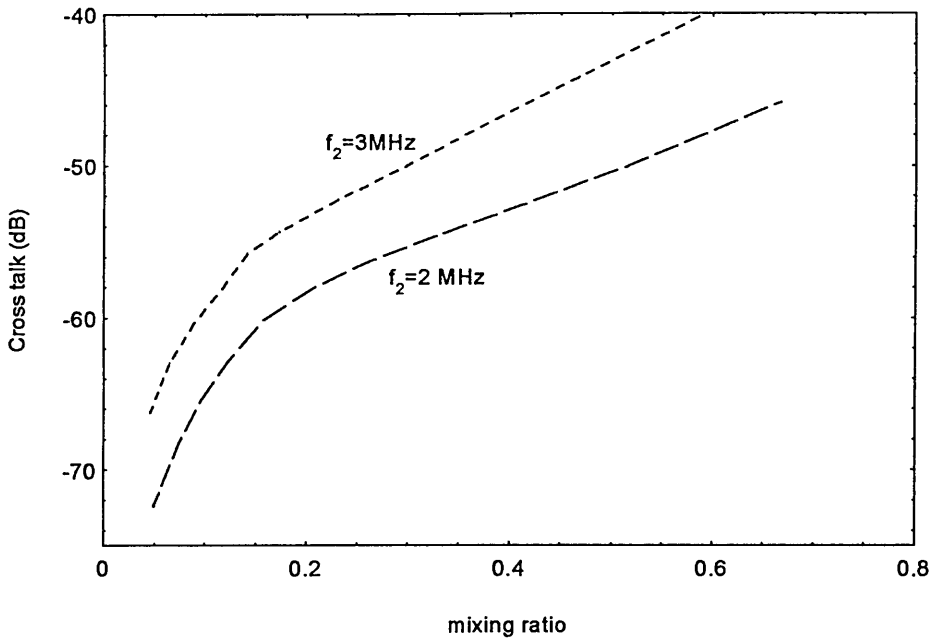


Fig. 4.18 Cross-talk in pulsed FWM system (from second channel to FM ($f_o = 21$ MHz, $\Delta f = 8$ MHz, third order Bessel band pass filter is assumed) [31].

On the other hand the cross-talk between the frequency modulated channel and the width modulated channel has been calculated for video signals only when filtering technique is used to separate the two multiplexed channels. Tanaka and Okamura have considered the fourth sideband component of the frequency modulated spectrum as the most dominant component which produces cross-talk in the system. It has been concluded that with proper choice of the frequencies and modulation indices a cross-talk of order -40 dB between any channels is possible. Furthermore, when the carrier frequency exceeds the video signal bandwidth the cross-talk component on the FM channel due to the PWM channel can be eliminated by the video filter.

As to the noise analysis, the *SNR* for the pulsed FWM system is given in this section. For comparison the *SNR* is also given for the case when the video signal and the PSK

modulated digital voice are multiplexed in the frequency domain then modulated using PFM. In the later case the SNR of the demodulated video and the carrier-to-noise (CNR) ratio of the PSK signal are given as;

$$SNR = \frac{12\beta^2}{(2\pi)^2 B_v f_o \sigma^2} \quad (4.7)$$

$$CNR = \frac{(m_v \Delta f / 2f_2)^2 / 2}{(2\pi)^2 B_a f_o \sigma^2} \quad (4.8)$$

where, B_v and B_a are the bandwidths of the video and the audio signals respectively, σ^2 is the noise jitter and m_v is the mixing ratio of the video signal (i.e. video signal level divided by the audio signal level). When the video signal is pulsed FM modulated and then PWM modulated by the voice carrier, the demodulated SNR of the video is the same as given in equation 4.7. The demodulated CNR of the voice carrier is given by;

$$CNR = \frac{[\sin^{-1}(m_a / \pi)]^2}{8B_a f_o \sigma^2} \quad (4.10)$$

where, m_a is mixing ratio of the PWM signal. Comparing equations 4.10 and 4.9, it can be concluded that both methods will give the same noise performance if;

$$m_a = \sin\left(\frac{m_v \Delta f}{2f_2}\right) \quad (4.11)$$

However, if we chose $\Delta f = f_2$, and $m_a = m_v$, the pulsed FWM will be better by 6 dB, indicating that transmission by multiplexing the voice signal on pulse width is better.

4.3.3 compound pulse frequency and width modulation

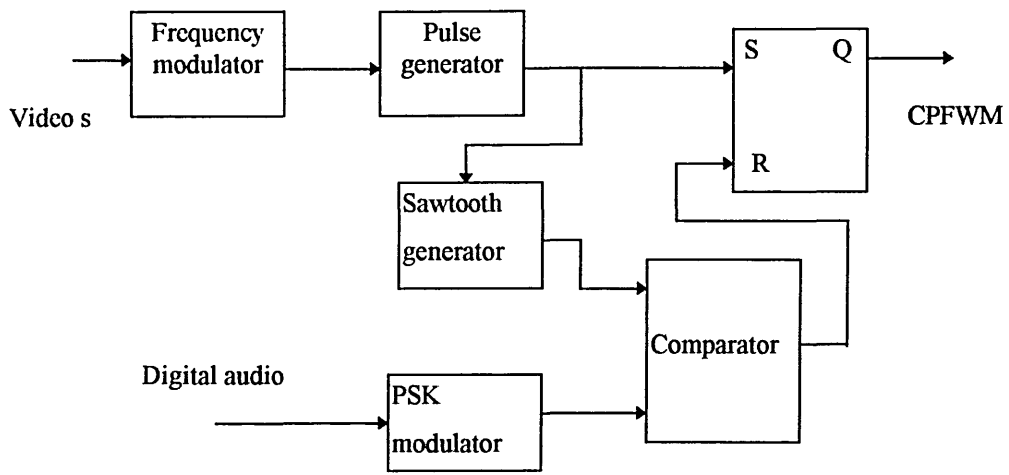
This technique has been used by Tanaka and Okamura [31], to transmit a video signal and audio message carried on a phase shift modulated carrier. The generation method of the compound pulse frequency and width modulation (CPWFM) is shown in Fig. 4.19, in which a video signal is used to modulate the frequency of a pulse train which is used to initiate a sawtooth generator. On the other channel a digital audio signal is used to modulate the phase of an audio sub-carrier. The phase shifted signal and the sawtooth waveform are applied to a voltage comparator. The comparator output and the frequency modulated pulse due to the first channel are used to set and reset a flip flop which produces the CPFWM signal, see Fig. 419- b.

At the receiver side, see Fig. 4.20, the two channels are demultiplexed by using edge separation techniques. The set pulse (PFM pulse) is generated from the rising edge of the received pulses, while the hold pulse is generated from the falling edge. The video message is then extracted from the set pulses by low-pass filtering. The set pulses (PFM pulses) are also used to initiate a sawtooth generator. The sawtooth output is sampled at the falling edge of the CPFWM signal position. The output of the sample and hold circuit is the PSK audio message which can then be extracted by PSK detector.

To conclude, PTM techniques have the disadvantage that both TDM and FDM multiplexing are not easy. TDM is difficult because the information is carried on one of the pulse characteristics, while the nature of PTM waveforms spectrum makes FDM not easy. CPTM techniques are alternative approaches to TDM and FDM multiplexing

schemes, and have the advantages of simplicity and good noise and cross-talk performance. Although, in theory, a number of possible CPTM techniques are available, only limited attempts have been made to develop them. Research showed that CPIWM scheme offers good cross-talk and noise performance with considerable low bandwidth. This makes it an attractive technique for wideband signal transmission. On the other hand, CPFWM is another alternative scheme which shows similar performance to that of CPIWM, but it is not characterised yet. Further study and investigation on the CPFWM scheme is therefore needed.

In the next chapter a detailed analysis of the performance of the CPFWM system will be given. This includes the modulation spectrum, noise, and cross-talk analysis.



(a)

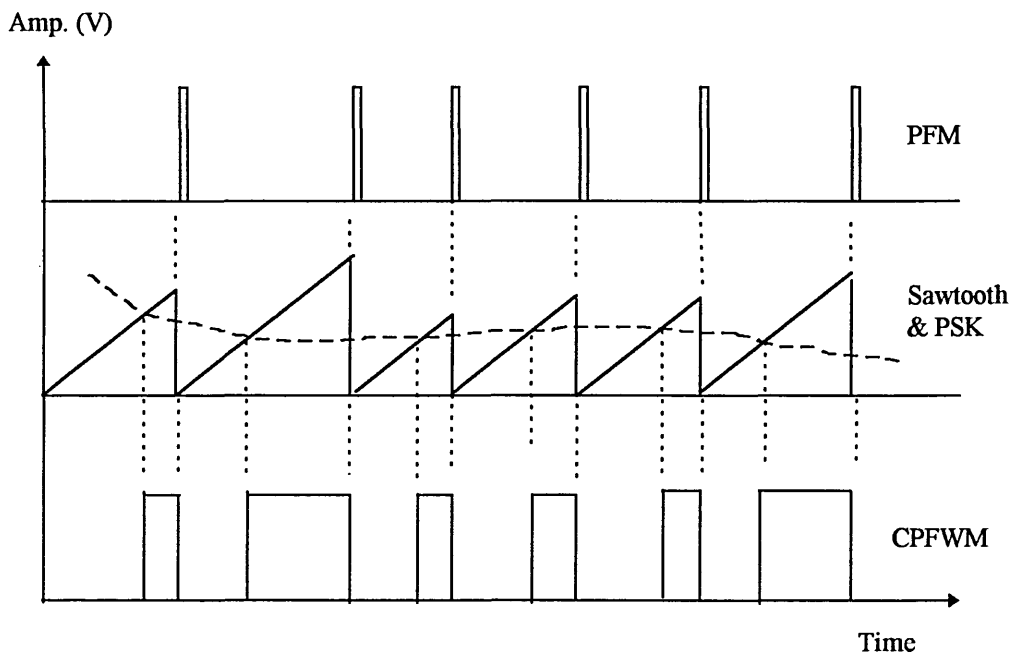
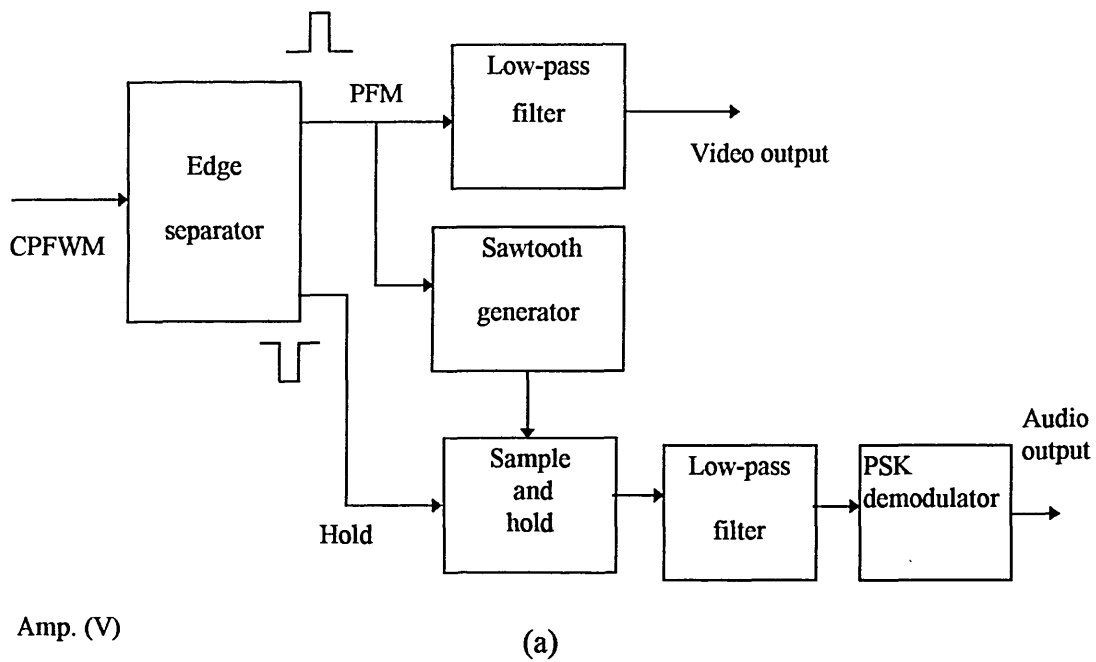


Fig. 4.19 CPFWM modulator: (a) Block diagram and (b) waveforms.



Amp. (V)

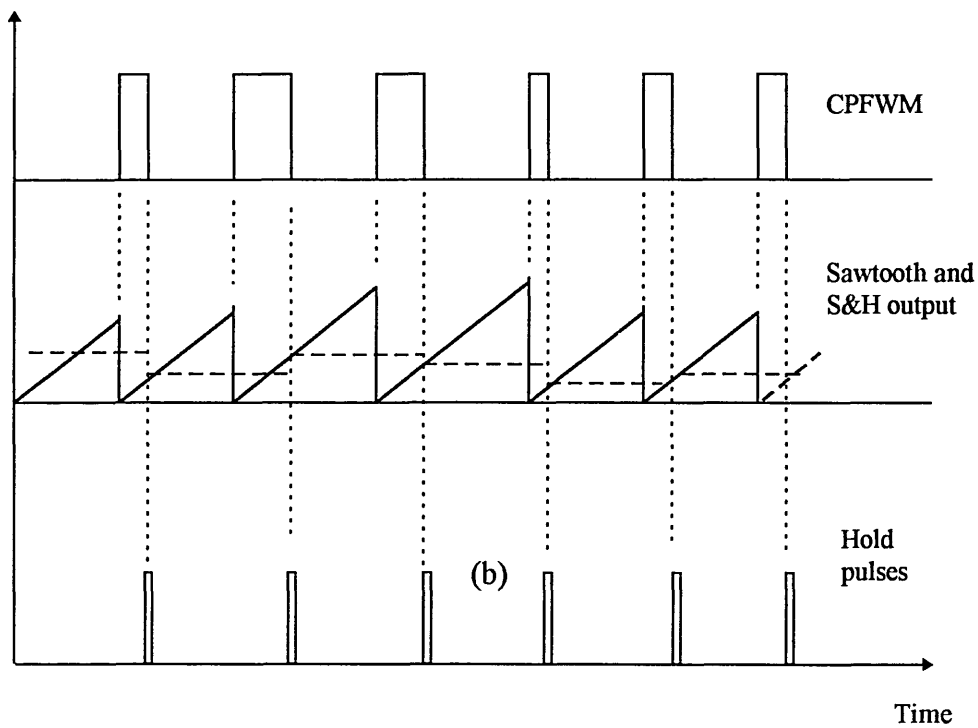


Fig. 4.20 CPFWM demultiplexer: (a) block diagram and (b) waveforms.

Chapter Five

Compound Pulse Frequency and Width Modulation

5.1 Introduction

Compound pulse frequency and width modulation (CPFWM), also known as the hybrid pulse frequency and width modulation, is an attractive alternative technique for multiplexing pulse time modulation signals. Like other combined pulse time modulation schemes, it is based on a combination of two PTM schemes; the PFM and the PWM. The main features of this technique may be summarised as; i) effective bandwidth utilisation, ii) channel separation without the need for demultiplexing and iii) channel synchronisation is not required for the demultiplexing process. These features make the CPFWM technique very attractive in a number of applications such as video distribution, where data and video signals can be provided independently.

Despite the fact that the principles of CPFWM were reported several years ago, most of the work carried out is based on experimental investigations, and very little work has been reported on theoretical analysis. In this chapter, the CPFWM technique is studied in detail. Mathematical characterisation, computer simulation, and experimental verification of the CPFWM generation and demodulation are presented.

5.2 CPFWM modulation and demodulation

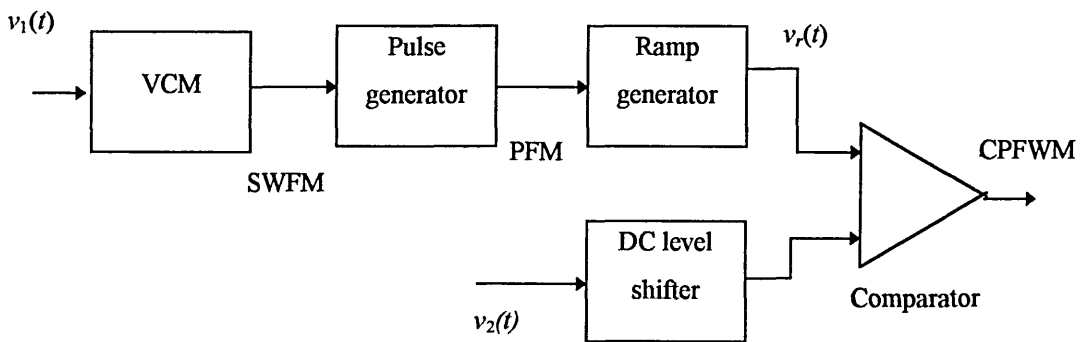
The approach used here in CPFWM generation is different from that reported by Tanaka et al [31] and discussed in the previous chapter. In this section, a theoretical analysis of the CPFWM modulator and demodulator is presented.

5.2.1 CPFWM Modulator

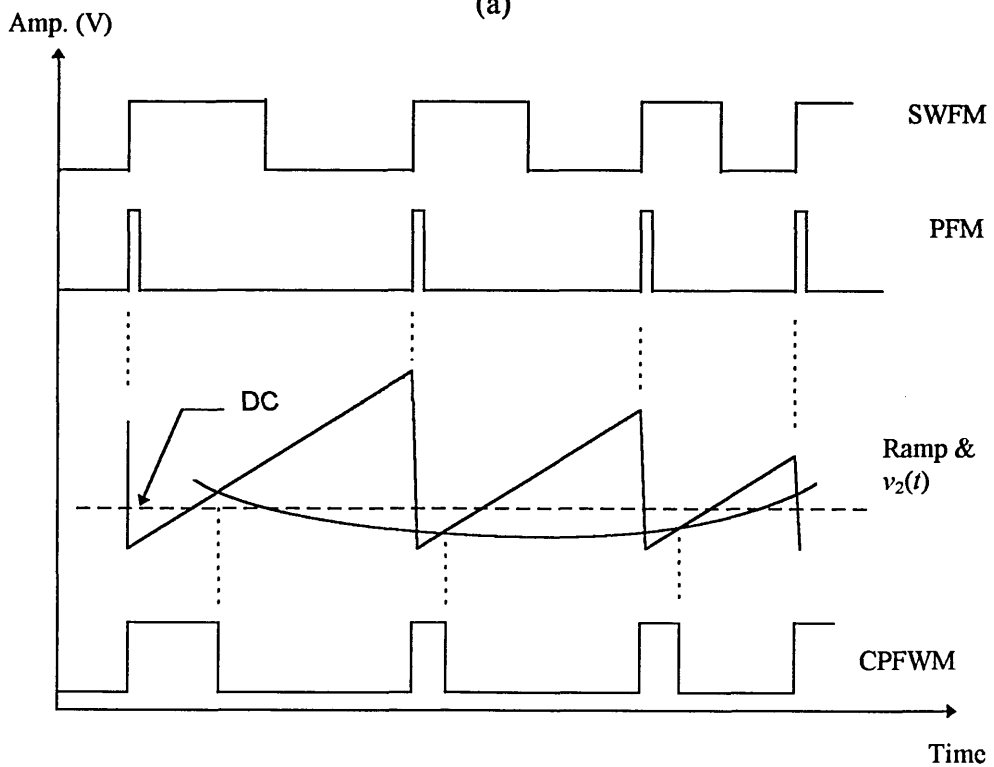
Figure 5.1 shows a block diagram of the CPFWM transmitter. A voltage controlled multivibrator (VCM) is used to generate SWFM. This anisochronous PTM method is closely related to both analogue FM and PFM systems and consists of a series of squarewave edges transitions occurring at the zero crossing points of the FM, see Fig. 5.1-b. The PFM waveform is derived directly from SWFM by passing it through a differentiator to generate low duty cycle pulses, see Fig. 5.2-b. The modulated pulses reset and initiate a constant slope ramp generator. The output of the ramp signal has variable amplitude and period which are proportional to the amplitude and frequency of the first input signal $v_1(t)$. After level shifting, the second modulating signal, $v_2(t)$ is compared with the ramp using a comparator. The output of the comparator is the desired CPFWM waveform which contains both of the input signals in the form of modulated period and duration, see Fig .5.1-b.

It is also possible to generate CPFWM by differentiating both edges of the SWFM, to produce a double edge PFM waveform. The PFM waveform is used to initiate a ramp generator, the amplitude of which is compared with the second modulating signal, see Fig. 5.2. It is clear that this technique will lead to doubling the frequency of the ramp generator. Consequently, the operating frequency of the CPFWM will be doubled also.

This technique has the advantage of reducing the filter order required in demodulating the PFM signal, and improving the noise performance since the sampling ratio for both channels are doubled. However, such advantages could also be achieved using the previous technique by doubling the free running frequency of the system.



(a)



(b)

Fig. 5.1 CPFWM modulator: (a) block diagram and (b) waveforms.

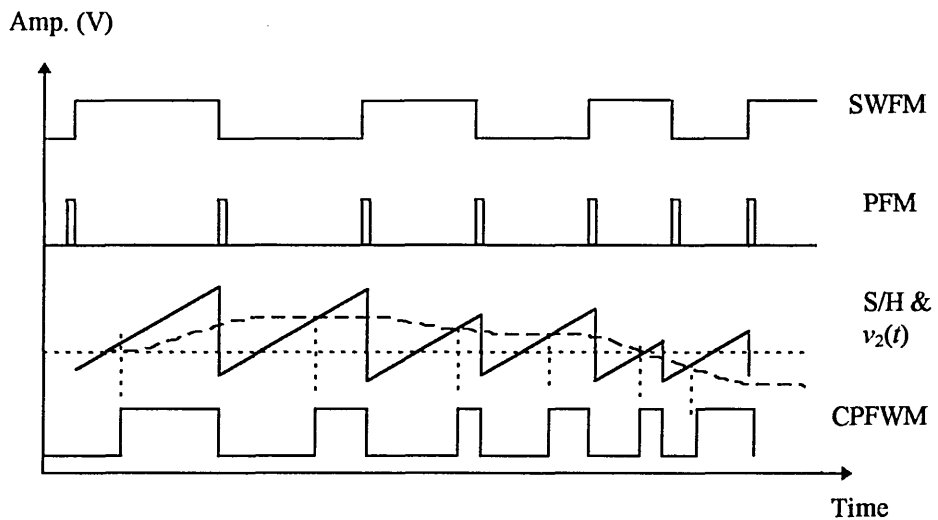


Fig. 5.2 CPFWM waveforms when using double edge differentiation.

The second modulating signal could either be used as a baseband waveform, or modulated by a sub-carrier, such as PSK or FSK. The principle of the modulator is the same, however, on the receiver side a proper demodulating technique should be applied after extracting the second modulating signal.

Removing the input signal from the PFM modulator results in removing the amplitude variation of the ramp signal. The output waveform becomes a leading edge PWM waveform, see Fig. 5.3.a. If the input signal to the comparator is removed, the ramp signal level will be compared with a constant DC level and the output signal will be an increased width PFM waveform, see Fig. 5.3.b.

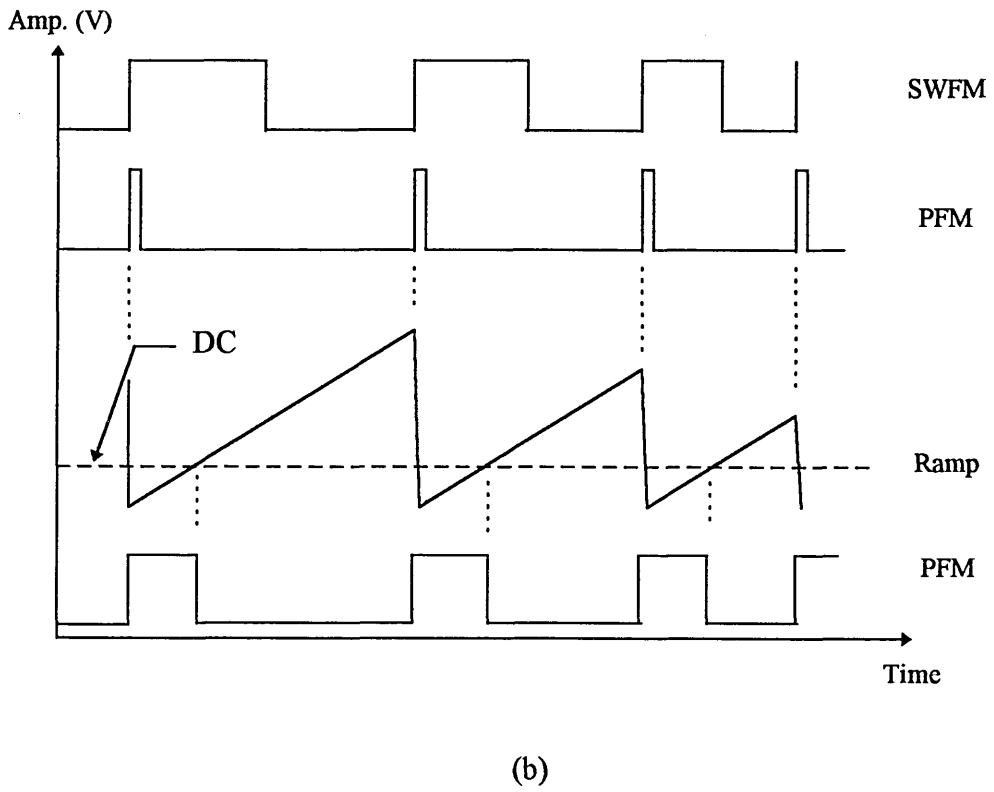
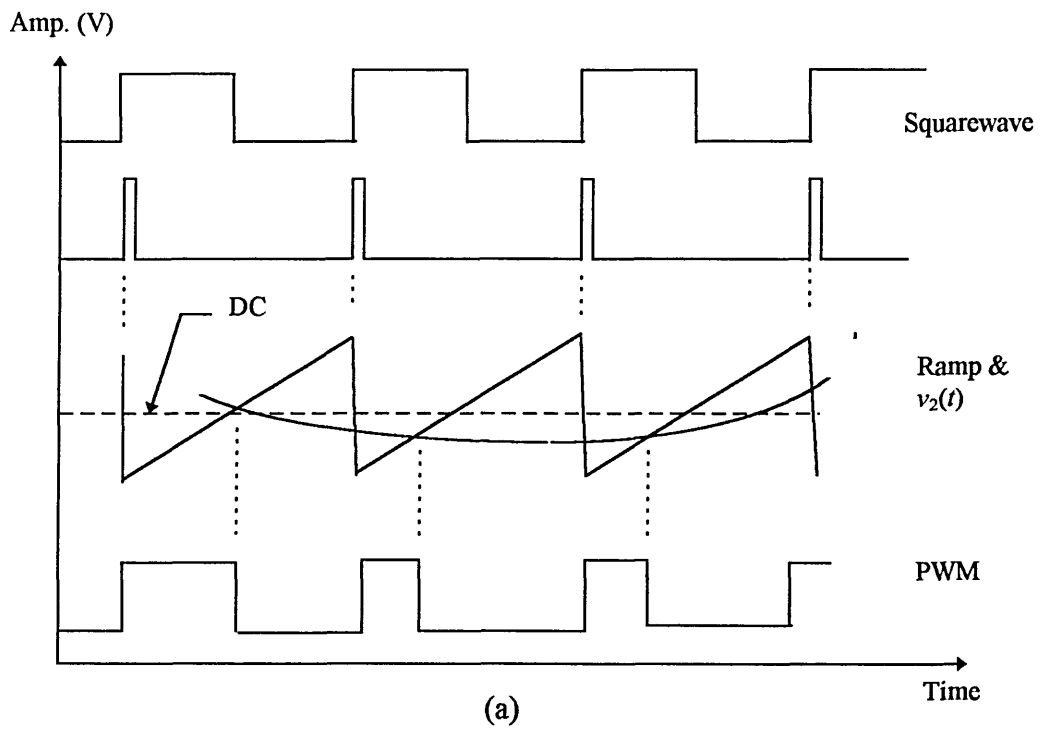


Fig. 5.3 Waveforms of the CPFWM modulator: (a) when the first input is removed and (b) when the second input is removed.

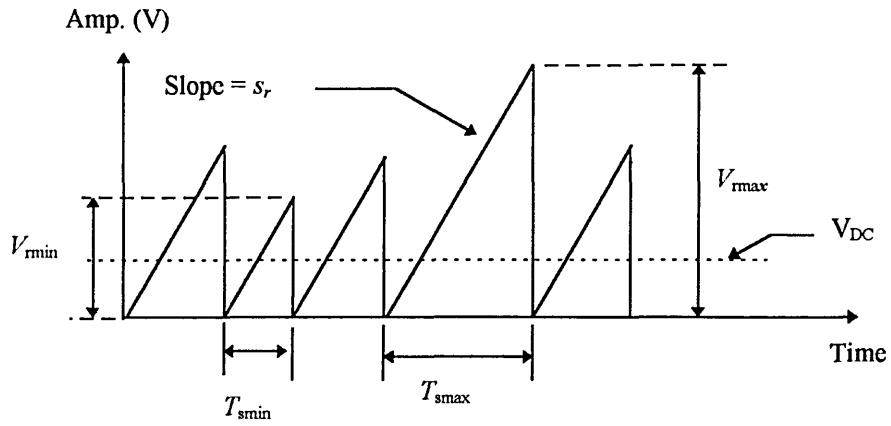


Fig. 5.4 Waveforms at the comparator inputs.

The principle of the modulation when both inputs are present is best explained using Fig. 5.4. If the slope of the ramp signal is s_r , the maximum and the minimum voltage levels of the ramp signal can be calculated as, respectively;

$$V_{r \min} = s_r T_{s \min} \quad (5.1)$$

and

$$V_{r \max} = s_r T_{s \max} \quad (5.2)$$

where, $T_{r \min}$ and $T_{r \max}$ are the minimum and the maximum period of the ramp signal, respectively. Subtracting equation 5.1 from 5.2, gives;

$$s_r = \frac{\Delta V}{\Delta t} \quad (5.3)$$

where, $\Delta V = V_{r\max} - V_{r\min}$, and $\Delta t = T_{s\max} - T_{s\min}$.

For optimum performance, the second modulating signal should be shifted by half of the minimum ramp voltage, i.e. $V_{DC} = V_{r\min} / 2$. The modulation index of the pulse width modulation channel (M) can be defined as the ratio between the second modulating signal level and the minimum ramp voltage, which can be written as;

$$M = \frac{V_2}{V_{r\min}} \quad (5.4)$$

Substituting equation 5.1 into 5.4, the following relation can be obtained;

$$\begin{aligned} M &= \frac{V_2}{s_r T_{r\min}} \\ &= \frac{V_2 (f_o + \beta f_1)}{s_r} \end{aligned} \quad (5.5)$$

where, f_o and f_1 are the carrier and the first modulating signal (to the PFM modulator) frequency, respectively, and β is the modulation index of the PFM waveform which is proportional to first input signal level.

Using k as the sensitivity of the VCM in (Hz/V), then the modulation index of the frequency modulation channel β may be calculated as;

$$\beta = \frac{V_1 k}{f_1} \quad (5.6)$$

The amplitude relationship between the two input signals is obtained by substituting equation 5.6 into 5.5. This results in;

$$V_2 = \frac{Ms_r}{f_o + V_1 k} \quad (5.7)$$

In order to combine PFM and PWM waveforms without introducing any non-linear distortion equation 5.7 should be satisfied.

However, the case when $V_{rmax} = 2V_{rmin}$, which represents the optimum mixing condition, gives the widest range of mixing ratio (V_2/V_1) between the two signals.

From equation 5.1 and 5.2 it can be shown that;

$$2T_{rmin} = T_{max} \quad (5.8)$$

or

$$2(f_o - \beta_p f_1) = f_o + \beta_p f_1 \quad (5.9)$$

where β_p is the optimum value for modulation index of the first channel (i.e. PFM), which is the value of β when equation 5.8 is satisfied. From equation 5.9, β_p can be given as;

$$\beta_p = \frac{f_o}{3f_1} \quad (5.10)$$

By substituting equation 5.10 into 5.5, the optimum modulation index for the second channel M_p can be obtained as;

$$M_p = \frac{4V_2 f_o}{3s_r} \quad (5.11)$$

Both equations 5.10 and 5.11 should be satisfied for optimum mixing between the two signals.

There are two special cases worth considering;

(a) when the first modulating signal is removed (i.e. $v_1 = 0$). This results in a PWM at the output of the CPFWM modulator and the value of β will be zero. In this case, equation 5.5 reduced to;

(b)

$$M = \frac{V_2 f_o}{s_r} \quad (5.12)$$

and the analysis for the optimum values of the modulation indices is not applicable.

(ii) When the second modulating signal is off (i.e. $v_2 = 0$) the modulation index will not be affected as it is always equal to $\Delta f/f_1$, also the analysis for optimum modulation index is not necessary.

On the other hand in order to minimise the interchannel cross-talk between channels it is essential to design the ramp generator so that the fall time is much smaller than the rise time of the ramp waveform. Otherwise, the variation in frequency of the ramp will cause changes in the pulse width of the CPFWM waveform. This will produce an interference component from the PFM channel to the PWM channel. Fig. 5.5 shows

the effect of the fall time on the pulse width of the waveform at the comparator output. For simplicity, let us assume that the PWM channel is off, while the frequency modulation is present, the change in the pulse width due to a non zero fall time can be given as;

$$\Delta\tau = \frac{V_r - V_{DC}}{s_f} \quad (5.13)$$

where V_r is the instantaneous amplitude of the ramp, and s_f is the slope of the falling edge, (see Fig. 5.5). The amplitude of the ramp can be evaluated as;

$$V_r = \frac{s_r}{f} \quad (5.14)$$

where f is the instantaneous frequency of the ramp waveform. If a single tone frequency modulation is assumed, f can be written as;

$$f = f_o + \Delta f \sin 2\pi f_1 t \quad (5.15)$$

where Δf is the maximum frequency deviation. Substituting equation 5.15 into 5.14 the V_r can be written as;

$$\begin{aligned} V_r &= \frac{s_r}{f_o \left(1 + \frac{\Delta f}{f_o} \sin 2\pi f_1 t\right)} \\ &\approx \frac{s_r}{f_o} \left(1 - \frac{\Delta f}{f_o} \sin 2\pi f_1 t\right) \end{aligned} \quad (5.16)$$

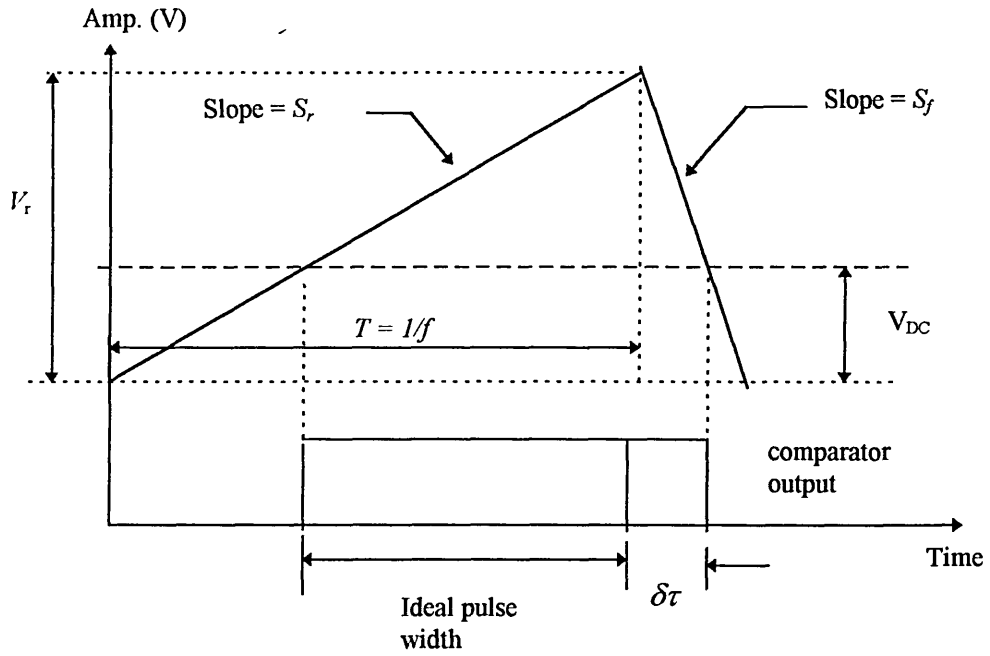


Fig. 5.5 Comparator output and ramp waveforms.

Finally, substituting equation 5.16 into 5.13 the change in the pulse width due to the existence of the frequency modulation can be obtained as;

$$\delta\tau = \frac{s_r}{s_f f_o} - \frac{V_{DC}}{s_f} - \frac{s_r \Delta f}{s_f f_o^2} \sin 2\pi f_1 t \quad (5.17)$$

The first and the second terms of equation 5.17 are constants which means they will introduce a constant shift in the pulse width. The last term represents the interference component which will cause cross-talk from the PFM channel into the PWM channel. The magnitude of this component depends on the ratio s_r/s_f which should be minimised.

5.2.2 CPFWM demodulator

At the receiver, after passing through a slicer the CPFWM signal is first demultiplexed by means of an edge separation technique using two differentiators, (see Fig. 5.6). The output from the first differentiator representing the rising edge, is a series of pulses corresponding to the PFM waveform, this is then passed to a monostable to produce a constant width PFM which passed through a low-pass filter to reconstruct the first modulating signal $v_1(t)$. The output from the second differentiator, representing the falling edge, is a pulse train which is used to control the sample and hold amplifier. The regenerated PFM pulses reset and initialise a ramp generator before being feed into the sample and hold amplifier for conversion into a PAM waveform, see Fig. 5.7. In order to minimise non-linear distortion it is important that both ramps at the receiver and transmitter should have the same shape and characteristics. Finally to recover the second modulating signal $v_2(t)$, the PAM waveform is passed through a low pass filter.

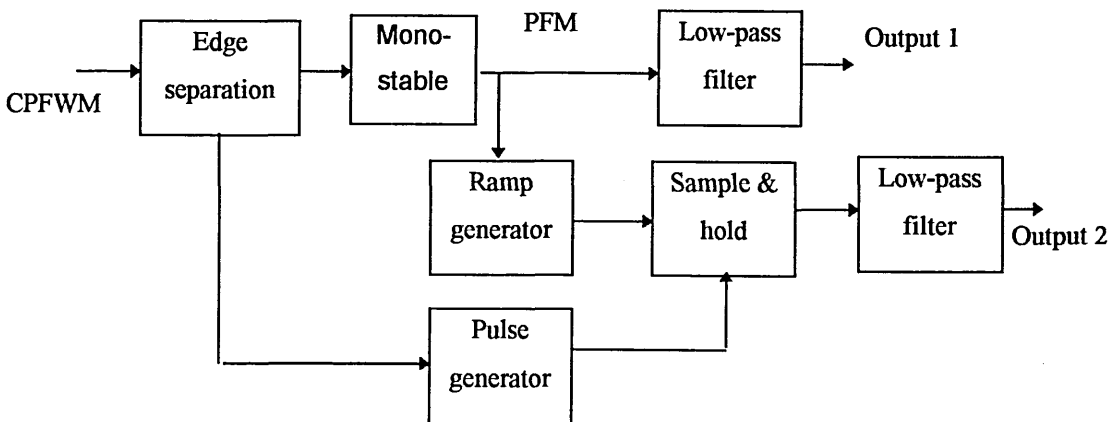


Fig. 5.6 Block diagram of the CPFWM receiver.

The pulse width of the CPFWM waveform is proportional to the amplitude of the second modulating signal, and has discrete values. The pulse width of the n th pulse may be given as;

$$\tau_n = \tau_o[1 + Mv_{2n}] \quad (5.18)$$

where, τ_o is the pulse width of the CPFWM waveform with the width modulation removed, and v_{2n} is the amplitude of the n th sample of the second modulating signal.

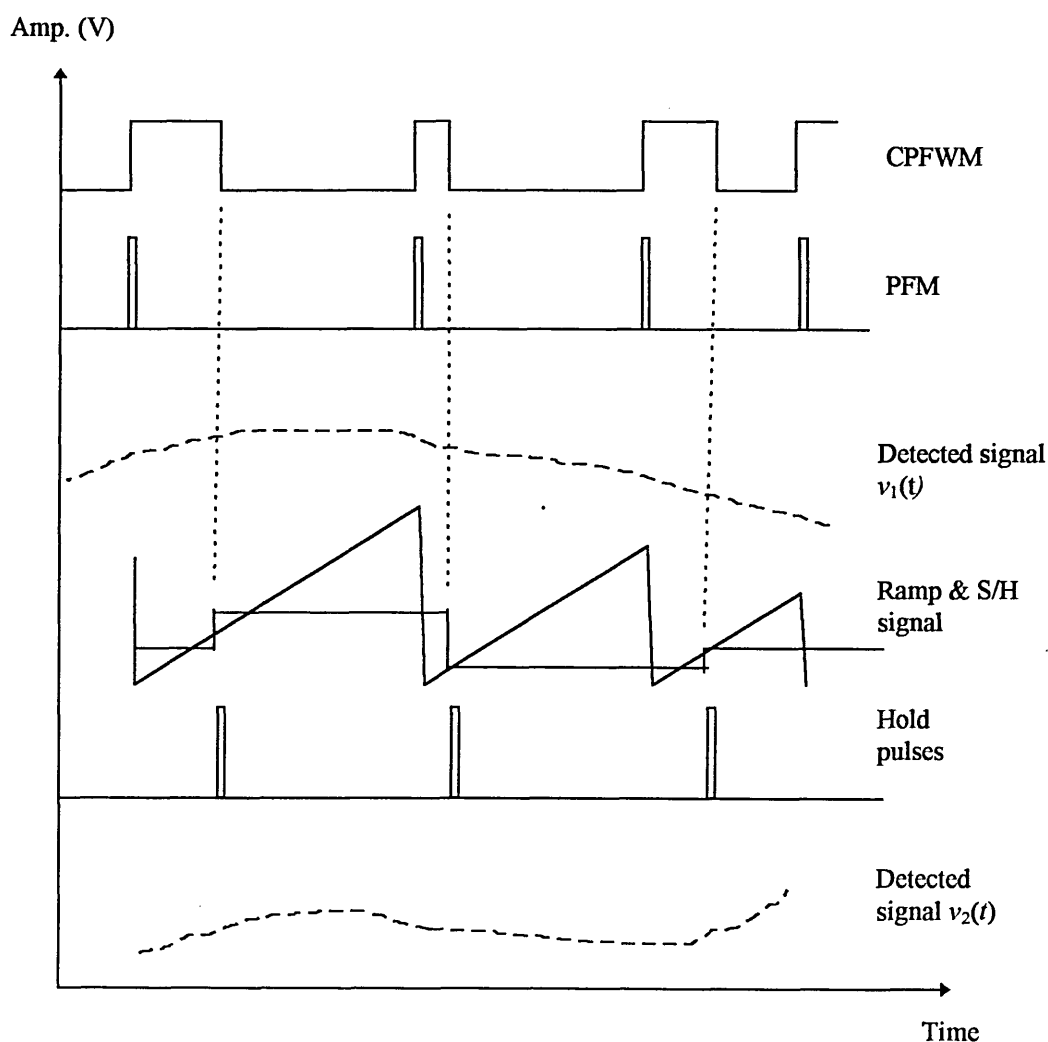


Fig. 5.7 Waveforms of the CPFWM demodulator.

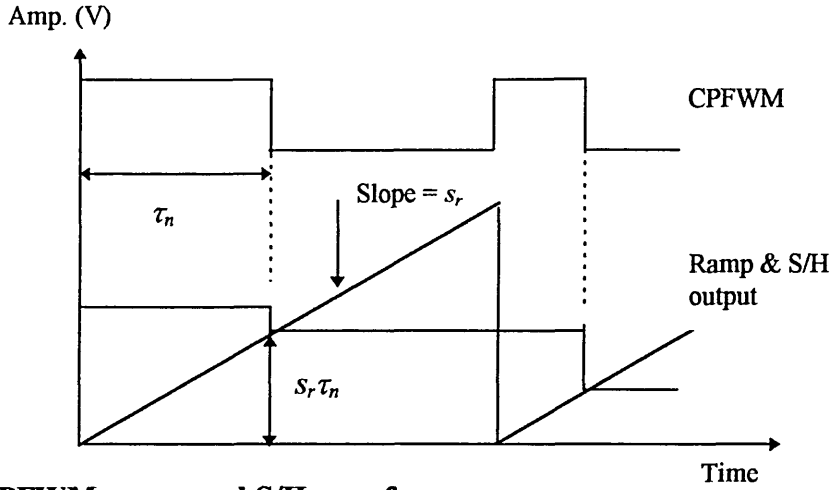


Fig. 5.8 CPFWM, ramp and S/H waveforms.

Figure 5.8 shows how the second channel is separated. The sample and hold amplifier stores discrete values and represents the reconstructed second channel. If the slope of the ramp waveform is the same as that at the transmitter, then the n th stored value from the sample and hold amplifier (i.e. the amplitude of the output of the sample and hold amplifier) can be calculated as;

$$v_{o2n} = s_r \tau_n = s_r \tau_o [1 + Mv_{2n}] \quad (5.19)$$

To recover both channels faithfully with minimum interchannel cross-talk, it is essential for the PFM pulse train to have a low duty cycle, see Fig. 5.9. If we assume that the maximum swing of $v_2(t)$ is unity, i.e. $|v_2(t)| \leq 1$, the maximum and the minimum pulse width of the CPFWM waveform can be determined from equation 5.18 as $\tau_o(1 \pm M)$. Thus, the pulse width of the reconstructed PFM waveform (τ_{PFM}) should satisfy the following relationship;

$$\tau_{PFM} < \tau_o(1 - M) \quad (5.20)$$

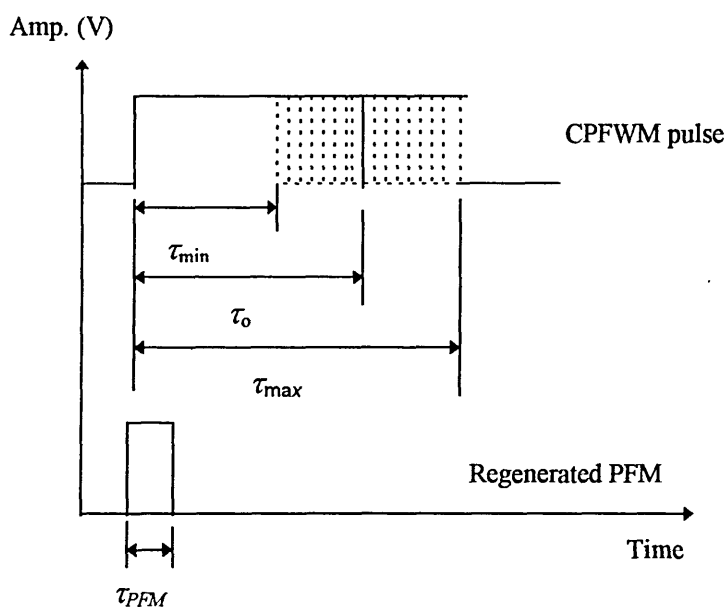


Fig. 5.9 Waveforms at the PFM pulse separation.

If the above condition is maintained, the PFM channel should be successfully separated from the PWM channel without any cross-talk. It is important to notice that lower duty cycle of PFM also means a higher modulation index and consequently higher signal-to-noise ratio for PWM channel. Since this takes place at the receiver, there is no bandwidth overhead penalty.

5.3 Computer simulation of the CPFWM system

Designing communication systems is often time consuming and expensive. Mathematical modelling and computer simulation are modern tools to speed up the design process and to provide the designer with an initial assessment of the system behaviour so that improvement or modification can be introduced before physically building the system. There are a number of general purpose simulation packages

available which are capable of simulating most electronic systems at different levels. One group of simulation packages, such as SPICE, is capable of simulating the electronic systems at the circuit element level. However, such packages are not suitable for communication systems simulation because such usually a very large number of circuit element are required to represent the system. This means the computer simulation will be very complicated and the amount of data needed for system simulation is very large, as well as the computational time being very long.

There exists a high level simulation that is used to simulate the circuits at conceptual level rather than circuit element level. As a result, systems can be created using block diagrams, which represent typical circuits such as VCOs, filters, amplifiers and so on.

Throughout the development of this work, a general purpose high level system simulation package, called TESLA, was used to simulate the CPFWM system. TESLA does not have any restriction on the topology of the circuit, and it is capable of dealing with analogue and digital circuits. The system block definitions can be entered either with a text editor or schematic editor. The CPFWM modulator and demodulator are simulated by a number of blocks, each block is defined by its transfer function, while outputs are always calculated and displayed in the time domain, as shown in the next sections.

5.3.1 simulation of the CPFWM modulator

The CPFWM modulator block diagram, shown in Fig. 5.1, has been simulated using TESLA assuming a single tone modulation in both channels. The schematic diagram of the simulated CPFWM system is shown in Fig. 5.10 together with the values of

frequencies and voltages used. The first modulating signal is represented by a sinusoidal waveform followed by a voltage control oscillator to produce the FM signal as a VCM is not available in the TESLA library. The FM signal is then passed through a zero crossing detector to produce a SWFM waveform at node 3, see Fig. 5.10. The SWFM is then differentiated and then passed through a rectifier to produce PFM pulses at the rising edges only (node 4). A voltage clipper is then used to ensure that all pulses are at TTL level at node 6. As TESLA does not provide a triggered ramp generator, an integrator with a DC input voltage is used to provide the ramp. The integrator is reset by an inverted PFM pulse train (nodes 6 and 7). The second modulating signal is simulated by a sinusoidal oscillator (node 10) to which a DC voltage is added by a summer (node 12). Finally, the ramp signal (node 9) and the level shifted second modulating signal (node 12) are compared to produce the required CPFWM waveform (node 13).

Time domain simulation is carried out using a carrier frequency of 2 MHz. The first modulating signal frequency chosen was 170 kHz, while the second modulating frequency was 70 kHz, as these values are harmonically independent. Time domain results of the simulation as shown in Fig. 5.11 clearly show the CPFWM, ramp and the second modulating signal waveform.

5.3.2 simulation of the CPFWM receiver

The simulation of the CPFWM receiver is based on the block diagram shown in Fig. 5.6, while the schematic diagram of the TESLA simulation is shown in Fig. 5.12. The CPFWM pulses from the modulator output are first differentiated (node 14) and passed through a voltage clipper to ensure TTL level for all pulses. The positive pulses

(representing the PFM) are separated by a rectifier (node 16) and then used to initiate a ramp generator which is constructed from an integrator as in the previous section. The first modulating signal is then recovered from the ramp envelope using a low-pass filter as it is not possible to recover it from the PFM pulses directly. This is because the pulse width of the PFM impulses is almost zero, which makes the extraction of the message signal impossible (i.e. causes errors in running the program). On the other hand, the hold pulses are generated from the negative impulses of the incoming CPFWM waveform. As TESLA does not provide negative rectification, the impulses at node 15 are first shifted by 5 Volt, then passed through voltage clipper at 5 Volt to remove all positive spikes and to obtain the hold pulses (node 20). Finally the second modulating signal is reconstructed by sampling the ramp waveform (node 19) at the trailing edge pulses (node 20) and passing the samples through a low-pass filter as shown in Fig. 5.12.

The ramp waveform, hold pulses and the generated waveform at the output of the sample and hold amplifier are shown in Fig. 5.13. Figure 5.14 illustrates the recovered modulating signals, clearly showing that the system is capable of faithfully recovering the input information

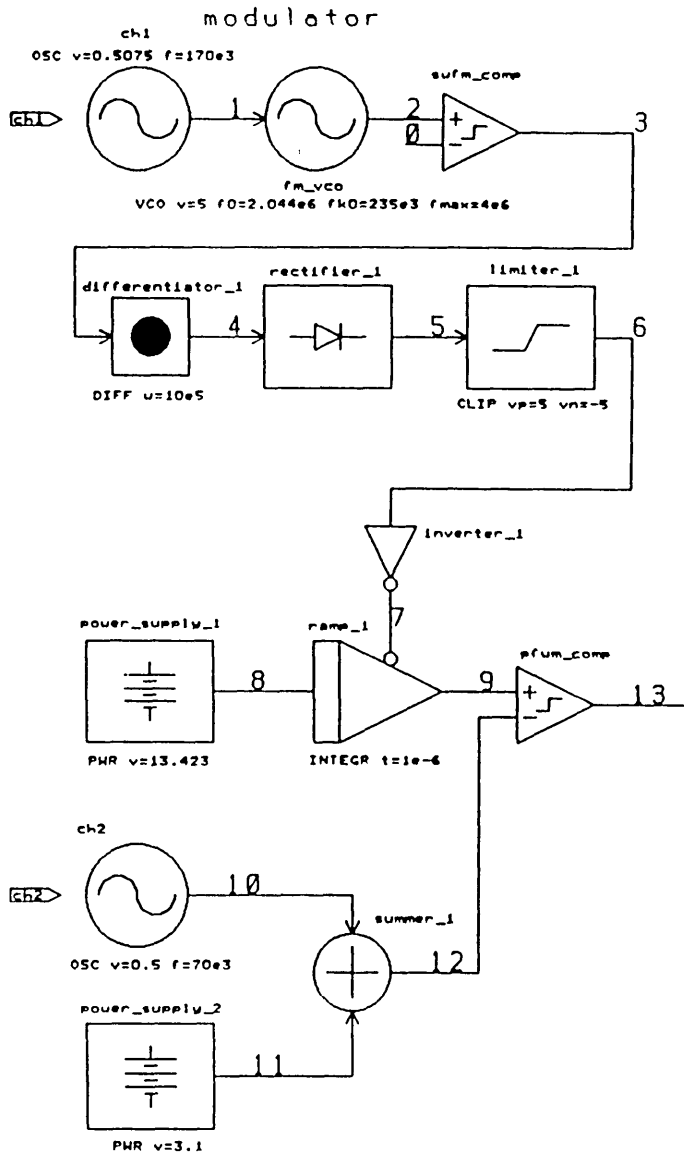


Fig. 5.10 CPFSK modulator block diagram.

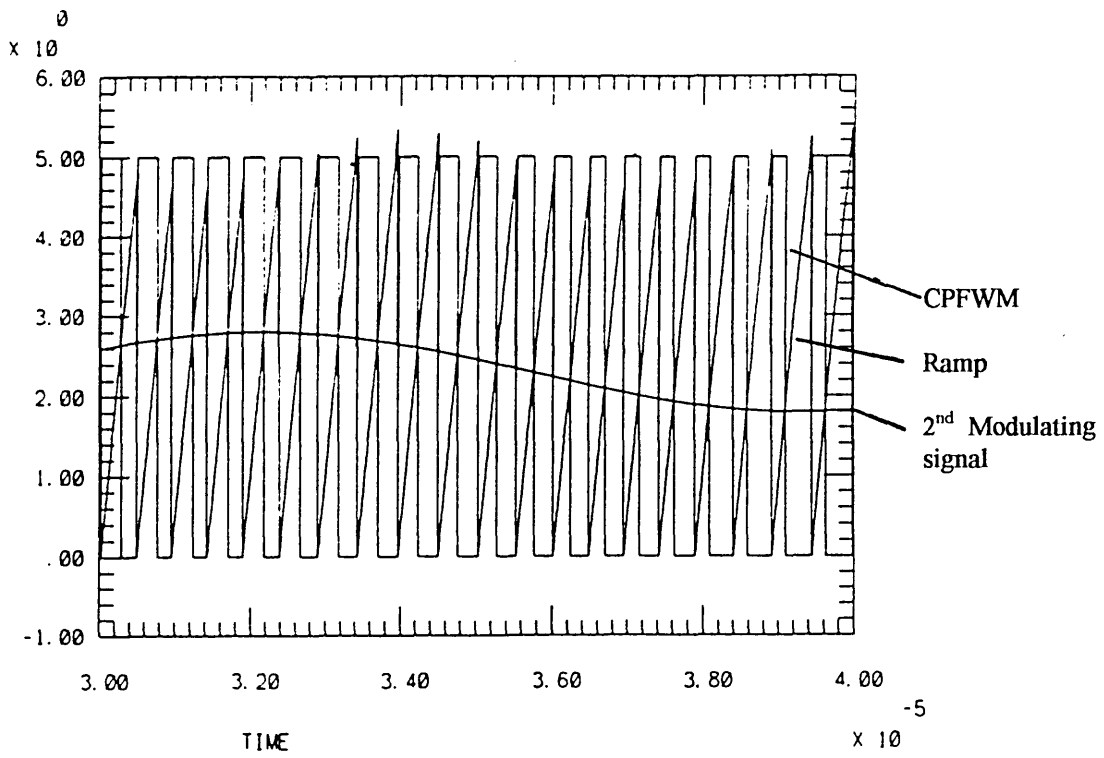


Fig. 5.11 Waveforms of the simulated CPFWM modulator.

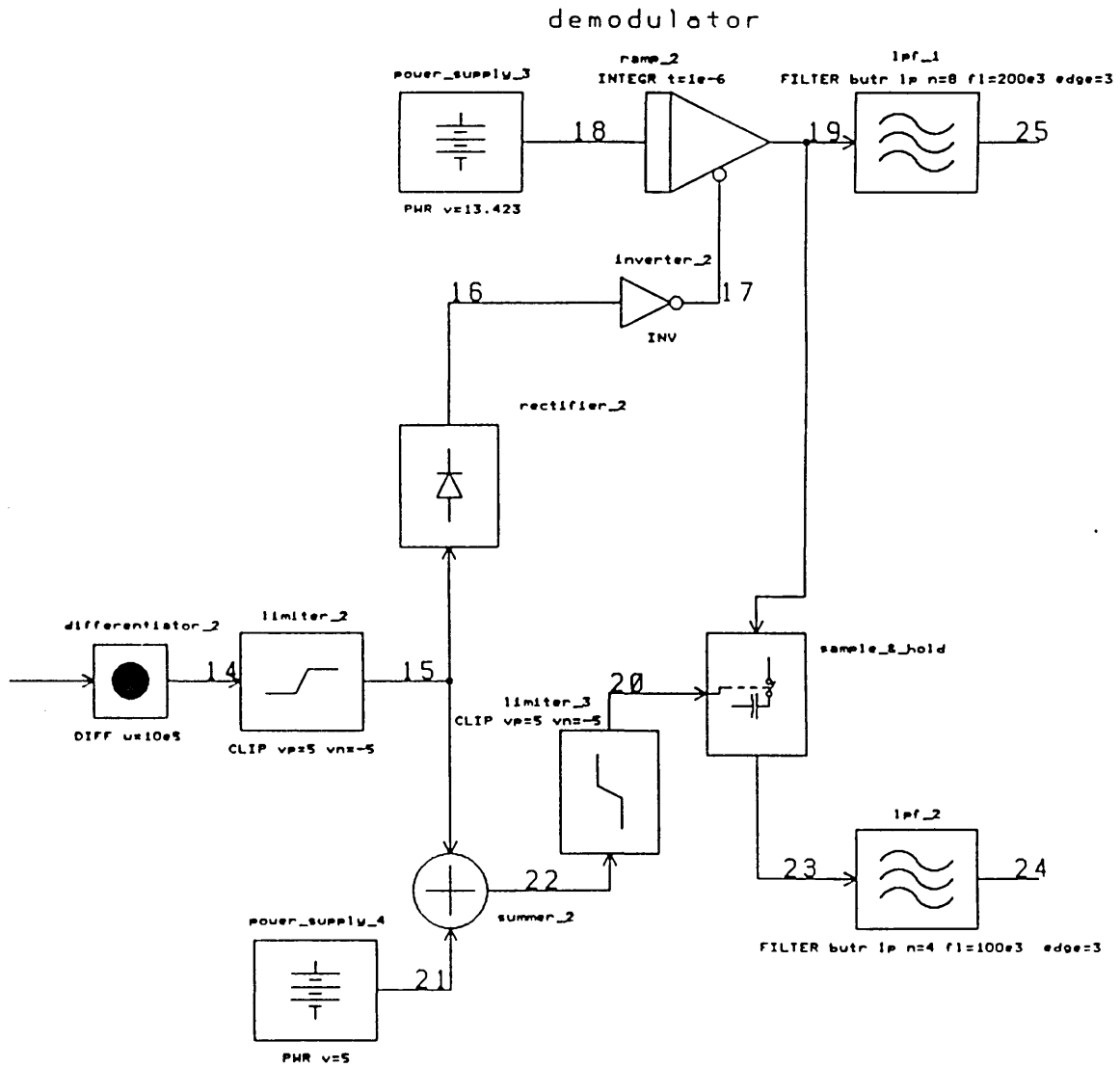


Fig. 5.12 Simulator block diagram of CPFWM demodulator.

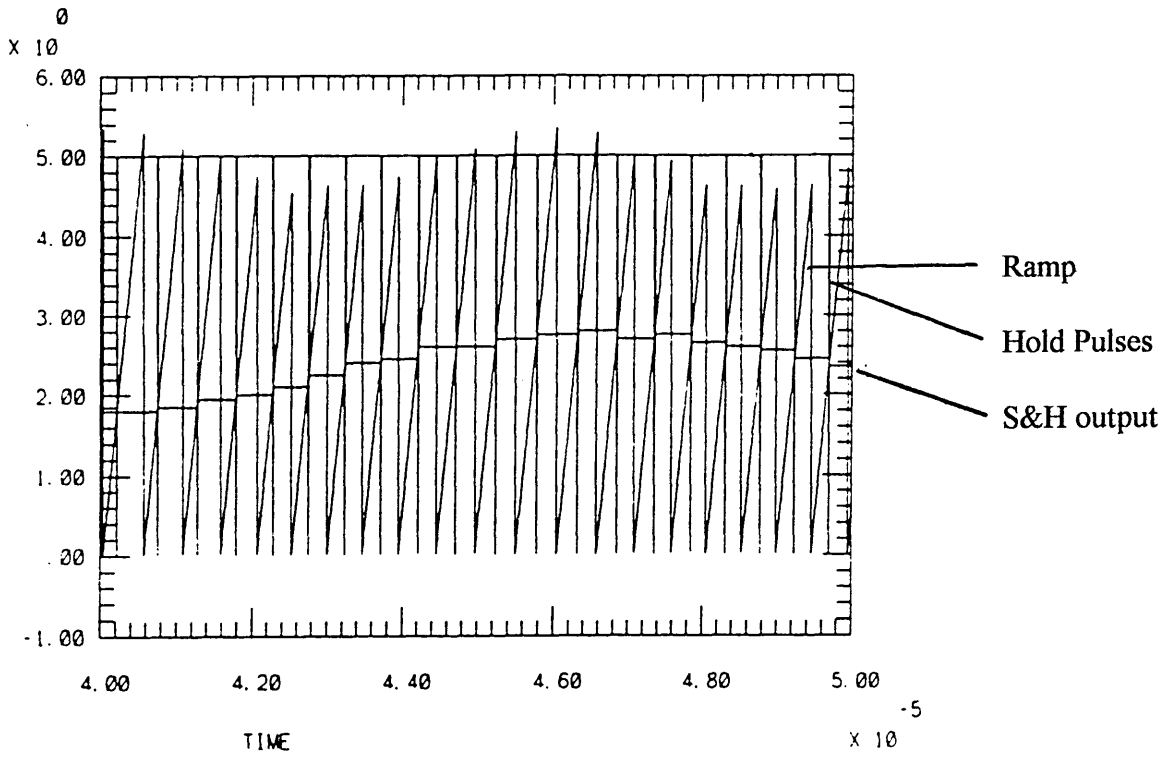


Fig. 5.13 Waveforms of CPFWM receiver.

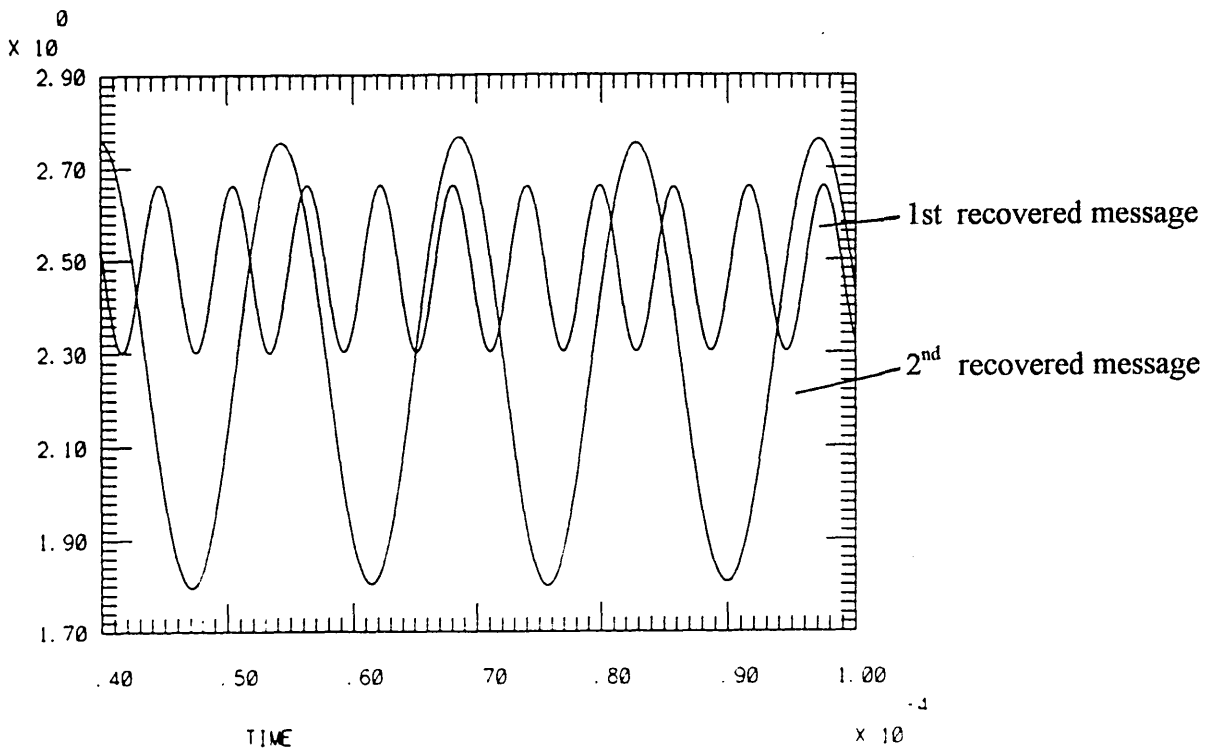


Fig. 5.14 Recovered modulating signals

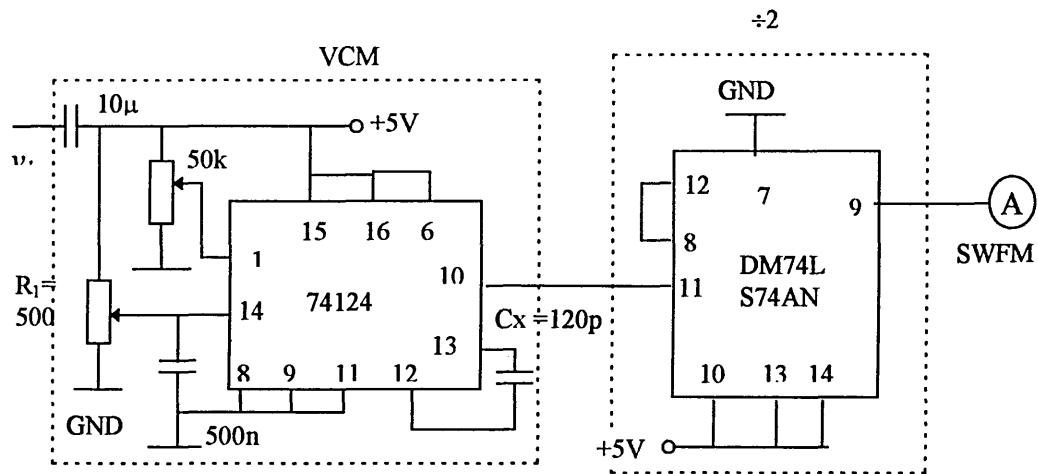
5.4 Experimental investigation of the CPFWM system

5.4.1 CPFWM modulator

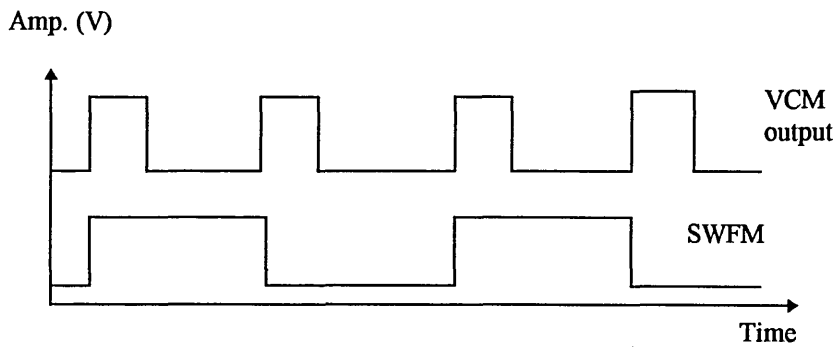
A low frequency experimental set-up for the CPFWM system has been built and tested. The CPFWM modulator is based on the block diagram given in Fig. 5.1 In this section the different elements of the modulator will be considered separately.

1. SWFM generation: The circuit diagram of the SWFM generator is shown in Fig. 5.15. An integrated circuit VCM is used to generate the SWFM waveform. The free running frequency of the VCM is given as $500/C_x$, where C_x is the external capacitance [68], see Fig. 5.15. The frequency can also be tuned by controlling the voltage at pin 14. However, the waveform generated is not a perfect squarewave, therefore a divide by two circuit is employed to resolve the problem. Thus the free running frequency of the VCM is 4 MHz, see Fig. 5.15-b for waveforms.

2. PFM pulses generation: PFM pulses are obtained by differentiating the SWFM. A simple RC differentiator is used followed by two NOT gates to re-shape the pulses. The circuit diagram and the waveforms of the differentiator are shown in Fig. 5.16. The values of the resistor and the capacitor are calculated for the free running frequency of the SWFM (i.e. 2 MHz). The pulse width of the output waveform of the differentiator will be the same as the fall time of the ramp. It must therefore kept as short as possible, the resistor R is chosen to be variable in order to minimise the pulse width of the PFM pulses.



(a)



(b)

Fig. 5.15 SWFM generator: (a) circuit diagram and (b) waveforms.

3. The ramp generator: The PFM pulses are used to initiate a ramp generator which consists of a constant current source to charge a capacitor. The capacitor is discharged through a transistor switch, see Fig. 5.17. The current mirror combination of Q1 and Q2 is used to construct a current source that provides a current of V_z/R , (where V_z is the zener diode voltage) which has been chosen to be 1 mA. The switching transistor Q3 is used to discharge the capacitor C. Finally, common collector transistor Q3 is used as a buffer.

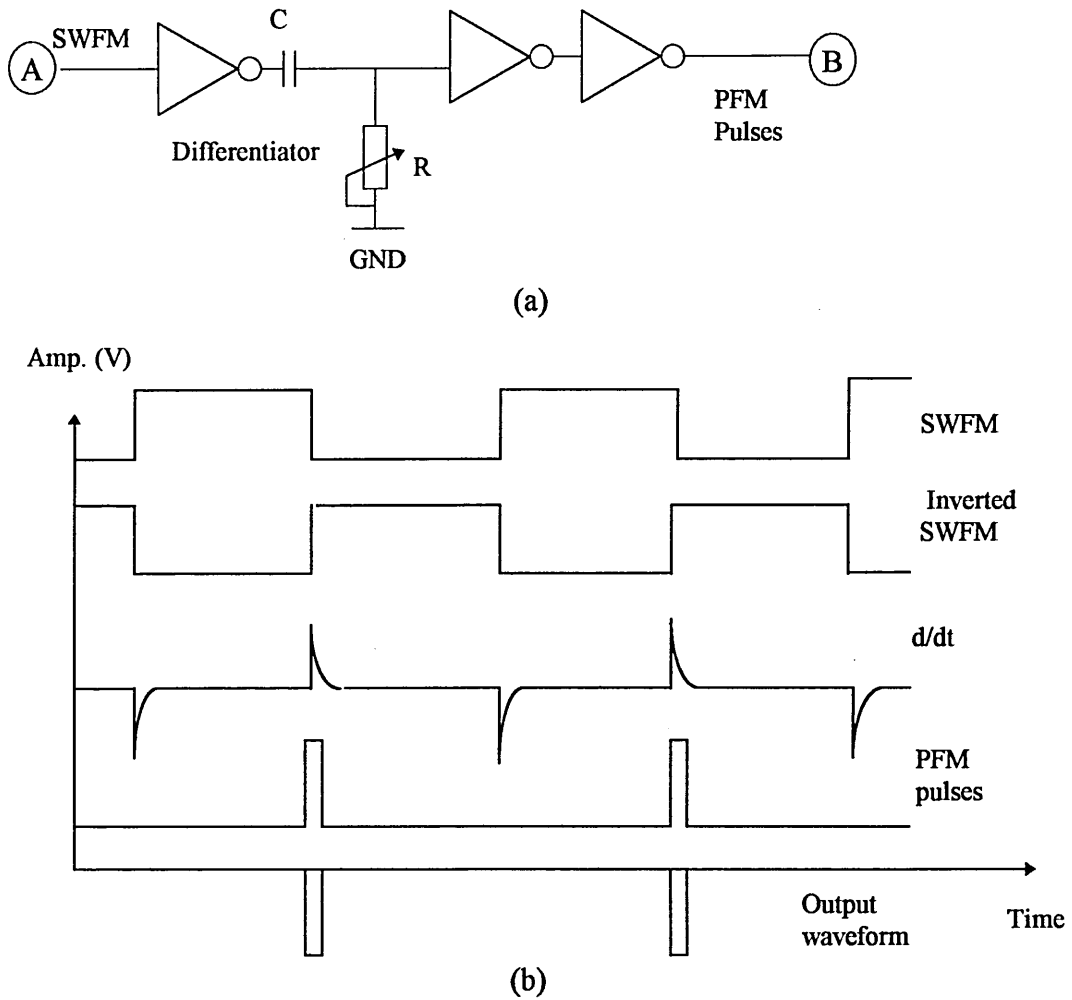


Fig. 5.16 SWFM pulses differentiation: (a) circuit diagram and (b) waveforms.

4. Voltage comparator : An integrated circuit analogue voltage comparator is used to compare the ramp voltage with the second modulating signal after DC shifting the latter. A simple passive adder circuit is used to shift the second modulating signal., see Fig. 5.18 for the circuit diagram. It should be noticed that the DC shifting in the second modulating signal is chosen to be half the minimum value of the ramp voltage when the frequency modulation index is a maximum. The output of the comparator is the required CPFWM waveform.

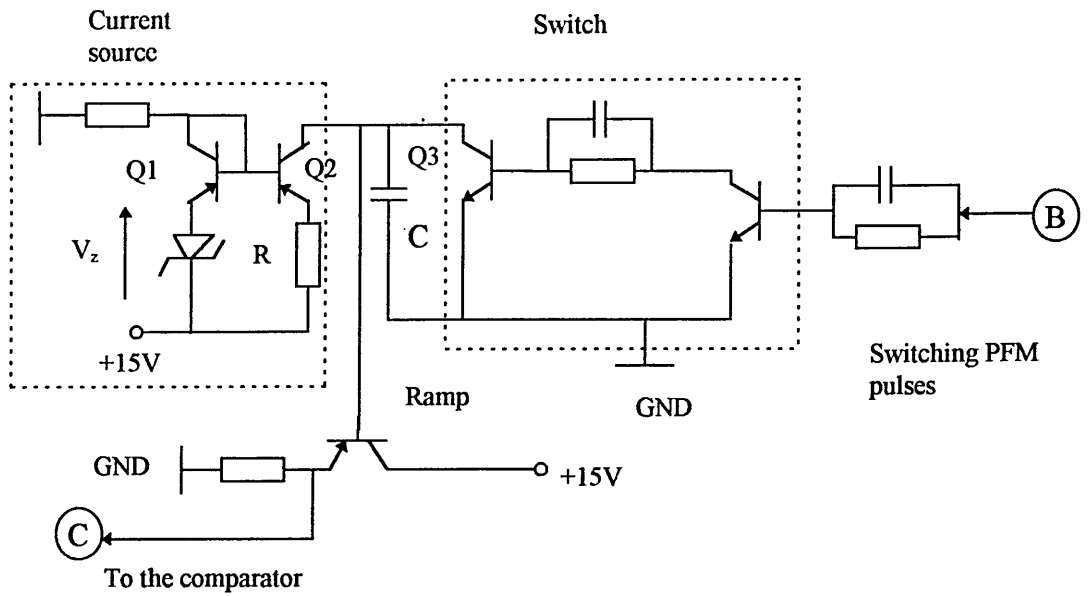


Fig. 5.17 Ramp generator.

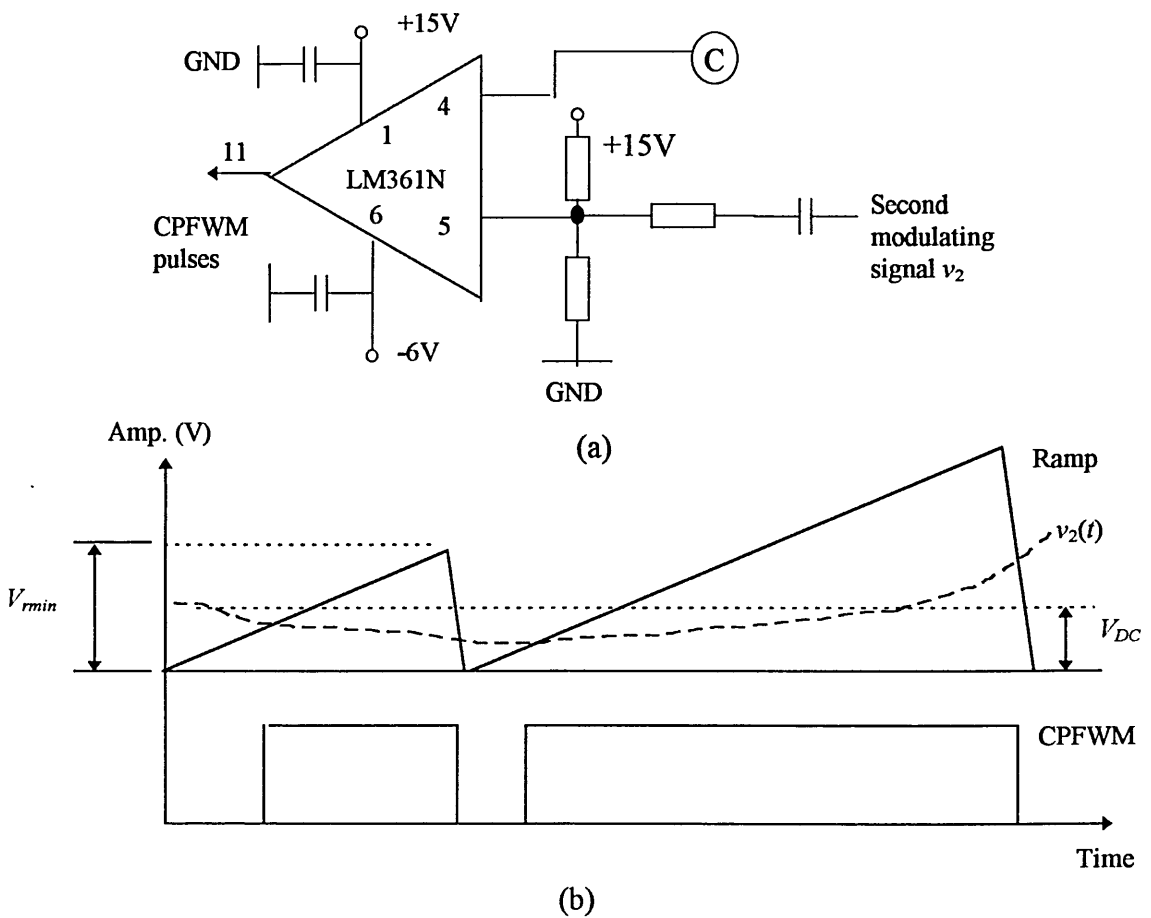


Fig. 5.18 Comparator: (a) circuit diagram and (b) waveforms.

5.4.2 CPFWM demodulator

The receiver has been built according to the principle explained in Fig. 5.6. The different sections of the receiver are explained individually as follows;

1. Edge separation and PFM demodulation: The received CPFWM pulses are first passed through an edge separation stage where the falling and the rising edges are completely separated. The rising edge contains the information carried by the first modulating signal, while the falling edge together with the rising edge are used to extract the information of the second modulating signal.

The circuit diagram of the edge separation technique used in this work is shown in Fig. 5.19. In this circuit, the resistor R is chosen to be variable to allow changing the pulse width of the regenerated PFM pulses. The regenerated PFM pulses are passed through a passive low pass filter, which has a bandwidth of 200 kHz, to extract the first message signal, see Fig. 5.19-b.

2. Ramp and sample and hold amplifier: The regenerated PFM pulses are used to initiate a ramp generator. The ramp used in the receiver is identical to that used in the transmitter side, see Fig. 5.17, to ensure using the same slope. On the other hand, the ramp is passed through a sample and hold amplifier, as shown in Fig. 5.20. The output of the sample and hold amplifier is passed through a passive fourth order low pass filter with a cut off frequency of 50 kHz to extract the second message.

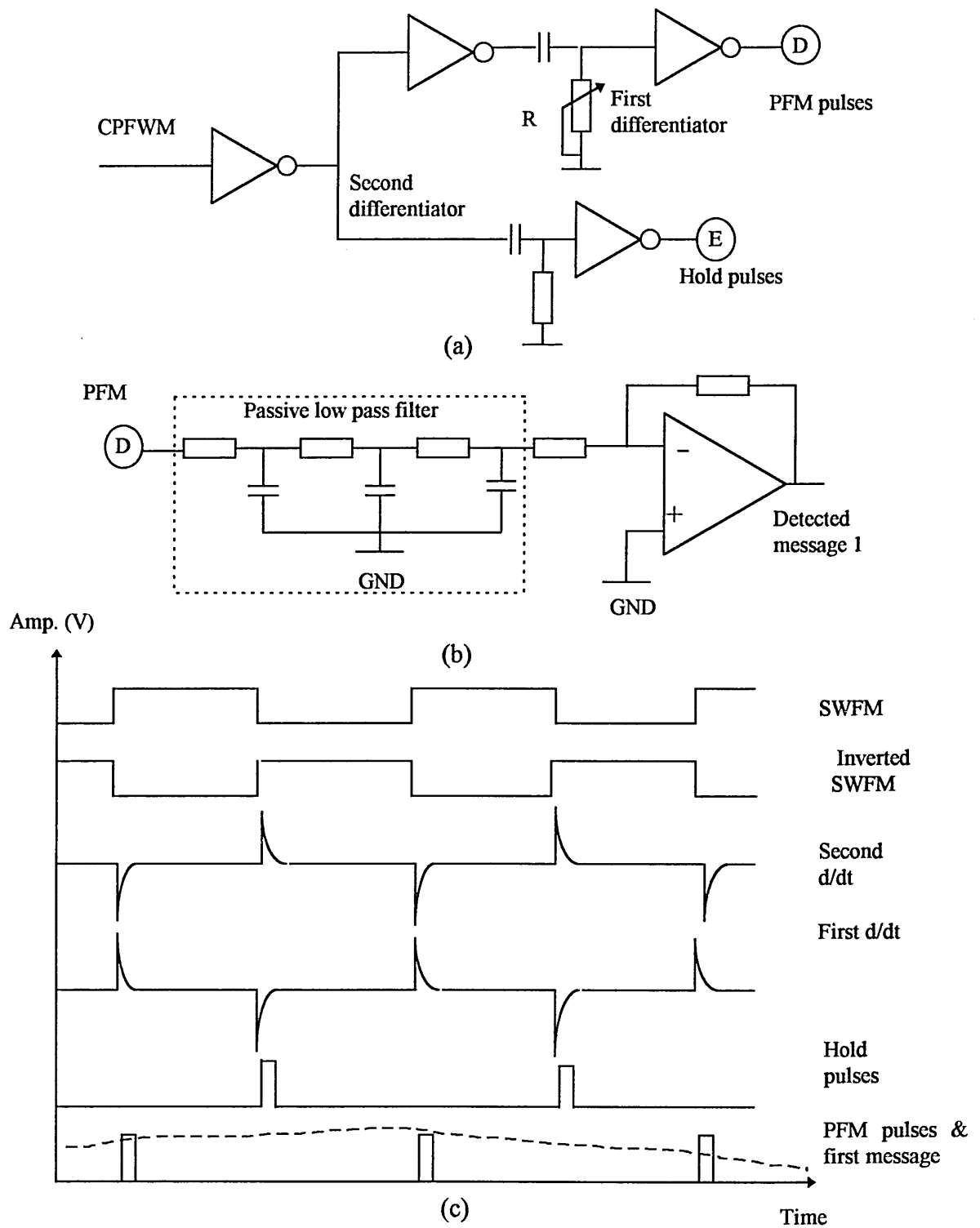


Fig. 5.19 Edge separation and PFM demodulation: (a) edge separation circuit diagram, (b) PFM demodulator and (c) waveforms.

5.4.3 Results

The circuit diagram of the CPFWM transmitter and receiver are shown in Figs. 5.21 and 5.22, respectively. The characteristics of the frequency modulator have been measured when the width modulation channel is off. The frequency at the comparator output (i.e. modulator output) is measured as a function of the first modulating signal level; for this purpose the capacitive coupling at the input of the VCM is removed then restored after the end of the test. The results are displayed in Fig. 5.23 together with the best linear curve fitting. This graph gives the linear dynamic range of the modulator, and the slope of the curve represents the sensitivity of the pulse frequency modulator (k). The modulation index of the pulse frequency modulation channel can then be evaluated from equation 5.6.

Similarly, the characteristics of the pulse width modulator are measured when the frequency modulation is off. The results are displayed in Fig. 5.24 together with the best linear curve fitting. The linear region of operation can be seen from Fig. 5.15, while the slope of the curve gives the sensitivity of the pulse width modulator (k_w). the modulation index of the width modulation channel can then be obtained as;

$$M = \frac{V_2 k_w}{\tau_o} \quad (5.21)$$

Waveforms at different nodes of the modulator circuit have been recorded in conditions when both modulating signals are present, when only the first modulating signal present, when only the second modulating signal is present and when both

modulating signals are absent. The wave forms are displayed in Figs. 5.25-5.28. It is clear that all the waveforms are in good agreement with the predicted waveforms and those obtained from computer simulation. Also, it can be seen that when the second modulating signal is absent, the modulator output represents a PFM waveform. However, when the first modulating signal is absent the output of the modulator is a PWM waveform, while when both modulating signals are present, the modulator output is a CPFWM waveform.

The waveforms at different points at the demodulator circuit have been recorded under different conditions; when both modulating signals are present, only the first modulating signal is present, only the second modulating signal is present and when both modulating signals are absent. The waveforms are displayed in Figs. 5.29-5.35. This shows that all the waveforms are in good agreement with the predicted waveforms and those obtained from computer simulation. Also, it can be seen that the two modulating signals are independently separated and detected.

A number of measurements has been taken to characterise the system distortion performance. The first measurements are displayed in Fig. 5.36 and show the relationship between the second harmonic distortion of the PWM channel with the variation of the CPFWM unmodulated duty cycle. The duty cycle has been changed by varying the DC level shift of the second modulating signal. Only the second harmonic of the PWM channel is considered as it is the most important harmonic component. The distortion at the PFM channel has not been shown as it was constant at about -45

dB. It can be noticed from this figure that the PWM channel shows flat distortion performance over the range of duty cycle between 0.4 to 0.55 of about - 40 dB.

Another set of measurements are shown in Figs. 5.37 and 5.38. these figures show the distortion characteristics of both channels as a function of the modulation index. It is clear that the PFM channel shows better distortion characteristics than the PWM. It should be mentioned that linearity of the current source is the most important factor in controlling the distortion at both channels. The second factor is the DC shift level of the second channel.

When comparing the resulting waveforms from the theoretical investigation which are shown in Figs. 5.2, 5.3, and 5.5 with those obtained from both the computer simulation as shown in Figs. 5.11 and 4.13- 5.14, and the recorded waveforms from the practical system which are shown in Figs. 5.25-5.36, it can be concluded that all the results from the theoretical analysis, practical implementation and computer simulation are in good agreement to each other. This confirms that the combination of the PFM and PWM schemes can be realised with simple circuitry. However, the separation of the compound scheme into its original components could also be carried out without synchronisation and using simple circuitry. The system performance is good and the system could be further improved if the ramp generators in both the receiver and the transmitter were designed to be identical and linear over the frequency of operation.

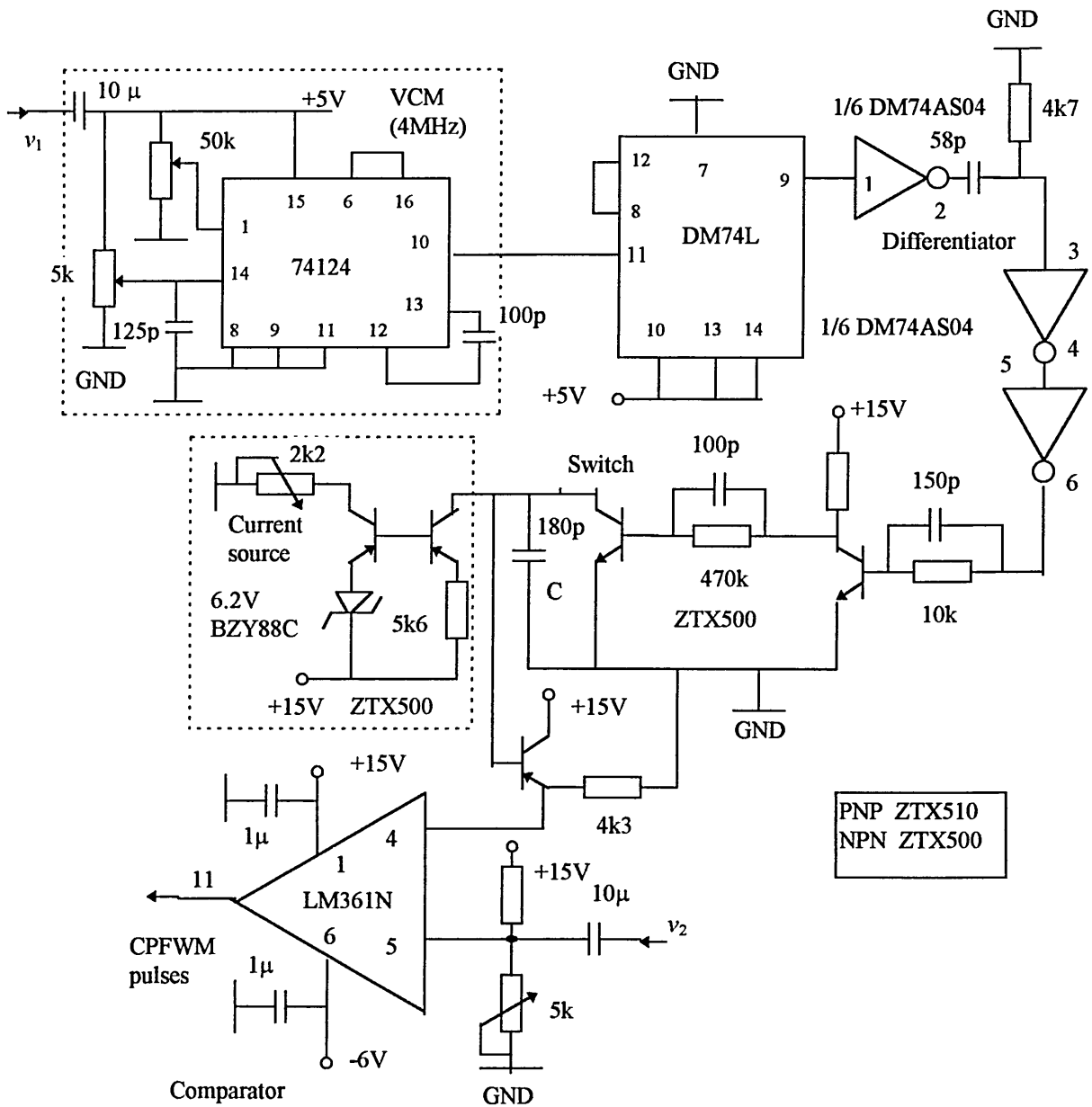


Fig. 5.21 Circuit diagram of the CPFWM modulator.

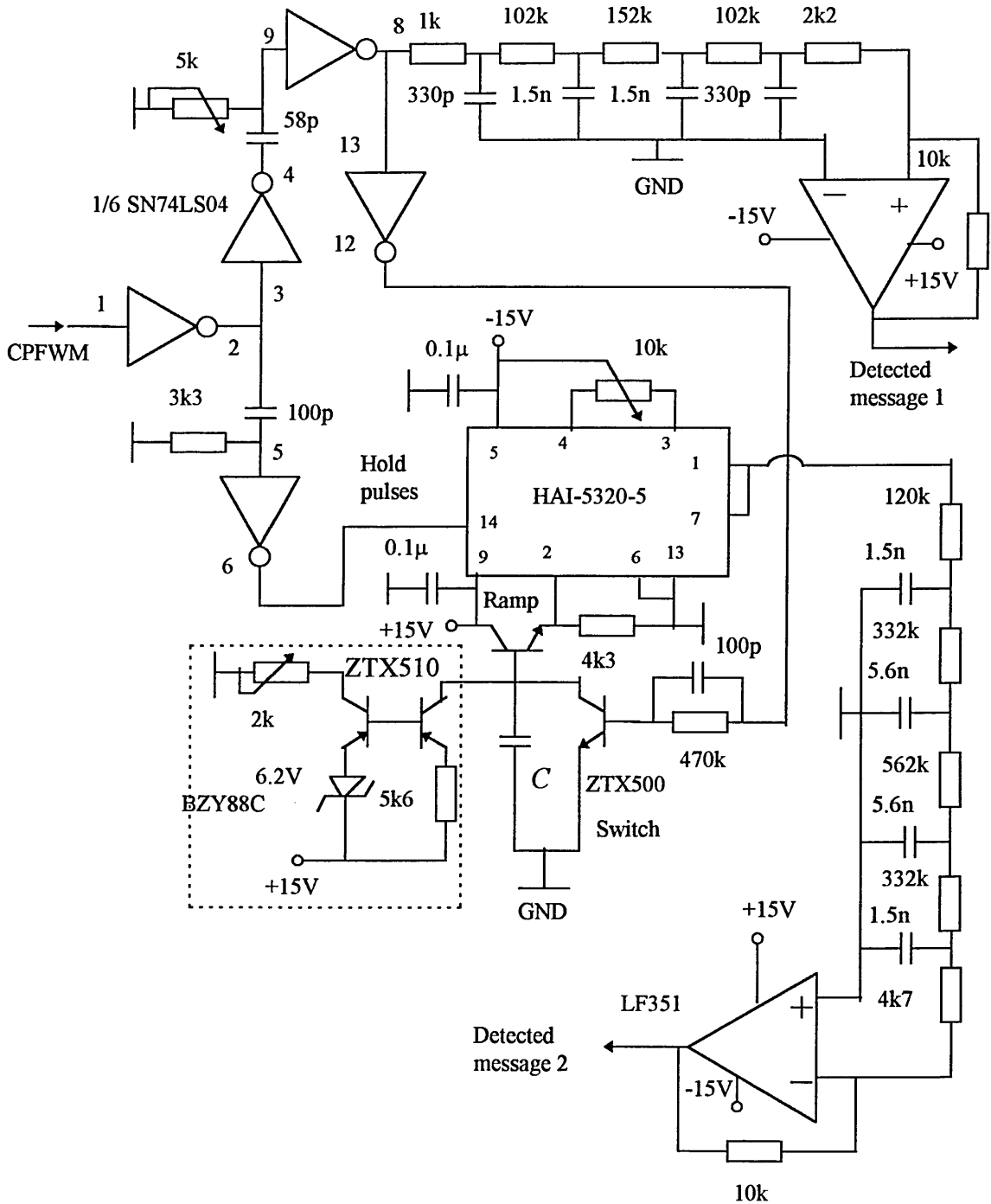


Fig. 5.22 Circuit diagram of the CPFWM demodulator.

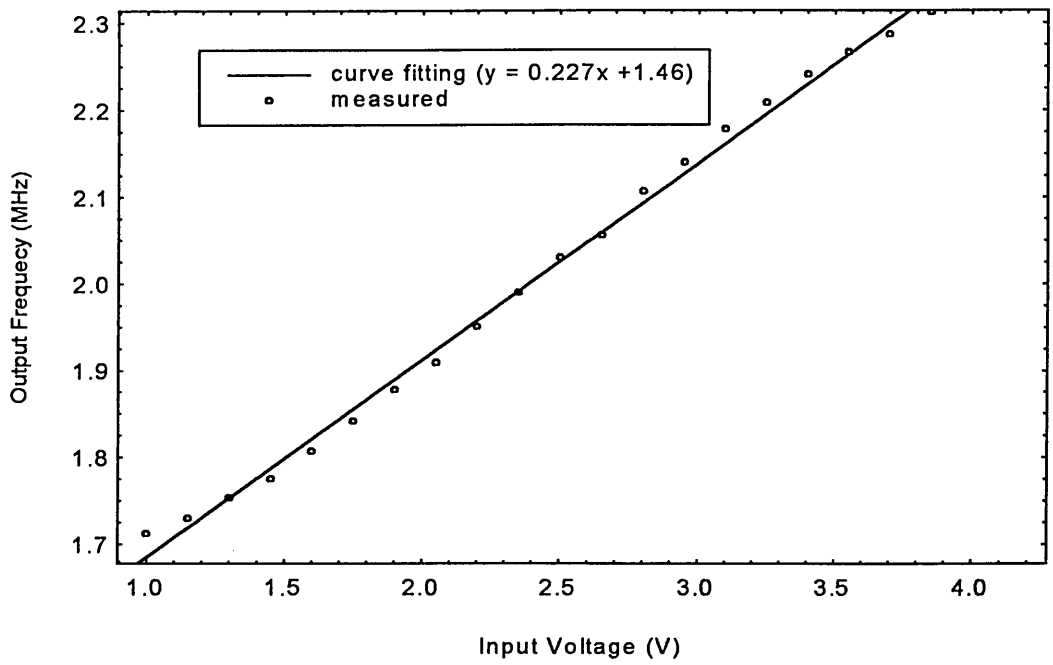


Fig. 5.23 Characteristics of the VCM.

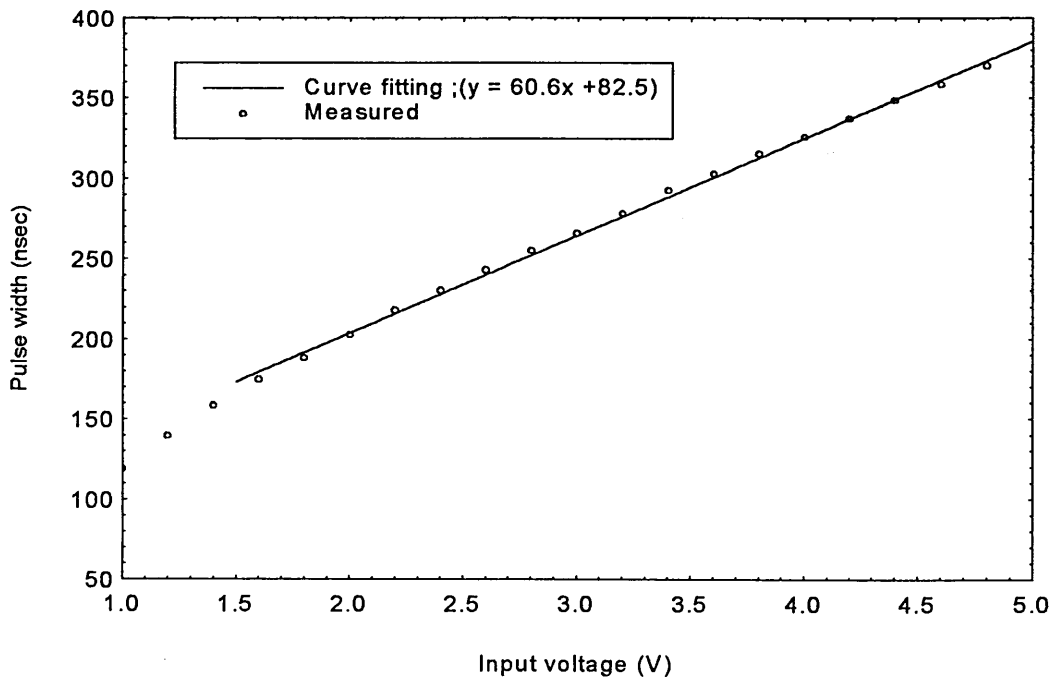


Fig. 5.24 Characteristics of the pulse width modulator (free running frequency = 2.04 MHz).

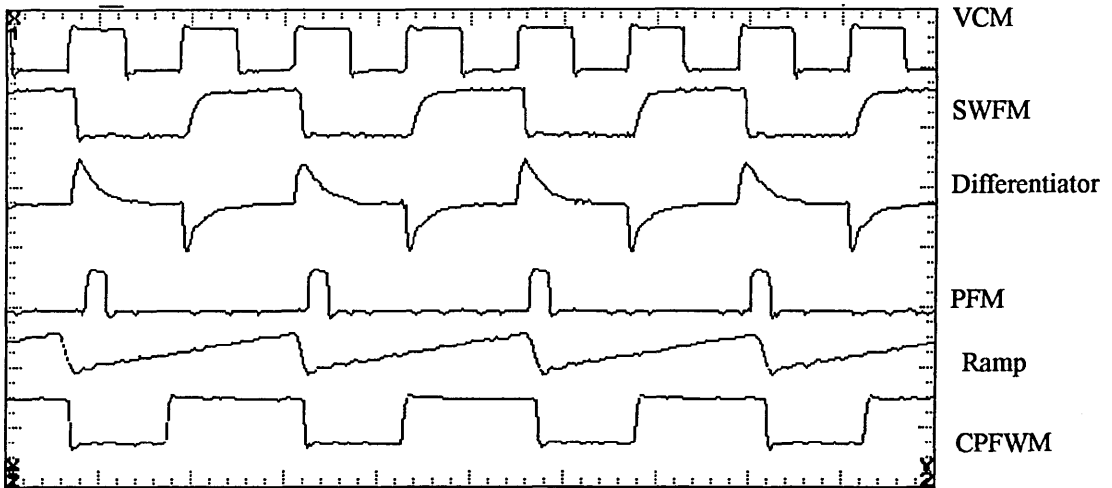


Fig. 5.25 Recorded waveforms at the CPFWM transmitter, when both modulating signals are absent (i.e. $M = \beta = 0$)

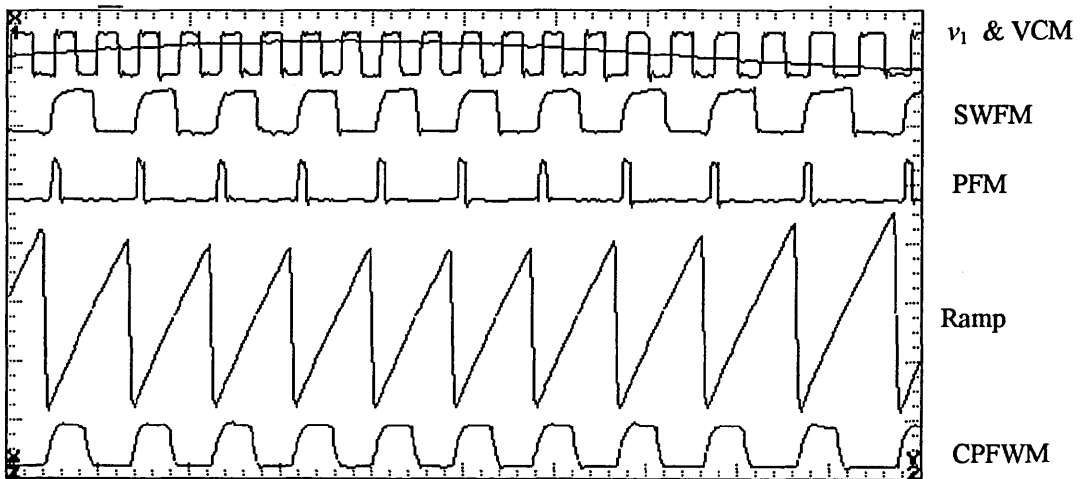


Fig. 5. 26 Recorded waveforms at the CPFWM, when $\beta = 1$ and $f_1 = 130$ kHz, and width modulation is absent ($M = 0$).

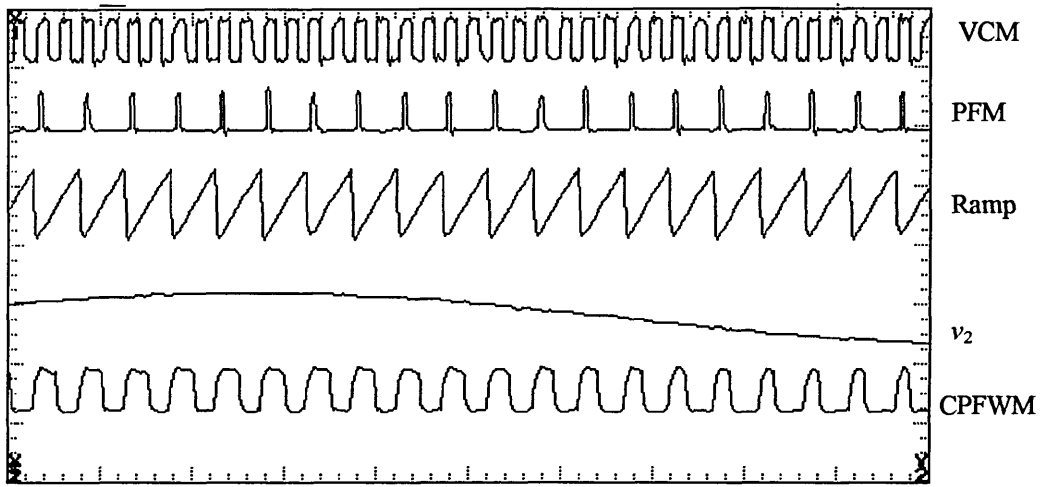


Fig. 5. 27 Recorded waveforms at the CPFWM, when $M = 15\%$ and $f_2 = 50$ kHz, and frequency modulation is absent ($\beta = 0$).

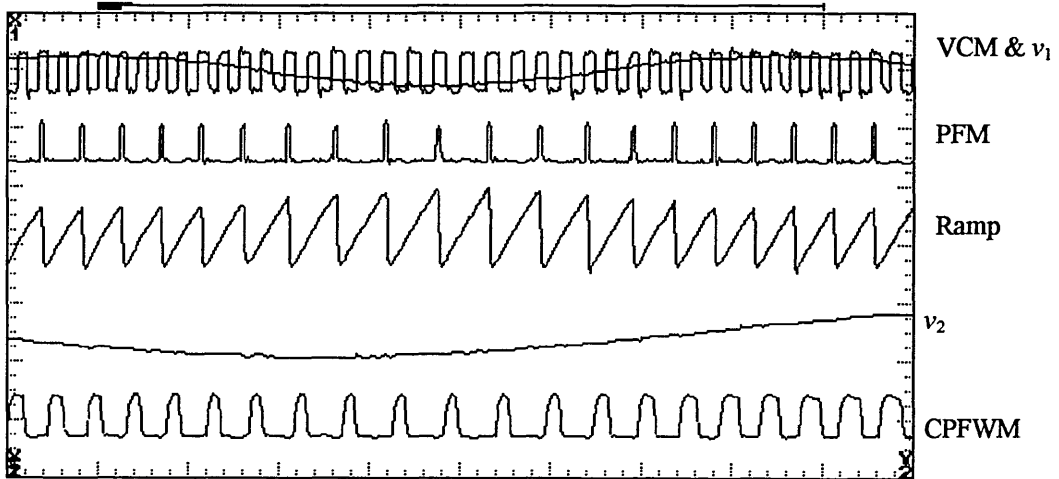


Fig. 5. 28 Recorded waveforms at the CPFWM, when both modulating signals are exist ($\beta = 1$, $M = 5\%$, $f_1 = 130$ kHz, $f_2 = 60$ kHz).

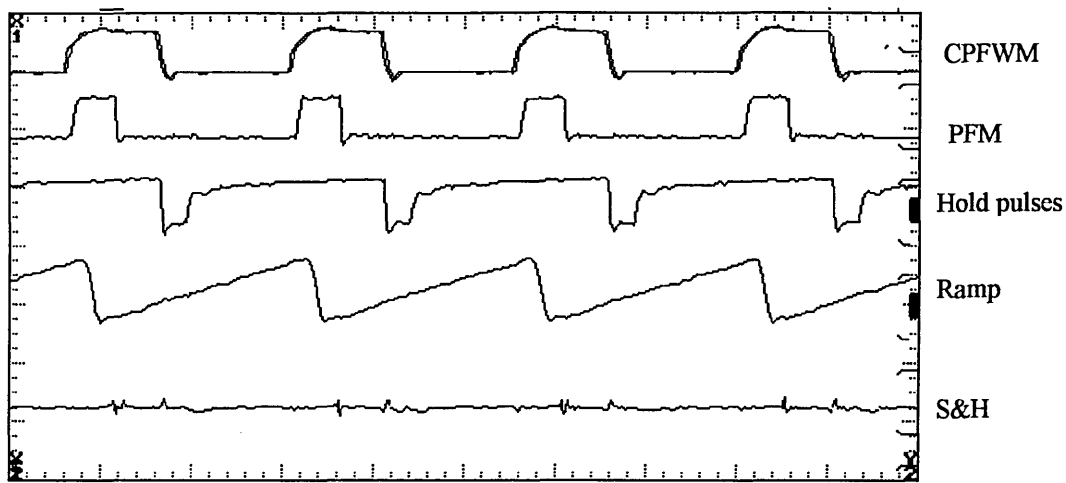


Fig. 5.29 Recorded waveforms at the receiver when both frequency and width modulations are absent ($\beta = M = 0$).

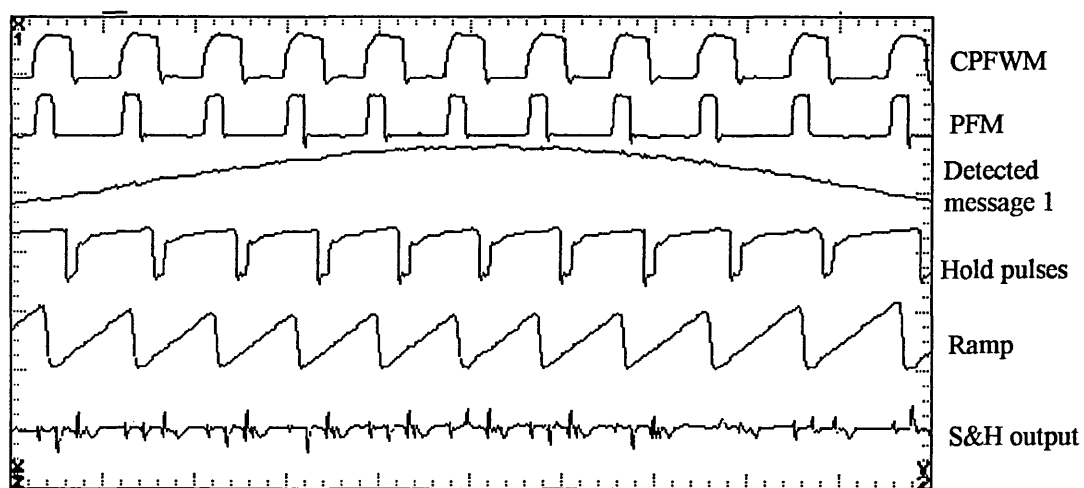


Fig 5. 30 Recorded waveforms at the receiver when width modulation is absent ($M = 0$), and $\beta = 1$, $f_i = 130\text{kHz}$.

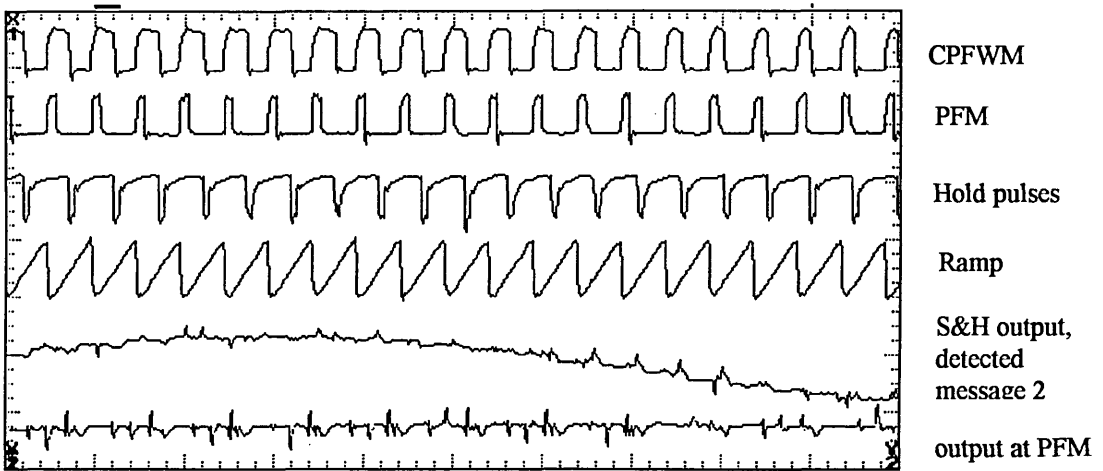


Fig 5. 31 Recorded waveforms at the receiver when frequency modulation is absent ($\beta = 0$), and, $M = 15\%$, $f_2 = 50$ kHz.

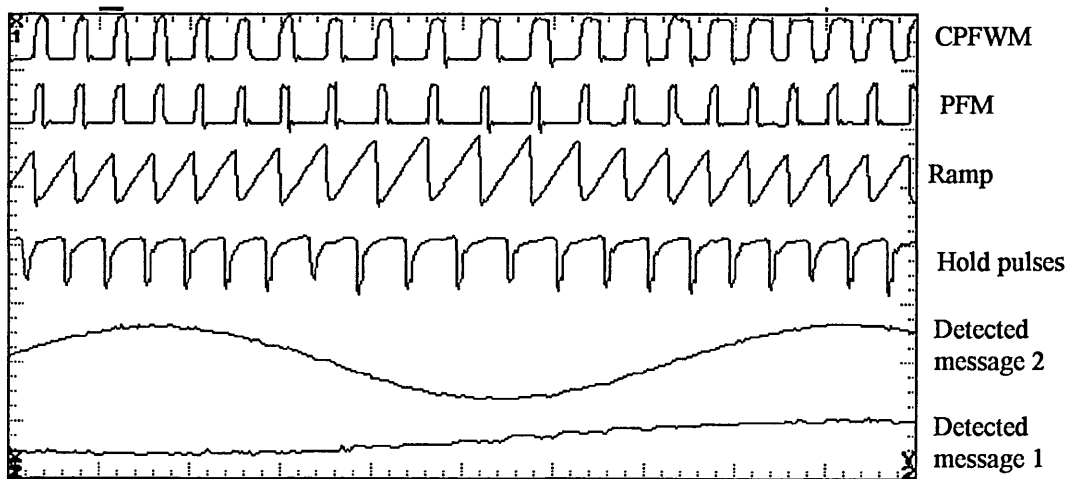


Fig 5. 32 Recorded waveforms at the receiver when both width frequency modulation and are exist, ($\beta = 1$, $M = 15\%$, $f_1 = 130$ kHz, and $f_2 = 60$ kHz).

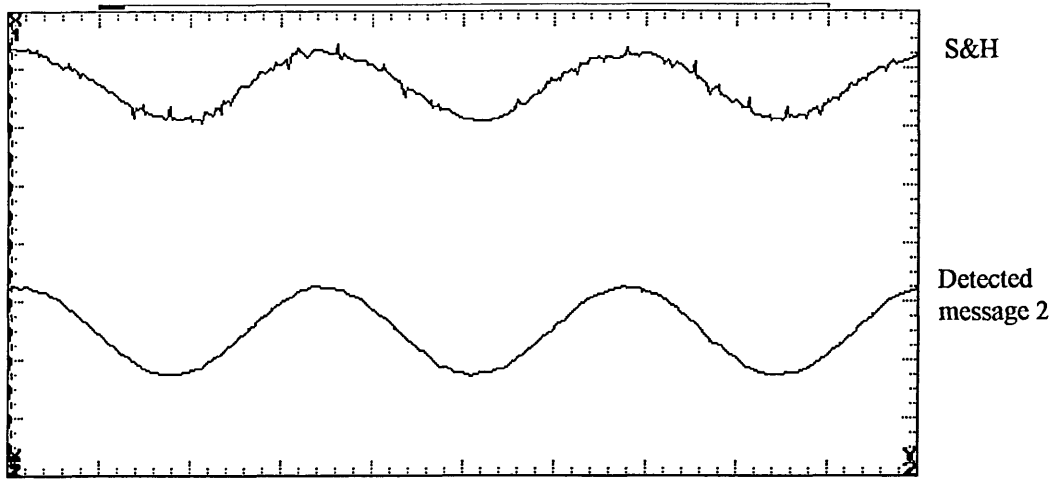


Fig. 5. 33 Recorded waveforms of the second detected message ($M = 15\%$, $\beta = 1$, $f_1 = 130$ kHz, $f_2 = 50$ kHz).

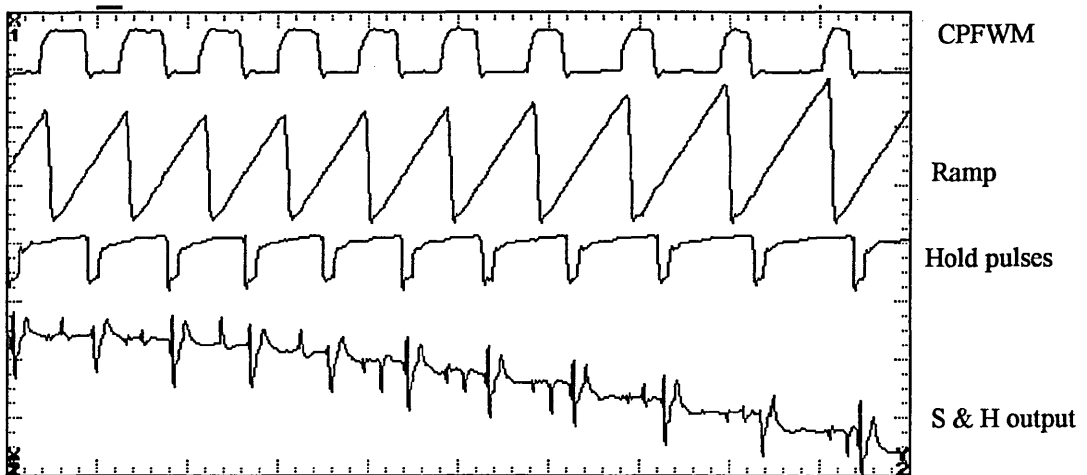


Fig. 5. 34 Recorded waveforms of the second channel demodulation (both modulation are exist, $M = 15\%$, $\beta = 1$, $f_1 = 130$ kHz, $f_2 = 50$ kHz).

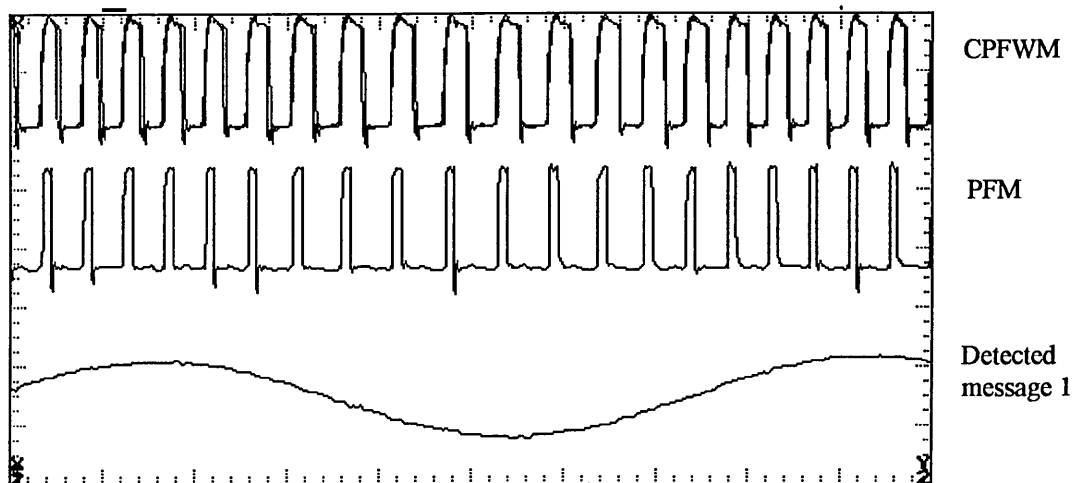


Fig. 5.35 Recorded waveforms of the first channel demodulation (both modulation are exist, $M = 15\%$, $\beta = 1$, $f_1 = 130 \text{ kHz}$, $f_2 = 50 \text{ kHz}$).

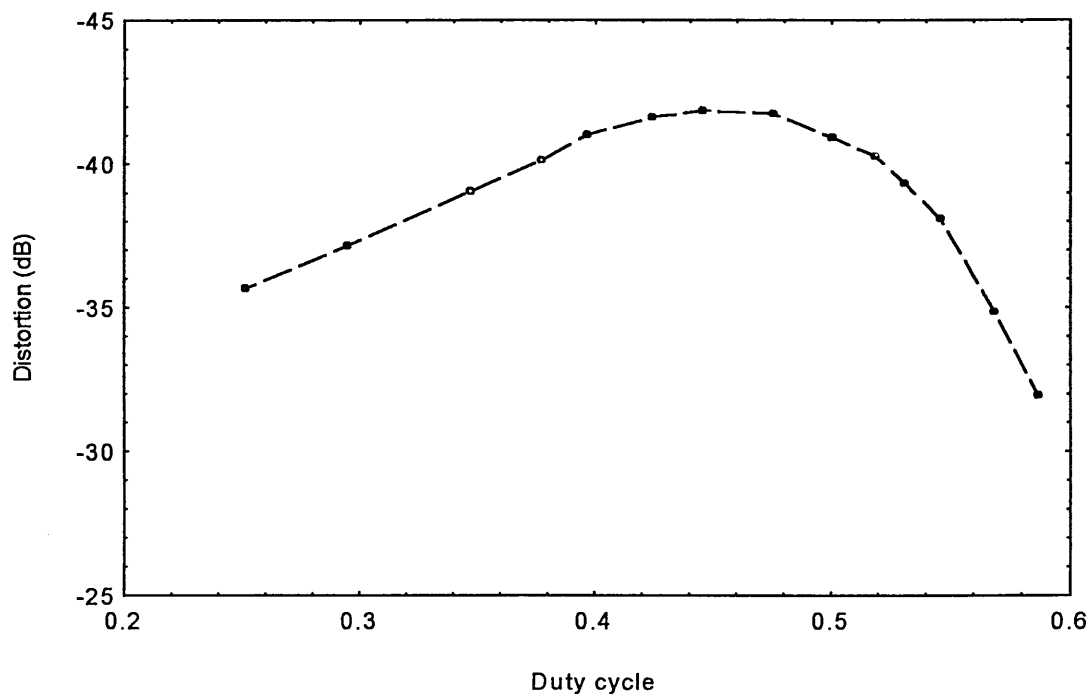


Fig. 5.36 Non-linear distortion in PWM channel as a function of duty cycle, $f_o = 1 \text{ MHz}$, $f_2 = 100 \text{ kHz}$, $M = 20\%$.

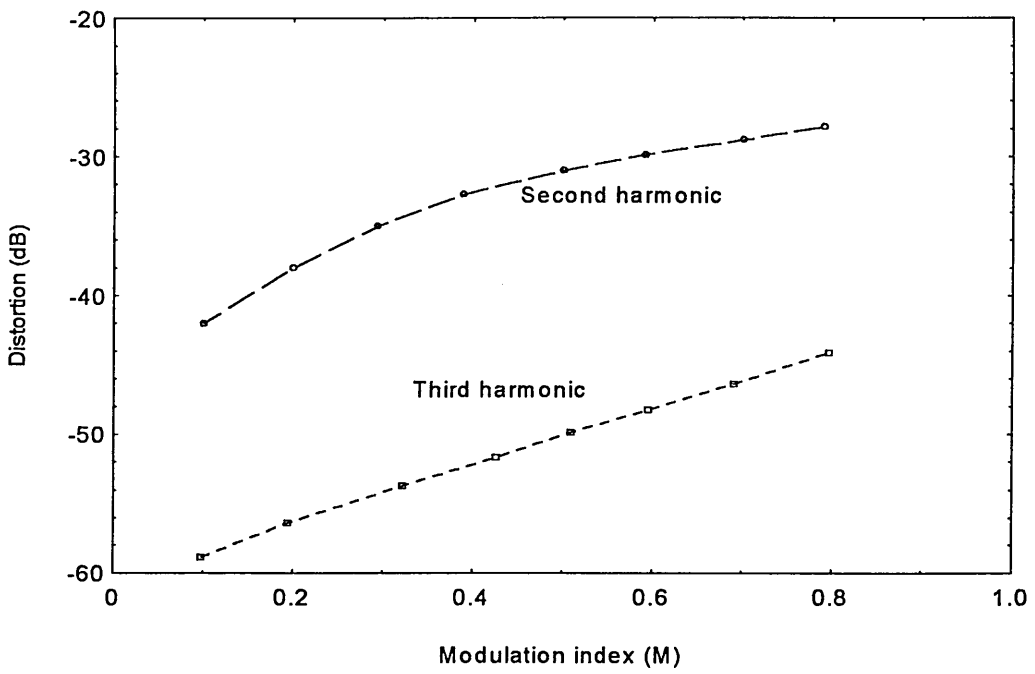


Fig. 5.37 Non-linear distortion in PWM channel, $f_o = 1$ MHz, $f_2 = 100$ kHz and 50% Duty cycle.

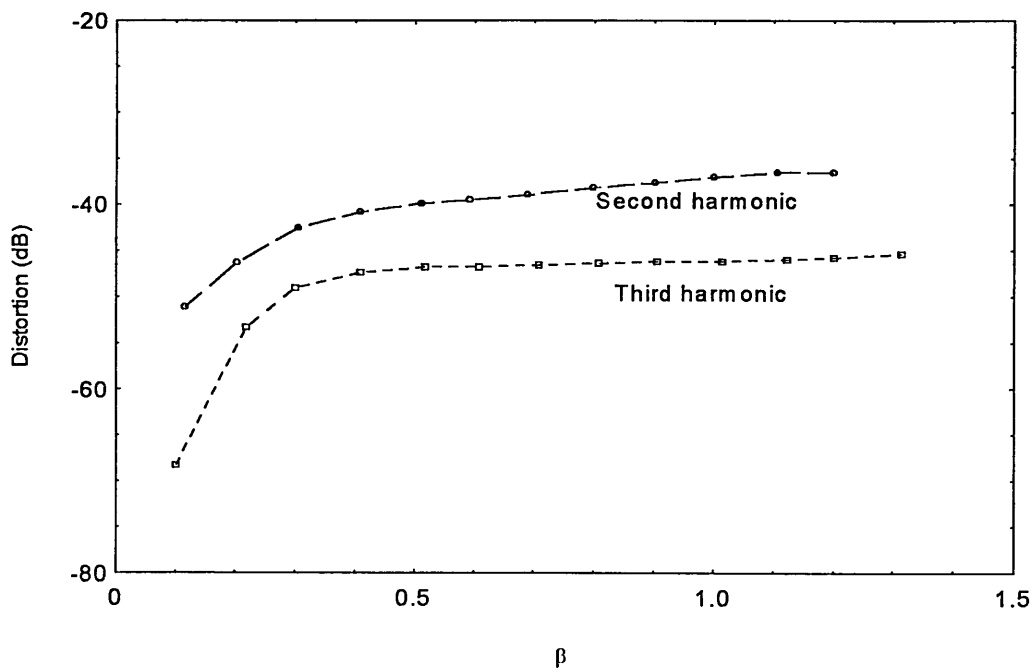


Fig. 5.38 Non-linear distortion in PFM channel, $f_o = 1$ MHz, $f_1 = 120$ kHz and 50% Duty cycle.

Chapter Six

Frequency spectrum of the CPFWM waveform

6.1 Introduction

The main advantages of using CPFWM techniques in wideband signal transmission are their effective bandwidth utilisation, and the ease of multiplexing and demultiplexing with very little cross-talk. These features make the CPFWM scheme attractive for many applications where transmission of wideband signals such as video, audio and high speed data are essential. However, to achieve the required performance, compromise between different factors governing the system implementation and performance is inevitable. One important factor is the transmission bandwidth, which should be minimised for the highest number of transmitted channels. Investigation of the efficiency of the bandwidth utility in CPFWM scheme is very important for future implementation, and for this reason, spectral investigation was carried out. So far only limited references have been made to the CPFWM modulation spectrum and were based on practical measurements only. In this chapter, a detailed theoretical analysis of the CPFWM modulation spectrum is reported. Computer simulation results together with experimental measurements are also presented and compared with the results obtained from newly derived mathematical expressions.

6.2 Theoretical analysis of CPFWM modulation spectrum

The modulation spectrum of CPFWM can be analysed by employing the same general approach introduced by Stuart [43]. According to this method, the CPFWM waveform can be considered as resulting from the integration of two modulated train of impulses of exactly the same repetition frequencies. The first train of impulses ($\delta_1(t)$), represents the rising edges of the CPFWM pulses, and is assumed to be frequency modulated by the first modulating signal. The second train of impulses, ($\delta_2(t)$), represents the trailing edges of CPFWM pulses, and is assumed to be; i) phase shifted by a constant value equal to the pulse width of CPFWM pulses when both modulating signals are off, ii) frequency modulated by the first modulating signal (like the first train of impulses) and iii) position modulated (phase modulated) by the second modulating signal, see Fig. 6.1. Throughout this analysis the amplitude of CPFWM is assumed equal to unity, also the modulating signals $v_1(t)$ and $v_2(t)$ are assumed to have unity amplitude (i.e. $|v_1(t)| \leq 1$ and $|v_2(t)| \leq 1$). However, gain factor could be introduced if needed.

Therefore, the CPFWM can be written as;

$$v(t) = \int_t [\delta_1(t) - \delta_2(t)] dt \quad (6.1)$$

The first train of impulses is frequency modulated by the first modulating signal, thus it can be written as;

$$\delta_1(t) = \sum_{n=-\infty}^{\infty} \frac{\omega_o + \Delta\omega v_1(t)}{2\pi} \exp\{jn[\omega_o t + \Delta\omega \int_t v_1(t) dt]\} \quad (6.2)$$

where, ω_o is the free running carrier frequency, and $\Delta\omega$ is the frequency deviation, while the second train of impulses may be written as;

$$\delta_2(t) = \sum_{n=-\infty}^{\infty} \frac{\omega_o - \Delta\phi \dot{v}_2(t) + \Delta\omega v_1(t - \tau)}{2\pi} \exp\{jn[\omega_o t - \omega_o \tau_o - \Delta\phi v_2(t) + \Delta\omega \int_{t-\tau}^t v_1(t) dt]\} \quad (6.3)$$

where

$$\tau = \tau_o + \frac{\Delta\phi}{\omega_o} v_2(t) \quad (6.3.a)$$

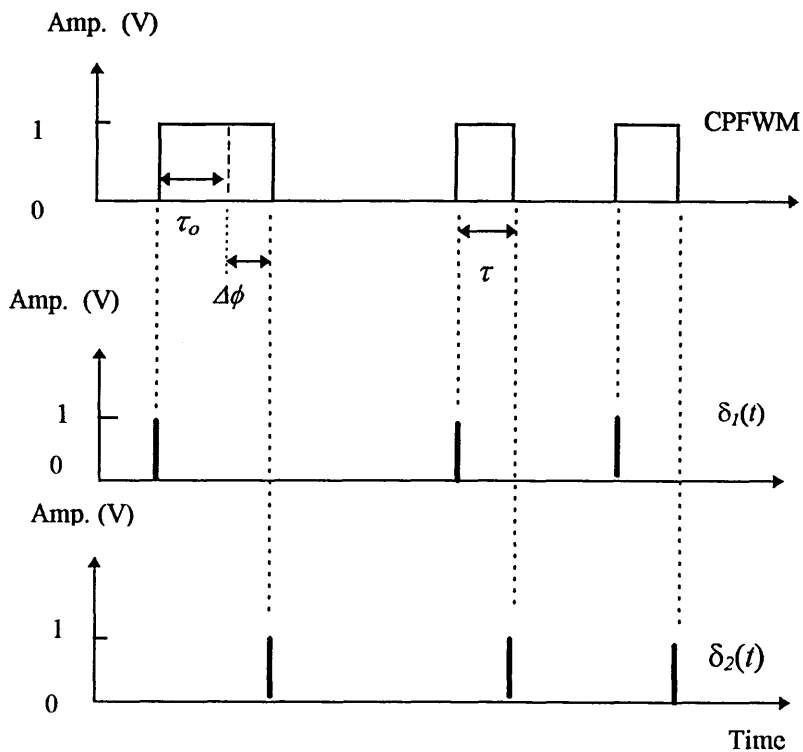


Fig. 6.1 CPFWM and impulse waveform.

τ_o is the pulse width when both modulating signals are off, $\Delta\phi$ is the maximum deviation in phase (position) and $\dot{v}_2(t)$ represents the time derivative of $v_2(t)$. Substituting equations 6.2 and 6.3 into equation 6.1, the CPFWM pulses can be written as;

$$v(t) = \sum_{n=-\infty}^{\infty} \frac{1}{2n\pi j} \left\{ \exp\{jn[\omega_o t + \Delta\omega \int v_1(t) dt]\} - \exp\{jn[\omega_o t - \omega_o \tau_o - \Delta\phi v_2(t) + \Delta\omega \int_{t-\tau}^{t-\tau_o} v_1(t) dt]\} \right\} \quad (6.4)$$

The above expression is a general exponential Fourier series representation of the CPFWM pulse train, which is applicable for any type of modulating signals.

Let us consider the following special cases;

a) When $v_1(t)$ is on and $v_2(t)$ is off: As shown in chapter five this is the case when the CPFWM waveform is reduced to a PFM pulse train. Substituting $v_2(t) = 0$ into equation 6.4 results in an expression for the given CPFWM waveform as;

$$v(t) = \sum_{n=-\infty}^{\infty} \frac{1}{2n\pi j} \left\{ \exp\{jn[\omega_o t + \Delta\omega \int v_1(t) dt]\} - \exp\{jn[\omega_o t + \Delta\omega \int_{t-\tau_o}^{t-\tau_o} v_1(t) dt]\} \right\} \quad (6.5)$$

Equation 6.5 is identical to an expression for PFM pulses given in the literature [61].

b) When $v_2(t)$ is on and $v_1(t)$ is off: This case represents pulse width modulation, as shown in chapter five. Substituting $v_1(t) = 0$ into equation 6.4, results in an expression for the PWM waveform similar to those reported in the literature [61];

$$v(t) = \sum_{n=-\infty}^{\infty} \frac{1}{2n\pi j} \left\{ \exp\{jn\omega_o t\} - \exp\{jn[\omega_o t - \omega_o \tau_o - \Delta\phi v_2(t)]\} \right\} \quad (6.6)$$

The modulation spectrum of CPFWM signal can be predicted from equation 6.4. It is far more complex to predict the modulation spectrum of the CPFWM waveform when employing a general modulating signal, and for this reason we have considered the case when both modulating signals are single tone sinusoidal modulation given as;

$$\left. \begin{array}{l} v_1(t) = \cos \omega_1 t \\ \text{and} \\ v_2(t) = \sin \omega_2 t \end{array} \right\} \quad (6.7)$$

where ω_1 and ω_2 are the frequencies of the first and the second modulating signals, respectively. Substituting equation 6.7 into equation 6.4, the CPFWM waveform can be rewritten as;

$$v(t) = \sum_{n=-\infty}^{\infty} \frac{e^{jn\omega_o t}}{2n\pi j} \left\{ \exp[jn\beta \sin \omega_1 t] - \exp\left\{-jn\left[\omega_o \tau_o + 2\pi M \sin \omega_2 t - \beta \sin \omega_1 \left(t - \tau_o - \frac{2\pi M}{\omega_o} \sin \omega_2 t\right)\right]\right\} \right\} \quad (6.8)$$

where β is the frequency modulation index, $\beta = \Delta\omega/\omega_1$ and M is the pulse width modulation index, where, $M = \Delta\phi/2\pi$. Equation 6.8 gives the modulation spectrum of

the CPFWM waveform in exponential series representation which can be further simplified by using the following series expansion;

$$e^{ja \sin x} = \sum_{k=-\infty}^{\infty} J_k(a) e^{jkx} \quad (6.9)$$

where, $J_k(x)$ is the Bessel function of order k and first kind. Substituting equation 6.9 into equation 6.8 yields in;

$$v(t) = \sum_{n=-\infty}^{\infty} \sum_{k=-\infty}^{\infty} \frac{J_k(n\beta) e^{j(n\omega_c + k\omega_1)t}}{2n\pi j} \left\{ 1 - e^{-j[(n\omega_o + k\omega_1) \frac{2\pi M}{\omega_o} \sin \omega_2 t + (n\omega_o + k\omega_1) \tau_o]} \right\} \quad (6.10)$$

The trigonometric term in equation 6.10 can also be converted into exponential form using equation 6.9. This leads to;

$$v(t) = \sum_{n=-\infty}^{\infty} \sum_{k=-\infty}^{\infty} \frac{J_k(n\beta) e^{j(n\omega_o + k\omega_1)t}}{2n\pi j} \times \left\{ 1 - \sum_{p=-\infty}^{\infty} (-1)^p J_p \left(2n\pi M + 2k\pi M \frac{\omega_1}{\omega_o} \right) \exp \left\{ -j[(n\omega_o + k\omega_1) \tau_o + jp\omega_2 t] \right\} \right\} \quad (6.11)$$

Using equation 6.8 (or 6.10 or 6.11) the low frequency components of the CPFWM waveform are evaluated when $n \rightarrow 0$. A full derivation is presented in Appendix I, as;

$$\begin{aligned}
\text{Baseband Frequency Components} &= \lim_{n \rightarrow 0} v(t) \\
&= \frac{\omega_o \tau_o}{2\pi} + M \sin \omega_2 t + \frac{\beta}{2\pi} \left\{ \sin \omega_1 t - \sum_{m=-\infty}^{\infty} J_m \left(2\pi M \frac{\omega_1}{\omega_o} \right) \sin [(\omega_1 - m\omega_2)t - \omega_1 \tau_o] \right\}
\end{aligned} \tag{6.12}$$

Therefore, equation 6.11 can be rewritten as;

$$\begin{aligned}
v(t) &= \frac{\omega_o \tau_o}{2\pi} + M \sin \omega_2 t + \frac{\beta}{2\pi} \left\{ \sin \omega_1 t - \sum_{m=-\infty}^{\infty} J_m \left(2\pi M \frac{\omega_1}{\omega_o} \right) \sin [(\omega_1 - m\omega_2)t - \omega_1 \tau_o] \right\} \\
&+ \sum_{\substack{n=-\infty \\ n \neq 0}}^{\infty} \sum_{k=-\infty}^{\infty} \frac{J_k(n\beta) e^{j(n\omega_o + k\omega_1)t}}{2n\pi j} \times \\
&\quad \left\{ 1 - \sum_{p=-\infty}^{\infty} (-1)^p J_p \left(2\pi M + 2k\pi M \frac{\omega_1}{\omega_o} \right) \exp \left\{ -j \left[(n\omega_o + k\omega_1)\tau_o + jp\omega_2 t \right] \right\} \right\}
\end{aligned} \tag{6.13}$$

The last term in equation 6.13 can be further simplified, see Appendix II, by using the properties of Bessel functions and exponential series and applying other mathematical manipulation the result is given in equation II.20. The time domain representation of the CPFWM waveform is then obtained by substituting equation II.20 into 6.13 as;

$$\begin{aligned}
v(t) &= \frac{\omega_o \tau_o}{2\pi} + M \sin \omega_2 t + \frac{\beta}{2\pi} \sin \omega_1 t - \frac{\beta}{2\pi} \sum_{m=-\infty}^{\infty} J_m \left(2\pi M \frac{\omega_1}{\omega_o} \right) \sin [(\omega_1 - m\omega_2)t - \omega_1 \tau_o] \\
&+ \sum_{n=1}^{\infty} \sum_{k=-\infty}^{\infty} \frac{J_k(n\beta)}{n\pi} \left\{ \sin(n\omega_o + k\omega_1)t - J_o \left[2\pi M \left(n + k \frac{\omega_1}{\omega_o} \right) \right] \sin(n\omega_o + k\omega_1)(t - \tau_o) \right\} \\
&- \sum_{n=1}^{\infty} \sum_{\substack{k=-\infty \\ k \neq 0}}^{\infty} \sum_{\substack{p=-\infty \\ p \neq 0}}^{\infty} \frac{J_k(n\beta)}{n\pi} J_p \left[2\pi M \left(n + k \frac{\omega_1}{\omega_o} \right) \right] \sin[(n\omega_o + k\omega_1 - p\omega_2)t - (n\omega_o + k\omega_1)\tau_o]
\end{aligned} \tag{6.14}$$

In the above equation, the carrier frequency component and its harmonics can be extracted by $k=0$, and $p=0$ into the fourth and the fifth term of equation 6.14, this leads to;

$$\text{Components (at } n\omega_o) = \sum_{n=1}^{\infty} \frac{J_o(n\beta)}{n\pi} \left\{ \sin n\omega_o t - 2J_o\left(2\pi M \frac{\omega_1}{\omega_o}\right) \sin[n\omega_o(t - \tau_o)] \right\} \quad (6.15)$$

The other frequency components can be obtained by substituting the appropriate values of n , k , and p into the last two terms of equation 6.14. Therefore, equation 6.14 can be rewritten as;

$$\begin{aligned} v(t) = & \frac{\omega_o \tau_o}{2\pi} + M \sin \omega_2 t + \frac{\beta}{2\pi} \sin \omega_1 t - \frac{\beta}{2\pi} \sum_{m=-\infty}^{\infty} J_m\left(2\pi M \frac{\omega_1}{\omega_o}\right) \sin[(\omega_1 - M\omega_2)t - \omega_1 \tau_o] \\ & + \sum_{n=1}^{\infty} \frac{J_o(n\beta)}{n\pi} \left\{ \sin n\omega_o t - 2J_o\left(2\pi M \frac{\omega_1}{\omega_o}\right) \sin[n\omega_o(t - \tau_o)] \right\} \\ & + \sum_{n=1}^{\infty} \sum_{k=-\infty}^{\infty} \frac{J_k(n\beta)}{n\pi} \left\{ \sin(n\omega_o + k\omega_1)t - J_o\left[2\pi M\left(n + k \frac{\omega_1}{\omega_o}\right)\right] \sin(n\omega_o + k\omega_1)(t - \tau_o) \right. \\ & \left. - \sum_{p=-\infty}^{\infty} J_p\left[2\pi M\left(n + k \frac{\omega_1}{\omega_o}\right)\right] \sin[(n\omega_o + k\omega_1 - p\omega_2)t - (n\omega_o + k\omega_1)\tau_o] \right\} \end{aligned} \quad (6.16)$$

Equation 6.16 gives a simplified Fourier series representation of a single tone CPFWM modulation waveform. The first term represents the DC component; the second and third terms are the baseband signal components, and the fourth term represents a series of diminishing sidetones spaced ω_1 apart around the highest baseband frequency component ω_2 . The fifth term represents a spectral components at the carrier

frequency ω_o and all its harmonics, diminishing in amplitude with harmonic number n . Finally the last term produces two frequency components: a diminishing series of sidetones separated by an amount equal to the baseband signal components ω_1 and ω_2 set around the clock frequency and its harmonics, along with a series of diminishing sub-sidetones spaced ω_1 apart around the sidetones corresponding to the highest input frequency ω_2 . The profile of these components changes as a function of sampling ratio ω_s/ω_1 and modulation indices M and β . In this respect, the sub-sidetone structure of CPFWM resembles that of the multitone PWM.

It is clear from the last two terms of equation 6.16 that the frequency spectrum profile of the CPFWM waveform is asymmetrical. Furthermore, CPFWM may be classified as an anisochronous PTM technique because the sampling frequency component in the modulation spectrum vanishes when the modulation indices M and β take on certain values. These values of the modulation indices can be evaluated from equation 6.15 as those values which set the magnitude of the fundamental component of the clock frequency to zero. This leads to the following condition;

$$\frac{J_o(\beta)}{\pi} \sqrt{1 + 4J_o^2(2\pi M \frac{\omega_1}{\omega_o}) - 4J_o(2\pi M \frac{\omega_1}{\omega_o})} = 0 \quad (6.17)$$

Equation 6.17 is a non-linear equation which has more than one root, one possible solution of equation 6.17 is when; $J_o(\beta) = 0$, this leads to $\beta = 2.404$. Another possible solution is when the square root term in equation 6.17 is equal to zero which leads to;

$$1 + 4J_o^2\left(2\pi M \frac{\omega_1}{\omega_o}\right) - 4J_o\left(2\pi M \frac{\omega_1}{\omega_o}\right) = 0$$

(6.18)

The solution of the above equation is given as $J_o\left(2\pi M \frac{\omega_1}{\omega_o}\right) = \frac{1}{2}$, which leads to

$M \frac{\omega_1}{\omega_o} = 0.242$. This condition gives the relationship between the sampling ratio and

the modulation index at which the carrier frequency component will vanish.

Now let us consider what happens to the modulation spectrum in the two special cases when modulating signals are on or off.

a) When $v_1(t)$ is on and $v_2(t)$ is off: In this case, the width modulation is absent and the CPFWM waveform can be represented as a PFM. Thus substituting $M = 0$ into equation 6.16 the following relationship will be obtained;

$$\begin{aligned} v(t) &= \frac{\omega_o \tau_o}{2\pi} + \frac{\beta}{2\pi} \sin \omega_1 t - \frac{\beta}{2\pi} \sin[\omega_1 t - \omega_1 \tau_o] \\ &+ \sum_{n=1}^{\infty} \frac{J_o(n\beta)}{n\pi} \{ \sin n\omega_o t - 2 \sin[n\omega_o(t - \tau_o)] \} \\ &+ \sum_{n=1}^{\infty} \sum_{k=-\infty}^{\infty} \frac{J_k(n\beta)}{n\pi} \{ \sin(n\omega_o + k\omega_1)t - \sin(n\omega_o + k\omega_1)(t - \tau_o) \\ &\quad - \sin[(n\omega_o + k\omega_1)t - (n\omega_o + k\omega_1)\tau_o] \} \end{aligned}$$

(6.19)

The above equation represents the frequency spectrum of PFM waveform, which is in agreement with those given in the literature[61]. Note that the phase disagreement between equation 6.19 and those given in the literature is due to the different initial assumptions made in the two cases.

b) When $v_2(t)$ is on and $v_1(t)$ is off: In this case the CPFWM waveform is the same as a PWM pulse train, and by substituting $\beta = 0$ in equation 6.16, the following equation can be derived;

$$\begin{aligned}
 v(t) = & \frac{\omega_o \tau_o}{2\pi} + M \sin \omega_2 t + \sum_{n=1}^{\infty} \frac{1}{n\pi} \left\{ \sin n\omega_o t - 2J_o \left(2\pi n M \frac{\omega_1}{\omega_o} \right) \sin [n\omega_o (t - \tau_o)] \right\} \\
 & + \sum_{n=1}^{\infty} \sum_{p=-\infty}^{\infty} \frac{1}{n\pi} \left\{ \sin(n\omega_o t) - J_o [2\pi M n] \sin[(n\omega_o)(t - \tau_o)] \right. \\
 & \quad \left. - J_p [2\pi M n] \sin[(n\omega_o - p\omega_2)t - n\omega_o \tau_o] \right\}
 \end{aligned}
 \tag{6.20}$$

Equation 6.19 is also in agreement with those given in literature [1].

6.3 Experimental and computer simulation results

To verify the theory a practical system has been designed and built and results obtained are compared with predicted values. Furthermore, results from computer simulation are also compared with practical and theoretical data.

For experimental measurements using the CPFWM system as explained in chapter five, the running frequency of the system was at 2.04 MHz and the two non-harmonically related input modulating frequencies were $f_1=170$ kHz and $f_2=70$ kHz. Measurements have been taken for a range of modulation indices of $M = 0.08, 0.15, 0.25,$ and $\beta = 0.09, 0.19, 0.38, 0.70, 1.00$. Measurements at higher modulation indices was avoided due to the presence of non-linear distortion resulting from the saturation of the active components in the circuit, and consequently the production of intermodulation harmonics. Since the sidetones and sub-sidetones around the carrier frequency are the spectrum components of most importance, the repeating pattern around the harmonics of the carrier frequency has been neglected. Tables 6.1 - 6.3 illustrate the experimental and theoretical results of the spectral components obtained at different modulation indices. The carrier frequency component has been taken as a reference component (0dB) in all measurements and calculations.

To facilitate comparison between the theoretical predictions and practical results, the differences in each table has been calculated together with the maximum, minimum and average differences for each component, see Table 6.3. These results reveal that the largest differences are less than 2 dB, while the majority of the differences are within 1dB.

In addition to the above results, Figures 6.2-6.6.10 show the captured spectrum of the CPFWM waveform for different modulation indices. As predicted, the amplitude of all the components and the number of side tones are functions of both the modulation indices and sampling ratio.

Results from computer simulation have been obtained using the TESLA, as explained in the previous chapter package (see Figs. 6.11 and 6.12). TESLA uses a fast Fourier transform (FFT) algorithm to predict the frequency spectrum of a time dependent signal. Accordingly, the choice of the resolution is an important factor as it will determine the number of data points and the sampling interval for the calculation. Obviously, using a very large number of data points over a long sampling intervals will produce more accurate results, and good resolution. However, if the number of data points is relatively low and the sampling interval is short, then a significant noise component will appear due to the inaccurate simulation. This noise components can be reduced by averaging the results (estimates) of several simulations.

Throughout this simulation resolution bandwidth was chosen to be 8kHz, and the final results was obtained by averaging 16 different estimates for each case. It was noticed that with these settings the resulting spectrum was reasonably clear as most of the components were distinguishable. Figures 6.11 and 6.12 show the simulated spectrum of CPFWM with exactly the same specifications as that for the experimental set up. For comparison the experimental and calculated results are also included. It can be seen that the experimental, calculated and simulated results are very close to each other within ± 1 dB range. These confirming the validity of the spectral equation.

Frequency component	(A) $\beta=0.38, M=0.09$		(B) $\beta=0.2, M=0.09$		(C) $\beta=0.09, M=0.09$		(D) $\beta=0.09, M=0.18$		(E) $\beta=0.19, M=0.18$	
	measured	calculated	measured	calculated	measured	calculated	measured	calculated	measured	calculated
f_1	-33.53	-33.84	-40.70	-40.08	-46.70	-46.63	-46.12	-46.46	-39.80	-40.72
f_2	-22.64	-23.05	-23.00	-23.28	-23.80	-23.34	-16.80	-17.13	-18.00	-17.88
f_1+f_2	-	-	-	-	-	-	-	-	-	-
f_1-f_2	-	-	-	-	-	-	-	-	-	-
f_0+f_1	-14.10	-14.27	-19.65	-20.05	-26.70	-26.50	-25.40	-26.60	-21.10	-20.89
f_0-f_1	-14.07	-14.7	-20.6	-20.44	-26.60	-27.30	-27.25	-27.35	-21.92	-21.64
f_0+f_2	-23.80	-23.58	-23.30	-23.42	-23.20	-23.42	-17.90	-17.40	-18.80	-18.21
f_0-f_2	-23.87	-23.58	-23.85	-23.42	-24.00	-23.42	-17.94	-17.40	-18.90	-18.21
$f_0+(f_1+f_2)$	-36.70	-36.96	-43.50	-43.14	-49.00	-49.66	-43.00	-43.67	-38.10	-37.97
$f_0+(f_1-f_2)$	-36.89	-36.96	-43.40	-43.14	-49.00	-49.66	-43.20	-43.67	-38.20	-37.97
$f_0-(f_1+f_2)$	-38.00	-38.39	-44.80	-44.57	-50.20	-51.09	-45.70	-45.04	-39.90	-39.33
$f_0-(f_1-f_2)$	-38.15	-38.39	-44.80	-44.57	-50.40	-51.09	-45.50	-45.04	-39.85	-39.33
f_0+2f_1	-33.22	-34.05	-45.70	-46.22	-58.00	-59.24	-	-61.00	-47.70	-47.10
f_0-2f_1	-34.00	-35.67	-46.23	-47.86	-58.40	-60.08	-	-60.00	-47.90	-48.10
f_0+2f_2	-47.30	-45.87	-47.50	-47.88	-48.10	-47.88	-36.40	-35.78	-36.35	-36.59
f_0-2f_2	-46.80	45.87	-47.50	-47.88	-47.54	-47.88	-36.50	-35.78	-36.50	-36.59
$2f_0$	-7.50	-7.84	-6.53	-7.07	-6.40	-6.86	-6.82	-7.58	-7.10	-8.37

Table 6.1 Measured and calculated relative amplitudes of frequency components at $f_1 = 170$ kHz, $f_2 = 70$ kHz. (All values are in dB and the component at carrier frequency has been taken as a reference at 0dB).

frequency component	(F) $\beta = 0.38, M = 0.18$		(G) $\beta = 0.70, M = 0.18$		(H) $\beta = 0.70, M = 0.25$		(I) $\beta = 1.00, M = 0.25$	
	measured	calculated	measured	calculated	measured	calculated	measured	calculated
f_1	-33.81	-34.70	-25.88	-26.21	-27.40	-27.24	-22.60	-22.94
f_2	-17.60	-17.91	-15.63	-15.88	-12.85	-12.25	-11.60	-11.05
f_1+f_2	-50.80	-51.85	-45.00	-46.74	-42.80	-42.75	-38.20	-38.61
f_1-f_2	-50.80	-51.85	-44.87	-46.74	-42.60	-42.75	-38.40	-38.61
f_0+f_1	-14.00	-13.94	-8.24	-8.47	-7.30	-8.26	-3.90	-4.53
f_0f_1	-14.88	-15.73	-8.21	-8.98	-8.20	-8.91	-4.92	-5.18
f_0+f_2	-19.00	-18.47	-17.90	-17.47	-14.40	-13.91	-14.29	-13.94
f_0f_2	-19.00	-18.47	-17.90	-17.47	-14.44	-13.91	-14.35	-13.94
$f_0+(f_1+f_2)$	-31.76	-32.08	-24.86	-25.36	-21.60	-21.85	-18.11	-18.14
$f_0+(f_1-f_2)$	-31.66	-32.08	-24.90	-25.30	-21.45	-21.85	-18.06	-18.14
$f_0-(f_1+f_2)$	-33.00	-33.46	-26.23	-26.75	-22.80	-23.11	-19.52	-19.41
$f_0-(f_1-f_2)$	-33.00	-33.46	-26.23	-26.75	-22.75	-23.11	-19.50	-19.41
f_0+2f_1	-34.80	-35.13	-22.67	-22.95	-22.79	-23.02	-15.40	-16.01
f_0-2f_1	-36.35	-36.65	-23.46	-24.07	-23.34	-24.33	-16.30	-17.32
f_0+2f_2	-36.52	-36.87	-37.50	-37.45	-29.60	-28.68	-29.74	-28.73
f_0-2f_2	-36.50	-36.87	-37.50	-37.45	-29.40	-28.68	-29.74	-28.73
$2f_0$	-8.50	-9.30	-11.66	-11.18	-12.50	-11.97	-19.63	-18.79

Table 6.2 Measured and calculated relative amplitudes of frequency components at $f_1 = 170$ kHz, $f_2 = 70$ kHz. (All values are in dB) and the component at carrier frequency has been taken as a reference at 0dB).

Column	f_1	f_2	f_1+f_2	f_1-f_2	f_1+f_1	f_1-f_1	f_1+f_2	f_1-f_2	$f_1+(f_1+f_2)$	$f_1+(f_1-f_2)$	$f_1-(f_1+f_2)$	$f_1-(f_1-f_2)$	f_1+2f_1	f_1-2f_1	f_1+2f_2	f_1-2f_2	$2f_1$
A	0.49	0.41	-	-	0.17	0.63	-0.22	-0.29	0.26	0.07	0.39	0.24	-	-	-1.43	-0.93	0.34
B	-0.62	0.28	-	-	0.4	-0.16	0.12	0.57	-0.36	-0.26	-0.23	-0.23	-	-	0.38	0.38	0.54
C	-0.07	-0.46	-	-	-0.2	0.7	0.22	-0.58	0.66	0.66	0.89	0.69	-	-	-0.22	0.34	0.46
D	0.34	0.33	-	-	0.2	-0.15	-0.5	-0.54	0.67	0.47	-0.66	-0.46	-	-	-0.62	-0.72	0.76
E	0.92	-0.12	-	-	-0.21	-0.26	-0.59	-0.69	-0.13	-0.23	-0.57	-0.52	-0.6	0.2	0.24	0.09	1.27
F	0.89	0.31	-	-	-0.06	0.85	-0.53	-0.53	0.32	0.42	0.46	0.46	0.33	0.3	0.35	0.37	0.8
G	-0.33	0.25	1.74	1.87	0.23	0.77	-0.43	-0.43	0.5	0.4	0.52	0.52	0.28	0.61	-0.05	-0.05	-0.48
H	-0.16	-0.6	-0.05	0.15	0.96	0.71	-0.49	-0.53	0.25	0.4	0.31	0.36	0.23	0.99	-0.92	-0.72	-0.53
I	0.34	-0.55	0.41	0.21	0.63	0.26	-0.35	-0.41	0.03	0.08	-0.11	-0.09	0.61	1.02	-1.01	-1.01	-0.84
Average	0.20	-0.02	0.70	0.74	0.24	0.37	-0.31	-0.38	0.24	0.22	0.11	0.11	0.17	0.62	-0.36	-0.25	0.26
Max.	0.92	0.41	1.74	1.87	0.96	0.85	0.22	0.57	0.67	0.66	0.89	0.69	0.61	1.02	0.38	0.38	1.27
Min.	-0.62	-0.6	-0.05	0.16	-0.21	-0.26	-0.69	-0.69	-0.36	-0.26	-0.66	-0.62	-0.6	0.2	-1.43	-1.01	-0.84
Overall Max																	1.87
Overall Min																	-1.43

Table 6.3. Error between measured and calculated in Tables 5.1 and 5.2.

Fig. 6. 2 Frequency spectrum of the CPFWM waveform, $f_0 = 2$ MHz, $f_1 = 170$ kHz, $f_2 = 70$ kHz, $M = 9\%$, $\beta = 0.38$.
 (- - Calculated | Measured)

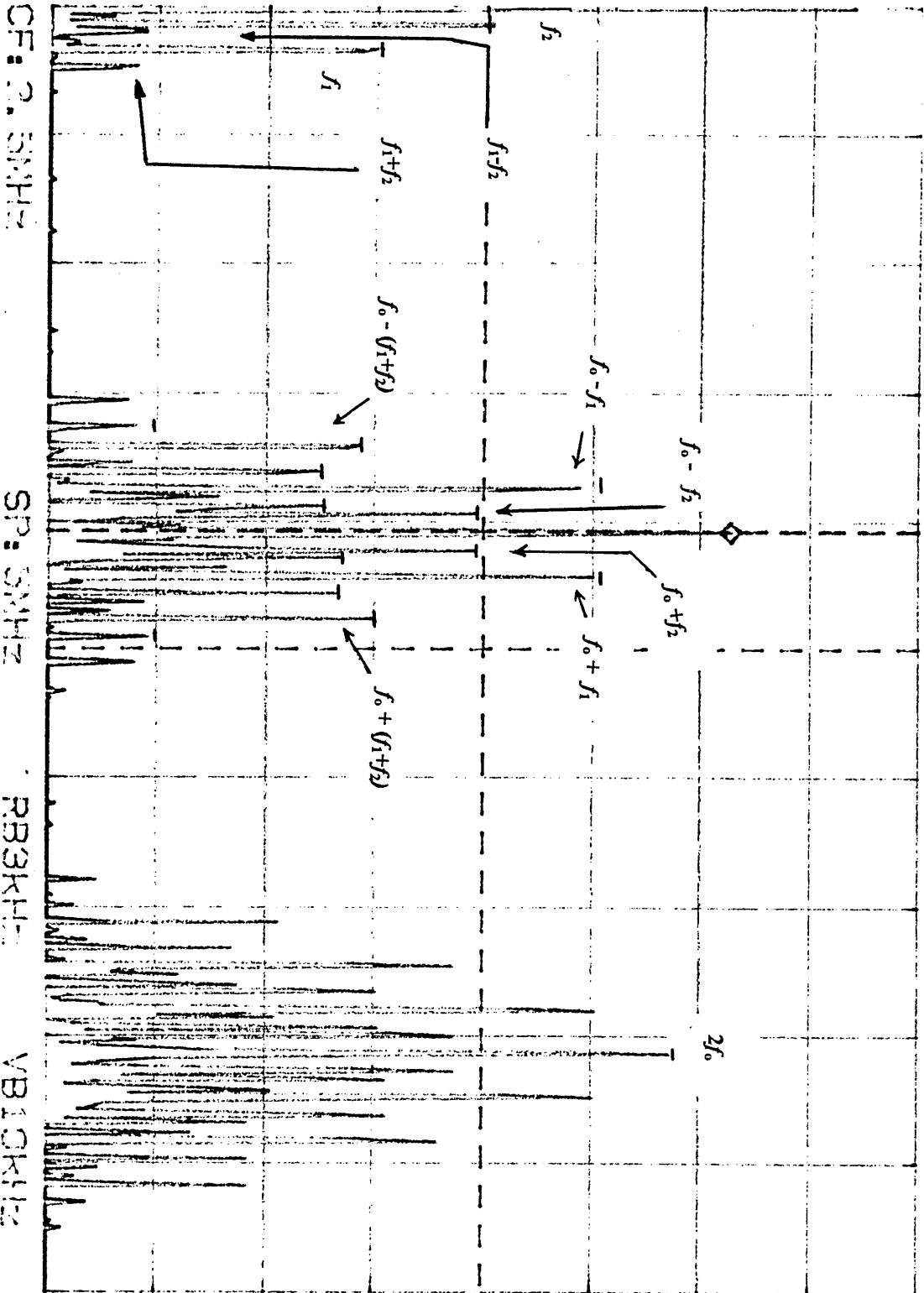


Fig. 6.3 Baseband frequency spectrum of the CPFSM waveform, $f_0 = 2$ MHz, $f_1 = 170$ kHz, $f_2 = 70$ kHz, $M = 9\%$, $\beta = 0.38$.
 (- Calculated | Measured)

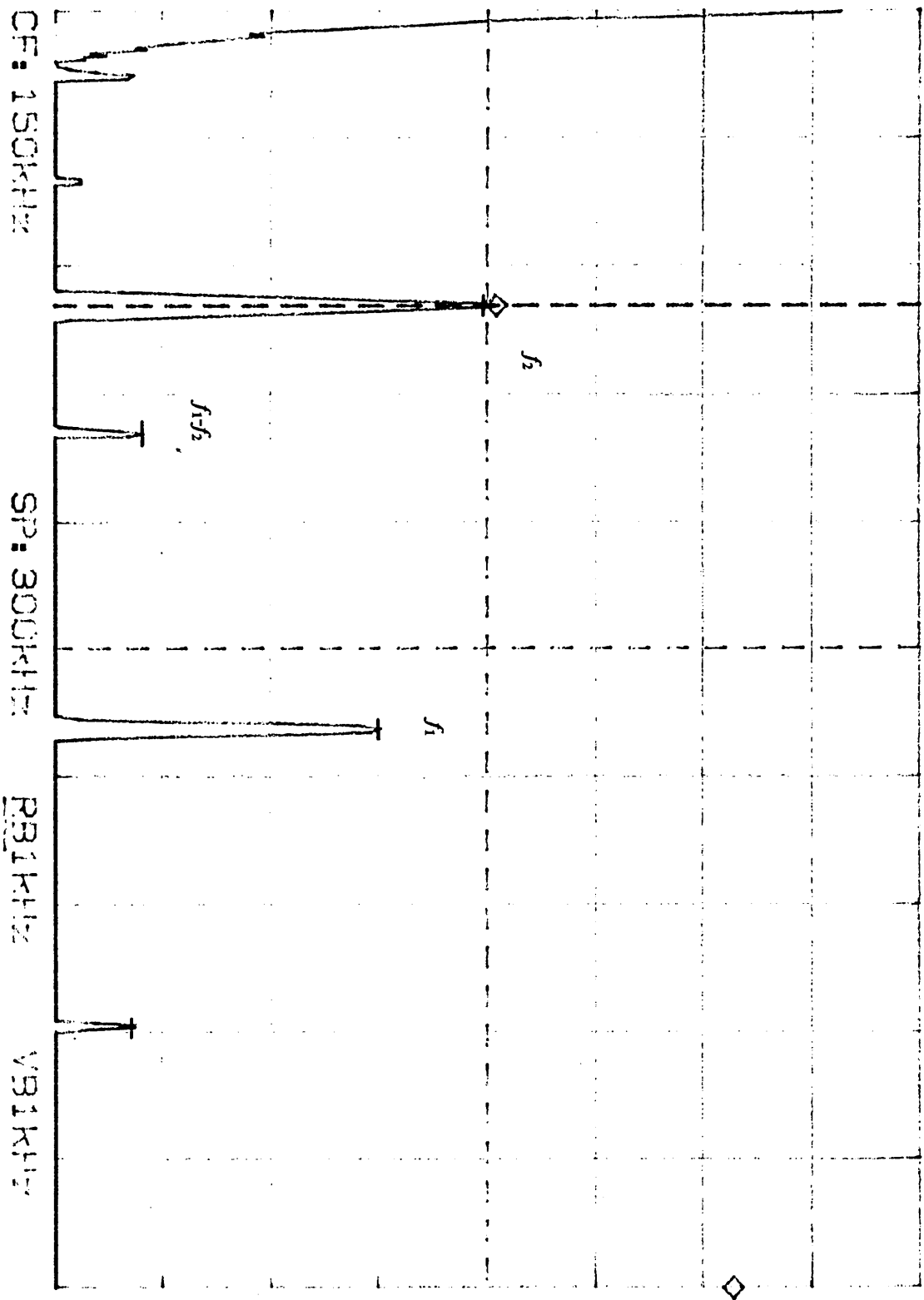


Fig. 6.4 Frequency spectrum components around the carrier, $f_0 = 2$ MHz, $f_1 = 170$ kHz, $f_2 = 70$ kHz, $M = 9\%$, $\beta = 0.38$.
 (- Calculated | Measured)

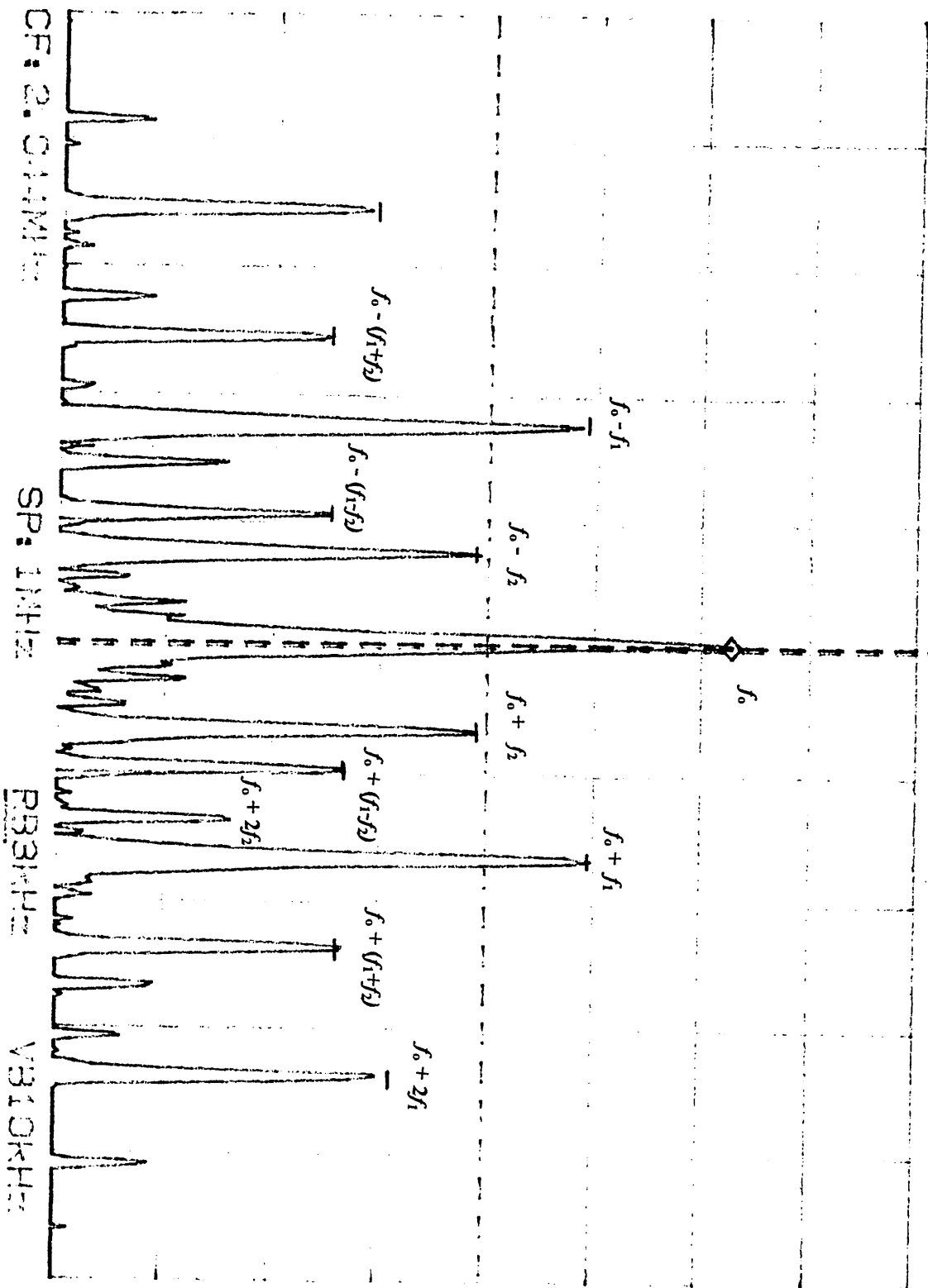


Fig. 6.5 Frequency spectrum of the CPFWM waveform, $f_0 = 2$ MHz, $f_1 = 170$ kHz, $f_2 = 70$ kHz, $M=9\%$, $\beta = 0.2$.
 (- - Calculated | Measured)

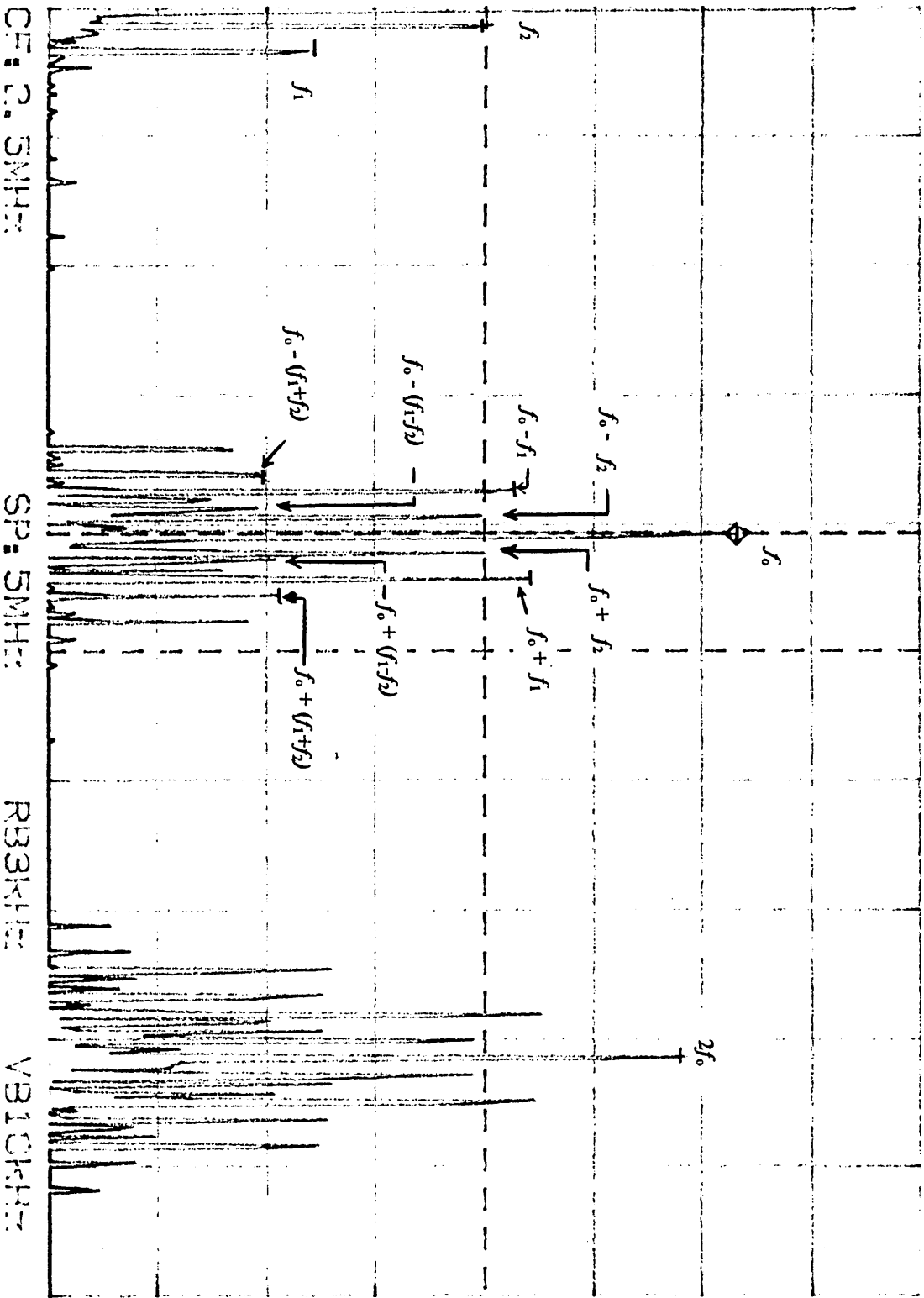


Fig. 6.6 Frequency spectrum of the CPFWM waveform, $f_0 = 2$ MHz, $f_1 = 170$ kHz, $f_2 = 70$ kHz, $M = 18\%$, $\beta = 0.38$.
 (- - Calculated | Measured)

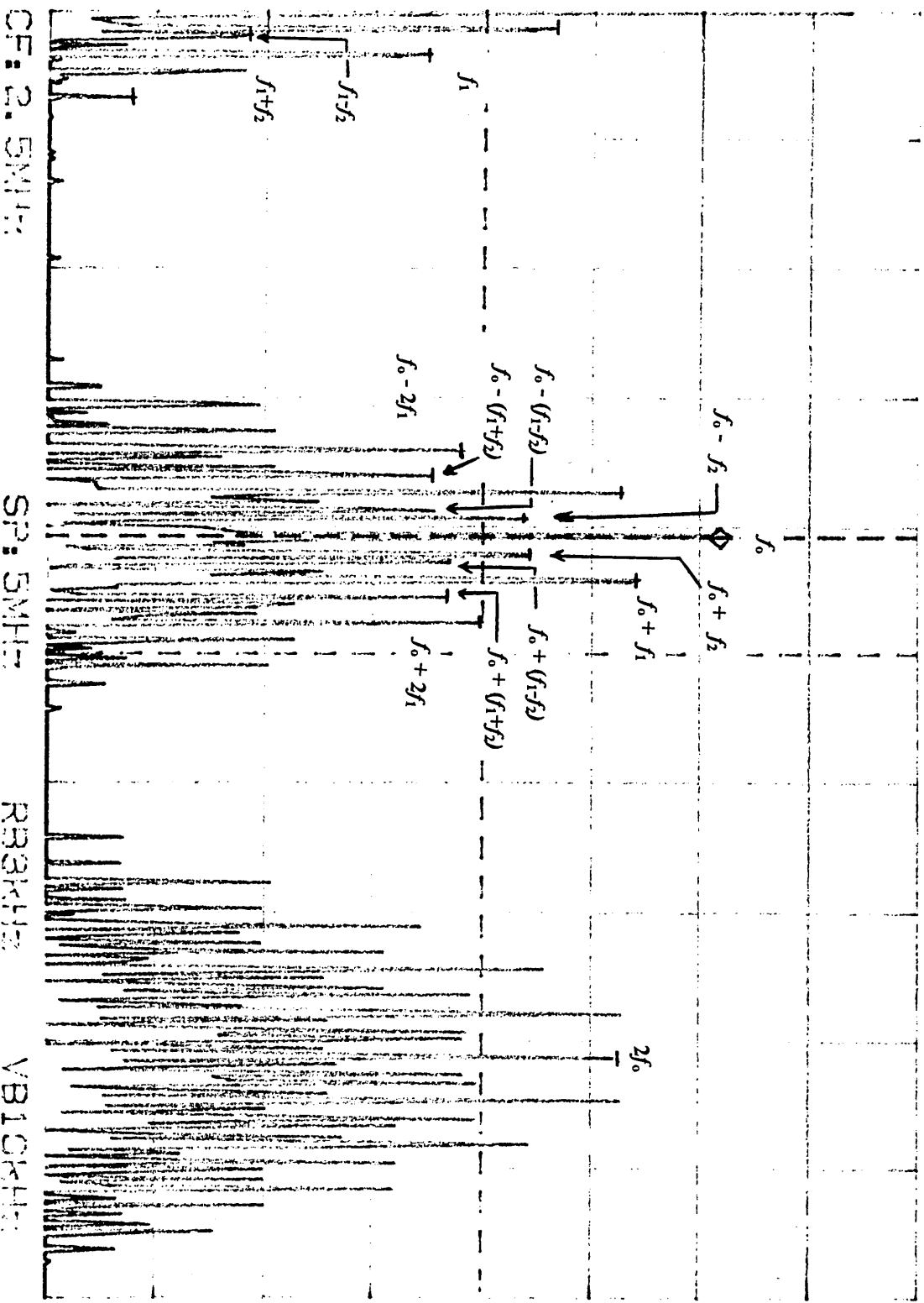


Fig. 6.7 Frequency spectrum of the CPFWM waveform, $f_0 = 2$ MHz, $f_1 = 400$ kHz, $f_2 = 98$ kHz, $M = 15\%$, $\beta = 0.24$
 (- Calculated | Measured)

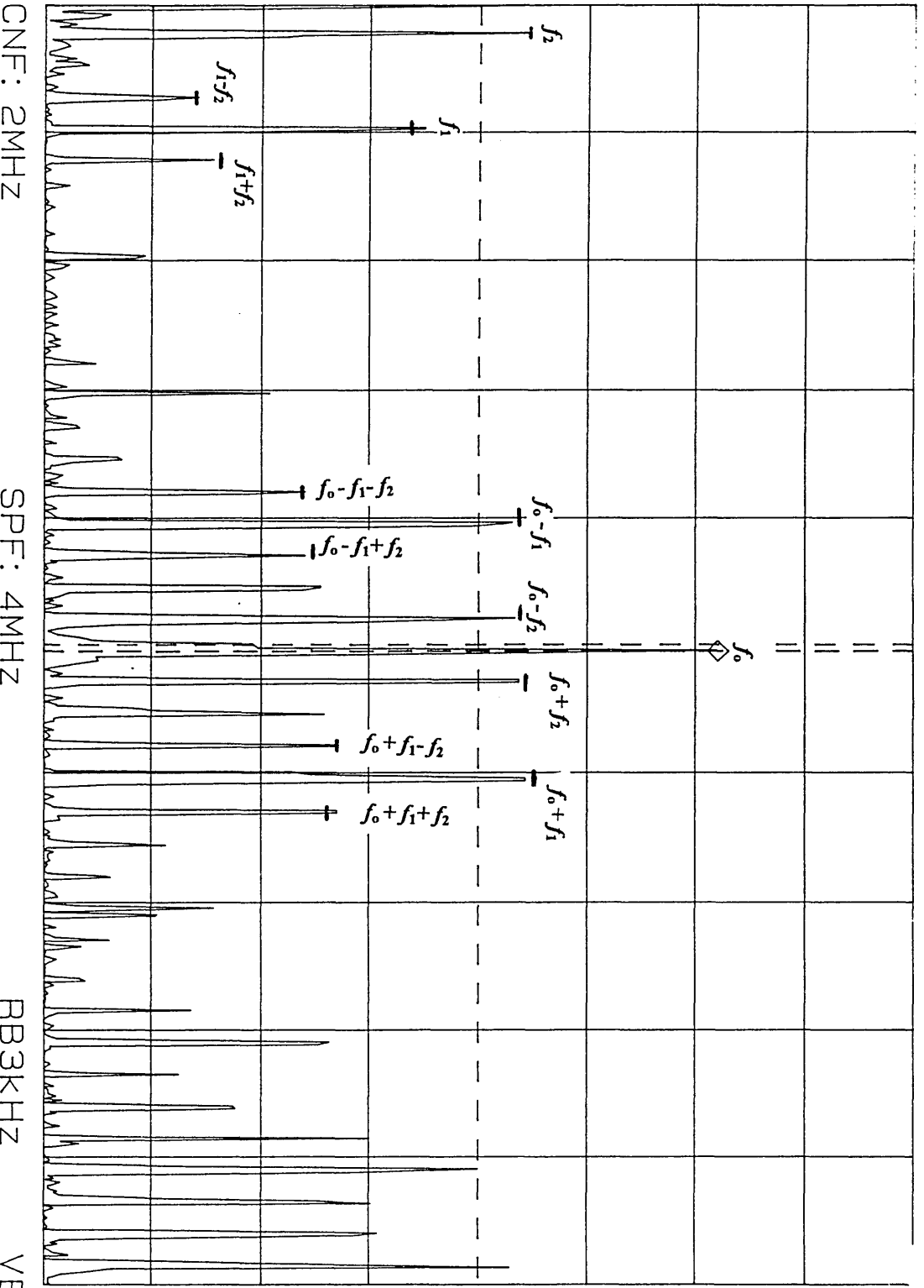


Fig. 6.8 Frequency spectrum of the CPFSM waveform, $f_0 = 2$ MHz, $f_1 = 800$ kHz, $f_2 = 98$ kHz, $M = 15\%$, $\beta = 0.2$.
 (- Calculated | Measured)

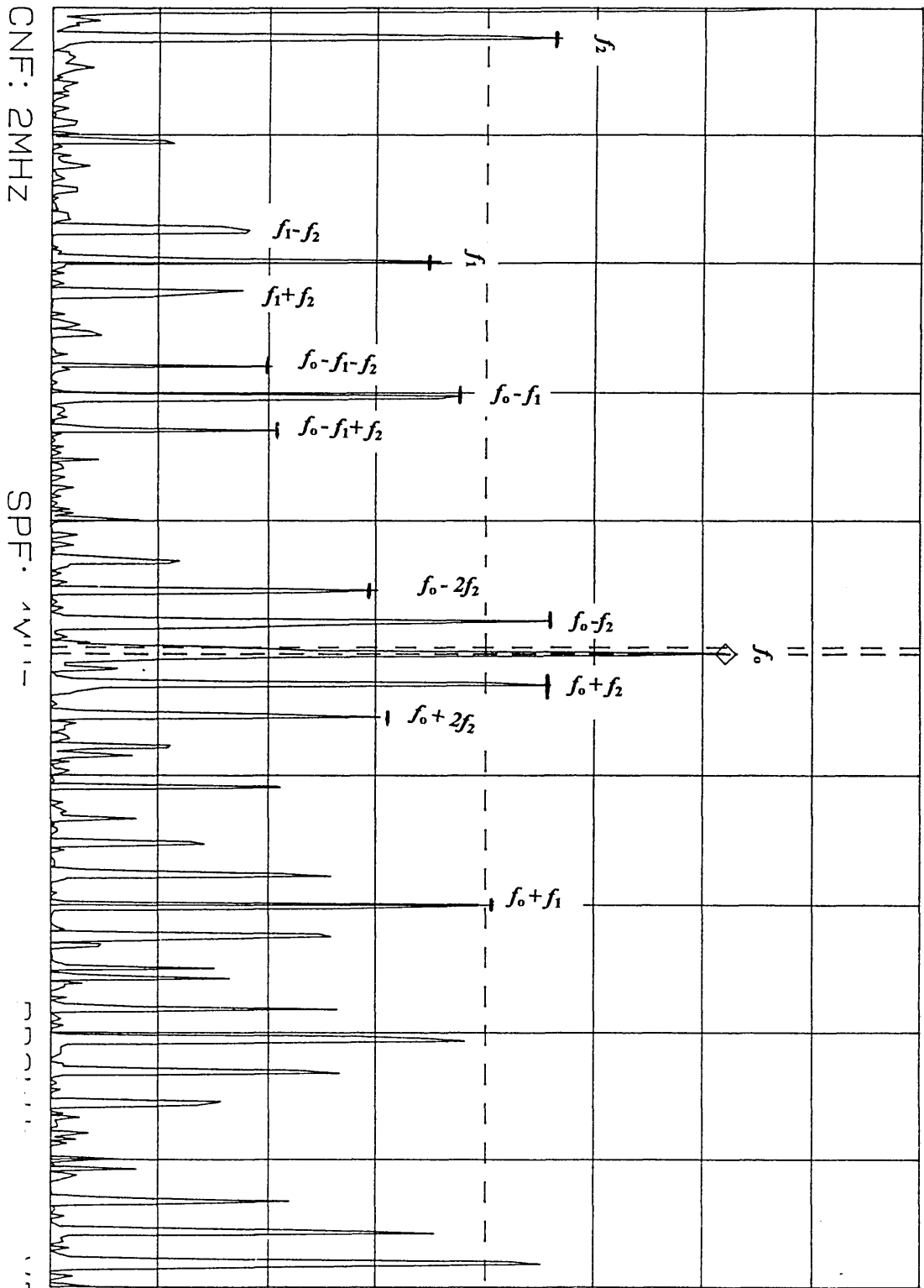
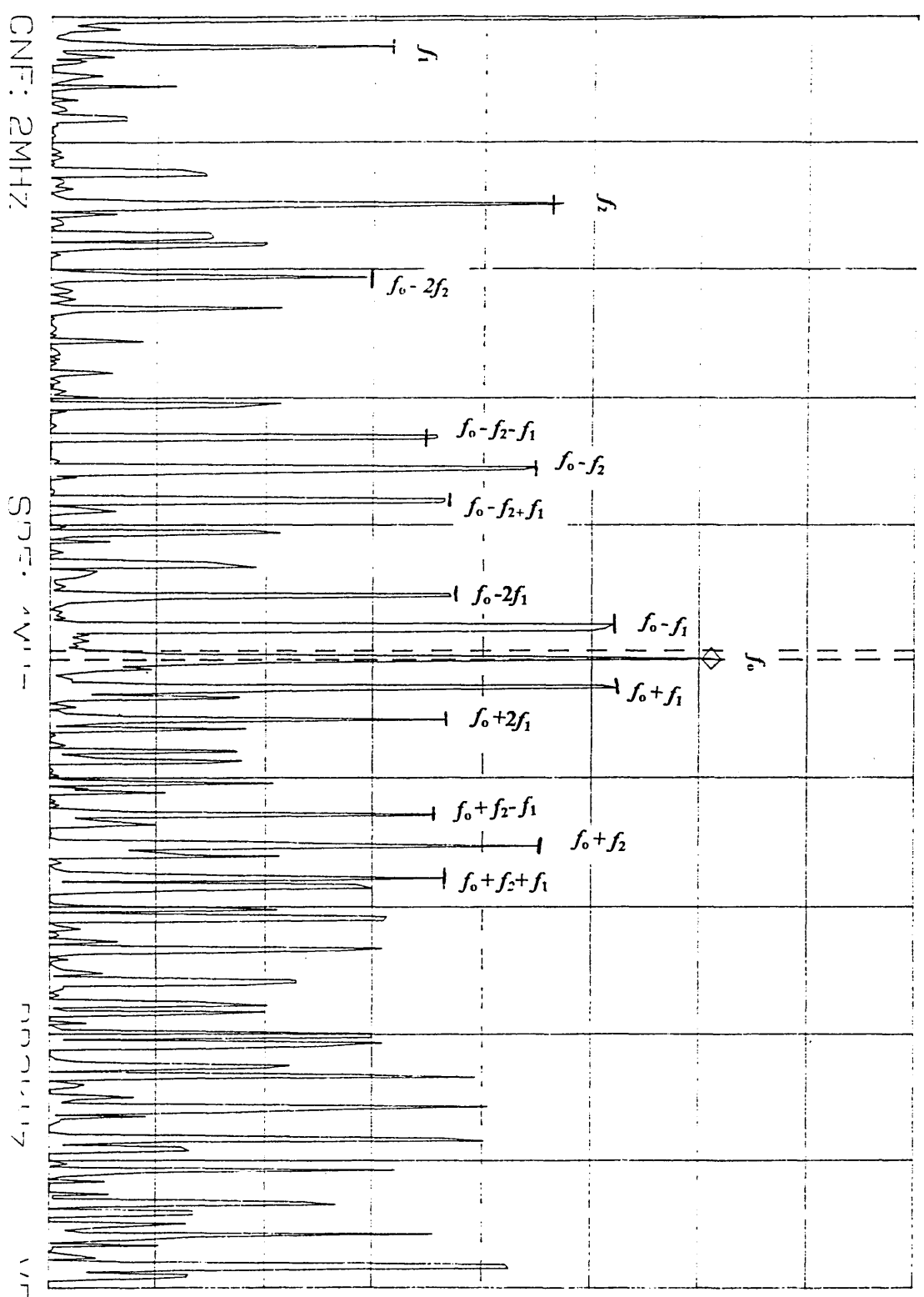


Fig. 6.10 Frequency spectrum of the CPFWM waveform, $f_0 = 2$ MHz, $f_1 = 100$ kHz, $f_2 = 600$ kHz, $M = 20\%$, $\beta = 0.63$.
 (- Calculated | Measured)



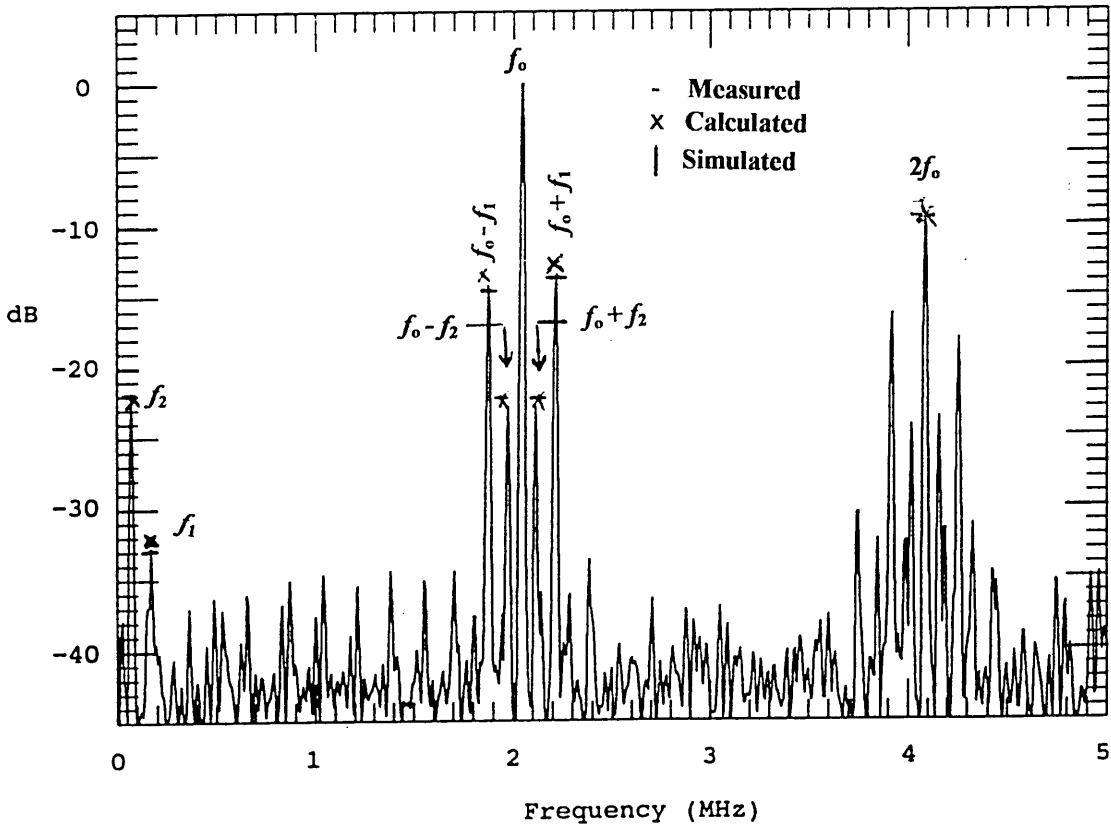


Fig. 6.11 Simulated frequency spectrum of the CPFWM waveform, $f_0 = 2$ MHz, $f_1 = 170$ kHz, $f_2 = 70$ kHz, $M = 9\%$, $\beta = 0.38$.

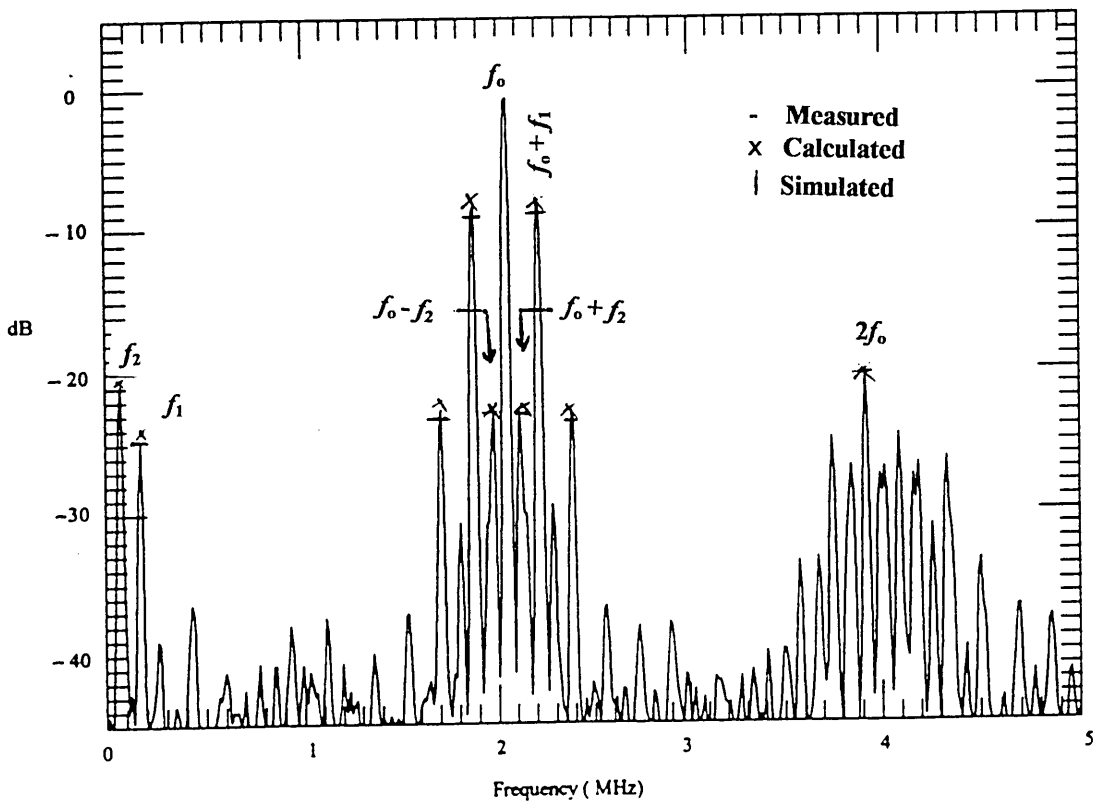


Fig. 6.12 Simulated frequency spectrum of the CPFWM waveform, $f_0 = 2$ MHz, $f_1 = 170$ kHz, $f_2 = 70$ kHz, $M = 9\%$, $\beta = 0.78$.

Chapter Seven

Cross-talk and Noise Performance

Analysis

7.1 Introduction

The most important characteristics of PTM systems are their noise reducing properties and the cross-talk performance. Noise has the effect of displacing the pulse edges from the values corresponding to the modulating signal. Noise impulses may also modulate other characteristics such as; amplitude, width, and slope of the pulse edges, but these are ultimately translated into pulse time displacement. This causes a random parasitic voltage fluctuation on the detected message, hence reducing the quality of the signal reception. The optimum noise performance of all PTM systems is realised when all effects of noise other than time displacement are eliminated or minimised.

On the other hand, another significant problem present in the development of pulse-multiplex communication systems is interchannel cross-talk. This problem has been studied in different multiplexed PTM systems such as PAM and PPM [90-92]. The key aspects of the investigations were to determine the factors that will minimise the usage of bandwidth and maximise the cross-talk ratio.

In multiplexed PTM systems, the most common form of cross-talk is caused by carryover of energy from one pulse to the next pulse. Thus, cross-talk may occur from one channel to the following channel, decreasing rapidly as the pulses are further separated in time. Cross-talk may be expressed as the ratio of the signal output of a given channel under normal modulation to the signal output of the same channel resulting from the modulation of some other channel. This ratio is customarily expressed in decibels. In CPTM systems, also similar phenomenon occurs, where energy from one modulated pulse edge (say the rising edge) is carried over to the following edge (the falling edge). Thus resulting in interchannel cross-talk.

This chapter investigates the interchannel cross-talk and noise performance in a CPFWM system. Theoretical analysis and experimental investigations of both problems are presented together with measured and predicted results. Throughout this chapter, the cross-talk performance is considered first followed by the noise analysis.

7.2 Cross-talk performance in CPFWM systems

In CPFWM system, see Fig. 7.1, cross-talk occurring in the PFM channel is due to width modulation by the second channel, and similarly the cross-talk in the PWM channel is due to the frequency modulation by the first channel. Although there are several causes of the cross-talk in both channels, however, there is a common cause which is called waveform interference [31, 90-92]. Waveform interference is the result of carryover of energy from one edge to the next edge.

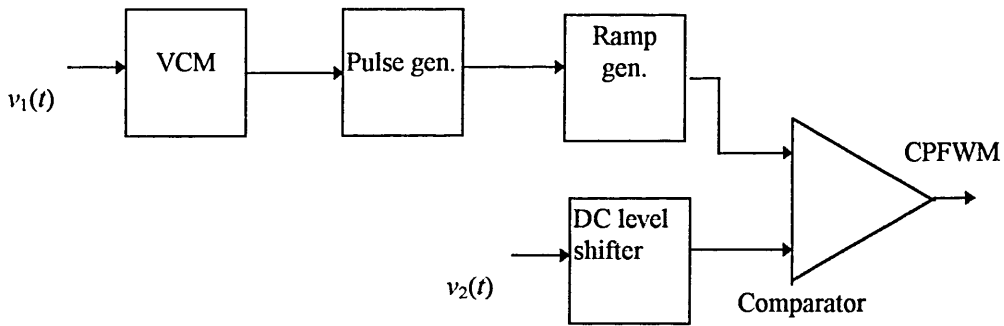


Fig. 7.1 Simplified block diagram of CPFWM transmitter.

In order to understand this phenomenon, let us consider a simplified received CPFWM waveform, as shown in Fig. 7.2. The shape of the received pulses is determined by the transfer function of the transmission medium, its bandwidth, and the time response characteristics of the input stages of the receiver. A typical waveform of the received CPFWM pulses (when both frequency and width modulations are absent) is shown in Fig. 7.2 together with their slope (i.e. the differential pulses). The slope is included in the diagram to show the effect of band limitation on the rise time of the edges. It is clear from Fig. 7.2 that the slope of the second pulse is affected by the first pulse. Since channel demultiplexing is carried out by separating the edges of the received CPFWM pulse train (i.e. differentiating the received pulses), the change in the slope of the rising edge of the received pulses will cause a phase shift (time jitter δT) in the separated edges. This phase shift depends on the following factors: the time interval from the fall to the rise of the pulse, and the shape of the received pulses (i.e. the transmission bandwidth and linearity of the transmission media). The amplitude of the received pulse is greatly affected by the interference between pulses, while the differential pulse is affected by the jitter.

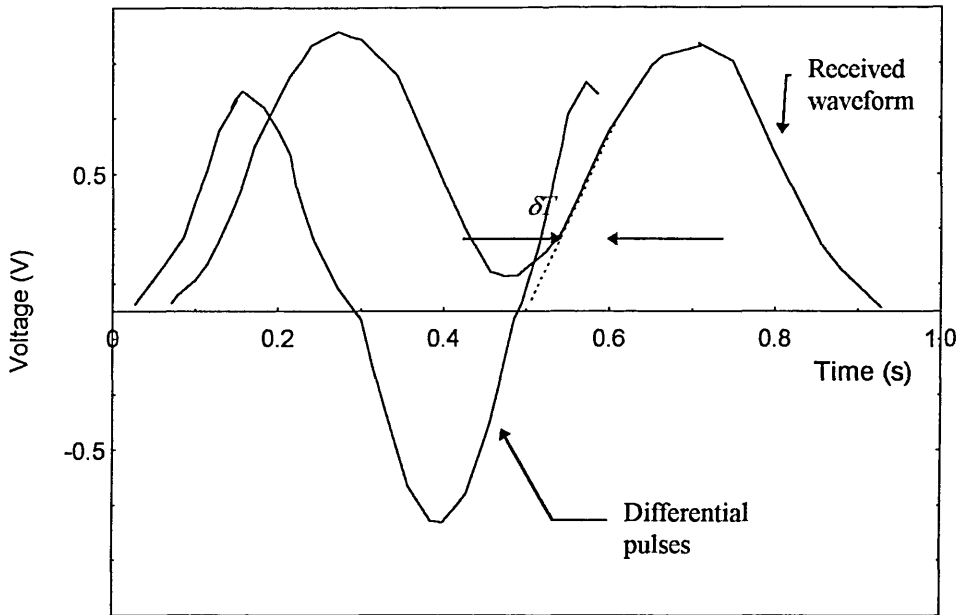


Fig. 7.2 Received CPFWM waveform of dual pulses and its slope.

Since time jitter depends on the time interval from the fall to the rise of the pulses, therefore, when width modulation exists the time jitter due to the waveform interference will vary according to the width modulation and thus cause cross-talk from the width modulation channel to the frequency modulation channel. However, when the pulse frequency is varied, the time interval from the fall of the pulse to the rise of the next pulse changes. Due to the limitation of the transmission bandwidth, the rising edge of the next pulse is modulated by the effect of the falling edge of the preceding pulses, which results in a cross-talk from the PFM signal to PWM signal. Furthermore, there are other causes for the cross-talk that will be considered later in this section. Next, the cross-talk in each channel will be considered individually, and both theoretical and experimental analysis will be given.

7.2.1 cross-talk from PWM signal to PFM signal

It was discussed in the previous chapters that the message carried by the frequency modulation channel is extracted by separating the frequency modulated edges of the carrier pulse train and then passing the resulting PFM pulses through a low pass filter. A block diagram of the PFM channel detector is shown in Fig. 7.3 together with its waveform diagram. In an ideal situation, there should be no cross-talk from the PWM signal to the PFM signal. However, in practice the received pulses are non ideal due to effects of the transmission channel bandwidth, thus resulting in cross-talk interference.

In order to analyse this situation, let us assume that a single tone modulating signal is used for both channels. Due to variation of the pulse width, the fall of the preceding pulse affects the rise time of the next pulse. Consequently, the PFM pulse train is phase modulated by the PWM modulating signal. As shown in Fig. 7.3.c, assume that the PFM pulse width T_o is modulated by $T_{PWM} \sin \omega_2 t$, where ω_2 is the frequency of the second modulating signal. Assume also that the jitter of δT is produced in the rise time of the pulse train, see Fig. 7.3.c. Then the pulse train regenerated by the pulse generator with repetition frequency of $f_o = 1/T_o$ is phase modulated by [31];

$$\theta(t) = \frac{\pi \delta T}{T_o} \sin(2\pi f_2 t) \quad (7.1)$$

Passing the regenerated PFM pulse train through a low pass filter, the cross-talk from the PWM signal to the PFM signal is obtained as;

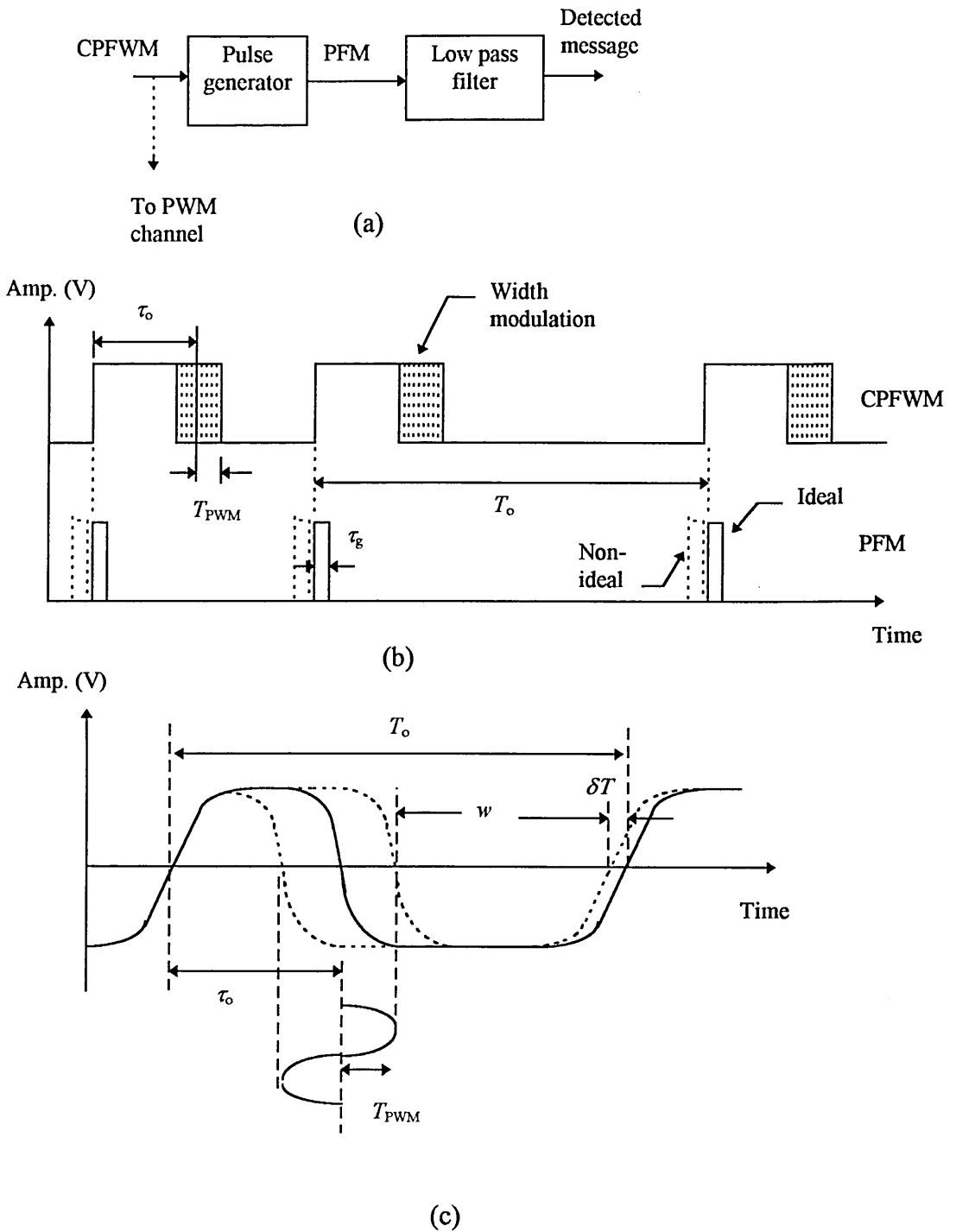


Fig. 7.3 Separation of the frequency modulated edges: (a) block diagram, (b) timing diagram and (c) received pulse.

$$CT_{WF} = \frac{|d\theta(t) / dt|}{2\pi \Delta f / \sqrt{2}} \quad (7.2)$$

substituting $\Delta f = \beta f_1$, then equation 7.2 becomes;

$$CT_{WF} = \frac{\sqrt{2}\pi \delta T (f_2 / f_1)}{T_o \beta} \quad (7.3)$$

where, β is the modulation index for the PFM channel. Equation 7.3 gives the cross-talk from the PWM signal to the PFM signal which depends on the modulating frequency of PWM signal as well as δT which in turn, depends on many factors such as; pulse width, pulse repetition frequency, channel bandwidth and β .

The theoretical evaluation of δT is not easy, as one needs to determine the shape of the received pulses. This requires determination of the transfer function of the transmission medium, input stages of the receiver and the time response of the transmitting elements. This is in addition to the stray capacitance and stray inductance in the receiver circuit. The time jitter δT can then be obtained as the change in the rise time of one edge due to the change in pulse width and/or the frequency of the received pulse. Usually complicated numerical analysis and /or computer simulation are required to determine the exact values of the time jitter.

Throughout this project, the variation of δT with T_{PWM} is measured for different values of received pulse rise time when the frequency modulation is turned off, and the results are shown in Fig. 7. 4. It can be seen that δT increases with the rise time (i.e. the decrease of the transmitting bandwidth) and its rate of increase is much higher at longer

rise time. This suggests that the cross-talk performance deteriorates significantly when the transmitting bandwidth is reduced.

Equation 7.3 is used to calculate cross-talk by keeping the pulse width deviation constant and using the measured values of δT . The predicted and measured data are plotted in Fig. 7.5 for different values of pulse rise time, showing good agreement to within ± 2 dB. This difference is due to the assumption made in obtaining the values of δT from practical measurement, that is at low β there is no PFM modulation on the rise edge. As expected, see equation 7.3, when β increases the signal power at the PFM channel demodulator increases while the level of the interference component from the PWM signal remains constant, therefore cross-talk decreases with β and increases with the pulse rise time.

In order to characterise the cross-talk performance from width modulation to frequency modulation channel a number of measurements was taken and results are displayed in Figs. 7.6 - 7.8 together with the calculated data. It can be seen from these figures that the calculated data show a good agreement (within ± 2 dB) with the measured results. It can be seen that cross-talk increases with the rise time, because the pulse distortion increases, and modulation index of the PWM channel.

Table 7.1 shows cross-talk data extracted from Figs. 7.6 - 7.8 which could be used to investigate the effect of the rise time and the modulation index β on the cross-talk. It can be seen that cross-talk is dramatically increasing when the rise time of the received CPFWM pulse is increasing. To illustrate this, when the pulse rise time is changed from 45 nsec to 100 nsec (i.e. almost doubled) the cross-talk deteriorated by about 23 dB.

However, for small values of rise time, a reduction of about 30% in the pulse rise time gives improvement of 10 dB in the cross-talk performance. The case is different when the rise time is high, an improvement of about 30% in the rise time gives only 6 dB improvement in the cross-talk performance. This is because δT increases with the pulse rise time, see Fig. 7.4. The effect of the modulation index β on the cross-talk can also be seen from Table 7.1. As predicted in equation 7.3, when β is doubled the cross-talk is improved by 6 dB.

β	Cross-talk (dB)							
	$t_R = 100$		$t_R = 77$		$t_R = 58$		$t_R = 45$	
	Calculated	Measured	Calculated	Measured	Calculated	Measured	Calculate	Measured
0.3	-9.3	-8.5	-15.4	-14.5	-22.5	-20.5	-31.0	-30.0
0.6	-15.3	-14.0	-21.4	-21.3	-28.0	-27.0	-38.0	-36.5
0.9	-19.0	-18.5	-25.0	-24.0	-32.0	-30.5	-42.0	-40.0

Table 7.1 Cross-talk from PWM channel to PFM signal when $2\pi M = 0.5$, $f_1 = 400$ kHz, $f_2 = 300$ kHz, $f_0 = 2.04$ MHz.

The cross-talk performance is also affected by the frequency of the second modulating signal applied to the PWM channel. This effect was studied and the measured results are displayed in Fig. 7.9. As the bandwidth of the second modulating signal is doubled the cross-talk increases by about 6 dB, as predicted by equation 7.3. A set of results displayed in Fig. 7.10 shows the relations between the modulation indices M and β necessary to produce -25 dB cross-talk on the PFM channel, for different values of the ratio (f_2/f_1). The area under these curves represents the region where the cross-talk from PWM on PFM is worst than -25 dB (i.e. greater than -25 dB). It also can be seen by reducing f_2/f_1 , the frequency modulation index required to keep the same cross-talk at the same width modulation index is reduced. For example, for -25 dB cross-talk and

width modulation of $2\pi M = 0.5$ and $f_2/f_1 = 0.25$, the frequency modulation index should be kept at $\beta = 0.12$. However, keeping the same width modulation, and increasing the frequency ratio f_2/f_1 to 0.75 will require an increase in β to 0.4 to result in -25.4 dB cross-talk. This set of results will be used later to predict the optimum operating modulation indices for the system.

Another factor which also affects the cross-talk performance of the PFM channel is the pulse width of the regenerated PFM pulses. This can be studied by considering Fig. 7.11 which shows the timing diagram of the pulse separation stage at the PFM signal demodulator. It can be seen that the pulse width of the regenerated PFM pulses (τ_g) is controlled by changing the RC time constant. When the time constant of the circuit is very short, the position modulation of the negative pulse at the differentiator output will not affect the falling edge of the regenerated PFM pulses. However, when the time constant of the circuit increases (i.e. τ_g increases), the falling edge of the PFM pulses will be phase modulated due to the modulation of the negative pulses. Obviously, this will introduce extra cross-talk. This cross-talk can be minimised, in an ideal case, by proper choice of τ_g such that; $\tau_g < \tau_{min}$. Since $\tau_{min} = \tau_o - T_{PWM}$, $T_o = 2\tau_o$ and $M = 2T_{PWM}/T_o$, therefore, the pulse width of the regenerated PFM pulses should be chosen so that $\tau_g < \tau_o(1 - M)$ in order to minimise cross-talk on PFM channel.

This phenomenon has been studied, and the cross-talk from width modulation channel to frequency modulation channel has been measured and the results are displayed in Fig. 7.12 for different values of the modulation index M . As expected, when the pulse width τ_g increases cross-talk increases, and when M increases the cross-talk performance deteriorates rapidly. Therefore, pulses with narrow width (τ_g) are needed to keep the

performance to its best possible values. For example, if we allow 3dB deterioration in cross-talk, as a result of increasing τ_g , then when $2\pi M = 1$ the value of τ_g / τ_o should not exceed 0.5. However if the modulation index increases to $2\pi M = 2$ the value of τ_g / τ_o will be reduced to 0.45.

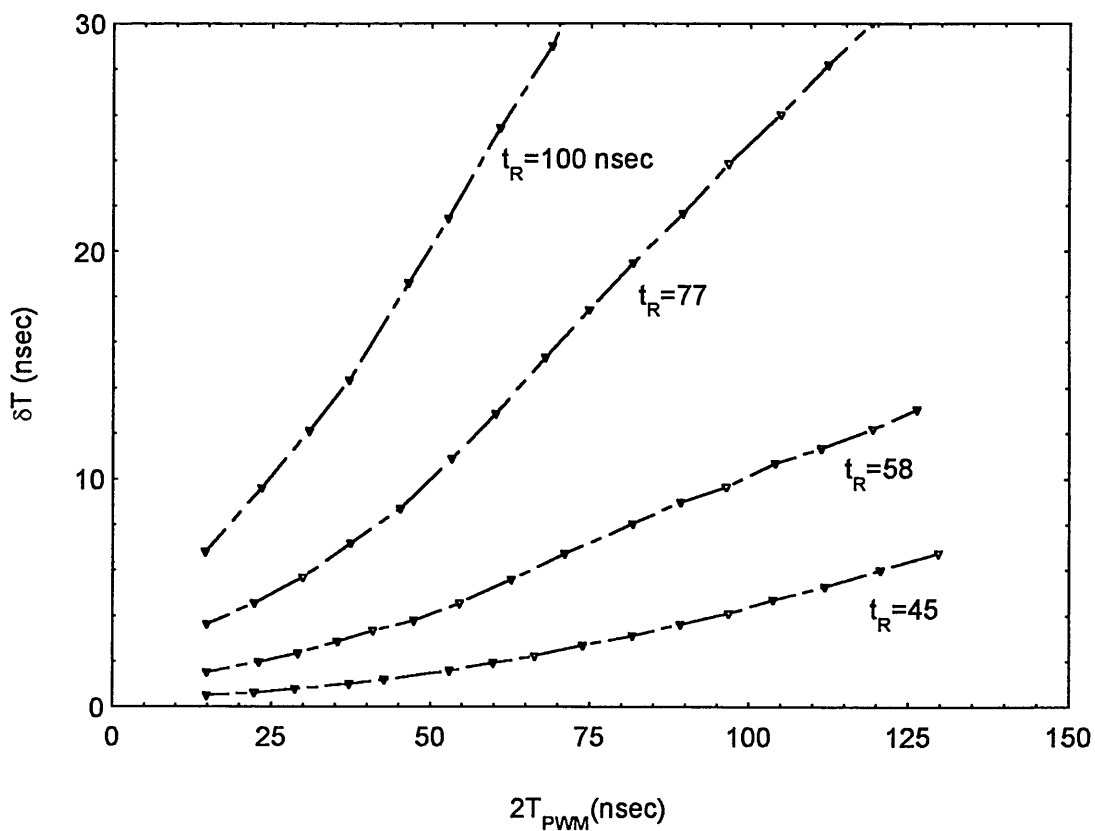


Fig. 7.4 Variation of time jitter with maximum pulse width deviation ($T_o=500$ nsec).

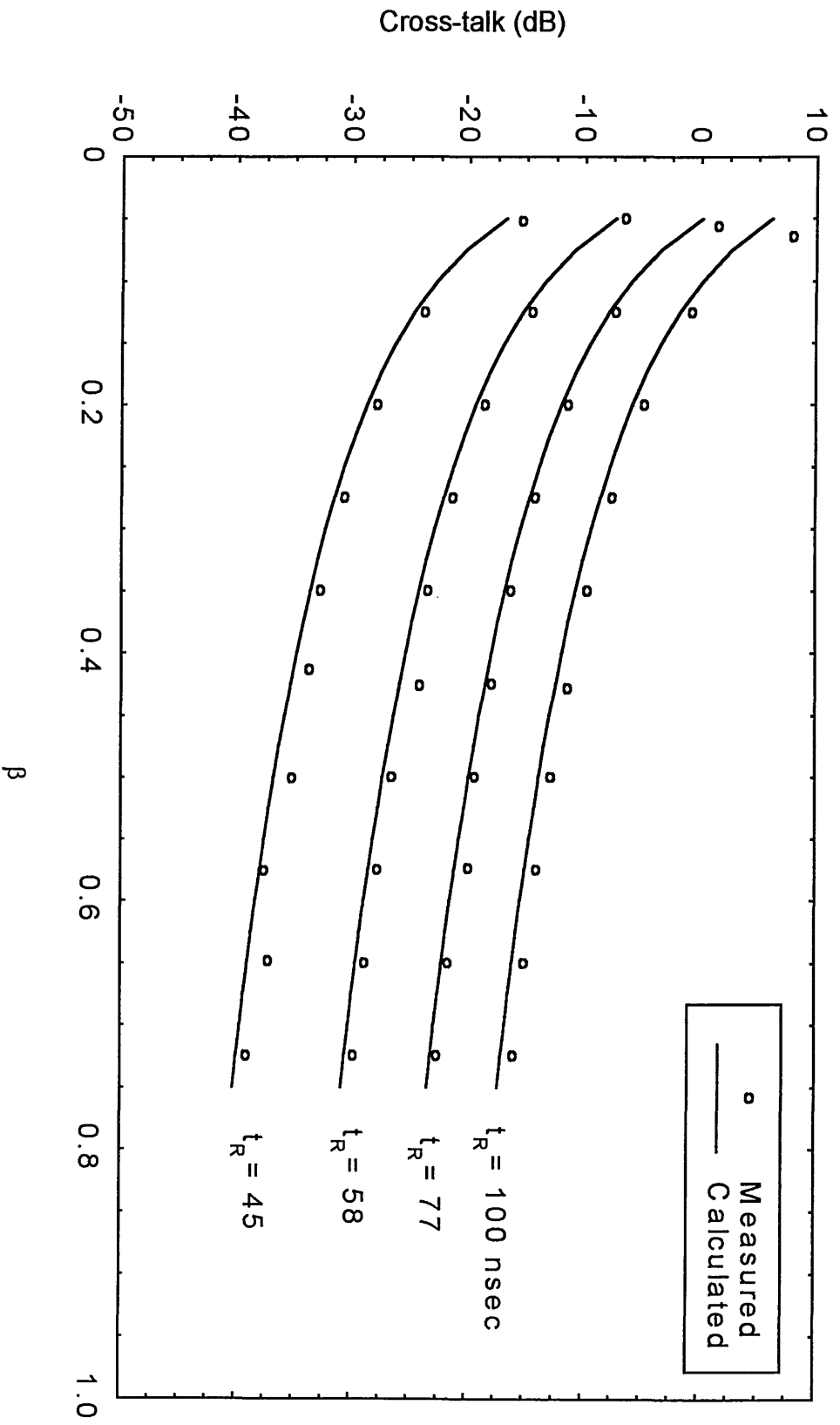


Fig. 7. 5 Cross-talk from the PWM channel to the PFM signal, $f_1 = 400$ kHz, $f_2 = 300$ kHz, $f_o = 2.04$ MHz, $2\pi M = 0.5$.

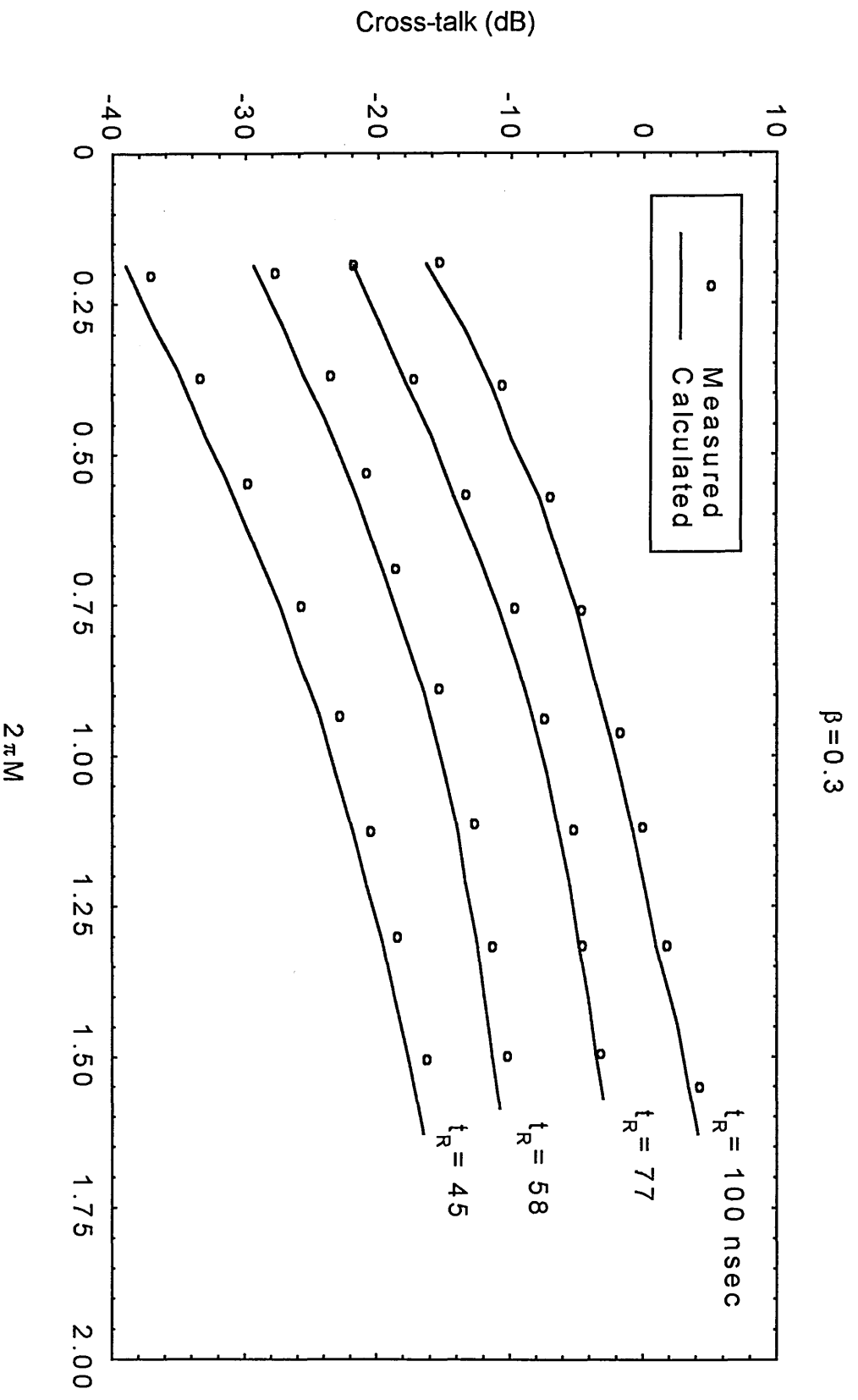


Fig. 7.6 Cross-talk from the PWM channel to the PFM signal, $f_1 = 400$ kHz, $f_2 = 300$ kHz, $f_o = 2.04$ MHz and $\beta = 0.3$.

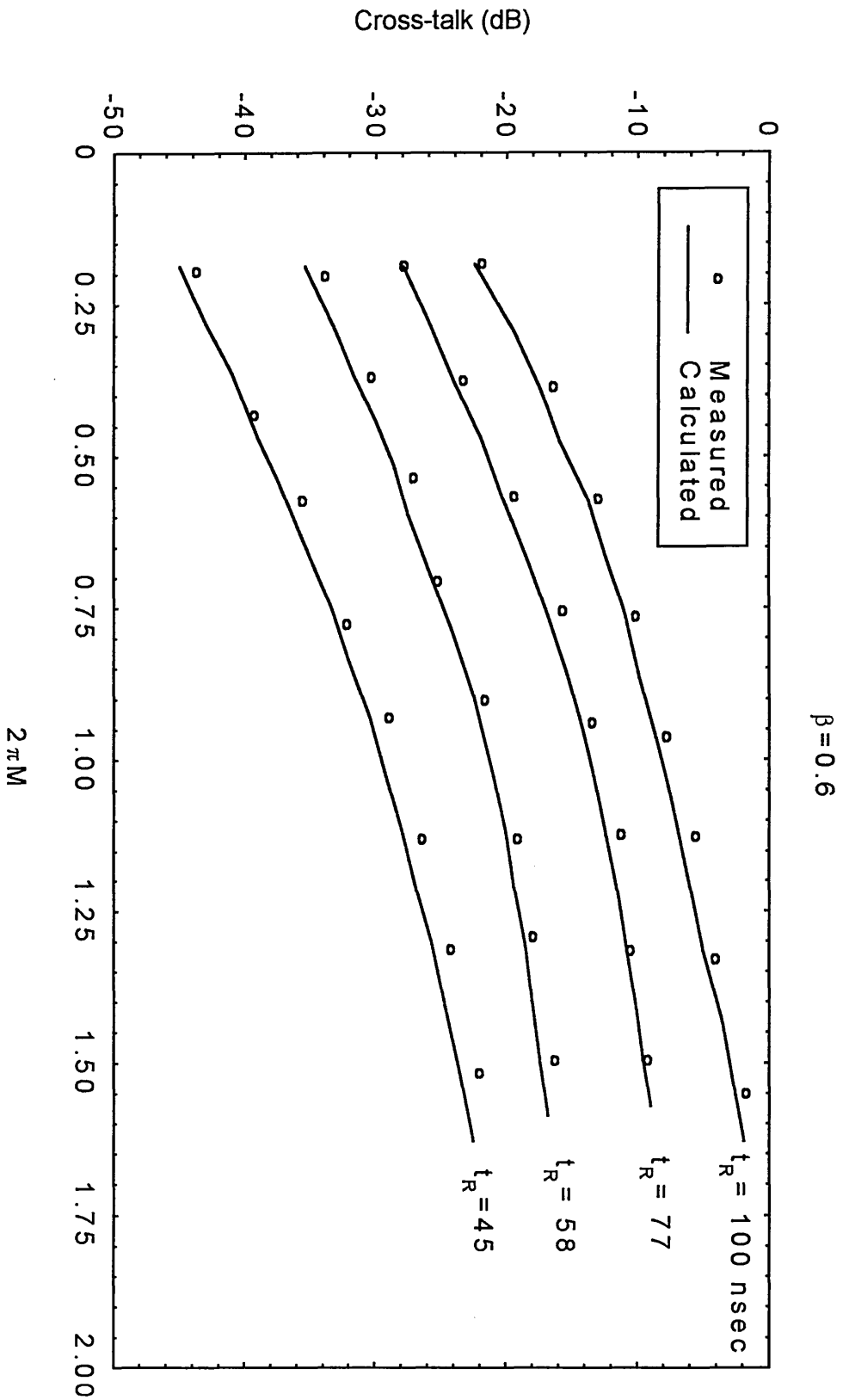


Fig. 7.7 Cross-talk from the PWM channel to the FPM signal, $f_1 = 400$ kHz, $f_2 = 300$ kHz, $f_o = 2.04$ MHz and $\beta = 0.6$.

$\beta = 0.9$

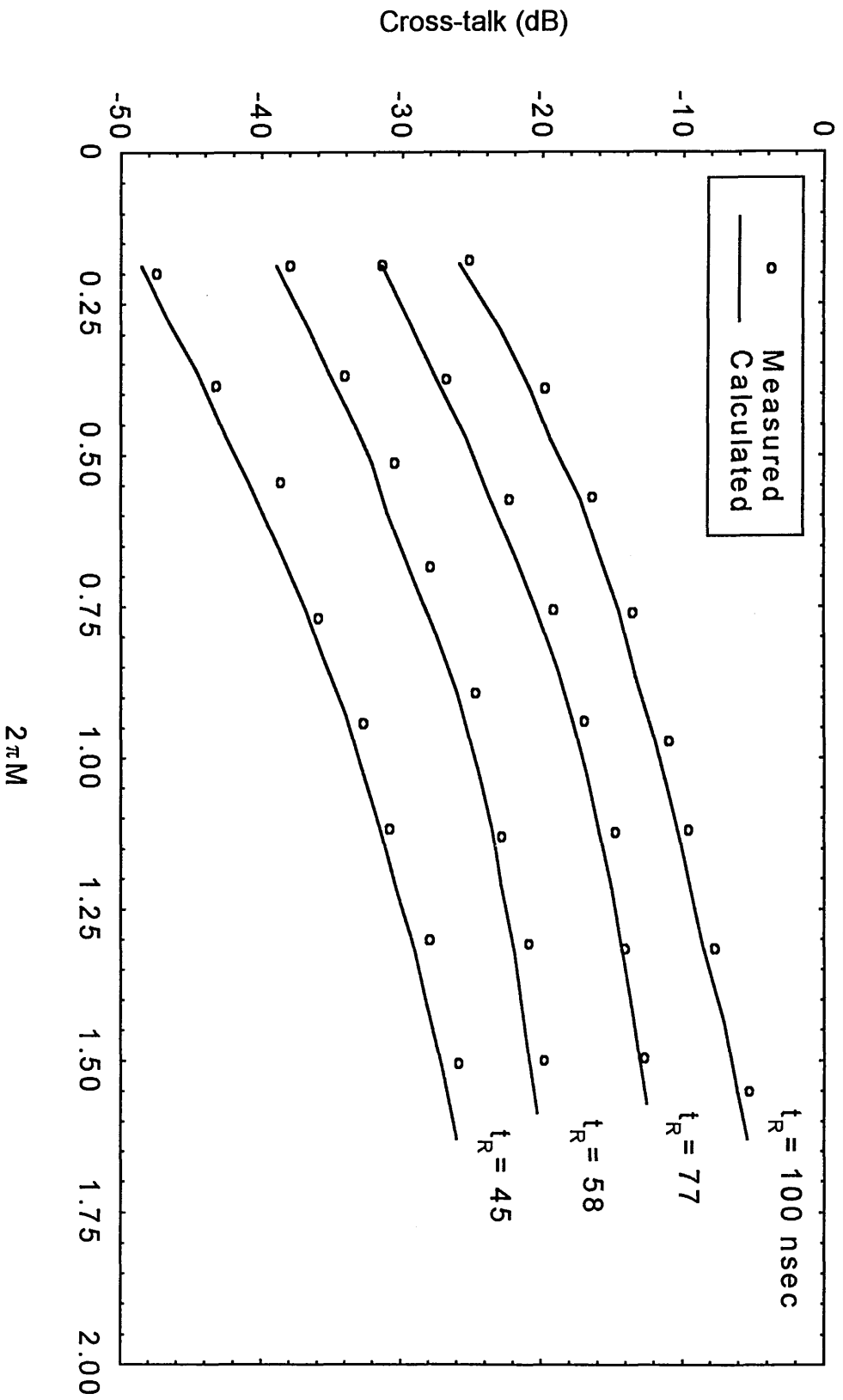


Fig. 7.8 Cross-talk from the PWM channel to the PFM signal, $f_1 = 400$ kHz, $f_2 = 300$ kHz, $f_o = 2.04$ MHz and $\beta = 0.9$.

$t_R = 58$

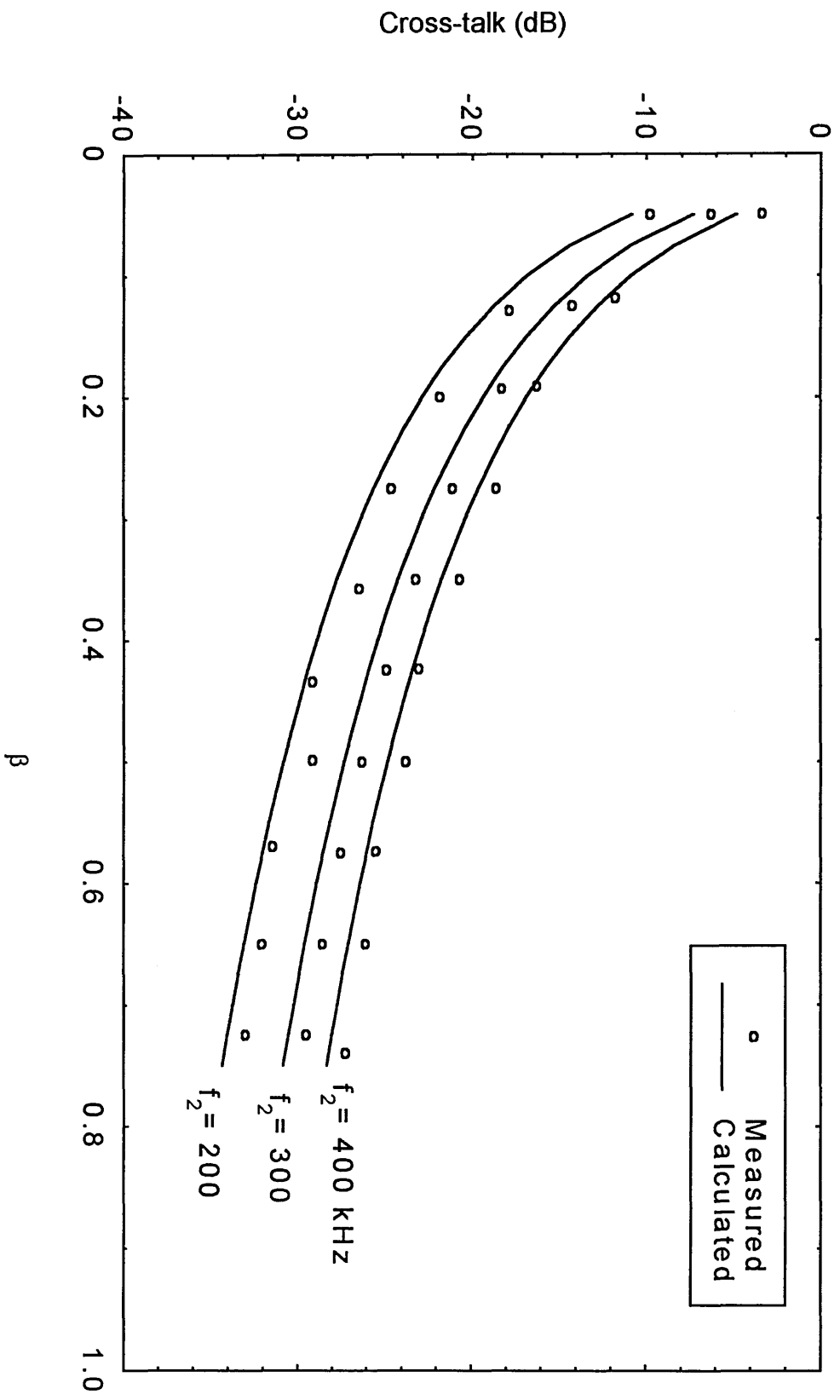


Fig. 7.9 Cross-talk from the PWM channel to the PFM signal, $f_1 = 400$ kHz, $f_o = 2.04$ MHz and $2\pi M = 0.5$, $t_R = 58$ nsec.

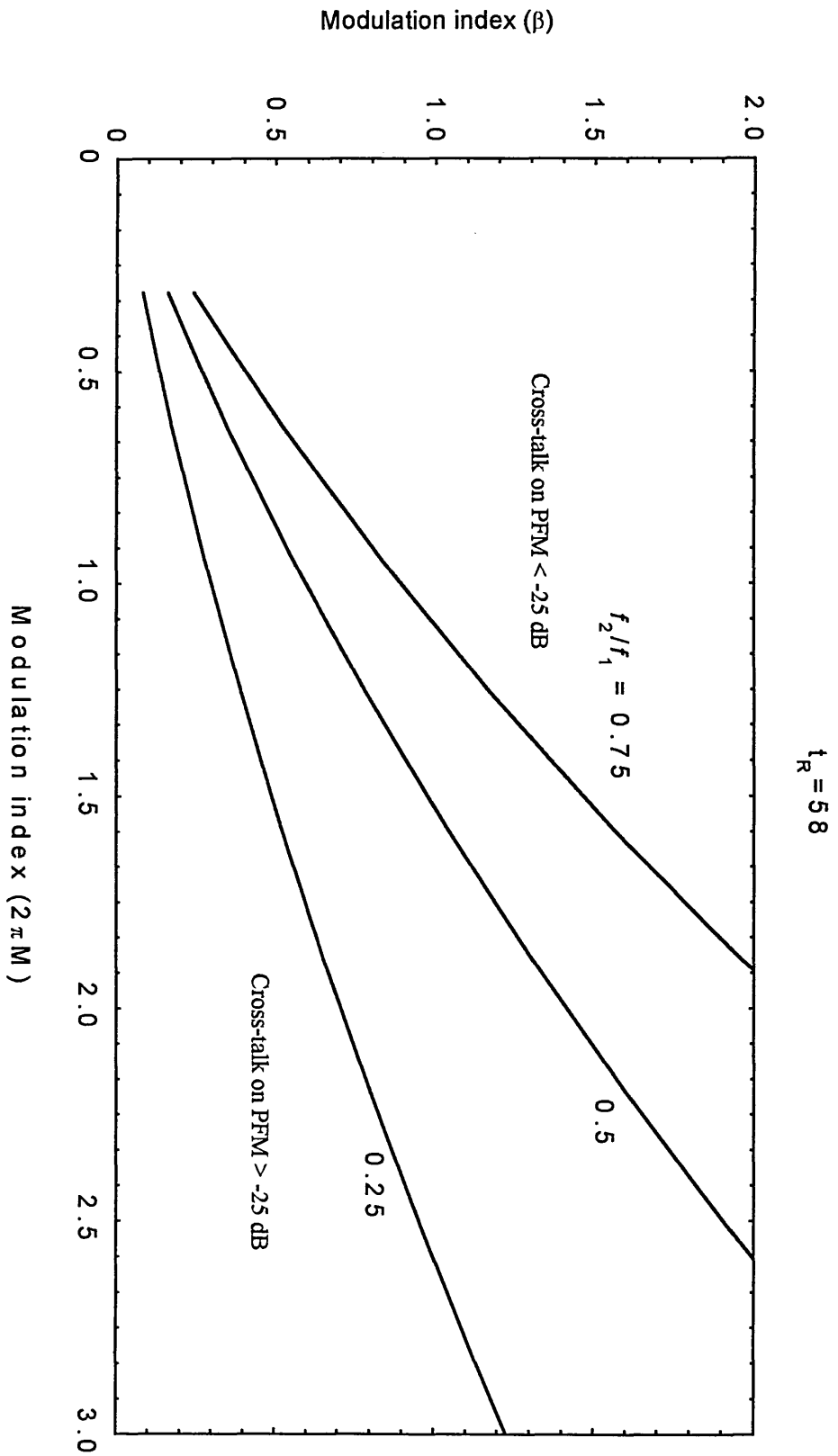


Fig. 7.10 Relation between modulation indices required to produce cross-talk on the PFM channel of -25 dB ($t_R=58$ nsec).

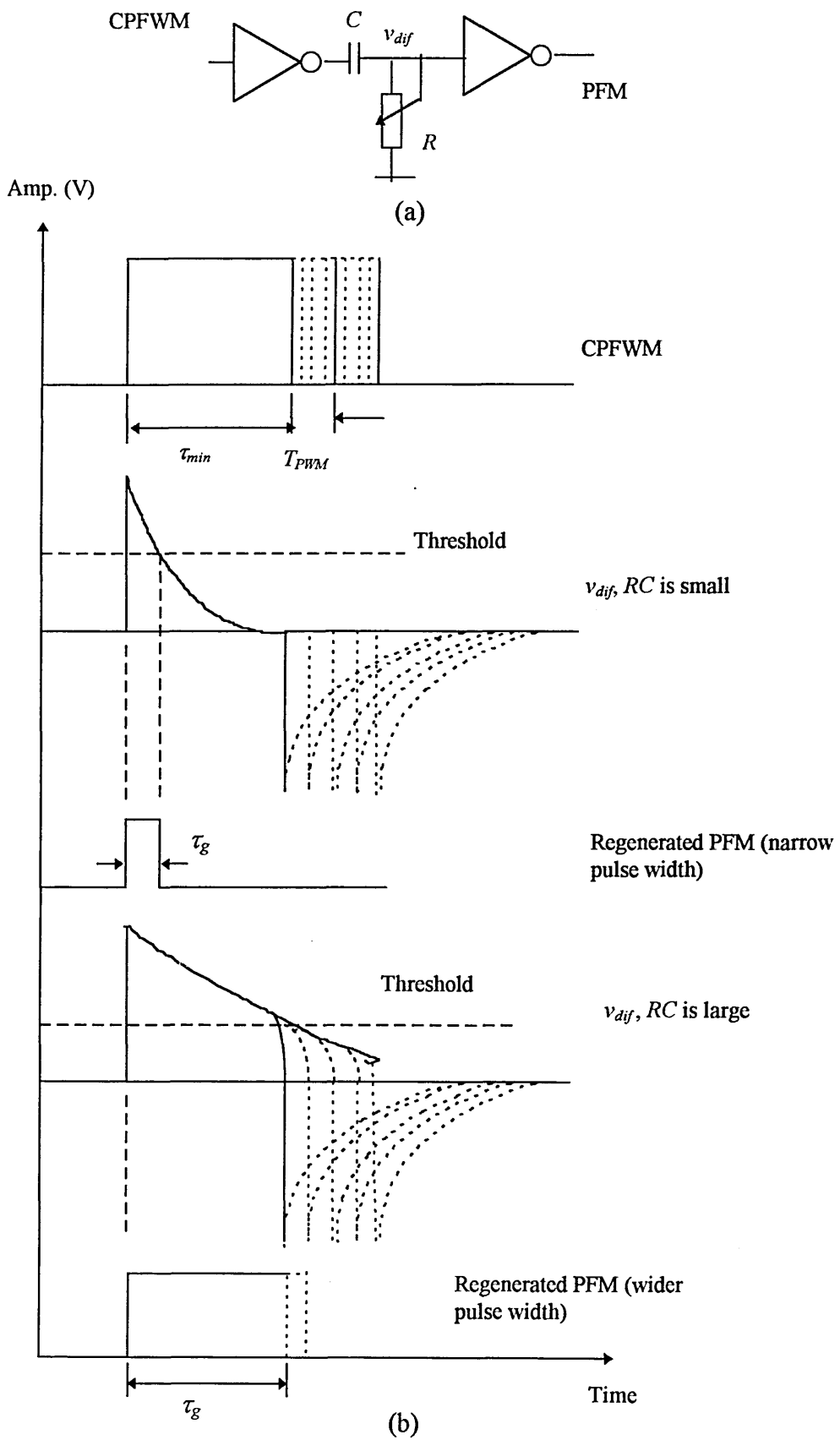


Fig. 7.11 Edge separation at the CPFWM receiver: (a) circuit diagram and (b) waveforms.

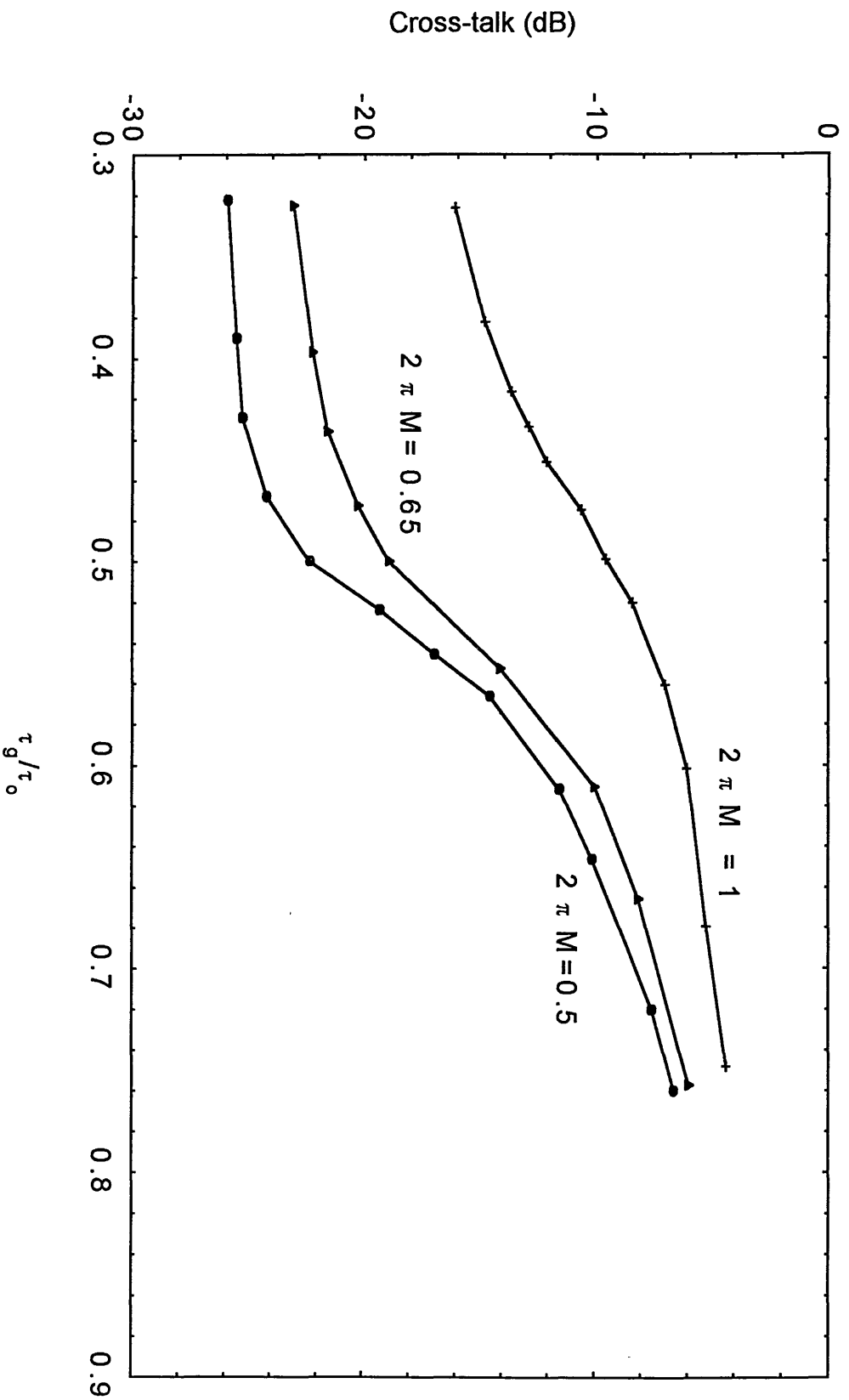


Fig. 7.12 Cross-talk from the PWM channel to the PFM signal, $f_1 = 400$ kHz, $f_2 = 300$ kHz, $f_o = 2.04$ MHz, $\beta = 0.3$ and $t_R = 58$ nsec.

7.2.2 Cross-talk from the PFM signal to the PWM signal

Figure 7.13 illustrates the block diagram and waveforms for demodulation of the PWM channel. The scheme is based on conversion of the received CPFWM pulse train into a PAM waveform, followed by low-pass filtering in order to recover the second modulating signal. Assuming that there is no distortion in the received CPFWM waveform, the demodulated PWM signal is represented as a PAM waveform with frequency modulated sampling pulses. It is this frequency modulation which results in a cross-talk from PFM signal to the PWM signal. In the absence of frequency modulation (i.e. no cross-talk), the frequency response of the PAM waveform may be given as;

$$e_1(f) = \text{sinc} \left(\frac{\pi f}{f_o} \right) \quad (7.4)$$

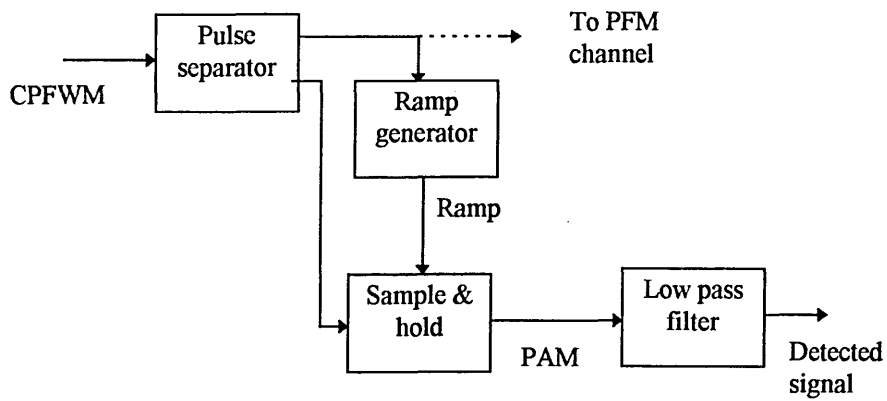
where, f_o is the sampling frequency.

However, in the presence of frequency modulation f_o changes to $(f_o \pm \Delta f)$ and equation 7.4 is rewritten as;

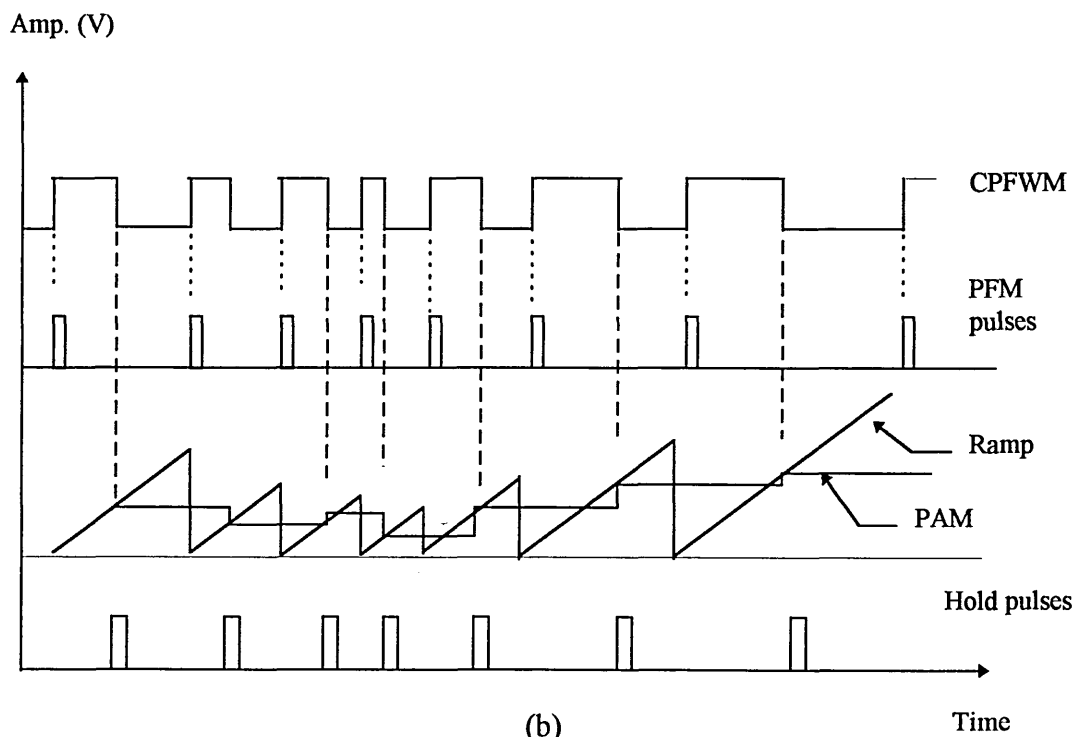
$$e_1(f) = \text{sinc} \left(\frac{\pi f}{f_o \pm \Delta f} \right) \quad (7.5)$$

where, Δf is the maximum frequency deviation. Equations 7.4 and 7.5 are plotted in Fig. 7.14, where the difference between the two responses correspond to the cross-talk given as;

$$CT_{FW1} = \left| \text{sinc} \left(\frac{\pi f_2}{f_o} \right) - \text{sinc} \left(\frac{\pi f_2}{f_o \pm \Delta f} \right) \right| \quad (7.6)$$



(a)



(b)

Fig. 7.13 Demodulation of the PWM channel: (a) block diagram and (b) waveforms.

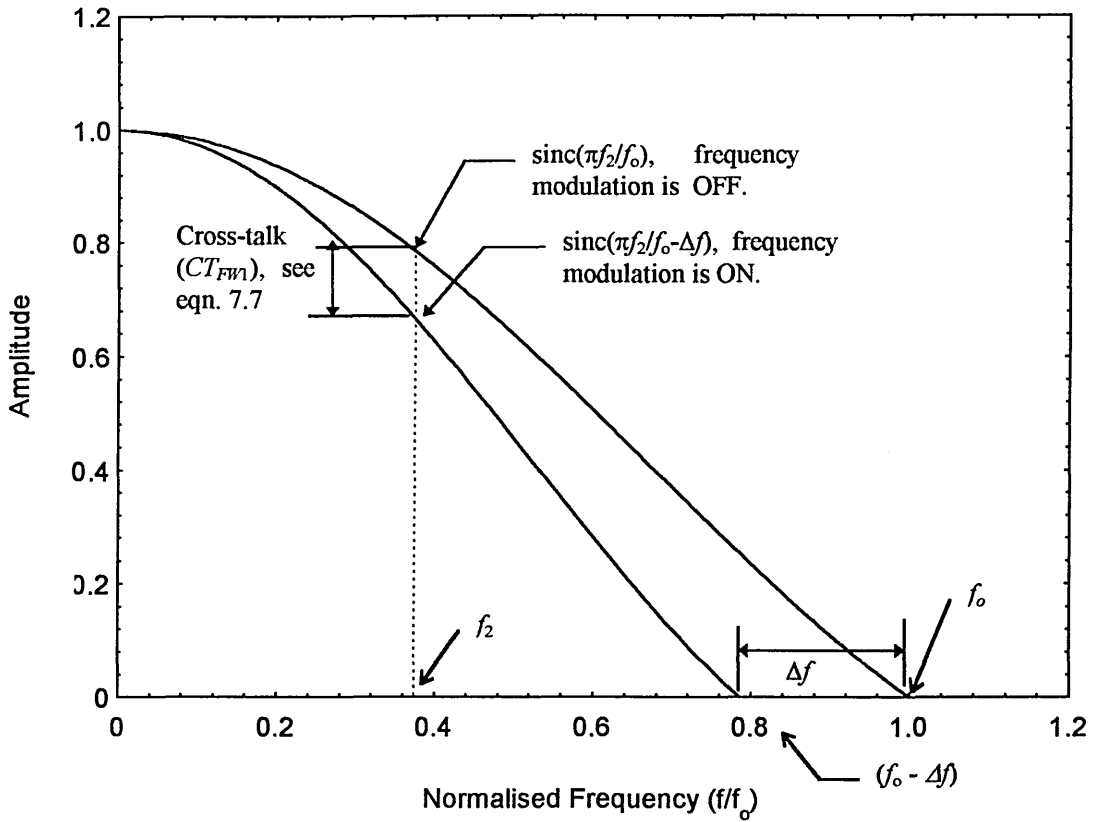


Fig. 7.14 Frequency response of PAM with frequency modulated sampling frequency.

Normalising it to f_0 , equation 7.6 can be rewritten as;

$$CT_{FW1} = \left| \text{sinc} \left(\frac{\pi f_2 / f_1}{f_0 / f_1} \right) - \text{sinc} \left(\frac{\pi f_2 / f_1}{f_0 / f_1 \pm \beta} \right) \right| \quad (7.7)$$

However, the modulation index β can be written in terms of the sampling ratio of the frequency modulation channel (f_1/f_0) as;

$$\beta = \frac{\Delta f}{f_1} = \frac{\Delta f}{f_0} \frac{f_0}{f_1} \quad (7.8)$$

Substituting equation 7.8 into 7.7, the cross-talk on PWM channel can be written in terms of the frequency modulation index as;

$$CT_{FW1} = \left| \text{sinc} \left(\frac{\pi f_2}{f_o} \right) - \text{sinc} \left(\frac{\pi f_2 / f_o}{1 \pm \beta(f_1 / f_o)} \right) \right| \quad (7.9)$$

In order to show the effect of both the modulation index β and the sampling ratio f_1/f_o on cross-talk, equation 7.8 and 7.7 are plotted in Fig. 7.15 for different values of the sampling ratios f_1/f_o and f_2/f_o . From equation 7.9 the sampling ratio f_1/f_o represents a scaling factor to the x-axis of Fig. 7.15. The graph of cross-talk versus β will have the same profile as that of cross-talk versus $\Delta f/f_o$. However, the only difference is in the x-axis which need scaling. This is simply done by incorporating a second set of graphs (dotted lines, see Fig. 7.15). To illustrate this let us look at an example: for cross-talk of -40 dB and $f_2/f_o = 0.25$, the required $\Delta f/f_o$ is 0.05 for a given set-up. This can also be reflected on β by simply intersecting the dotted lines as shown, i.e. for the same cross-talk and f_2/f_o , β could be either 0.25 at $f_1/f_o = 0.2$ or 0.1 at $f_1/f_o = 0.5$. This graph gives an ability to select various parameters of the system if one or two of them are already given.

The dynamic range of the system may be obtained by operating at Nyquist sampling rate for both channels. This rate (i.e. f_1/f_o or f_2/f_o) represents the maximum sampling rate in many applications, above which the non-linear distortion will increase. Figure 7.15 can also be used to define the dynamic region of the system as identified by the area between the curve for $f_2/f_o = 0.5$ and the dotted line for $f_1/f_o = 0.5$.

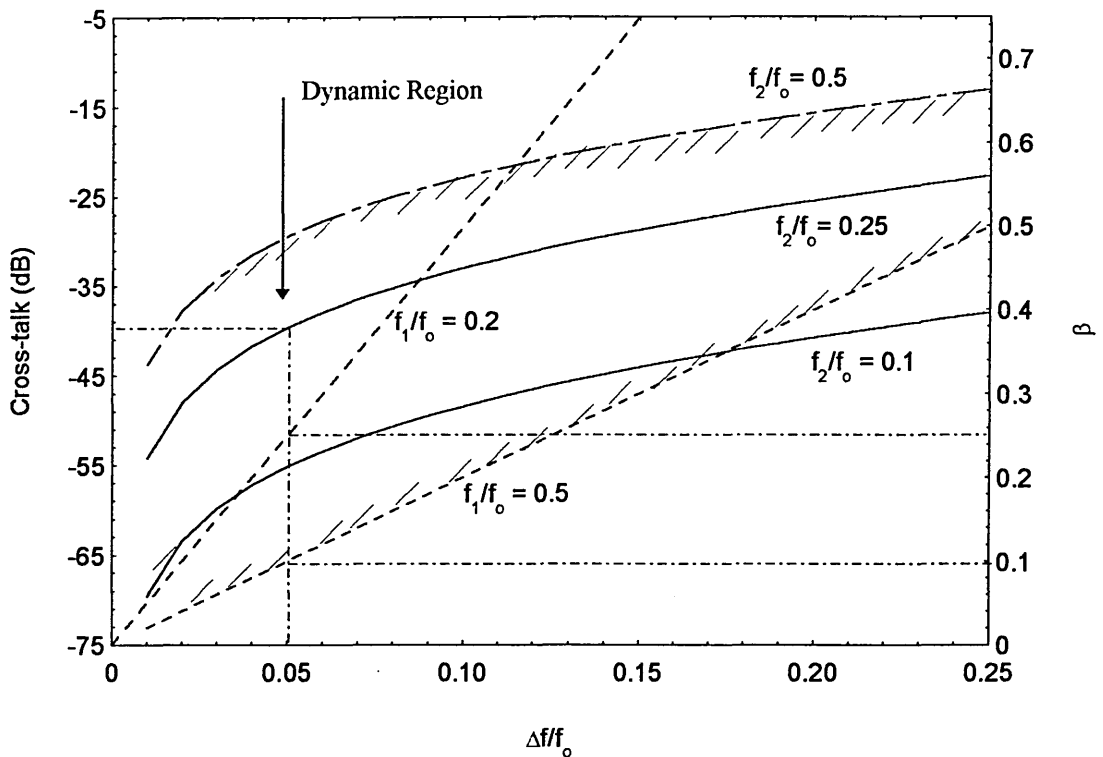


Fig 7.15 Cross-talk from PFM signal to PWM signal in an ideal transmission, the dotted lines represents the critical cases where the sampling ratio is 1:2.

Figures 7.14 and 7.15 also show that the cross-talk increases with the frequency deviation Δf . The increase in cross-talk is mainly due to the second term of equation 7.7 which increases with Δf . At sampling ratio $f_2/f_0 = 0.1$, cross-talk is -53 dB when $\Delta f/f_0$ is 0.05. Doubling the frequency deviation the cross-talk will increase by 5 dB. The cross-talk also increases with the frequency of the second modulating signal. This is because of the nature of the frequency response of the PAM waveform, see Fig. 7.13. At frequency deviation of 0.1 and sampling ratio (f_2/f_0) of 0.1, the cross-talk is -48 dB. However cross-talk will be -33 dB (i.e. increased by 15 dB) when the sampling ratio increases to 0.25.

In the above cross-talk analysis, it was assumed that the system is ideal with no waveform distortion present. However, in non-ideal case, where signal distortion plays an important role, it is vital to take distortion into account. When the pulse frequency changes, the time interval from the fall of the pulse to the rise of the next pulse (T_w) also changed, see Fig. 7.16. The rise of the next pulse is modulated by the preceding pulse, see Fig. 7.1. This produces a cross-talk from the PFM signal to the PWM signal which depends on the time jitters δT produced by the frequency modulation, as illustrated in Fig. 7.16. The cross-talk due to the non-linear distortion can be given as;

$$CT_{FW2} = \frac{\delta T}{2T_{PWM}} \quad (7.10)$$

where, T_{PWM} is the maximum pulse width deviation of the width modulated channel. The overall system cross-talk may be evaluated by adding both components given in equations 7.10 and 7.7. This leads to;

$$CT_{FW} = \sqrt{CT_{FW1}^2 + CT_{FW2}^2} \quad (7.11)$$

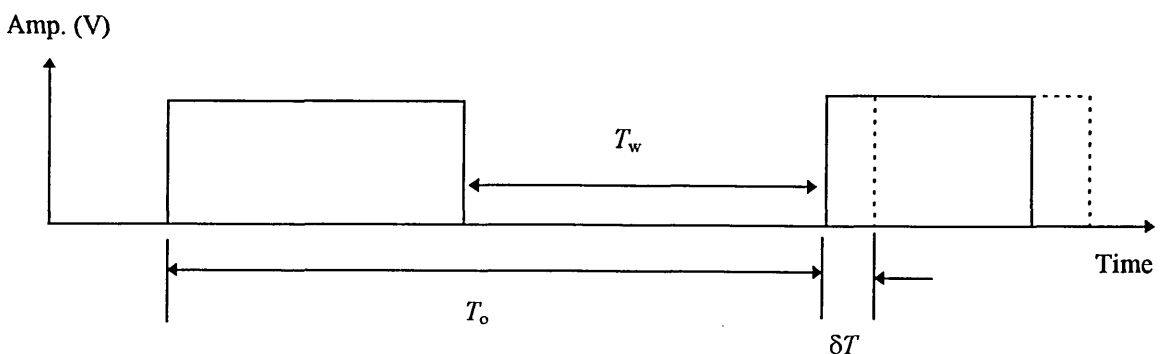


Fig. 7.16 CPFWM waveform.

When the signal distortion is low and the rise time of the received pulses is very small (i.e. pulses almost ideal) the overall cross-talk is mainly due to the first term of equation 7.11. However, in the case of high distortion and longer rise time, the total cross-talk is dominated by the second term of equation 7.11, and this is the case in most practical systems.

In order to characterise the cross-talk performance from frequency modulation to width modulation channel, a number of measurements were taken and the results are shown in this section. The first measurement set is shown in Fig. 7.17, in which the time jitter is measured as a function of the change in the channel frequency. The same method used in the previous section; the width modulation index is kept constant, and the carrier frequency is now changed and the change in δT is measured as a function of the change in the carrier frequency. It is clear from Fig. 7.17 that the time jitter is increasing with the rise time of the pulse and the change in the frequency. Consequently the cross-talk is deteriorating with the rise time and the frequency modulation index.

Another set of results displayed in Figs. 7.18-7.20 shows both the measured and calculated cross-talk from PFM channel to PWM channel as a function of the modulation index $2\pi M$ for different values of frequency modulation index β and pulse rise time t_R . Cross-talk increases with β due to an increase in time jitter as one would have expected. On the other hand cross-talk can be reduced by increasing the width modulation (i.e. increasing the signal strength). Doubling the modulation index (M) results in about 6 dB improvement in the cross-talk. As outlined earlier cross-talk can also be reduced by reducing the rise time of the waveform (or by increasing the transmission bandwidth). Shorter rise time means more time for modulation and less

time for edge-to-edge energy overlap. A summary of the effect of the rise time of the received waveform is given in Table 7.2. This table shows that the difference between the measured and the calculated results is within ± 1 dB. Figure 7.21 shows the variation of cross-talk with modulation index β . It is clear that when β increases, the time jitter increases and consequently the cross-talk performance will deteriorate.

$2\pi M$	Cross-talk (dB)							
	$t_R = 100$		$t_R = 77$		$t_R = 58$		$t_R = 45$	
	Calculated	Measured	Calculated	Measured	Calculate	Measured	Calculate	Measured
0.4	-9.5	-9.0	-14.1	-12.7	-16.6	-16.0	-18.9	-18.0
0.6	-13.0	-12.0	-17.6	-17.0	-20.1	-20.0	-22.4	-22.0
0.8	-15.5	-	-20.1	-	-22.6	-	-25	-24.0

Table 7.2 Summary of cross-talk from the PFM channel to the PWM channel for different rise time values.

Another set of results displayed in Fig. 7.22 shows the relationship between the modulation indices, β and M when cross-talk is kept at a constant value (i.e. for example -25 dB) and for different rise time of the received pulse. The areas under these curves represent the region where the cross-talk from PFM channel on PWM channel is better than -25 dB (i.e. smaller than -25 dB). Also evident is that as the rise time increases the frequency modulation index needs to be reduced to result in the same cross-talk at the same width modulation. To illustrate, for $t_R = 45$ nsec and cross-talk = -25 dB, the maximum frequency modulation index is 1.0. However, if t_R increases to 77 nsec, then the maximum value of β required to keep the same cross-talk drops to 0.65. This means in order to keep the same cross-talk performance with less transmission bandwidth the noise performance must be degraded.

The relationships between modulation indices in both channels can be obtained by combining Fig.7.10 and Fig. 7.22. A typical case has been displayed in Fig. 7.23 when $f_2/f_1 = 0.5$, and rise time of 58 nsec. In this figure, four different regions can be distinguished;

- region A; where cross-talk in both channels is better than -25 dB,
- region B; where cross-talk in both channel is worse than -25 dB,
- region C; where cross-talk in PFM channel is better than that at PWM channel
- region D; where cross-talk in PWM channel is worst than that at PFM channel.

The optimum region to operate would be region A, where both channels will have cross-talk less than -25 dB.

To compare cross-talk performance in both channels, as well as with other systems, a set of results is displayed in Fig. 7.24. In this figure, the cross-talk in both channels is measured as a function of modulation index β , and keeping the width modulation $2\pi M$ at a fixed value. It can be observed that the cross-talk from PWM channel to PFM channel decreases with the increase of the modulation index β . This is because when β increases the level of the detected signal at the frequency modulation channel increases, and since the width modulation is fixed at certain value, then the only parameter which effect the cross-talk is the time jitter δT . δT also increases with β , but the rate of the increase is much smaller than that of the recovered signal (at the PFM channel). The case is different when we consider the cross-talk from PFM to PWM; for a fixed value of $2\pi M$ the level of the detected signal at the PWM channel is also fixed. When β increases, δT increases, which leads to an increase in the waveform interference. Therefore, the cross-talk will increase with the increase of the modulation index β . Thus the optimum value of β is 0.6 resulting in -30 dB cross-talk at $2\pi M=1$.

For comparison, cross-talk of the CPFWM system and a typical two channel PPM time division multiplexed (TDM-PPM) system are also shown in Fig. 7.24. The detailed mathematical analysis of cross-talk performance of the TDM-PPM is given in Appendix-III. The CPFWM system shows a comparable performance with the TDM-PPM system, provided that the TDM-PPM duty cycle is high. At low β cross-talk on the PWM channel is better than that for TDM-PPM system with low duty cycle. CPFWM system will give better performance than TDM-PPM, provided the channel bandwidth is limited. On the other hand, TDM-PPM with low duty cycle will outperform CPFWM by about 10 dB, but the system is more complex and will require very large bandwidth and time synchronisation at the receiving end.

Figure 7.25 shows cross-talk in the CPFWM system as a function of the unmodulated pulse duty cycle together with cross-talk performance of the CPFWM and TDM-PPM systems. As can be seen when the pulse duty cycle increases cross-talk on the PWM channel decreases. At duty cycle of 0.5 and beyond the fall in cross-talk is significant. This is because of the edge-to-edge overlapping being highest when operating at a low duty cycle. On the other hand, as the duty cycle increases the maximum PWM modulation index decreases by the same amount thus resulting in increased non-linear distortion and reduced signal-to-noise ratio performance in PWM channel (see Fig. 7.25). Therefore, just like a PTM system, there exist cross-talk, non-linear distortion and *SNR* trade-off, and one might have one or two improved for a certain set-up but not all. The improvement in the cross-talk is due to the increase in the spacing between the rising and the falling edge of the received pulse. This results in less energy overlap from the rise edge (PFM channel) and the falling edge (PWM channel). The

signal-to-noise ratio deterioration results from the reduction in the maximum modulation index and the increase in the system non-linearity.

The effect of increasing duty cycle on cross-talk from PWM to PFM is different from the previous case. Here, the cross-talk increases with duty cycle. This is due to the narrower separation between the falling edge and the rising edge of the received pulse. It can be seen from Fig. 7.25 that the system (i.e. both channels of CPFWM) shows best balance between the non-linear distortion, and cross-talk performance when the duty cycle is around 0.5.

The TDM-PPM system behaviour with the duty cycle is completely different. Figure 7.25 shows the cross-talk in one channel of TDM-PPM system when the maximum modulation index of the first channel used is ($M_2 = 0.5$) and the second channel (the interfering channel) is kept at reasonably low modulation index ($M_1 = 0.16$). Cross-talk performance significantly deteriorates when duty cycle increases. Unless duty cycle is kept small (i.e. very short pulse width), the cross-talk between TDM-PPM channels will be serious.

Finally, CPFWM shows reasonable balance between the cross-talk performance, non-linear distortion and signal-to-noise ratio at 50% duty cycle. Comparing it with a low duty cycle TDM-PPM system shows that the CPFWM system offers comparable cross-talk performance, and in some cases, it shows an improved performance. However, the main advantage of using a CPFWM system over a TDM-PPM system is its simplicity and self synchronisation characteristics.

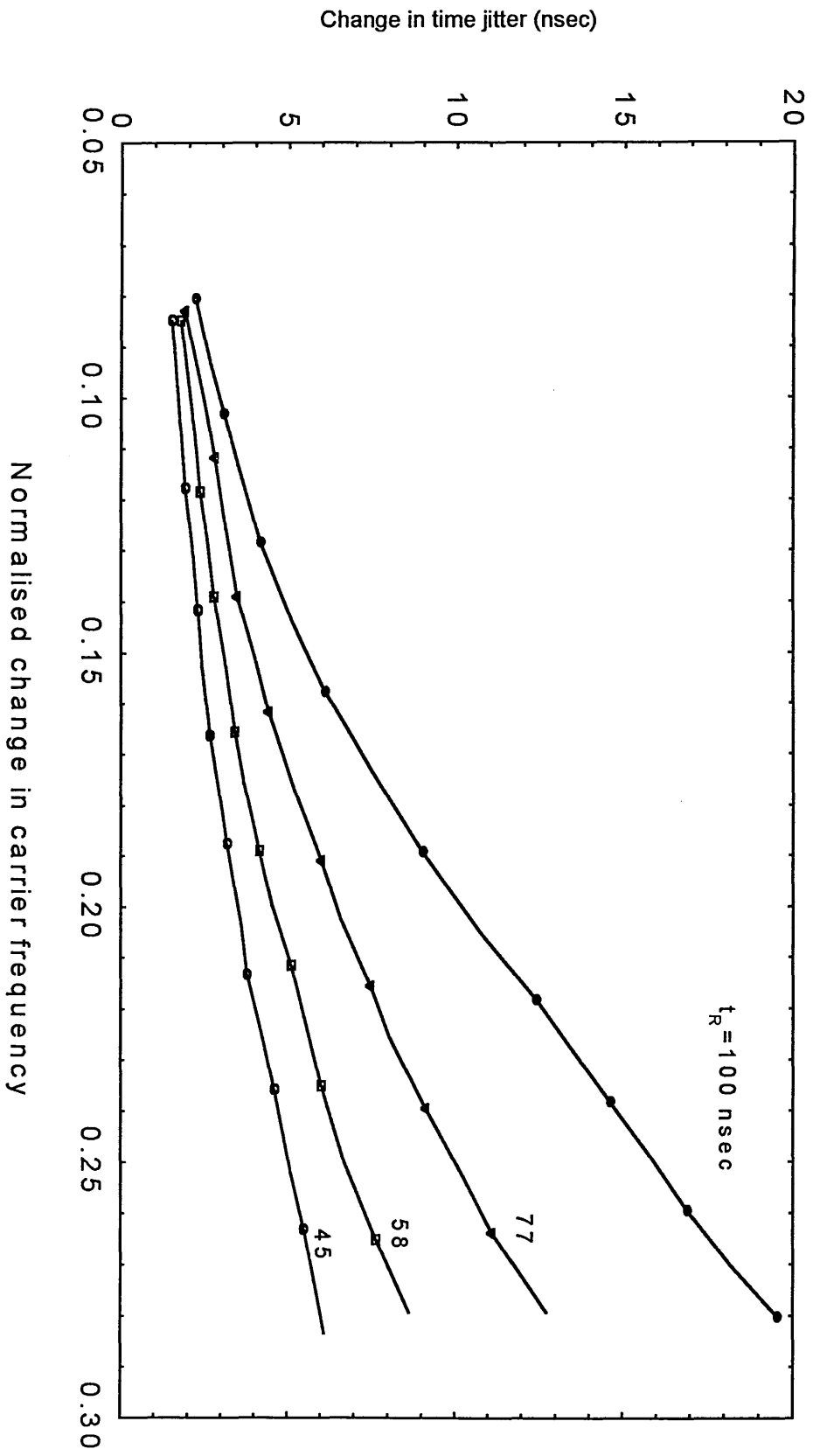


Fig. 7.17 Variation of time jitter with change in carrier frequency (i.e. $\Delta f/f_1$) ($T_0 = 500$ nsec).

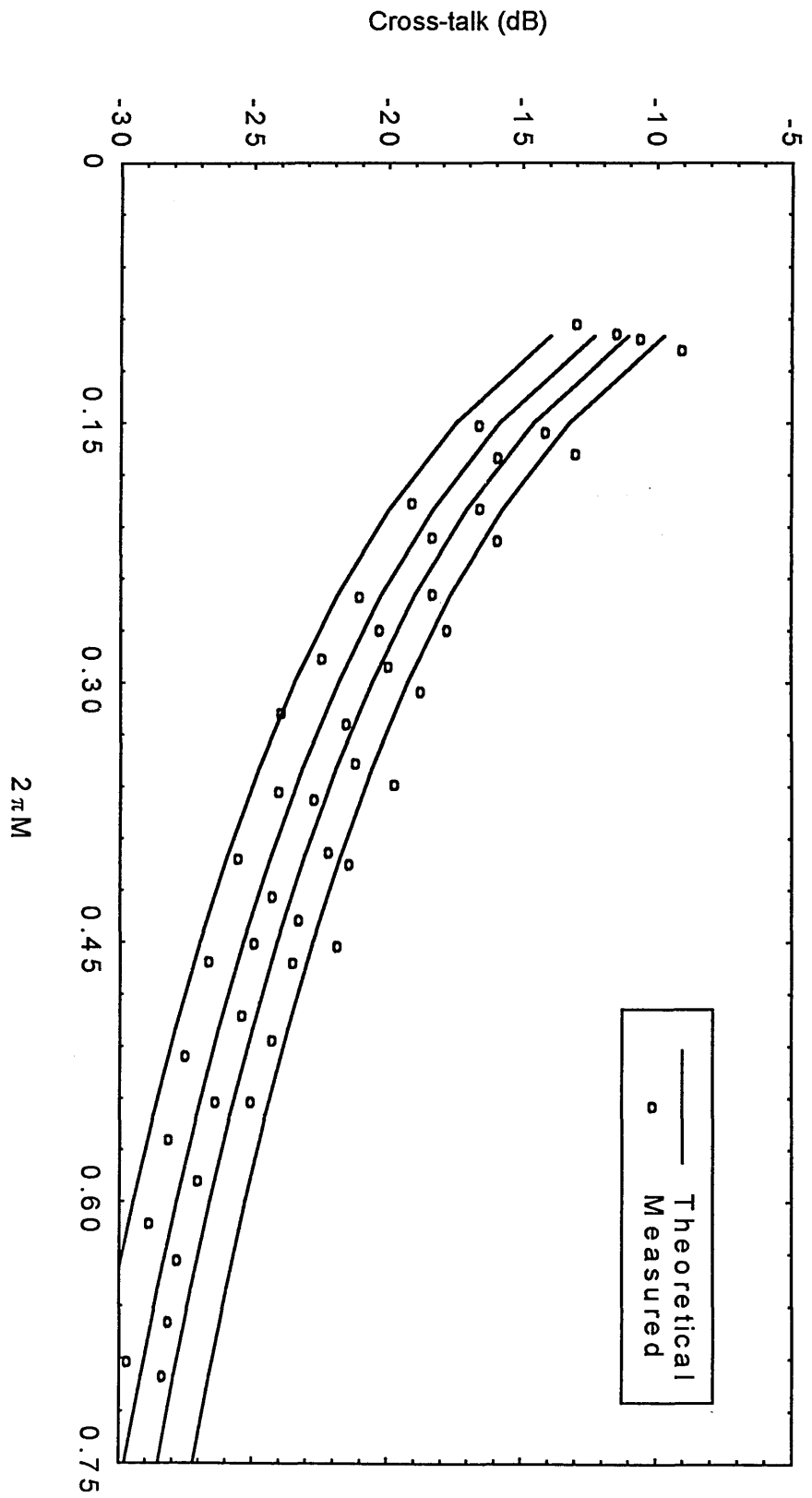


Fig. 7.18 Cross-talk from the PFM channel to the PWM signal, $f_1 = 400$ kHz, $f_2 = 305$ kHz, $f_o = 2.04$ MHz, $\beta = 0.5$.

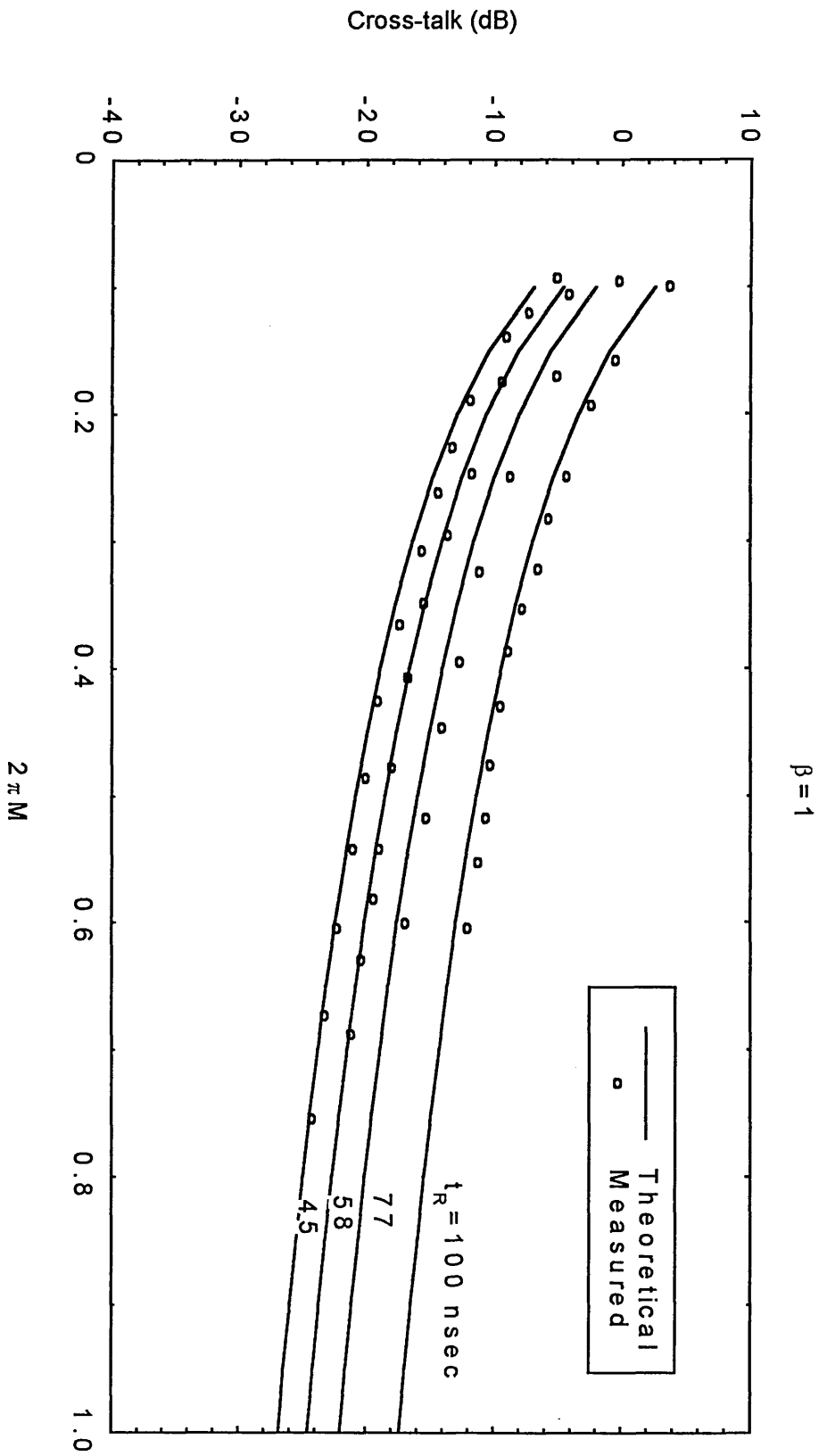


Fig. 7.19 Cross-talk from the PFM channel to the PWM signal, $f_1 = 400$ kHz, $f_2 = 305$ kHz, $f_o = 2.04$ MHz, $\beta = 1$.

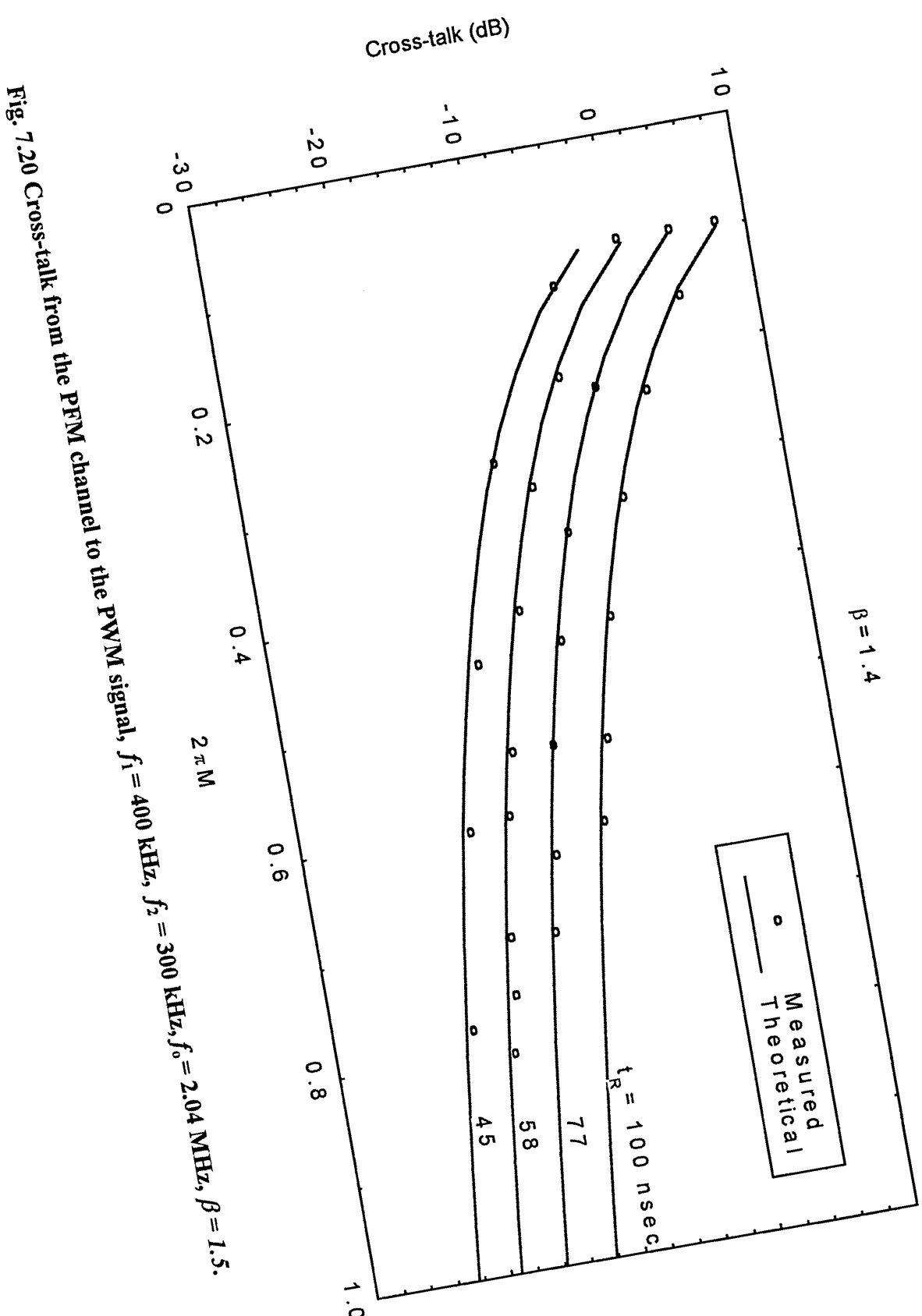


Fig. 7.20 Cross-talk from the PFM channel to the PWM signal, $f_1 = 400 \text{ KHz}$, $f_2 = 300 \text{ KHz}$, $f_0 = 2.04 \text{ MHz}$, $\beta = 1.5$.

$2\pi M = 0.5$

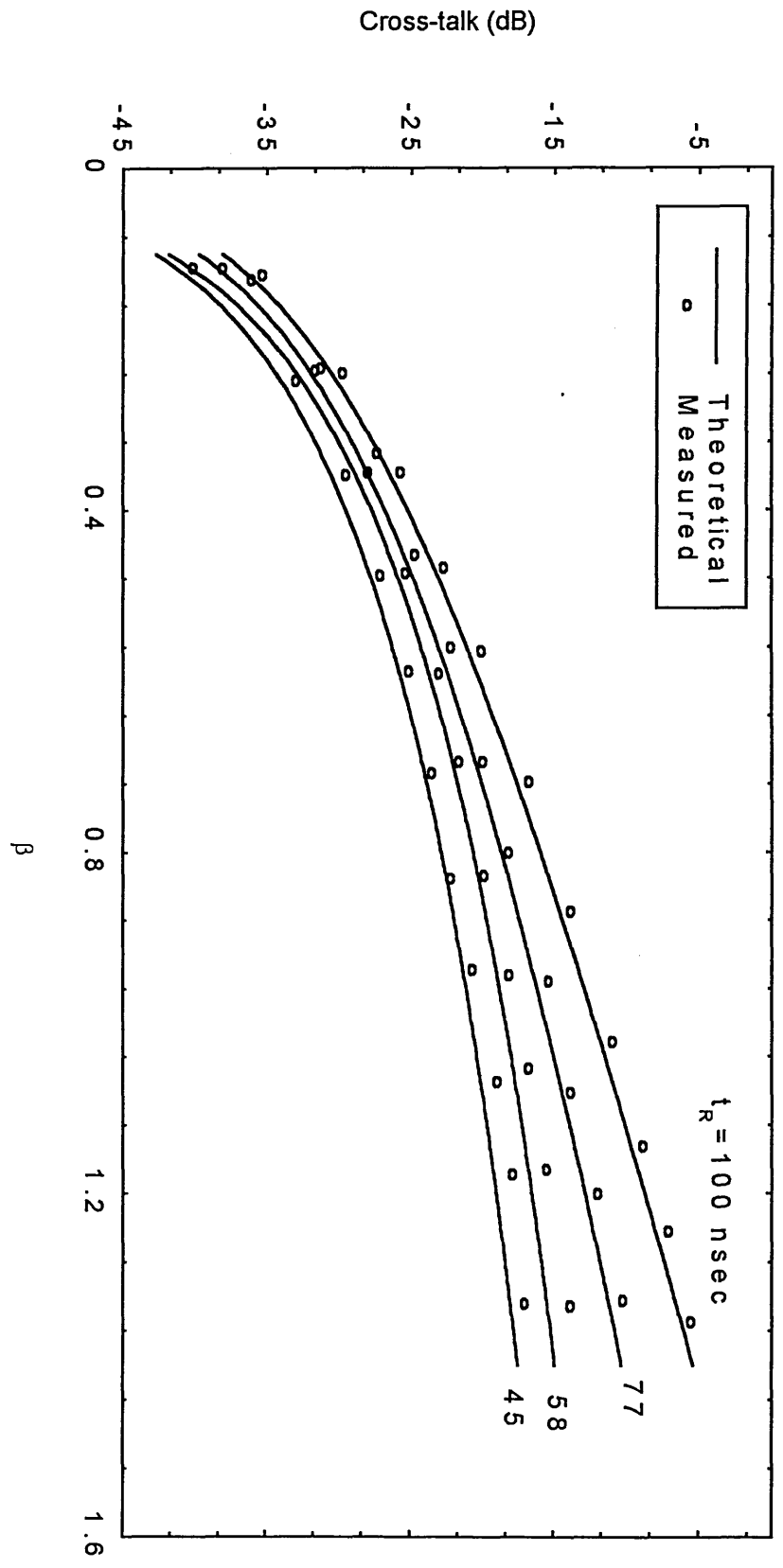


Fig. 7.21 Cross-talk from the PFM channel to the PWM signal, $f_1 = 400$ KHz, $f_2 = 300$ KHz, as $f_o = 2.04$ MHz, $2\pi M = 0.5$.

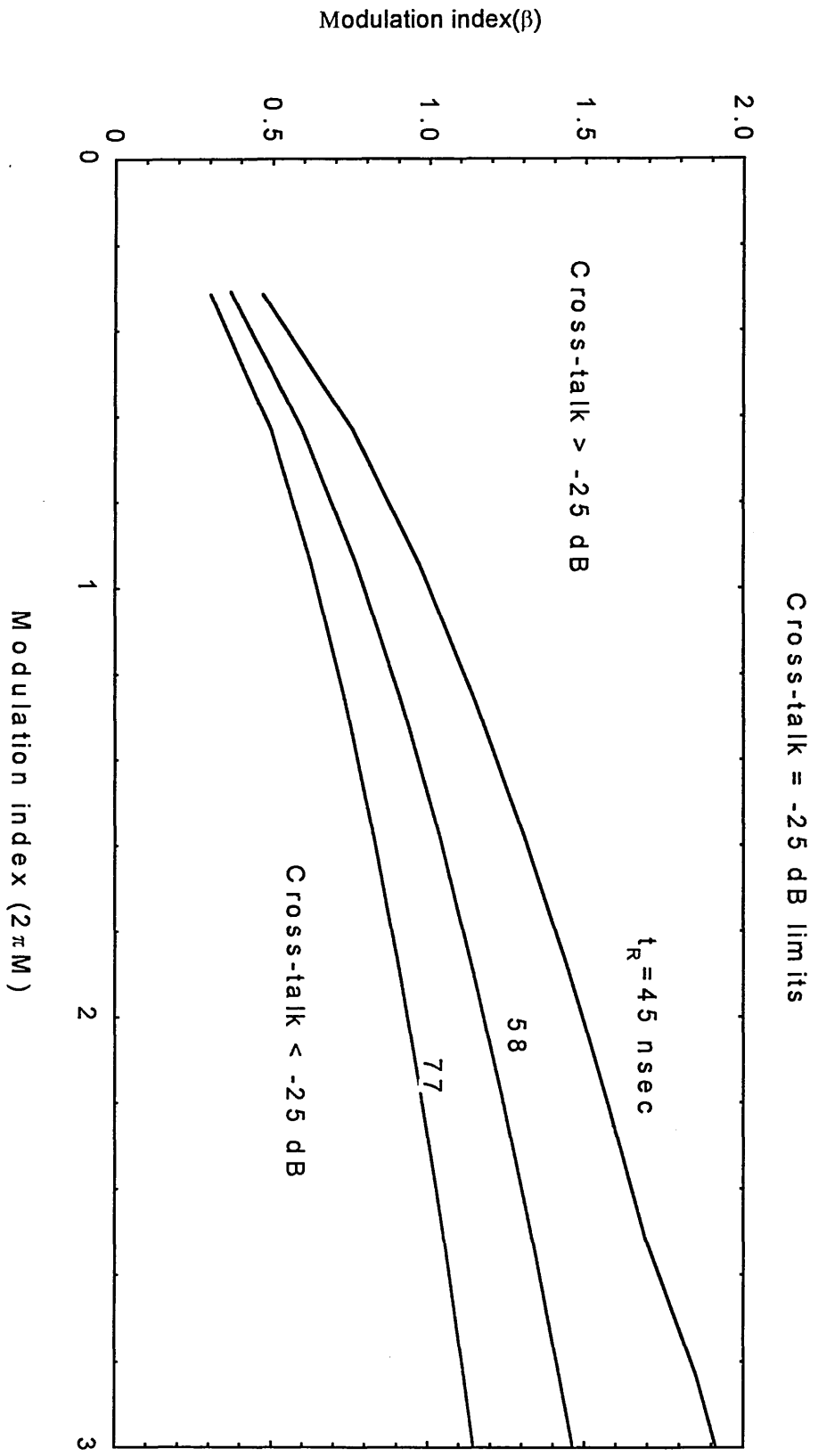


Fig. 7.22 Relationships between modulation indices to produce cross-talk of -25 dB at different values of pulse rise time.

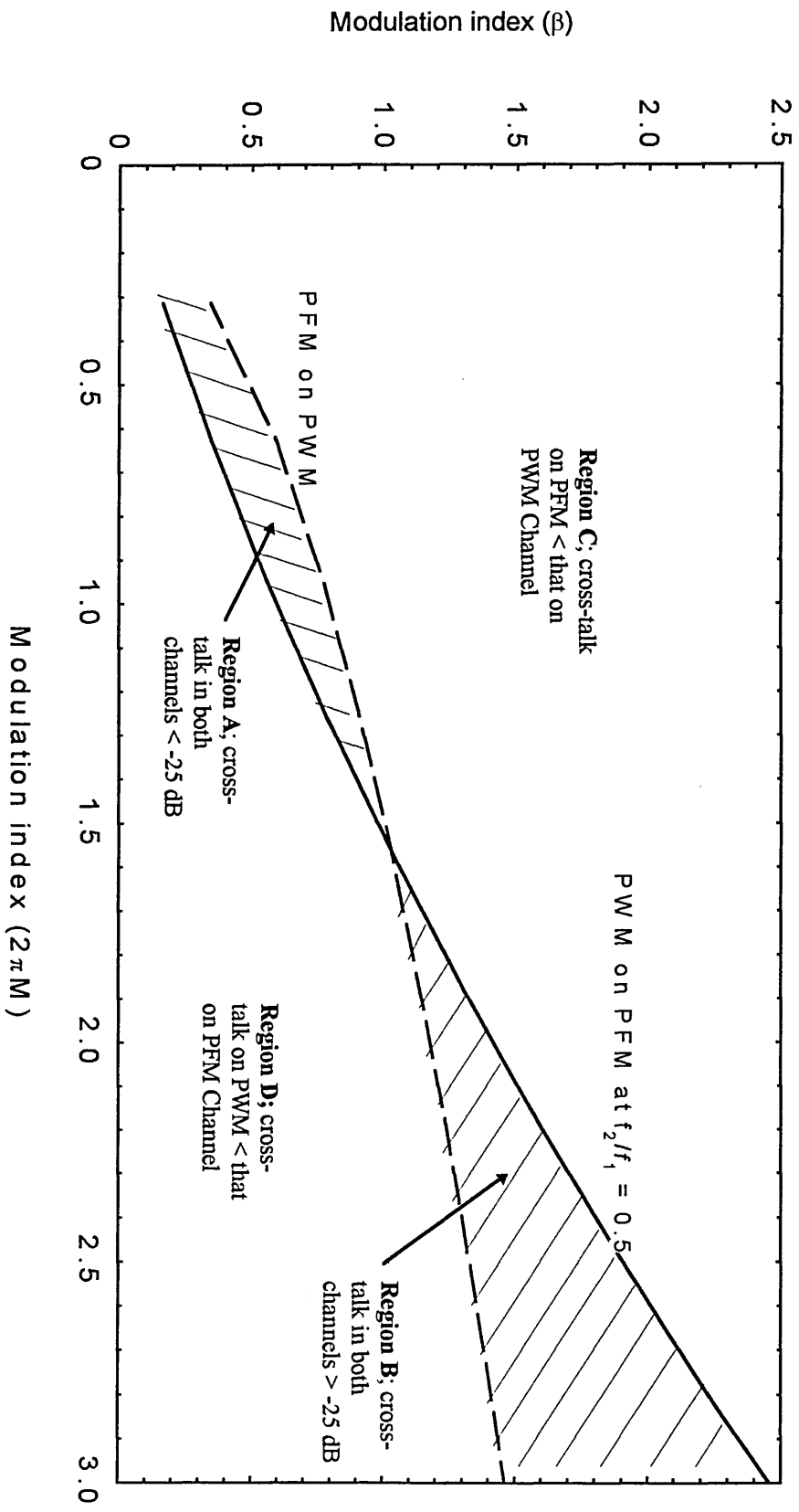


Fig. 7.23 Relation between modulation indices for both channels.

$M \text{ or } M_1 = 0.158$

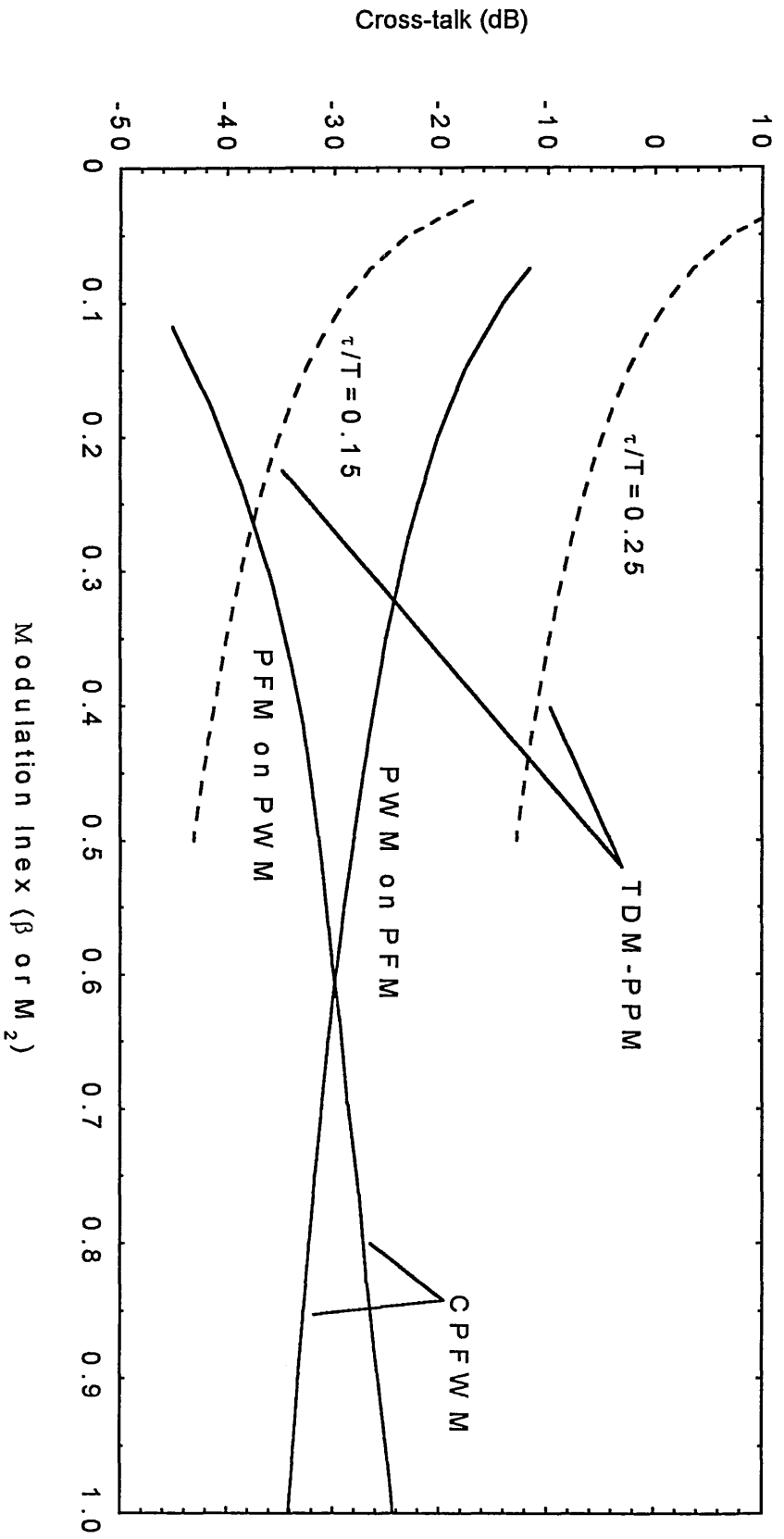


Fig. 7.24 Cross-talk performance of the CPFWM and theTDM-PPM system (TDM-PPM at $2\pi M_1 = 1$, $t_R = 58$ nsec, and CPFWM at $2\pi M = 1$ and $t_R = 58$ nsec).

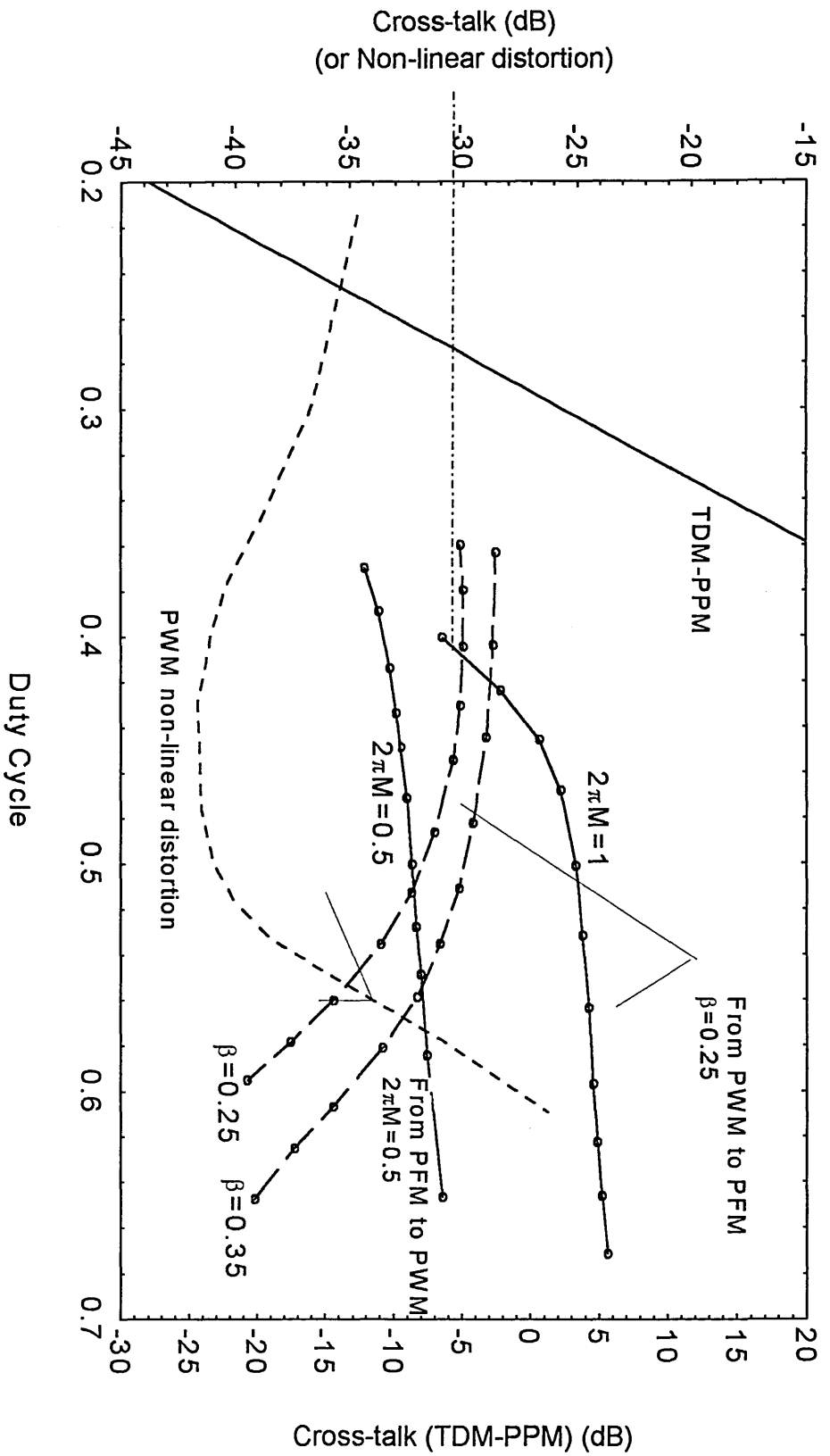


Fig. 7.25 Cross-talk performance of the CPFWM and the TDM-PPM system as a function of the unmodulated Pulse duty cycle, CPFWM at; $f_1 = 200$ KHz, $f_2 = 120$ KHz, $f_0 = 2.04$, $\beta = 0.25$, TDM-PPM the same as CPFWM and $2\pi M_I = 0.158$, $M_2 = 0.5$).

7.3 Noise performance of the CPFWM system

A typical PTM receiver block diagram is shown in Fig. 7.26, where signal plus noise is passed through the slicer before being demodulated. The signal-to-noise ratio analysis is based on the following assumptions;

- the received CPFWM pulses are trapezoidal with equal fall and rise times.
- the noise displaces both edges.
- the input noise is white Gaussian with a constant power spectral density.
- the slicer is set at half the amplitude of the received pulse.

The instantaneous amplitude of the received pulse $v(t)$ will be displaced by n_t , the instantaneous value of the noise, see Fig. 7.27-b. The effect of the noise is to offset the actual edge displacement, due to modulation, by n_t . $n_t > 0$ will cause longer pulses, while $n_t < 0$ will result in shorter pulses. The slicer eliminates the amplitude variation and then the displacement is given as[93, 94];

$$\Delta t = t_R \frac{n_t}{A} \quad (7.12)$$

The random noise is proportionally converted into random jitter, which can be replaced by a narrow pulse train shown in Fig. 7.25 - C. Noise power spectral density can then be obtained by Fourier transformation of the autocorrelation function of the equivalent pulse train [94-96]. The output noise power and the SNR can then be obtained as explained earlier in chapter 2.

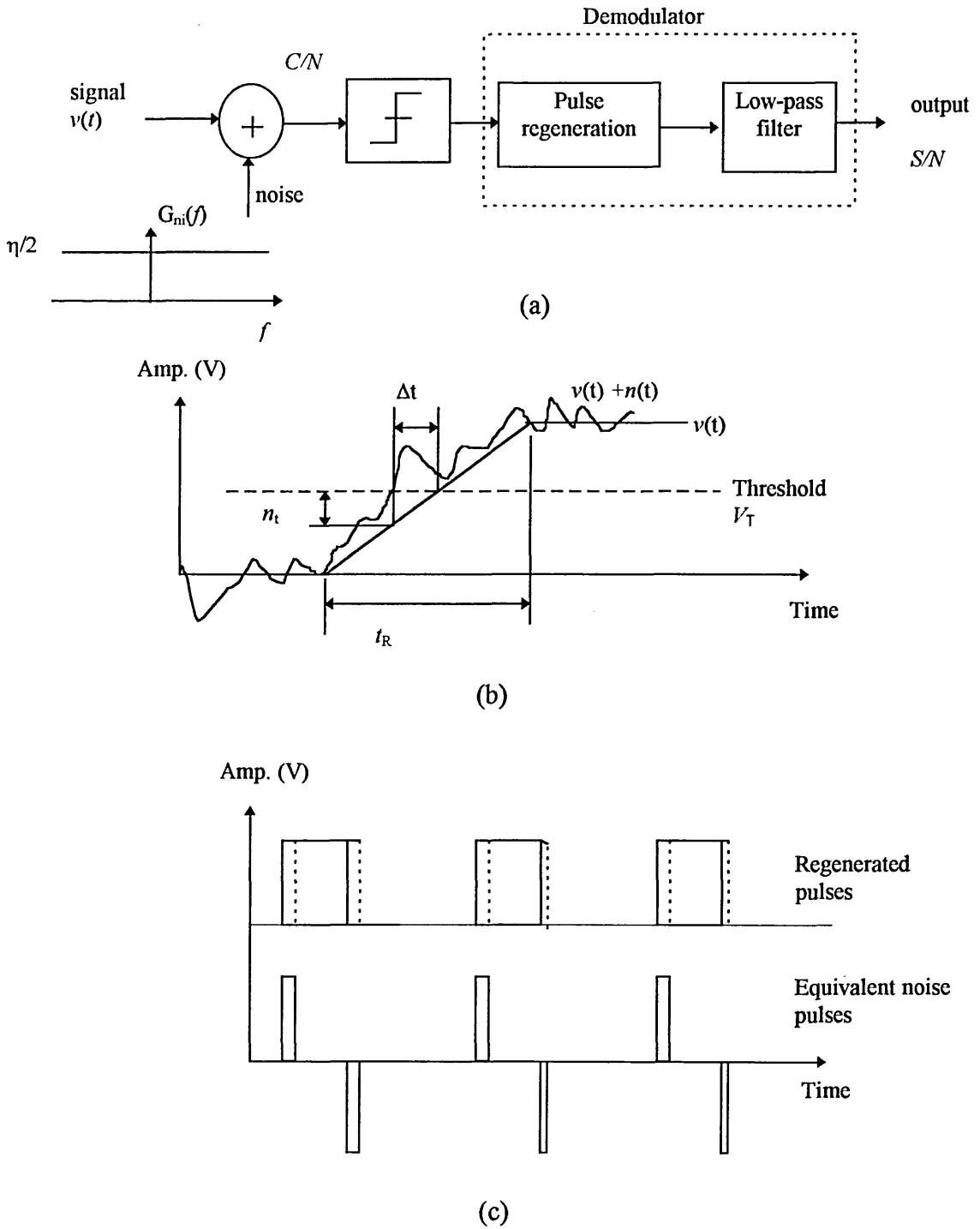


Fig. 7.25 Typical PTM receiver: (a) block diagram, (b) received pulse with noise and (c) time diagram.

7.3.1 noise performance of the PFM channel

A simplified diagram for the PFM demodulation is given in Fig. 7.27. The received CPFWM is passed through a pulse edge separation stage to generate a stream of pulses of constant width equal to τ_g . When noise is added to the CPFWM, the regenerated pulses are displaced by $x(t_o)$. This is equivalent to adding the pulse pair $y(t)$ to the undisplaced pulses, see Fig. 7.27.

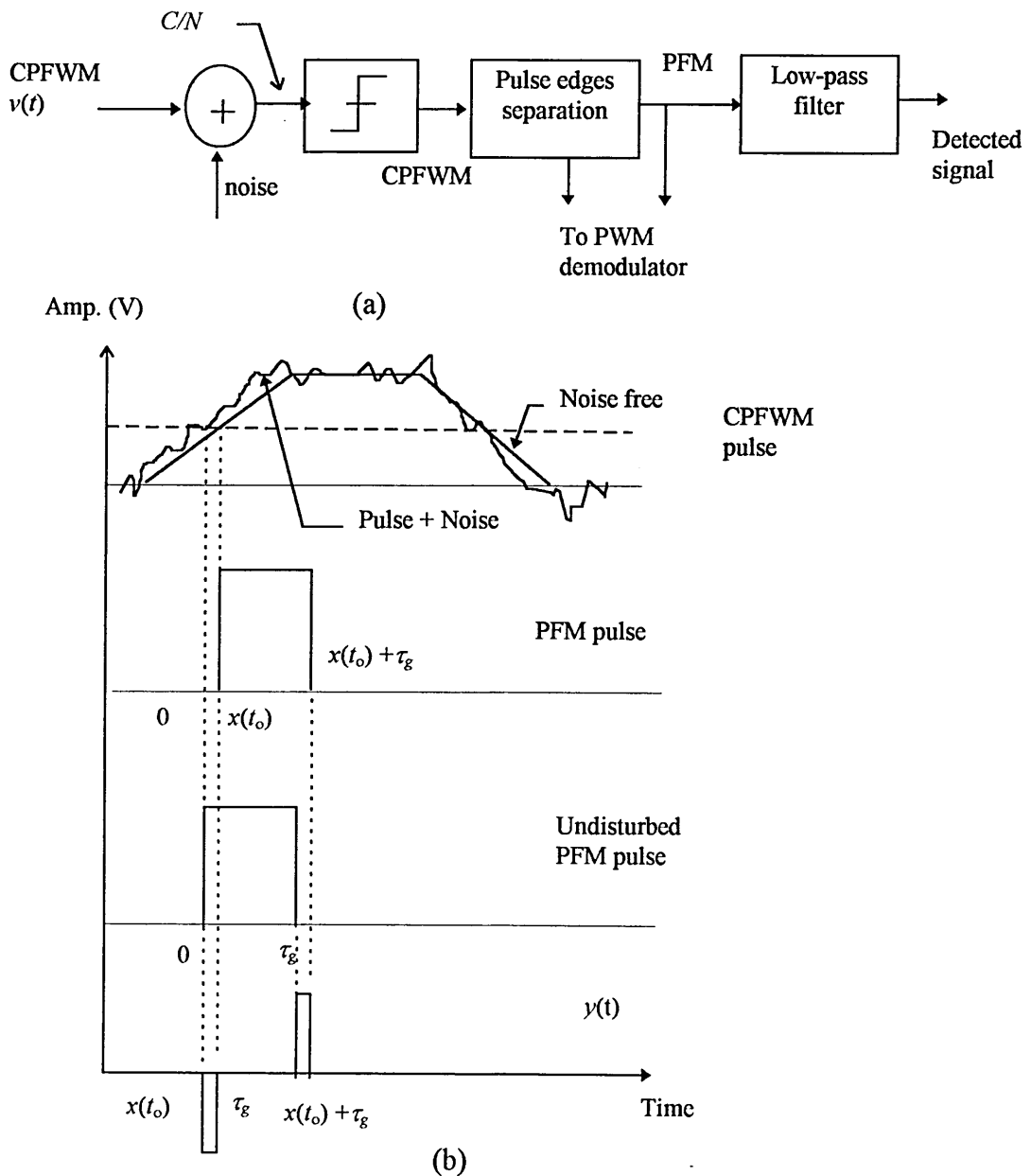


Fig. 7. 27 PFM demodulator with noise: (a) block diagram and (b) waveforms.

The analysis adopted here is the same as the one used for PFM system [94-96]. Drukarev [96] has treated the PFM system when the noise level is above and below the threshold level. However, ignoring the impulsive noise, and following the derivation given by Drukarev [96], the signal-to-noise ratio (S/N) can be obtained [31, 94-96];

$$S / N = \frac{3\left(\frac{\Delta f}{f_1}\right)^2}{4\pi^2 f_o f_1 \overline{\sigma^2}} \quad (7.13)$$

where $\overline{\sigma^2}$ is the edge jitter power which can be given as;

$$\overline{\sigma^2} \approx \frac{\overline{n^2(t)}}{[\dot{v}(t)]^2} \quad (7.14)$$

where $\overline{n^2(t)}$ is the noise power at the detection threshold. Using equation 7.14 into

7.13 and substitute for $\dot{v}(t) = A / t_R$, the following formula can be obtained;

$$\begin{aligned} S / N &= \frac{3\beta^2}{4\pi^2 f_o f_1 t_R^2} \frac{A^2}{\overline{n^2(t)}} \\ &= \frac{3\beta^2}{4\pi^2 f_o f_1 t_R^2} CNR \end{aligned} \quad (7.15)$$

where β is the frequency modulation index. Note that the term $\frac{A^2}{\overline{n^2(t)}}$ represents the carrier-to-noise ratio (CNR) or the input signal-to-noise ratio. Equation 7.15 is valid only when operating above the threshold.

The measured signal-to-noise ratio versus CNR for different values of rise time is shown in Figs. 7.28 and 7.29, agreeing well the predicted results (within ± 2 dB). As is the case with all PTM scheme, the SNR shows a threshold effect at about 22 dB, below which the SNR deteriorates rapidly.

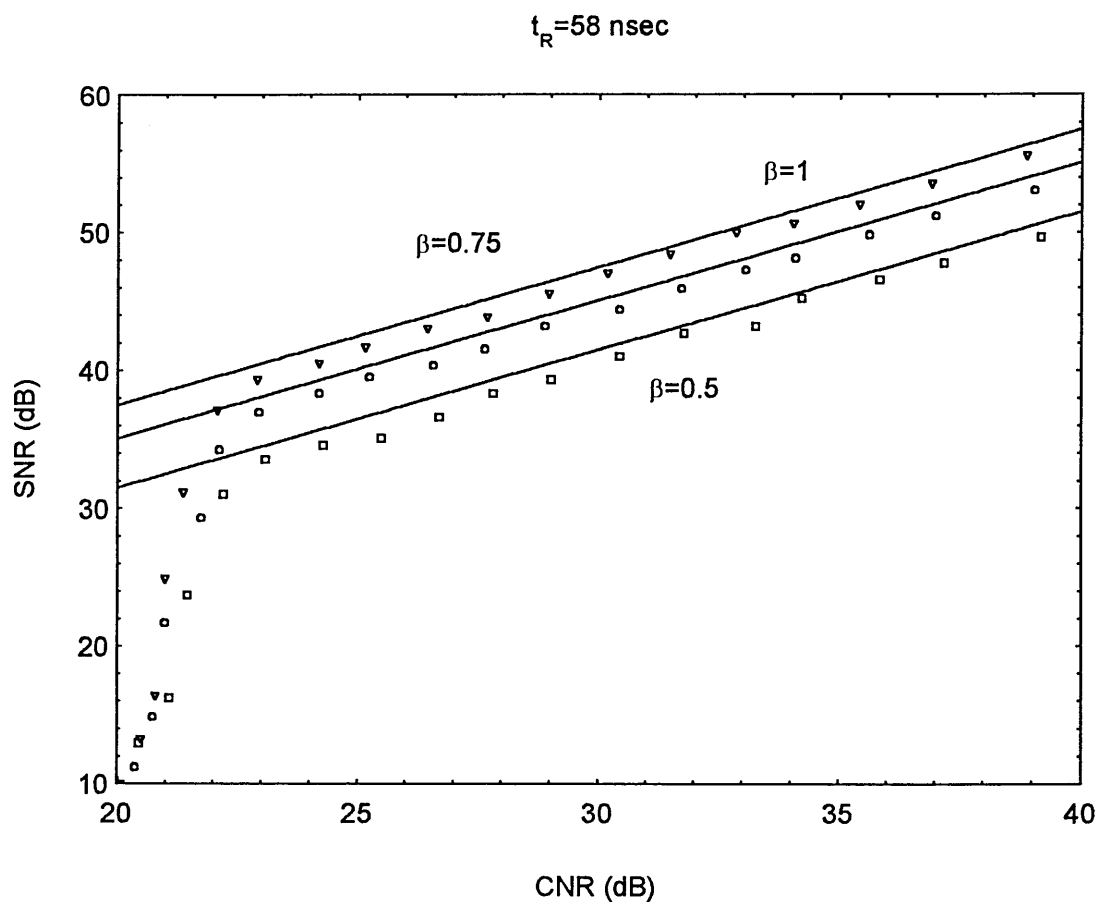


Fig. 7.28 Noise performance of the PFM channel, $f_1 = 200 \text{ kHz}$, $f_o = 2.04 \text{ MHz}$, (solid line represents theoretical values).

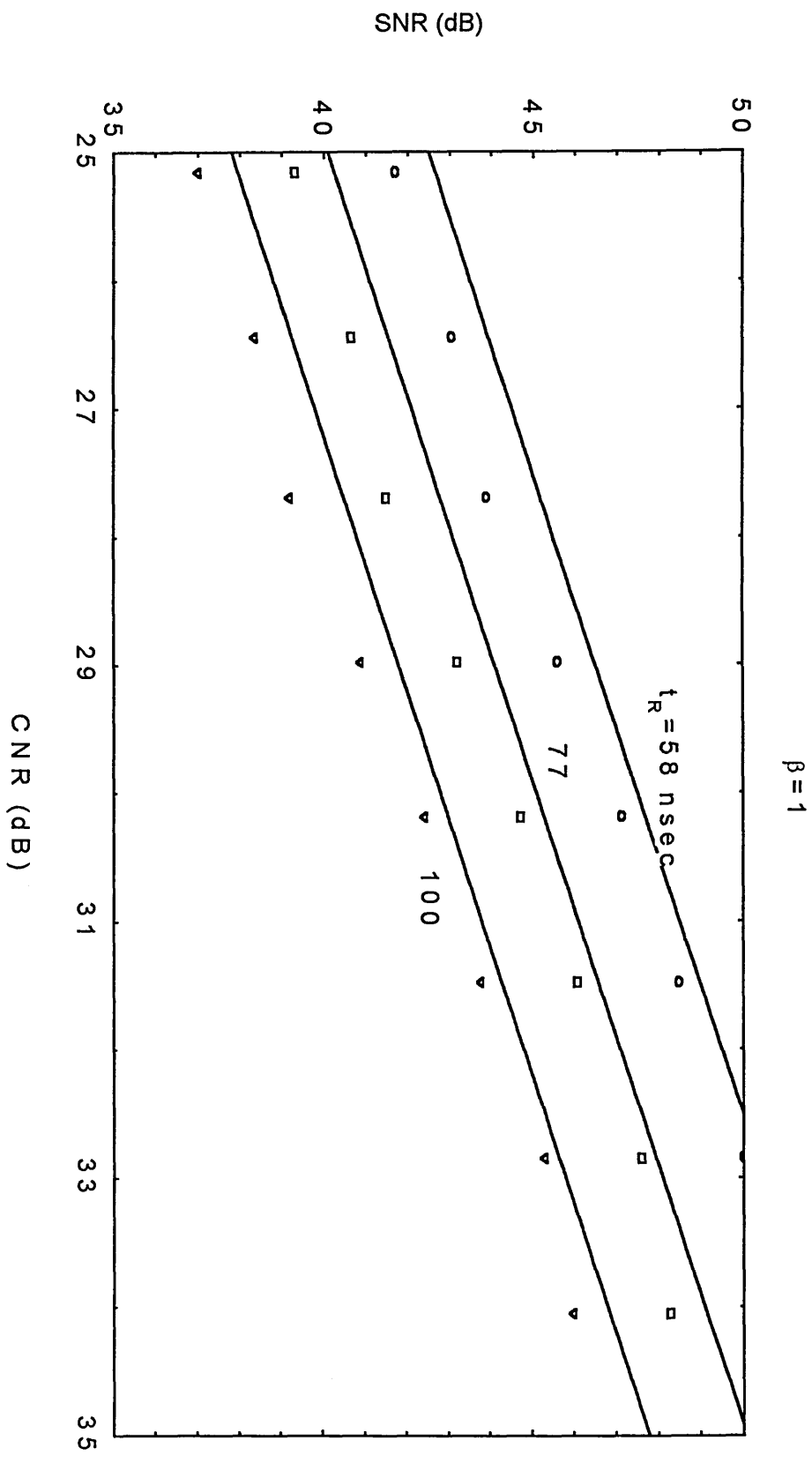


Fig. 7.29 Noise performance of the PFM channel, $f_1 = 200 \text{ kHz}$, $f_o = 2.04 \text{ MHz}$, $\beta = 1$ (solid line represents theoretical values).

7.3.2 noise performance of the PWM channel

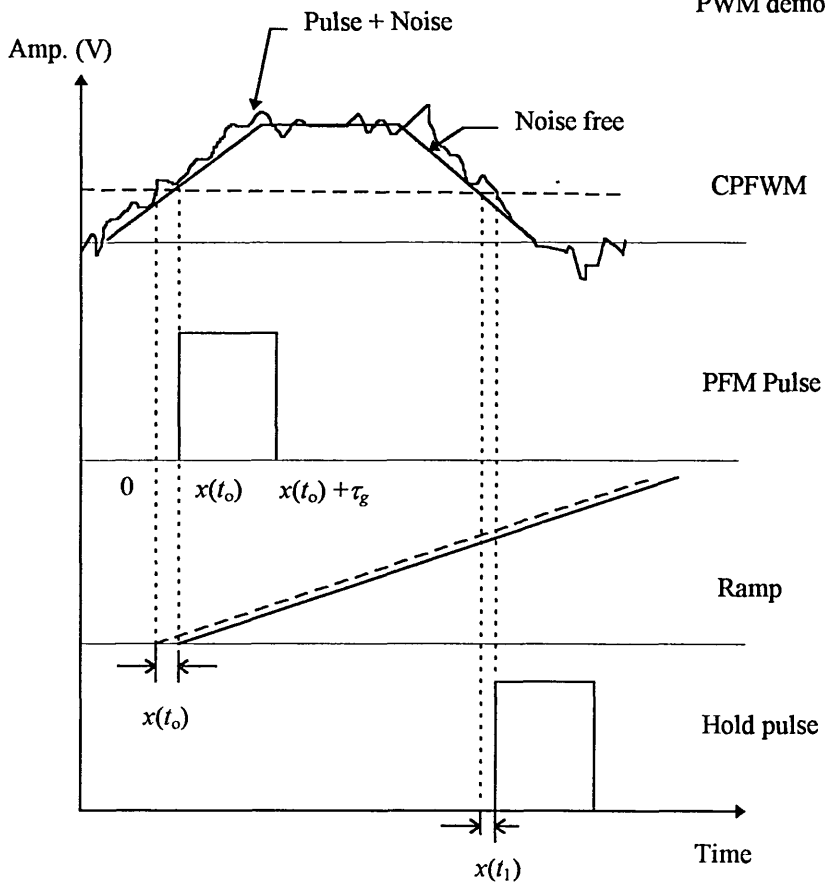
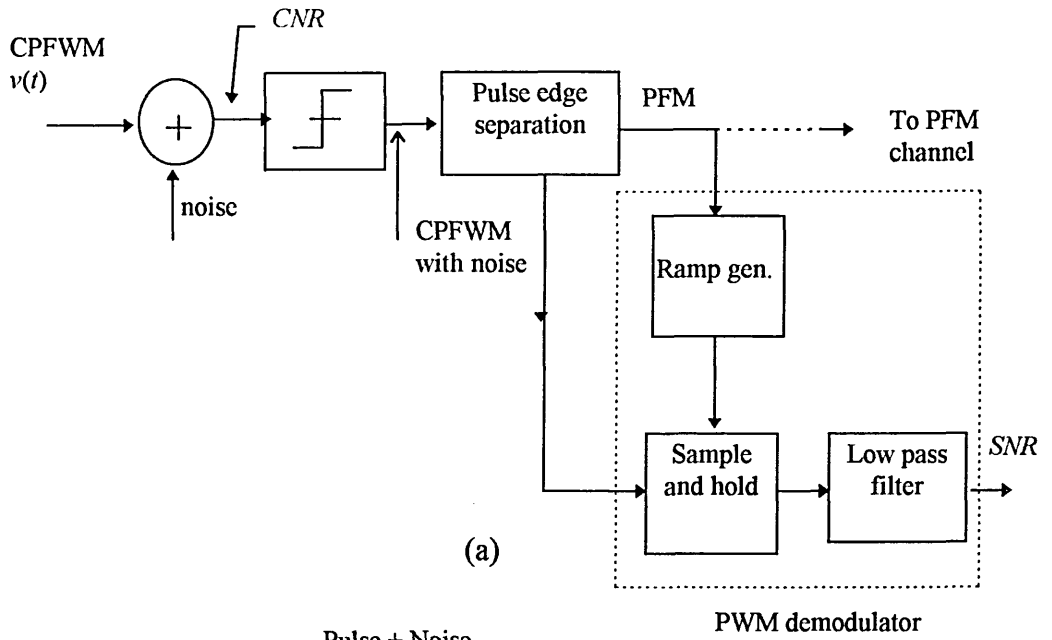
The block diagram of the PWM demodulator is shown in Fig 7.30 (a), where both the leading and trailing edges of the CPFWM waveform are used to extract the information carried by the pulse width. The effect of noise is to displace both the leading and trailing edge by $x(t_0)$ and $x(t_1)$ respectively, with leading edge driving the ramp generator, the ramp waveform will also be displaced by $x(t_0)$. Consequently, the sampled waveform at the output of the sample-and-hold amplifier will be affected by both displacements $x(t_0)$ and $x(t_1)$. The noise voltage level at the sample and hold output can be evaluated as;

$$n_o(t) = k[x(t_0) - x(t_1)] \quad (7.16)$$

where k is the time to voltage conversion factor of the sample and hold amplifier (i.e. the slope of the ramp).

Effectively, the above noise voltage is equivalent to the case where a pulse pair $y(t)$, see Fig. 7.31, is added to the undisplaced PWM pulse and the resultant pulse is passed through a low pass filter. If we assume that $x(t_0)$ and $x(t_1)$ are statistically independent, then the PWM signal-to-noise ratio can be obtained as [31];

$$SNR = \frac{(T_{PWM} / T_o)^2}{8f_2f_o\sigma^2} \quad (7.17)$$



(b)

Fig. 7.30 PWM Channel demodulation with noise: (a) block diagram and (b) waveforms.

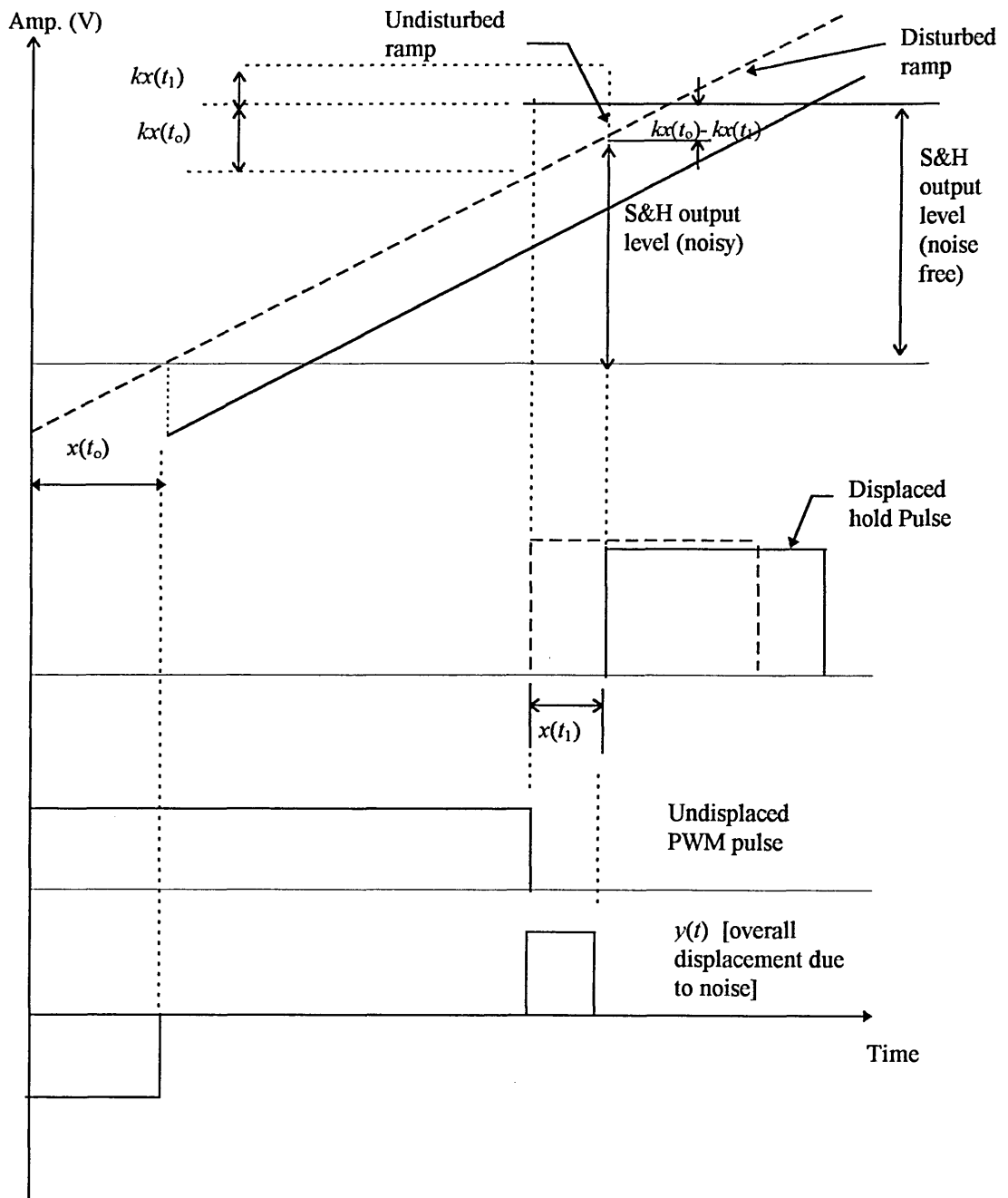


Fig. 7.31 Regenerated signal at the sample and hold amplifier when noise is present.

where $T_{P_{WM}}$ is the maximum pulse width deviation, T_o is the unmodulated period, ($T_o=1/f_o$). With $v(t) = A/t_R$, substituting equation 7.14 into 7.17, and the SNR presented as;

$$S / N = \frac{(T_{P_{WM}} / T_o)^2}{8f_2 f_o t_R^2} \frac{A^2}{n^2(t)} \quad (7.18)$$

With modulation index $M=2T_{P_{WM}}/T_o$, equation 7.18 can be written as;

$$S / N = \frac{M^2}{32f_2 f_o t_R^2} CNR \quad (7.19)$$

where $CNR = \frac{A^2}{n^2(t)}$

Experimental confirmation of the SNR performance for different values of pulse rise time is given in Figs. 7.32 and 7.33, showing good agreement with predicted results obtained from equation 7.19. Doubling the rise time reduces the SNR by about 5 dB. These figures show a CNR threshold point at almost $CNR = 23$ dB, where the SNR deteriorates rapidly just like PFM system.

Table 7.3 shows comparison between theoretical and measured results for both PFM and PWM channels. It can be seen that in both channels the theoretical results agree with those measured to within 2 dB.

CNR (dB)	PWM ($M = 30\%$)		PFM ($\beta = 1$)	
	SNR (Measured)	SNR (Theoretical)	SNR (Measured)	SNR (Theoretical)
25.0	34.0	34.7	41.0	42.5
30.0	38.0	39.0	46.5	47.5
35.0	44.0	45.0	51.0	52.5

Table 7.3 Measured and calculated SNR for PFM and PWM channels.

For both channels to have the same SNR, the following condition may be applied by equating equation 7.15 with 7.19, this leads to;

$$\frac{\beta}{M} = 0.64 \sqrt{\frac{f_1}{f_2}} \quad (7.20)$$

Let the slope of the pulse width modulator and the slope of the VCO be k_f (Hz/V) and k_w (s/V), respectively. Thus equation 7.20 can be rewritten in terms of the mixing ratio as;

$$\frac{v_1}{v_2} = 1.28 \frac{k_w}{k_f} f_o^2 \left(\frac{f_1}{f_o}\right) \sqrt{\frac{f_1 / f_o}{f_2 / f_o}} \quad (7.21)$$

Equations 7.20 and 7.21 are valid for any transmission bandwidth. Equation 7.20 could be combined with the results obtained from the cross-talk performance to show how the modulation indices can be chosen to obtain an optimum performance from the system. Two values of f_1/f_2 have been considered to show the effect of the sampling rate on the system behaviour and the results are displayed in Fig. 7.34. There are in total six

identifiable regions; four for cross-talk (see also Fig. 7. 23) and two for SNR , as shown in Figs. 7.34.b and 7.34.a, respectively. The above figures are best described by referring to table 7.4 which summarises the cross-talk and SNR characteristics of the system. At $\beta = 1$, $2\pi M = 1.65$ and $f_1/f_2 = 2$, cross-talk at both channels will be -25 dB and SNR of PFM channel will be 12 dB higher than that for PWM channel. Keeping the same modulation indices, but doubling f_1/f_2 results in improvement in cross-talk performance for both channels and deterioration of PFM SNR by 3 dB.

Region	SNR performance	Cross-talk performance
A	$SNR_{PWM} < SNR_{PFM}$	Optimum for both channels ($CT < - 25$ dB)
B	$SNR_{PWM} < SNR_{PFM}$	Worst case for both channels ($CT > - 25$ dB).
C	$SNR_{PWM} < SNR_{PFM}$	$CT_{WF} < CT_{FW}$
D	$SNR_{PWM} < SNR_{PFM}$	$CT_{FW} < CT_{WF}$
E	$SNR_{PWM} > SNR_{PFM}$	$CT_{FW} < CT_{WF}$

Table 7.4 Summary of SNR and cross-talk characteristics of the PFWM system (also see Fig. 7.34).

The difference (in dB) between the SNR of the PFM and PWM channel can be evaluated by dividing equation 7.19 by 7.15, then converting the results into decibels.

This leads to;

$$SNR_{PFM} - SNR_{PWM} = 6.87 + 10 \log\left(\frac{\beta^2}{M^2} \frac{f_2}{f_1}\right) \quad (7.22)$$

When both channels are identical in bandwidth and modulation indices, the last term in equation 7.22 is zero. This means that the PFM channel has an advantage of ~ 7 over the PWM channel. Equation 7.22 is plotted in Fig. 7.36 for different values of β/M and f_2/f_1 . As expected PFM channel shows better SNR performance compared to PWM for wide range of modulation indices ratio β/M .

The results obtained clearly indicate the potential of PFM for applications which require good SNR performance such as video and other wideband signals. Applications requiring less SNR performance can be carried in the PWM channel. The optimum performance of the overall system is best determined by properly choosing the modulation indices, sampling ratios and channel bandwidth so that a good balance between the cross-talk and SNR performance can be achieved.

Finally, the noise performance of CPFWM system is compared with digital modulation scheme (PCM with 8-bit) and an analogue modulation scheme (AM with 100% modulation). See Fig. 7.37. It is clear that the CPFWM system shows noise performance between the two systems. Taking into consideration that the transmission bandwidth of the CPFWM system is much less than any digital system, it can be concluded that the CPFWM represents a good balance between bandwidth and noise performance requirements. At low SNR (say 25 dB), CPFWM is superior to AM but is not as good as PCM. However, this can be improved provided the CNR and channel bandwidth are increased.

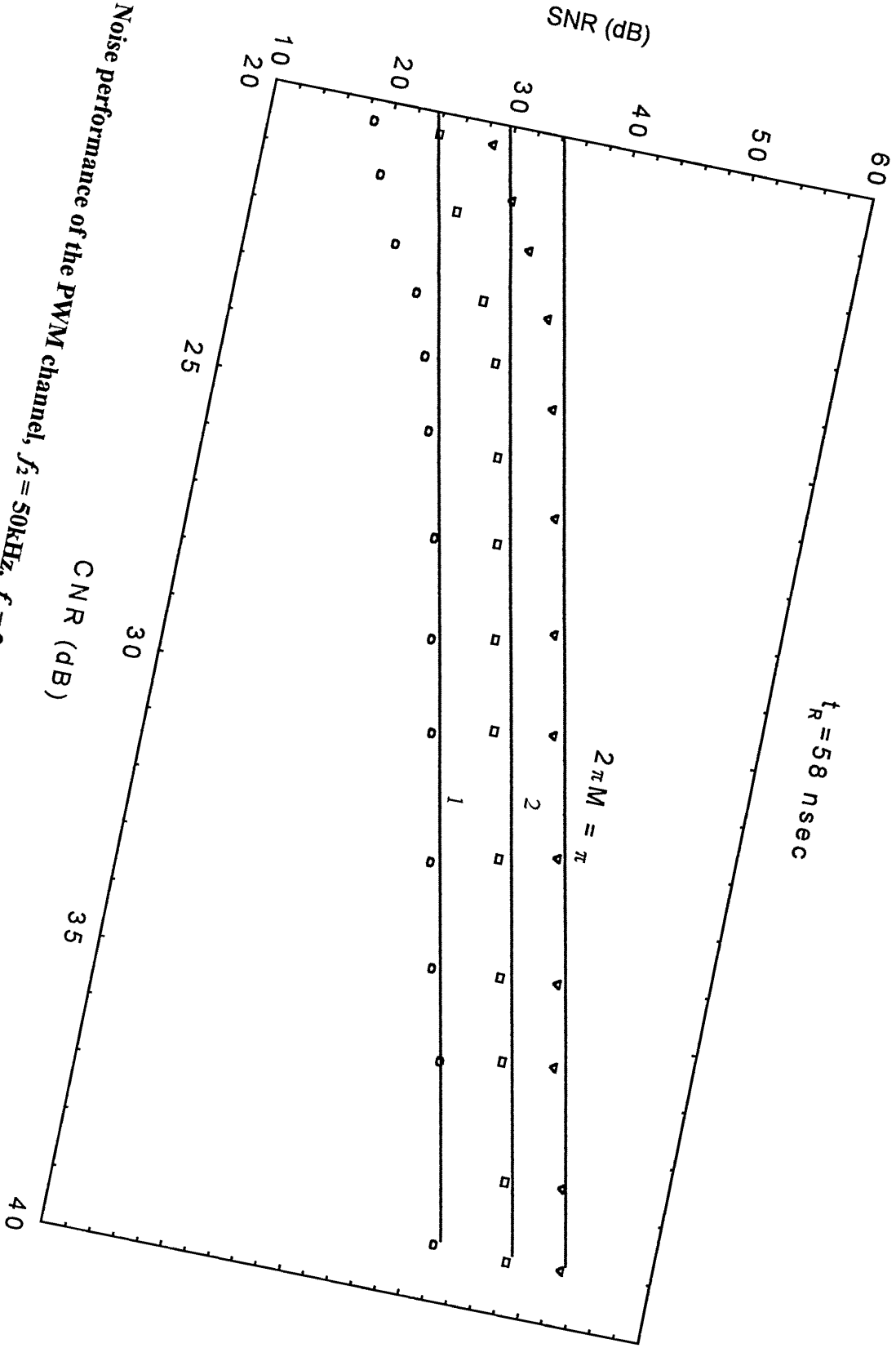


Fig. 7.32 Noise performance of the PWM channel, $f_1 = 50\text{kHz}$, $f_c = 2.04\text{MHz}$, $t_r = 58 \text{ nsec}$.

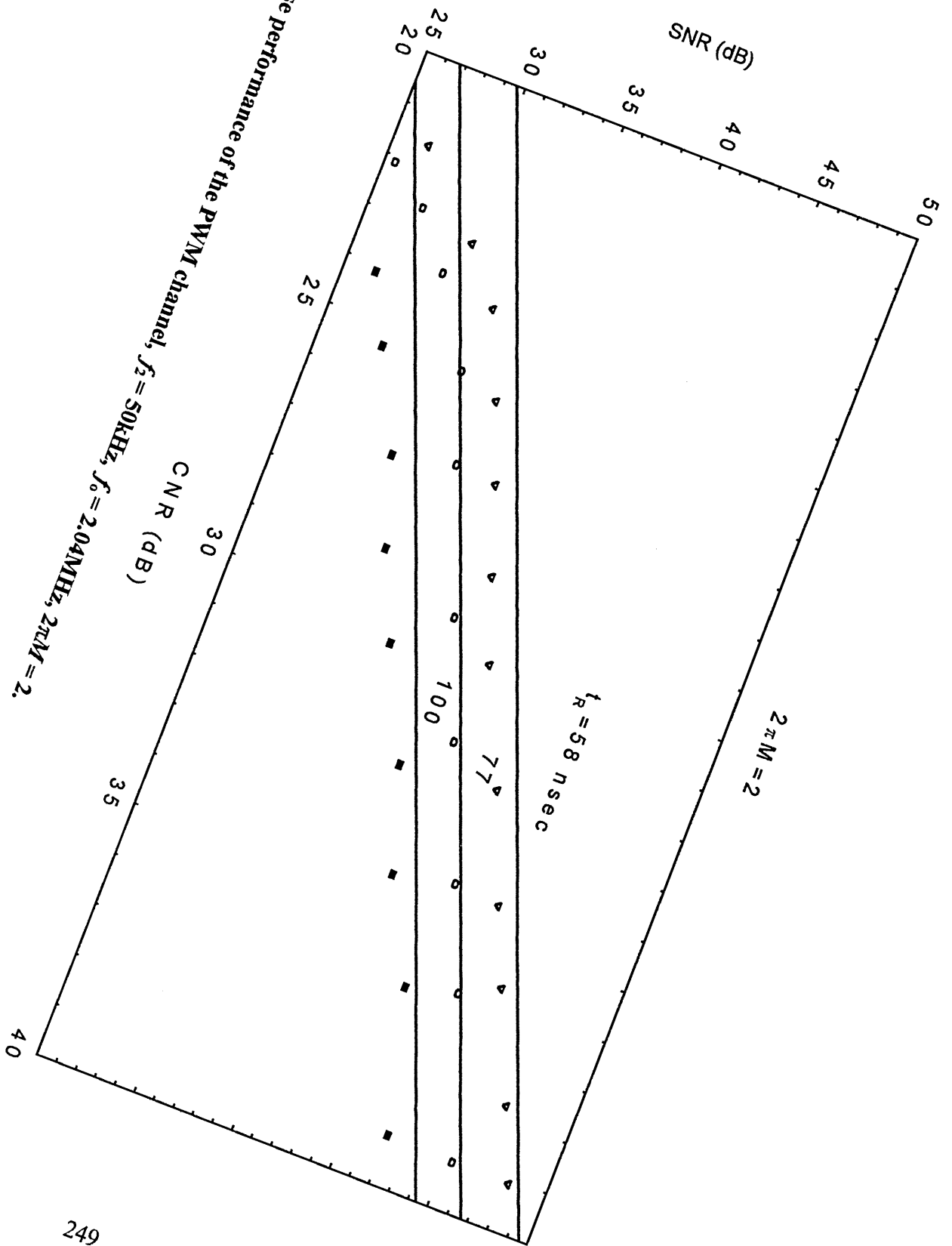


Fig. 7.33 Noise performance of the PWM channel, $f_s = 50$ kHz, $f_c = 2.04$ MHz, $2\pi M = 2$.

$t_R = 58$

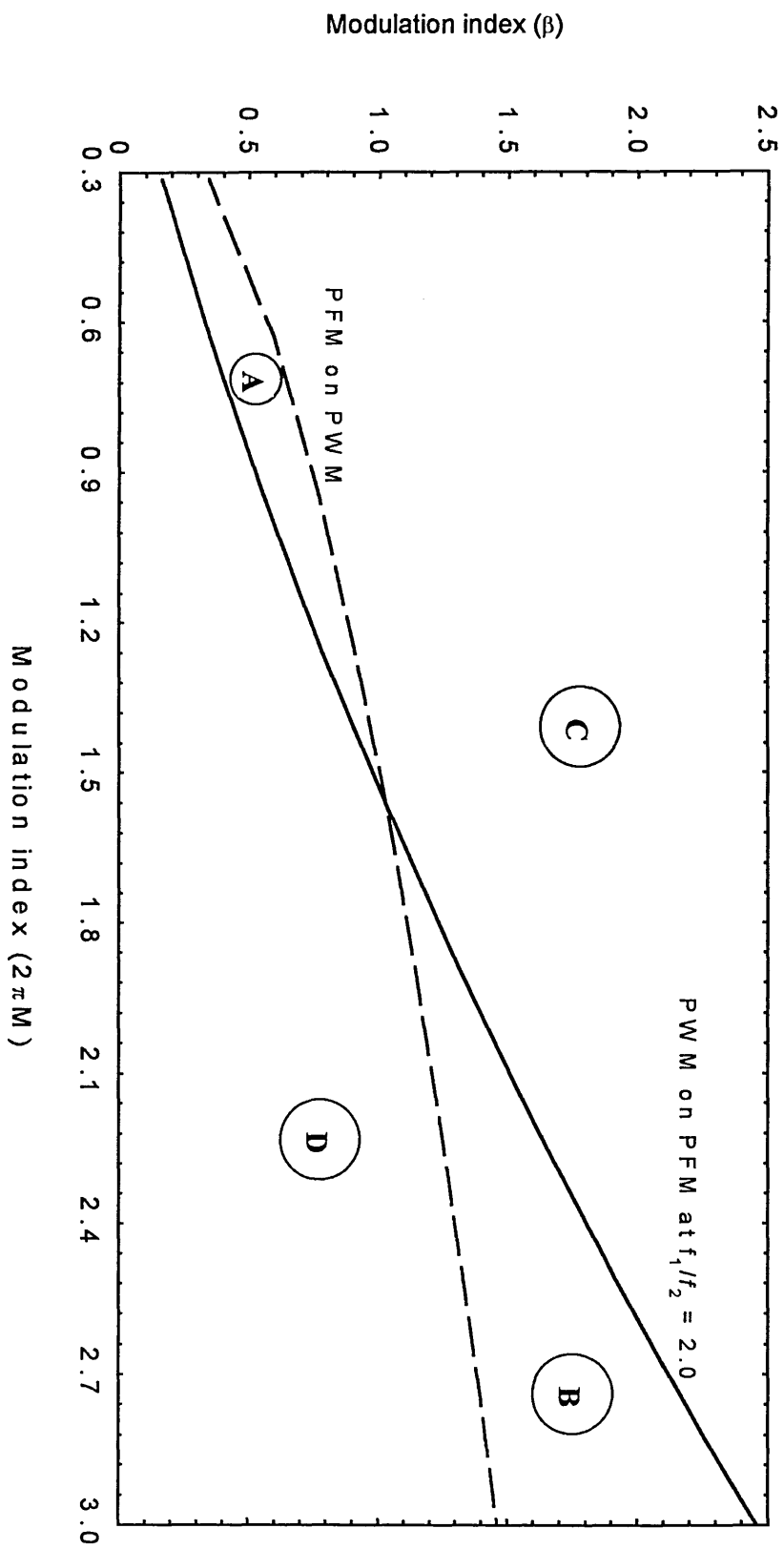


Fig. 7. 34 (a) Relationships between modulation indices for optimum operation ($f_1/f_2=2$, $t_R = 58$ nsec).

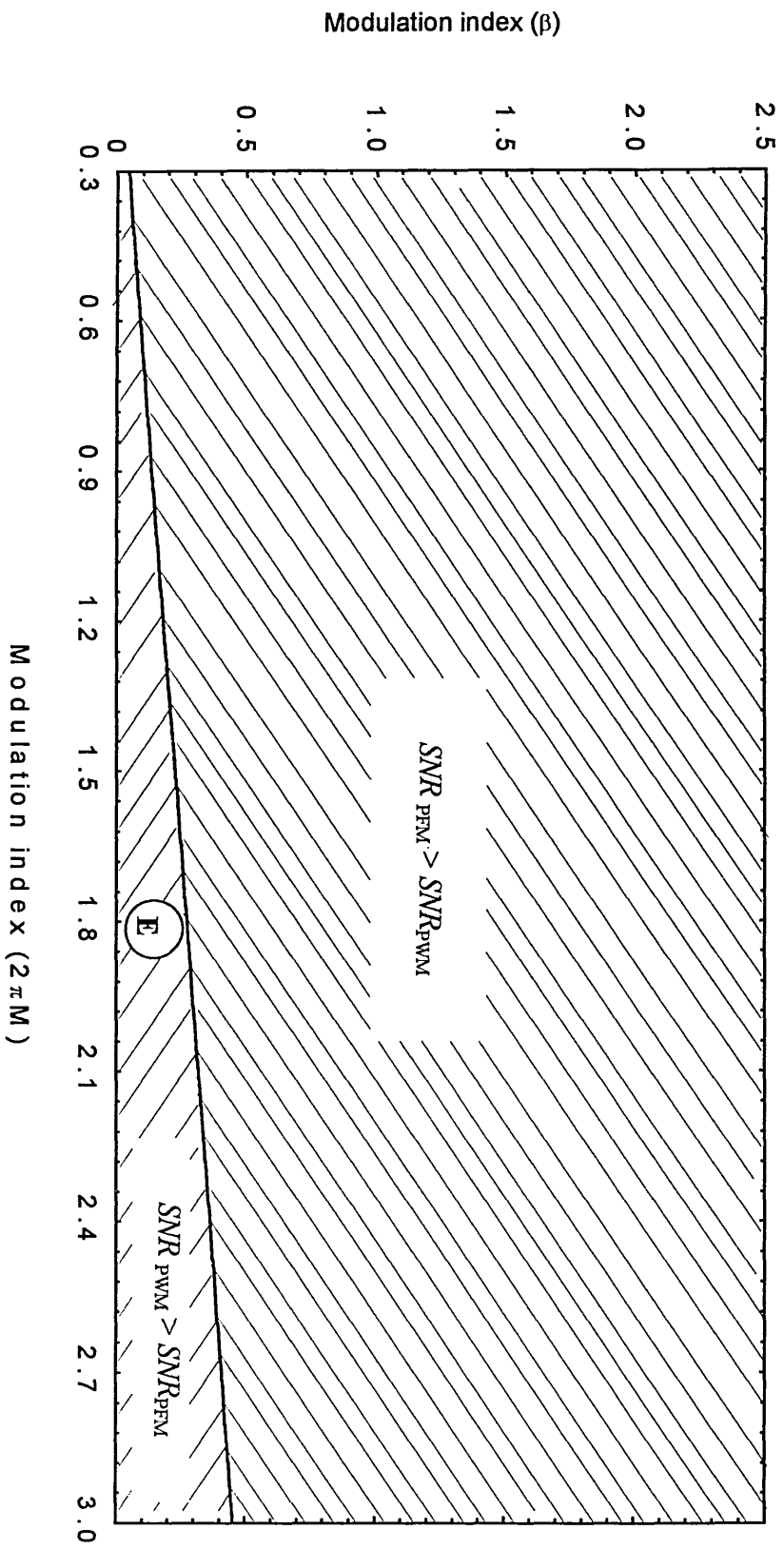


Fig. 7. 34 (b) Relationships between modulation indices for optimum operation ($f_1/f_2=2$, $t_R = 58$ nsec).

$t_R = 5.8$

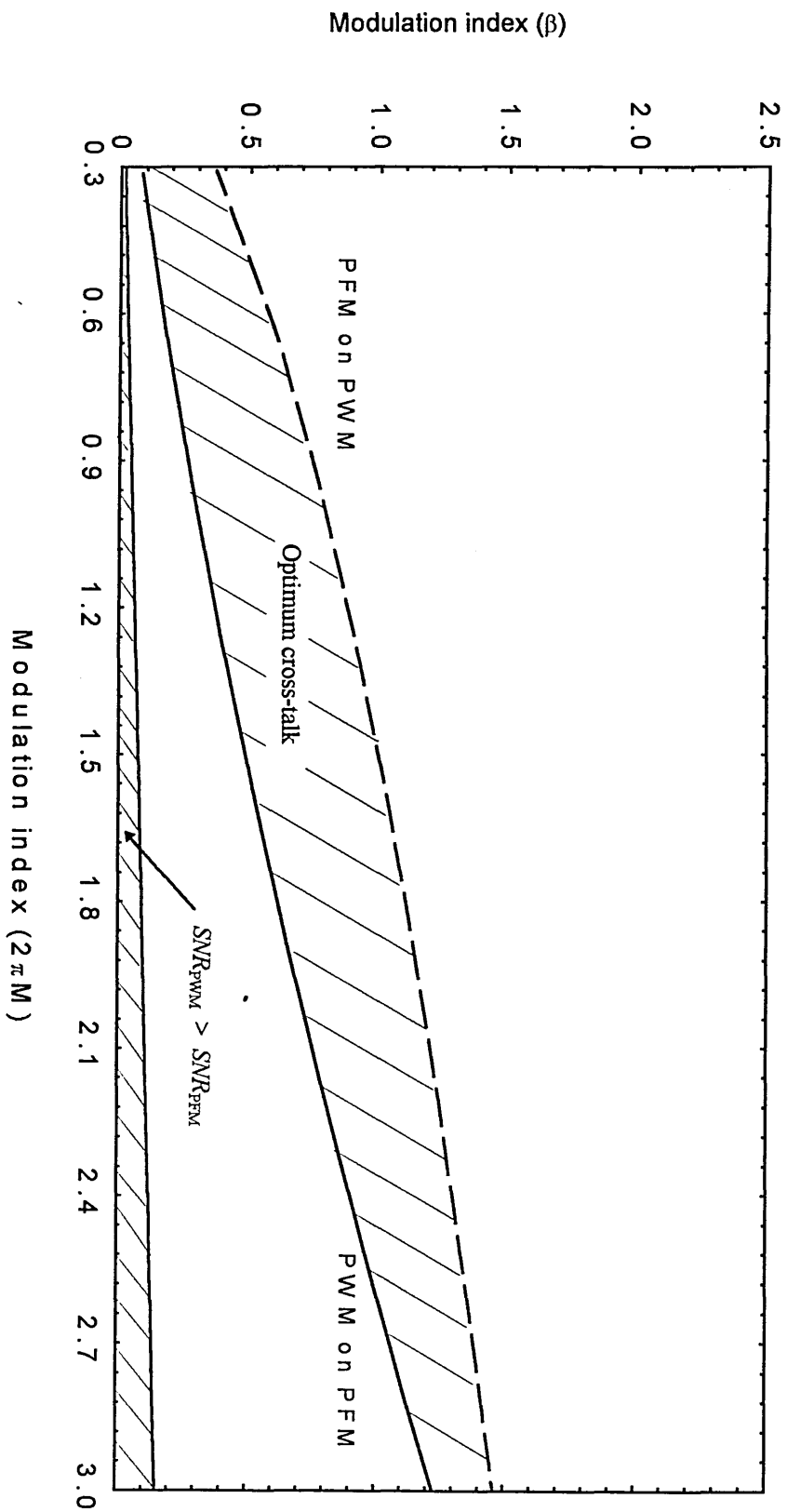


Fig. 7.35 Relationships between modulation indices for optimum operation ($f_1/f_2 = 4$).

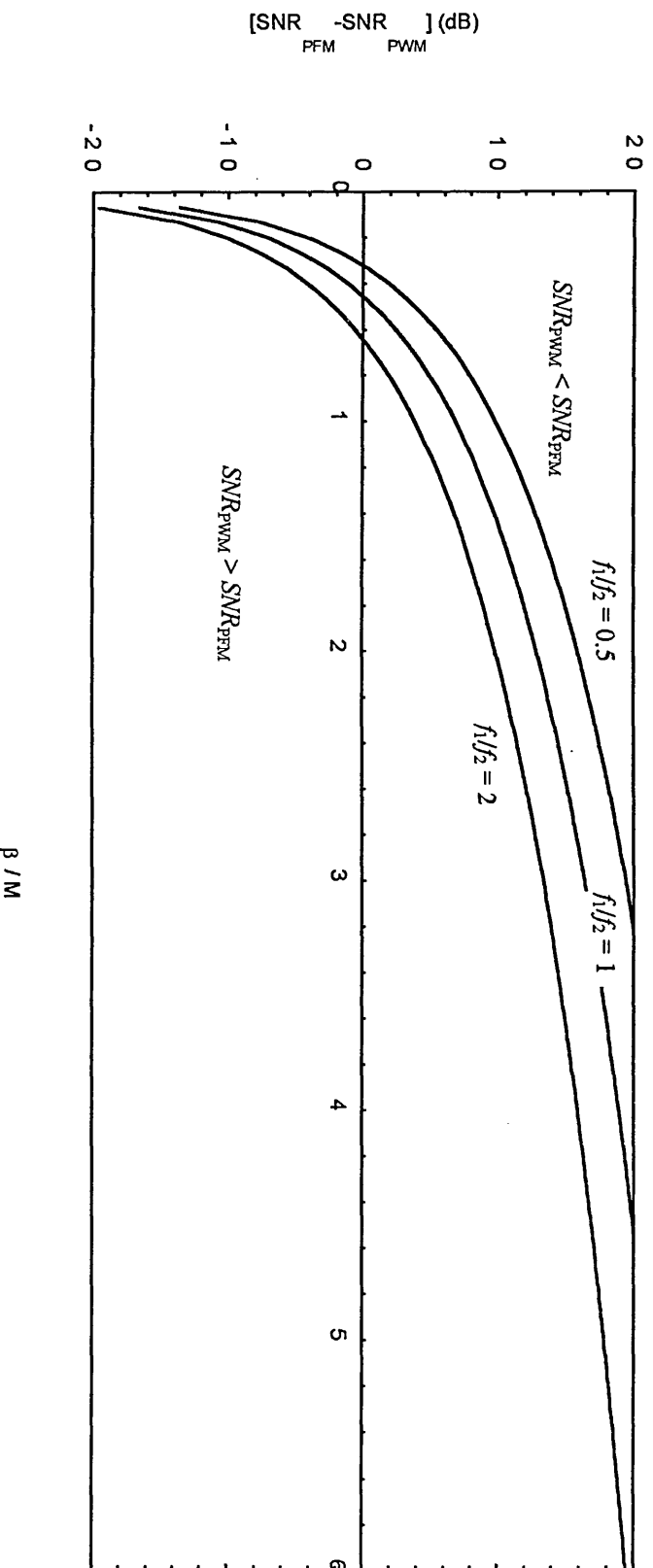


Fig. 7.36 Comparison between the noise performance of both PFM and PWM channels.

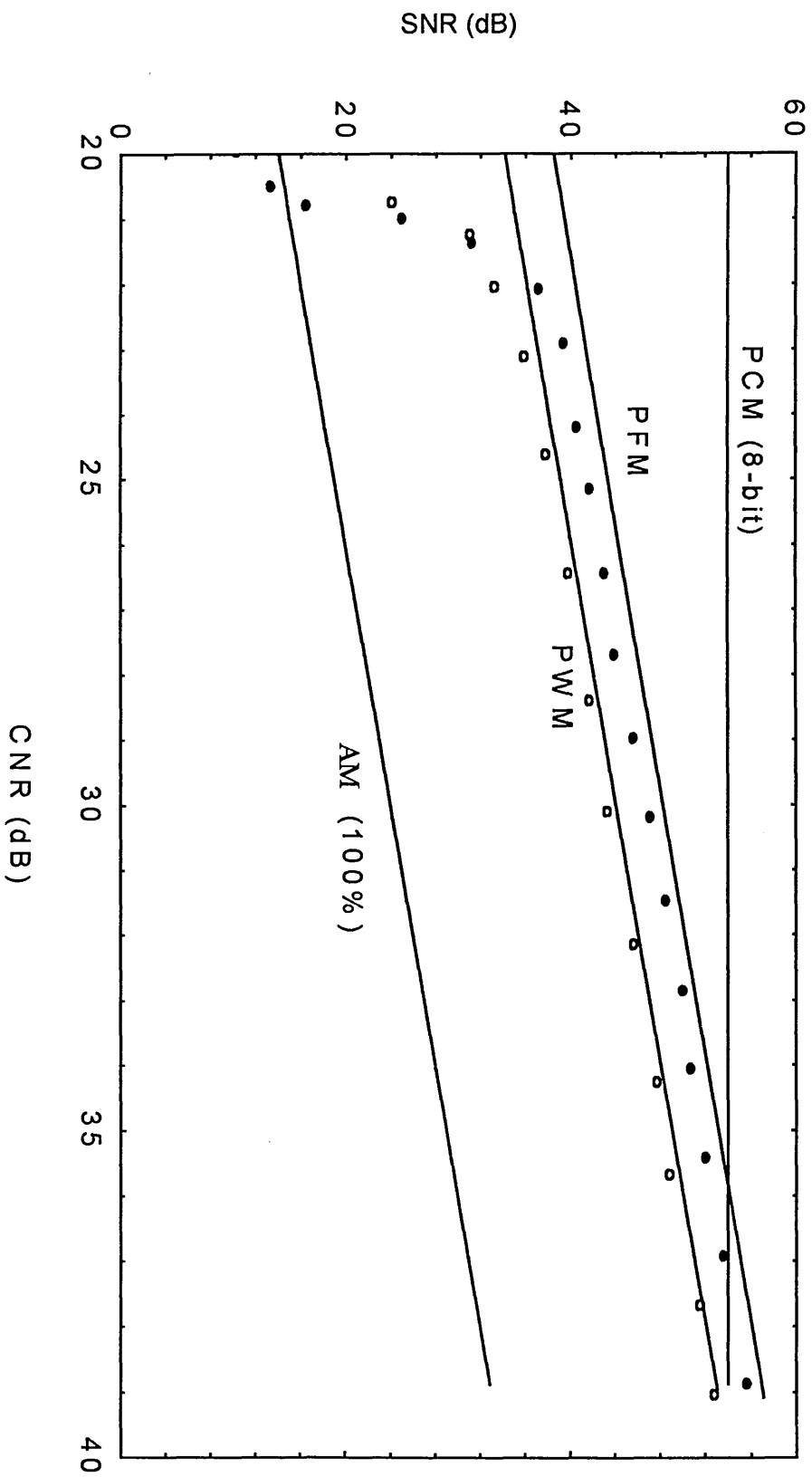


Fig. 7.37 Noise performance of the CPM system and other standard systems (CPM; $\beta=1$, $M=0.5$, $f_2 = 50\text{kHz}$, $f_1=200\text{ kHz}$, AM, 100% modulation, PCM at 8-bit).

Chapter Eight

Conclusions

As a part of this project, trapezoidal and triangular PSM waveforms have been analysed. These types are very similar in nature, and triangular PSM can be considered as a special case from trapezoidal PSM waveform. Mathematical analysis shows that triangular PSM has wider dynamic range than trapezoidal. Triangular PSM requires less power to carry the same modulation index than trapezoidal PSM, and consequently shows better noise performance.

The frequency spectrums of both trapezoidal and triangular PSM are very similar. In both types of the PSM waveforms, the amplitude of the baseband frequency components is inversely proportional to the modulating signal. Therefore, it is not possible to recover the message signal by passing the regenerated pulses through a low-pass filter. Traditionally, demodulation of PSM waveform is carried out by using a differentiator followed by low-pass filter. This technique has the disadvantage of poor noise performance. This is because of the high-pass frequency characteristics of the differentiator. Slicing and gating has been applied to reduce the amount of noise entering the receiver and thus to improve the noise performance of the PSM system.

A novel receiver design for the PSM system has been developed. This receiver offers simplicity and improved performance compared to classical receivers, and eliminates the use of the differentiator and the need for voltage slicing or gating. The novel receiver design can be used with any type of the PSM waveforms. The disadvantage of this receiver design is the requirement of synchronisation which can be achieved using the falling edge of the PSM waveform as a reference.

A new *SNR* formula has been presented for the first time enabling prediction of the system noise performance of the PSM system. Close experimental confirmation has been obtained between the formula's prediction and practical measurements taken at a variety of system parameters. As expected, the *SNR* of the PSM system increases with the transmission bandwidth and the modulation index. Unlike an AM system, the PSM system has inherent noise suppression, and can produce a positive improvement factor over a wide range of modulation indices when the transmission bandwidth is limited.

The compound PTM technique has also been investigated, as a solution to the problem of multiplexing PTM waveforms. The CPFWM system has been theoretically and experimentally investigated. Mathematical characterisation of the CPFWM waveform has been developed enabling calculation of the modulation conditions required for optimum performance. Computer simulation shows that the CPFWM waveform can be successfully generated and demultiplexed using simple circuits. Good agreement has been obtained between simulation, practical and theoretical results.

When designing CPFWM systems, the ramp generators (both in the transmitter and receiver) should be chosen to be identical, and with a high degree of linearity. The free running frequency of the ramp generators should be twice that of the carrier. Ramp generators with poor linearity can cause significant reduction in the system linearity. Therefore, at a high frequency operation, more attention should be given to the ramp generators to minimise non-linear distortion problem. Further, a non-zero fall time of the ramp will cause a cross-talk component from PFM channel to appear. The amplitude of this cross-talk component is proportional to the ratio between the rise and the fall time of the ramp, and the frequency modulation condition.

Increasing the pulse width of the regenerated PFM pulses causes deterioration in cross-talk performance of the PFM channel, and reduces the maximum allowable modulation index at the width modulation channel for optimum cross-talk performance. Consequently, this also degrades the overall *SNR* performance of the PWM channel.

At the receiving end, the pulse width of the regenerated PFM must very short. Increasing the pulse width of the regenerated PFM pulses reduces the cross-talk performance of the PFM channel, and reduces the maximum allowable modulation index at the width modulation channel for optimum cross-talk performance. Consequently, this degrades the overall *SNR* performance of the PWM channel.

A newly derived spectral modulation formula for CPFWM waveform is presented in this work. Tests on an experimental CPFWM system and computer simulation have shown that excellent agreement to within ± 1 dB is obtained with theoretical prediction

from the new modulation formula. The characteristics of CPFWM render it suitable for bandwidth efficient and low-cost analogue transmission.

Frequency spectrum investigation showed that CPFWM can be classified as anisochronous PTM technique because the sampling frequency component in the modulation spectrum vanishes when modulation indices M and β taken certain values. Removing either of the two input signals results in a modulation spectrum similar to PWM or PFM alone. The baseband components show overlapping between components from the first and the second modulating signals. This means that it is not possible to separate the modulating signals using only filters.

In an ideal situation, there should be no cross-talk from the PWM channel to the PFM channel. However, cross-talk occurs in PFM channel due to width modulation by the second channel, and similarly cross-talk in PWM channel is due to the frequency modulation by the first channel. Although there are many causes of cross-talk in both channels, the main cause is waveform interference which is a result of carryover of energy from one edge to the other. This results in phase modulation (time jitter) in the separated edges. The time jitter mainly depends on the linearity and the bandwidth of the transmission medium, and increases with the increase in the waveform distortion..

Cross-talk in PFM channel dramatically deteriorates when the rise time of the received pulse increases (i.e. less transmission bandwidth), and it is proportional to the modulating signal frequency ratio (f_2/f_1). Cross-talk performance in PFM can be improved by choosing the message signal with wide bandwidth to be carried on the

PFM channel, while the message with narrow bandwidth to be carried on the width modulation channel. This choice also has the advantage of improving the *SNR* performance of the system and the difference between the *SNR* in the PFM channel and the PWM channel will be reduced.

In CPFWM system, when the duty cycle increases the maximum PWM modulation index decreases by the same amount. This also causes deterioration in the non-linear distortion of PWM channel. The effect of this will be; an improvement in cross-talk in PWM channel, deterioration in *SNR* and increase in non-linear distortion. However, when duty cycle increases, cross-talk in PFM channel will improve. The best balance between the non-linear distortion, cross-talk and *SNR* is obtained when duty cycle is 50%.

Unlike cross-talk in the PFM channel, cross-talk in the PWM channel is present even in an ideal situation. There are many causes for cross-talk in the PWM channel, each cause produces a cross-talk component. The overall cross-talk results from the summation of all individual components. One component of this cross-talk is due to the nature of the PWM demodulator, which is based on conversion to PAM signal followed by low-pass filtering. The strength of this component can be minimised by reducing the frequency modulation index and increasing the sampling ratio. The second component of cross-talk in the PWM channel is due to the non-zero fall time of the ramp waveform, which can be minimised by minimising the fall time. This component is usually very small and has a negligible effect as the fall time of the ramp is usually very small. The third and main component of the cross-talk is due to waveform

interference, which increases with the rise time of the received pulses and frequency modulation index.

Unlike CPFWM, TDM-PPM cross-talk performance is very sensitive to unmodulated pulse duty cycle. Increasing the duty cycle can cause serious deterioration in the cross-talk performance of the TDM-PPM. The CPFWM system shows comparable cross-talk performance with the TDM-PPM system and in some cases it shows an improved performance. Taking into consideration that TDM-PPM with narrow pulse width requires wide transmission bandwidth, it can be concluded that CPFWM shows a good balance between bandwidth and cross-talk performance.

An optimum region of cross-talk performance in both channels can be determined by proper choice of the modulation indices and the ratio f_1/f_2 . Increasing the ratio f_1/f_2 results in an increase in optimum cross-talk region for both channels but deterioration of *SNR* performance of the PFM channel.

When both channels are identical in bandwidth and modulation indices, the *SNR* of the PFM channel has an advantage of about 7 dB over the PWM channel. Unless the frequency modulation index is very small, the *SNR* of the PFM channel is always superior to that of PWM. At the optimum cross-talk region of operation, the *SNR* of the PFM channel is superior to PWM channel. When the CPFWM system is used to the best of its performance, the PFM channel will have better signal quality than the PWM channel. Therefore, the PFM channel should be used for those signals which require quality transmission; such as video or other wideband signals. However, the

PWM channel is more suitable for applications which are less restricted on *SNR* performance.

CPFWM system shows noise performance between the digital and analogue systems. Taking into consideration that the transmission bandwidth of the CPFWM system is much less than any digital system, it can be concluded that the CPFWM represents a good balance between bandwidth and noise performance requirements.

As a suggestion for future work, CPFWM transmission can be improved if only the edges of the CPFWM waveform are transmitted. This can be realised by differentiating the CPFWM waveform before transmission, which has the advantage of power saving during the transmission and therefore improves *SNR*. It is also expected that cross-talk performance will be improved as a very narrow pulse width (very low duty cycle) will be used for transmission. Another advantage of this technique is that the possibility of employing a laser source in an optical transmission. However, synchronisation is necessary in order to separate and discriminate the two distinct channels. A solution for this problem could be by transmitting synchronisation pulses which would be used at the receiving end as a reference to discriminate between the two channels, but this has the disadvantage of reducing the maximum transmission rate. Another solution would be to use different pulse width for each channel, however this technique loses the merit of power saving and increases the receiver complexity.

List of papers published from this project

1. **A. Issa, Z. Ghassemlooy and A. Ray**” *Noise performance of the pulse slope modulation system*” *Electronic Letters*, Vol. 29, No. 25, 1993, pp. 2171-2173.

2. **Z. Ghassemlooy, A. Issa, and B. Wilson**, “ *Spectral prediction for hybrid pulse frequency and width modulation*” *Electronic letters*, Vol. 30, No. 12, 1994, pp. 933-935.

3. **A. Issa, R. Geotz, and Z. Ghassemlooy**, “ *Compound pulse frequency and width modulation technique*” *Communication Networks Symposium*, the Manchester Metropolitan University, July 1994, Manchester.

4. **Z. Ghassemlooy, A. Issa, and B. Wilson**, "*Hybrid Frequency Width Modulation Technique for Analogue Fibre Optic Communications*", *The Proceedings of ICEE Conference*, May 1994, Thran, Iran.

5. **Z. Ghassemlooy, A. Issa, R. Wickramasinghe and A. Simmonds**, “ *Compound pulse frequency and width modulation technique*”, *Inter. J. Optoelectronics*. Vol. 10, No. 1, 1995, pp. 19-23.

References

- [1] **B. Wilson, and Z. Ghassemlooy**, “*Pulse time modulation techniques for optical communications: a review*”, IEE Proc. Pt-J, Vol. 140, No. 6, 1993, pp. 346-357.
- [2] **B. Rhomberg**, “*Optical fibre technology; Optical video transmission system*”, Electrical Communication, Vol. 56, No. 4, 1981, pp. 407-411.
- [3] **K. S. Shanmugan**, “*Digital and analogue communication systems*”, J. Wiley, New York, 1979.
- [4] **C. Haber and E. Nossen**, “*Analogue versus digital antijam video transmission*”, IEEE Trans. Communication . Vol. COM-25, No. 3, 1977, pp. 310-317.
- [5] “*Using fibre optics to remote RGB raster video workstation*”, **ARTEL** Communication Corporation, Massachusetts, Application note CG-3.
- [6] “*Fibre optics in computervision instaview CAD/CAM systems*”, **ARTEL** communication corporation, Application note CG-4.
- [7] **M. Schwartz, W. Bennett and S. Stein**, “*Communication systems and techniques*”, McGraw-Hill, NewYork, 1966.
- [8] **D. Heatley**, “*Unrepeated video transmission using pulse frequency modulation over 100 km of monomode optical fibre*”, Electronics Letters, Vol. 18, No. 9, 29th April 1982, pp 369-370.

- [9] **G. Nicholson**, “*Modulation techniques for cable television distribution on optical fibres*”, A. T. R. Vol. 17, No. 2, 1983, pp. 25-37.
- [10] **T. Tsuboi, H. Obara and K. Asatani**, “*Fibre optic high-definition television on transmission system*”, Review of Electrical communication Lab., Vol. 33, No. 4, 1985, pp. 609-614
- [11] **D. Brace, and D. J. T. Heatley**, “*Wideband transmission by optical fibre system*”, The British Cinematography Sound and Television Society Journal, Vol. 63, Pt. 2, Feb. 1981, pp. 152-155.
- [12] **I. Garrett**, “*Towards the fundamental limits of optical-fibre communications*”, J. Lightwave Technology, Vol. LT-1, No. 1, 1983, pp. 131-138.
- [13] **P. Cochrane and D. Heatly**, “*Future directions in long haul optical fibre systems*”, British Telecom. Engineering Journal, Vol. 9, pp 268-280, 1991.
- [14] **K. Sato and K Astani**, “*Analogue baseband TV transmission experiments using semiconductor laser diodes*”, Electron. Letter, Vol. 15, No. 22, 1979, p. 794.
- [15] **B. Wilson, Z. Ghassemlooy and C. Lu**, “*High-speed pulse time modulation techniques*”, OE/Fibres 92, 1992, Boston USA, Paper 1787-26.
- [16] **J. P. Frankurt, et-al**, “*Analog transmission of TV channels on optical fibres with non-linearity correction by regulated feedforward*”, Electrical and Electronic Engineering, Vol. 12, Pt. 9, pp. 298-304.

[17] **L. Pophiliat**, "*Video transmission using a 1.3 μm LED and monomode fibre*", 10th European Conference on Optical Communications, Stuttgart, W. Germany, 1984, pp238-239.

[18] **R. E. Epworth**, "*The phenomenon of modal noise in analog and digital optical fibre systems*", Proc. 4th European conference on optical communication, Genoa, Italy, 1978, pp. 492-501.

[19] **K. Sato, et-al**, "*Fibre optic analog transmission techniques for broadband signals*", Review of Electrical Communication Labs. Vol. 32, No. 4, 1984, pp. 586-597.

[20] **B. Wilson, Z. Ghassemlooy, and D. J. T. Heatly**, "*Properties and applications of pulse time modulation techniques for fibre broadband communication networks*", International conference on Information Engineering, pp 693-702, July 1991.

[21] **D. Cooke, D. Jelonek, Z. Oxford, E. Fitch**, "*Pulse Communication*", J. IEE, Vol. 94, Pt. IIIA, 1947, pp. 83-105.

[22] **M. Levy**, "*Some theoretical and practical considerations of pulse communication*", J. IEE, Vol. 94, Pt. IIIA, 1947, pp. 565-572.

[23] **E. Fitch**, "*The spectrum of modulated pulses*", J. IEE, Vol. 94, Pt. IIIA, 1947, pp. 556-564.

[24] **S. Moskowitz, and D. Grieg**, "*Noise suppression characteristics of pulse time modulation*", Proceedings of the I. R. E., April, 1948, pp. 446-450.

- [25] **Z. Jelonek**, “*Noise problem in pulse communication*”, J. IEE, Vol. 94, Pt. IIIA, 1947, pp 533-545.
- [26] **O. Kruse**, “*Variable slope pulse modulation*”, Proc. IRE, Vol.4, No. 11, 1952
- [27] **J. Das**, “*Pulse slope modulation: A new method of modulating video pulses and its possible application on line circuit*”, Indian J. Phys. , Vol. 28, 1954, pp. 449-4462.
- [28] **O. Kruse, D. Lewis and J. Jackson**, “*Combination leading and trailing edge variable slope pulse modulation*”, Electronic Engineering, March 1967, pp. 174-176
- [29] **J. Das**, “*Signal analysis and audio characteristics of pulse-slope modulation*”, Electronic Engineering, Nov. 1955, pp482-487.
- [30] **N. Al anani, Z. Ghassemlooy, and A. Ray**, “*An experimental optical fibre communication link using pulse slope modulation*”, Int. Symp. On Communication Theory and Applications, July 1993, Lancaster, pp. 106-110.
- [31] **T. Tanaka and N. Okamura**, “*Multiple transmission systems using PFM and PWM*”, Electronics and Communications in Japan, Pt-1, Vol. 74, No. 1, 1991, pp. 65-80.
- [32] **Z. Ghassemlooy, B. Wilson and A. Lok**, “*Hybrid pulse time modulation techniques*”, Int. Symposium on fibre optic networks and video communications, April 1993, Berlin, Germany, Paper 1974-14.

- [33] **K. Sato**, "*Intensity noise of semiconductor laser diodes in fibre optic analog transmission*", IEEE J. Quantum Electronics, Vol. QE-19, Sept. 1983. pp. 1380-1391.
- [34] **K. Sato and K. Astani**, "*Linearity in fibre optic analog transmission system using laser diodes*", Trans. IECE Japan, Vol. E64, Oct. 1981, pp. 646-656.
- [35] **A. Carlson**, "Communication systems" McGraw-Hill, 1975, Second Edition.
- [36] **M. Berry and J. Arnold**, "*Pulse width modulation for optical fibre transmission of video*", IEE Int. Conference on Impact of VLSI Technology on Communication Systems, London, 1983.
- [37] **S. Suh**, "*Pulse width modulation for analogue fibre-optic communications*", IEEE J. Lightwave, LT-5, No. 1, 1987, pp. 102-112.
- [38] **B. Wilson and Z. Ghassemlooy**, "*Optical fibre transmission of multiplexed video signals using PWM*", Int. J. Optoelectronics, No. 4, 1989, pp. 3-17.
- [39] **B. Wilson, and Z. Ghassemlooy**, "Optical pulse width modulation for electrically isolated analogue transmission", J. Phys. Pt. E, Vol. 18, 1985, pp. 954-958.
- [40] **D. Xianda, C. Englefield, P. Goud and R. Razdan**, "*Four level pulse width modulation for fibre optic communications*", IEEE Trans. Communications, Vol. COM-30, No.8, 1982, pp1959-1963.
- [41] **H. Black**, "Modulation Theory", 1953, Van Nostrand, NewYork.

[42] **W. Bennett**, "*New results in the calculation of modulation components*", Bell System Tech. J., Vol. 12, 1933, pp. 228-243.

[43] **R. Stuart**, "*An Introduction to Fourier Analysis*", 1962, Chapman and Hill, London.

[44] **B. Wilson, and Z. Ghassemlooy**, "*Multiple sidetone structure in pulse width modulation*", Electronic Letters, Vol. 24, No. 9, 1988, pp. 516-518.

[45] **B. Wilson, Z. Ghassemlooy and A. Lok**, "*Spectral structure of multitone pulse width modulation*", Electronic Letters, Vol. 27, No. 9, 1991, pp. 702-703.

[46] **Z. Ghassemlooy, and B. Wilson**, "*Optical PWM data link for high quality video and audio signals*", IEEE Trans. Consumer Electronics, Vol.40, No.1 Feb 1994, pp. 55-63.

[47] **Z. Ghassemlooy**, "*Pulse position modulation spectral investigation*", Int. J. Electronics, Vol. 74, No. 1, 1993, pp. 153-158.

[48] **J. Das and P. Sharama**, "*Pulse interval modulation*", Electronic Letter, Vol. 3, 1976, pp. 288-289.

[49] **A. Okazaki**, "*Pulse interval modulation applicable to narrow band transmission*", IEEE Trans. On Cable TV, Vol. CATV-3, 1978, pp. 155-164.

[50] **R. S. Fyath, S. Abdullah, and A. Glass**, "*Spectrum investigation of pulse interval modulation*", Int. J. Electronics, Vol. 59, No. 5, 1985, pp. 597-601.

- [51] **J. N. Tripathi**, “*Spectrum measurements of pulse interval modulation*”, Int. J. Electronics, Vol. 49, 1980, pp. 415-419.
- [52] **M. Sato, M. Murata, and T. Namekawa**, “*Pulse interval and width modulation for video transmission*”, IEEE Trans. Cable Television, Vol. CATV-3, No. 4, 1978, pp. 165-173.
- [53] **M. Sato, M. Murata, and T. Namekawa**, “*A new optical communication systems using the pulse interval and width modulated code*”, IEEE Trans. Cable Television, Vol. CATV-4, No-1, 1979, pp. 1-9.
- [54] **B. Wilson, Z. Ghassemlooy, and J. Cheng**, “*Optical pulse interval and width modulation for analogue fibre communications*”, IEE Proceedings, Pt-J, Vol. 139, No. 6, 1992, pp. 376-382.
- [55] **B. Wilson, Z. Ghassemlooy and J. Cheng**, “*Spectral predictions for pulse interval and width modulation*”, Electronics Letters, Vol. 27, No. 7, 1991, pp. 580-581.
- [56] **B. Wilson, and Z. Ghassemlooy**, “*Recent theoretical developments in pulse time modulation*”, International Symposium on Communication Theory and Applications, pp. 765-767, May 1994.
- [57] **S. Heker, et-al**, “*Video transmission in optical fibre communication systems using pulse frequency modulation*”, IEEE Trans. Communications, Vol. COM -36, No. 2, 1988, pp 191-193.

- [58] **D. J. T. Heatley, and T. Hodgkinson**, "*Video transmission over cabled monomode fibre at 1.23 μm using PFM with 2- PSK heterodyne detection*", *Electronic Letters*, Vol. 20, No. 3. , 1984, pp110-111.
- [59] **S. Cowen**, "*Fibre optic video transmission system employing pulse frequency modulation*", *Ocean '79, 5th Annu. Combined Conference*, San Diego, CA, Sep. 1979, pp. 17-19.
- [60] **M. Wenyon**, "*Pulse frequency modulation for broadband transmission*", *Laser Focus*, June 1981, pp. 170-173.
- [61] **L. Chao**, "*Optical Transmission of wideband video signal using SWFM*", PhD Thesis, Department of Electrical Engineering and Electronics, UMIST, Oct. 1990.
- [62] **K. Sato, S. Aoygai, and T. Kitami**, "*Fibre optic video transmission employing square wave frequency modulation*", *IEEE Trans. Communications*, Vol. COM-33, No. 5, 1985, pp. 417-423.
- [63] **B. Wilson, Z. Ghassemlooy, and C. Lu**, "*Optical fibre transmission of high definition television signals using squarewave frequency modulation*", *Third Bangor Symp. on Communications*, University of Wales, Bangor, May, 1991, pp. 258-262.
- [64] **Z. Ghassemlooy, B. Wilson, and I. Darwazeh**, "*Optical fibre transmission of video and audio signals using square wave frequency modulation*", *IEEE Trans. On Consumer Electronics*, Vol. 39, No. 1, 1993, pp. 33-39.
- [65] **R. Cryan, et-al**, "*Optical fibre digital pulse position modulation assuming a Gaussian received pulse shape*", *IEE Proc. Pt-J*, Vol. 137, 1990, pp. 89-96.

[66] **S. VandenBrink, P. Goud, and C. Englefield**, "*Implementation of the pulse interval modulation code 3B17P for 90 Mbit/s LED single mode fibre system*", IEEE Pacific Conference on Communication, Computers and Signal Processing, June, 1989, pp. 423-425.

[67] **J. Das**, "*Quantitative noise reduction in pulse time modulation*", Electronic Engineering, Sep. 1955, pp 406-409.

[68] **C. Timmermann**, "*Signal-to-noise ratio of a video signal transmitted by a fibre-optic system using pulse-frequency modulation*", IEEE Trans. on Broadcasting, Vol. BC-23, No.1, 1977, pp 12-16.

[69] **V. Di Biase, P. Passeri, and R. Pietroiusti**, "*Pulse analogue transmission of TV signal on optical fibre*", Alta Frequenza, Vol. LVI, No. 4, 1987, pp. 195-203.

[70] **R. Webb**, "*Output noise spectrum from demodulator in an optical PFM system*", Electronic Letters, Vol. 18, No. 4, 1982, pp. 634-636.

[71] **D. J. T. Heatley**, "*SNR comparison between two designs of PFM demodulator used to demodulate PFM or FM*", Electronic Letters, No. 5, 1984, pp. 214-215.

[72] **C. Timmermann**, "*Noise in receivers for pulse frequency modulated optical signals*", A. E. U., Vol. 30, 1977, pp. 285.

[73] **P. Sharma, and J. Tripathi**, "*Signal-to-noise ratio studies of PIM and PIM-FM systems*", Int. J. Electronics, Vol. 28, 1970, pp. 129-141.

[74] **S. Marougi, and K. Sayhood**, “*Signal-to-noise performance of the pulse - interval and width modulation system*”, *Electronic Letters*, Vol. 19. No. 14, 1983, pp 528-529.

[75] **Y. Ueno, and T. Yasugi**, “*Optical fibre communications using pulse-interval modulation*”, *NEC Research and Development*, No. 48, 1978, pp. 45-52.

[76] **I. Gradshteyn, and I. Ryzhik**, “*Tables of integrals, series, and products*”, Academic Press, Fourth Edition, 1965, NewYork.

[77] **M. Abramowitz, and L. Stegun**, “*Handbook of mathematical functions with formulas, graphs, and mathematical tables*”, Dover Publications, Ninth Printing, 1970, NewYork.

[78] **O. Kruse, D. Lewis, and R. Metz**, “*Spectrum analysis of a train of modulated combination leading- and trailing-edge variable-slope pulses*”, *Electronic Engineering*, Feb. 1968, pp. 100-102.

[79] **O. Krause, and R. Montgomery**, “*Spectrum of a train of modulated trailing edge variable slope pulses*”, *Electronic Engineering*, Sept. 1966, pp. 593-595.

[80] **O. Kruse**, “*Spectrum analysis of variable slope pulse modulation waves*”, *The Texas Journal of Science*, No. 4, Dec. 1949, pp.378-389.

[81] **D. Grieg, and A. Levine**, “*Pulse-time modulated multiplex radio relay system-terminal equipment*”, *Electrical Communications*, Vol. 23, 1946, pp. 159-178.

- [82] **H. Baeyer**, “*The basic principles of multi-channel transmission with modulated impulses*”, The Brown Boveri Review, March. 1946, pp. 65-69
- [83] **Venkatesan, P. Natarajan, and J. Orson**, “*Transmission of FDM wideband data and video channels over a single-mode fibre using 1300 μm LED*”, Electronic Letters, Vol. 24 No. 7, 1988, pp 387-389.
- [84] **J. M. Senior**, “*Optical fibre communications; principles and practice*”, Prentice-Hall International, 2nd Edition, 1992.
- [85] **A. Lowery, and R. Geels**, “*LED spectral slicing for single mode local loop applications*”, Electronic letters, Vol. 24, No. 7, 1988, pp389-390.
- [86] **R. Olshansky, V. Lanzisera, and P. Hill**, “*Subcarrier multiplexed lightwave systems for broadband distribution*”, J. Lightwave Technology, Vol. 7, No. 9, 1989, pp. 132-134.
- [87] **B. Wilson, and Z. Ghassemlooy**, “*Optical fibre transmission of multiplexed video signals using PWM*”, Int. J. Optoelectronics, Vol. 4, 1989, pp. 3-17.
- [88] **M. Sato, T. Murata, and T. Namekawa**, “*A simplified voice two channel transmission experiment by pulse interval-width modulation*”, Trans. IEICE, No. 7, 1979, pp. 712-713.
- [89] ALS/AS Logic Databook, National Semiconductor Corporation, 1987.

[90] **J. Flood and J. Tillman**, “*Cross talk in amplitude-modulated time division multiplex systems*”, Proceedings of the Institution of Electrical Eng., Paper No. 1130, 1951, pp.279-293.

[91] **E. Kretzmer**, “*Interference characteristics of pulse time modulation*”, Proceedings of the IRE, March, 1950, pp. 22-255.

[92] **S. Moskowitz, L. Diven, and R. S. Feit**, “*Cross-talk considerations in time division multiplex systems*”, Proceedings of the I. R. E. Nov. 1950, pp.1330-1336.

[93] **C. Shannon**, “*Communication in the presence of noise*”, Proceedings of the I.R.E., Jan. 1949, pp10-23.

[94] **T. Kanada, K. Hakoda, and E. Yoneda**, “*SNR fluctuation and non-linear distortion in PFM optical NTSC video transmission systems*”, IEEE Trans. Communications, Vol. COM-30, No. 8, 1982, pp. 1868-1875.

[95] **E. Yoneda, T. Kanada, and K. Hakoda**, “*Design and performance of optical fibre transmission systems for colour television signals*”, Review of the Electrical Communication Lab. Vol. 29, No. 11-12, 1981, pp. 1107-1117.

[96] **A. Drukarev**, “*Noise performance and SNR threshold in PFM*”, IEEE Trans. Communications, Vol. COM-33, No. 7, 1985, pp. 708-7111.

Appendix - I

Derivation of the baseband components of the CPFWM waveform

The baseband components of the CPFWM waveform can be derived from equation 6.8 as the value of $v(t)$ when $n \rightarrow 0$. Therefore,

$$\begin{aligned}
 \text{Baseband Components} &= \lim_{n \rightarrow 0} v(t) \\
 &= \lim_{n \rightarrow 0} \left[\frac{e^{jn\omega_c t}}{2n\pi j} \left\{ \exp[jn\beta \sin \omega_1 t] \right. \right. \\
 &\quad \left. \left. - \exp\left\{-jn\left[\omega_c \tau_o + \pi M \sin \omega_2 t - \beta \sin \omega_1 \left(t - \tau_o - \frac{\pi M}{\omega_o} \sin \omega_2 t\right)\right]\right\} \right\} \right]
 \end{aligned} \tag{I.1}$$

The power series expansion of exponential function is given as;

$$e^y = 1 + y + \frac{y^2}{2!} + \frac{y^3}{3!} + \dots \tag{I.2}$$

Substituting the above power series expansion (equation I.2) into equation I.1, all the terms will vanish except the first order terms which can be written as;

$$\lim_{n \rightarrow 0} v(t) = \frac{1}{2\pi} \left(\beta \sin \omega_1 t + \omega_c \tau_o + 2\pi M \sin \omega_2 t - \beta \sin \omega_1 x \right) \tag{I.3}$$

where,

$$x = t - \tau_o - \frac{\pi M}{\omega_o} \sin \omega_2 t \tag{I.4}$$

The last term in equation I.3 can be simplified as follows;

$$\begin{aligned}
\sin \omega_1 x &= \sin \left[\omega_1 (t - \tau_o) - 2\pi M \frac{\omega_1}{\omega_c} \sin \omega_2 t \right] \\
&= \sin \omega_1 (t - \tau_o) \cos \left(2\pi M \frac{\omega_1}{\omega_c} \sin \omega_2 t \right) - \cos \omega_1 (t - \tau_o) \sin \left(2\pi M \frac{\omega_1}{\omega_c} \sin \omega_2 t \right)
\end{aligned}
\tag{I.5}$$

The above equation can be further simplified by expanding the trigonometric terms in terms of Bessel functions, this leads to;

$$\begin{aligned}
\sin \omega_1 x &= \sin \omega_1 (t - \tau_o) \left\{ J_o \left(2\pi M \frac{\omega_1}{\omega_c} \right) + \sum_{n \text{ even}}^{\infty} 2J_n \left(2\pi M \frac{\omega_1}{\omega_c} \right) \cos n\omega_2 t \right\} \\
&\quad - \cos \omega_1 (t - \tau_o) \left\{ \sum_{n \text{ odd}}^{\infty} 2J_n \left(2\pi M \frac{\omega_1}{\omega_c} \right) \sin n\omega_2 t \right\}
\end{aligned}
\tag{I.6}$$

The above equation can be further simplified by using the following identity;

$$\sin \alpha \cos \beta = \frac{1}{2} [\sin(\alpha + \beta) + \sin(\alpha - \beta)]
\tag{I.7}$$

Substituting equation I.7 into I.6 the following can be obtained;

$$\begin{aligned}
\sin \omega_1 x &= J_o \left(2\pi M \frac{\omega_1}{\omega_c} \right) \sin(t - \tau_o) + \sum_{n \text{ even}} J_n \left(2\pi M \frac{\omega_1}{\omega_c} \right) \\
&\quad \times \left\{ \sin[(n\omega_2 + \omega_1)t - \omega_1 \tau_o] + \sin[(\omega_1 - n\omega_2)t - \omega_1 \tau_o] \right\} \\
&\quad - \sum_{n \text{ odd}} J_n \left(2\pi M \frac{\omega_1}{\omega_c} \right) \left\{ \sin[(n\omega_2 + \omega_1)t - \omega_1 \tau_o] - \sin[(\omega_1 - n\omega_2)t - \omega_1 \tau_o] \right\}
\end{aligned}
\tag{I.8}$$

But

$$J_{-n}(a) = (-1)^n J_n(a) \quad (\text{I.9})$$

Therefore, equation I.8 can then be written as;

$$\sin \omega_1 x = \sum_{n=-\infty}^{\infty} J_n(2\pi M \frac{\omega_1}{\omega_c}) \sin\{(\omega_1 - n\omega_2)t - \omega_1 \tau_o\} \quad (\text{I.10})$$

Substituting equation I.10 into I.3, the baseband components can then be given as;

$$\lim_{n \rightarrow 0} v(t) = \frac{\omega_c \tau_o}{2\pi} + \frac{\beta}{2\pi} \sin \omega_1 t + M \sin \omega_2 t \quad (\text{I.11})$$
$$- \frac{\beta}{2\pi} \sum_{m=-\infty}^{\infty} J_m(2\pi M \frac{\omega_1}{\omega_c}) \sin\{(\omega_1 - m\omega_2)t - \omega_1 \tau_o\}$$

The above equation represents the baseband components and has been used in chapter.

Appendix-II

Derivation of the carrier components and their harmonics

The carrier frequency components and their harmonics as well as the sidetones around them can be derived from the last term in equation 6.14, which can be written as;

$$C = \sum_{\substack{n=-\infty \\ n \neq 0}}^{\infty} \sum_{k=-\infty}^{\infty} \frac{J_k(n\beta)e^{j(n\omega_c+k\omega_1)t}}{2n\pi j} \times \left\{ 1 - \sum_{p=-\infty}^{\infty} (-1)^p J_p(2n\pi M + 2k\pi M \frac{\omega_1}{\omega_c}) \exp\{-j[(n\omega_c + k\omega_1)\tau_o + jp\omega_2 t]\} \right\} \quad (\text{II.1})$$

The above can be split into two terms as follows;

$$C = C_1 + C_2 \quad (\text{II.2})$$

where,

$$C_1 = \sum_{\substack{n=-\infty \\ n \neq 0}}^{\infty} \sum_{k=-\infty}^{\infty} \frac{J_k(n\beta)e^{j(n\omega_c+k\omega_1)t}}{2n\pi j} \quad (\text{II.3})$$

and

$$C_2 = \sum_{\substack{n=-\infty \\ n \neq 0}}^{\infty} \sum_{k=-\infty}^{\infty} \sum_{p=-\infty}^{\infty} (-1)^p \frac{J_k(n\beta)e^{j(n\omega_c+k\omega_1)t}}{2n\pi j} J_p(2n\pi M + 2k\pi M \frac{\omega_1}{\omega_c}) \times \exp\{-j[(n\omega_c + k\omega_1)\tau_o + jp\omega_2 t]\} \quad (\text{II.4})$$

The first term of equation II.3 can be simplified as follows; equation II.3 can be rewritten as;

$$C_1 = \sum_{n=1}^{\infty} \sum_{k=1}^{\infty} \left\{ \frac{J_k(n\beta)e^{j(n\omega_c+k\omega_1)t}}{2n\pi j} + \frac{J_{-k}(-n\beta)e^{-j(n\omega_c+k\omega_1)t}}{-2n\pi j} \right. \\ \left. + \frac{J_k(-n\beta)e^{j(-n\omega_c+k\omega_1)t}}{-2n\pi j} + \frac{J_{-k}(n\beta)e^{j(n\omega_c-k\omega_1)t}}{2n\pi j} \right\} \quad (\text{II.5})$$

Consider the following identities;

$$\left. \begin{aligned} J_{-n}(x) &= (-1)^n J_n(x) \\ \text{and} \\ J_{-n}(-x) &= J_n(x) \end{aligned} \right\} \quad (\text{II.6})$$

Using the above identities into equation II.5, the following can be obtained;

$$C_1 = \sum_{n=1}^{\infty} \sum_{k=1}^{\infty} \frac{J_k(n\beta)}{2n\pi j} \left[\{e^{j(n\omega_c+k\omega_1)t} - e^{-j(n\omega_c+k\omega_1)t}\} + (-1)^k \{e^{j(n\omega_c-k\omega_1)t} - e^{-j(n\omega_c-k\omega_1)t}\} \right] \quad (\text{II.7})$$

However, the above exponential functions can be converted into trigonometric forms using the following identity;

$$\sin x = \frac{e^{jx} - e^{-jx}}{2j} \quad (\text{II.8})$$

therefore, equation II.7 can be rewritten as;

$$C_1 = \sum_{n=1}^{\infty} \sum_{k=1}^{\infty} \frac{J_k(n\beta)}{2n\pi j} \left[\sin(n\omega_c + k\omega_1)t + (-1)^k \sin(n\omega_c - k\omega_1)t \right] \quad (\text{II.9})$$

Using the same above approach, the second term C2 can also be simplified. C2 can then be rewritten as;

$$C_2 = \sum_{n=1}^{\infty} \sum_{k=1}^{\infty} \sum_{p=1}^{\infty} \{ (f(n, k, p) + f(-n, -k, -p)) + (f(n, k, p) + f(-n, -k, -p)) + (f(n, k, p) + f(-n, -k, -p)) + (f(n, k, p) + f(-n, -k, -p)) \} \quad (\text{II.10})$$

where;

$$f(n, k, p) = (-1)^p \frac{J_k(n\beta)}{2n\pi j} J_p(2n\pi M + 2k\pi M \frac{\omega_1}{\omega_c}) \times \exp\{-j[(n\omega_c + k\omega_1)\tau_o + j(n\omega_c + k\omega_1 + p\omega_2)t]\} \quad (\text{II.11})$$

For simplicity, the terms between brackets in equation II.10 will be simplified separately. Therefore, using the identities in II.6 into the first two terms of II.10, the following can be driven;

$$f(n, k, p) + f(-n, -k, -p) = (-1)^p \frac{J_k(n\beta)}{2n\pi j} J_p(2n\pi M + 2k\pi M \frac{\omega_1}{\omega_c}) \times \{ \exp\{j[(n\omega_c + k\omega_1 + p\omega_2)t - (n\omega_c + k\omega_1)\tau_o]\} - \exp\{-j[(n\omega_c + k\omega_1 + p\omega_2)t - (n\omega_c + k\omega_1)\tau_o]\} \} \quad (\text{II.12})$$

Equation II.12 can be written as;

$$f(n, k, p) + f(-n, -k, -p) = (-1)^p \frac{J_k(n\beta)}{n\pi} J_p(2n\pi M + 2k\pi M \frac{\omega_1}{\omega_c}) \times \{ \sin[(n\omega_c + k\omega_1 + p\omega_2)t - (n\omega_c + k\omega_1)\tau_o] \} \quad (\text{II.13})$$

Similarly, the other terms of II.10 can be simplified as follows;

$$f(n, k, -p) + f(-n, -k, p) = -\frac{J_k(n\beta)}{n\pi} J_p(2n\pi M + 2k\pi M \frac{\omega_1}{\omega_c}) \times \{\sin[(n\omega_c + k\omega_1 - p\omega_2)t - (n\omega_c + k\omega_1)\tau_o]\} \quad (\text{II.14})$$

$$f(n, -k, p) + f(-n, k, -p) = (-1)^{k+1} \frac{J_k(n\beta)}{n\pi} J_p(2n\pi M - 2k\pi M \frac{\omega_1}{\omega_c}) \times \{\sin[(n\omega_c - k\omega_1 + p\omega_2)t - (n\omega_c - k\omega_1)\tau_o]\} \quad (\text{II.15})$$

and

$$f(n, -k, -p) + f(-n, k, p) = (-1)^{k+1} \frac{J_k(n\beta)}{n\pi} J_p(2n\pi M - 2k\pi M \frac{\omega_1}{\omega_c}) \times \{\sin[(n\omega_c - k\omega_1 - p\omega_2)t - (n\omega_c - k\omega_1)\tau_o]\} \quad (\text{II.16})$$

Substitute equations II.13- II.16 into equation II.10, the later can be rewritten as;

$$C_2 = \sum_{n=1}^{\infty} \sum_{k=1}^{\infty} \sum_{p=1}^{\infty} \{(-1)^{p+1} \frac{J_k(n\beta)}{n\pi} J_p(2n\pi M + 2k\pi M \frac{\omega_1}{\omega_c}) \times \{\sin[(n\omega_c + k\omega_1 + p\omega_2)t - (n\omega_c + k\omega_1)\tau_o]\} - \frac{J_k(n\beta)}{n\pi} J_p(2n\pi M + 2k\pi M \frac{\omega_1}{\omega_c}) \times \{\sin[(n\omega_c + k\omega_1 - p\omega_2)t - (n\omega_c + k\omega_1)\tau_o]\} + (-1)^{k+1} \frac{J_k(n\beta)}{n\pi} \times J_p(2n\pi M - 2k\pi M \frac{\omega_1}{\omega_c}) \{\sin[(n\omega_c - k\omega_1 + p\omega_2)t - (n\omega_c - k\omega_1)\tau_o]\} + (-1)^{k+1} \frac{J_k(n\beta)}{n\pi} J_p(2n\pi M - 2k\pi M \frac{\omega_1}{\omega_c}) \{\sin[(n\omega_c - k\omega_1 - p\omega_2)t - (n\omega_c - k\omega_1)\tau_o]\} \} \quad (\text{II.17})$$

Using the identity in II.5 in II.17 the latter may be written as;

$$C_2 = \sum_{n=1}^{\infty} \sum_{k=-\infty}^{\infty} \sum_{p=-\infty}^{\infty} \left\{ (-1)^{p+1} \frac{J_k(n\beta)}{n\pi} J_p \left(2n\pi M + 2k\pi M \frac{\omega_1}{\omega_c} \right) \times \right. \\ \left. \{ \sin[(n\omega_c + k\omega_1 + p\omega_2)t - (n\omega_c + k\omega_1)\tau_o] \} \right\} \quad (\text{II.18})$$

Using the identity in II.6 in equation II.18, then change the variables $-p$ to p , equation II.18 can be rewritten as;

$$C_2 = - \sum_{n=1}^{\infty} \sum_{k=-\infty}^{\infty} \sum_{p=-\infty}^{\infty} \left\{ \frac{J_k(n\beta)}{n\pi} J_p \left(2n\pi M + 2k\pi M \frac{\omega_1}{\omega_c} \right) \times \right. \\ \left. \{ \sin[(n\omega_c + k\omega_1 - p\omega_2)t - (n\omega_c + k\omega_1)\tau_o] \} \right\} \quad (\text{II.19})$$

Substitute equations II.19 and II.9 in II.2. The latter can be written as;

$$C = \sum_{n=1}^{\infty} \sum_{k=1}^{\infty} \frac{J_k(n\beta)}{2n\pi j} \left[\sin(n\omega_c + k\omega_1)t + (-1)^k \sin(n\omega_c - k\omega_1)t \right] \\ - \sum_{n=1}^{\infty} \sum_{k=-\infty}^{\infty} \sum_{p=-\infty}^{\infty} \left\{ \frac{J_k(n\beta)}{n\pi} J_p \left(2n\pi M + 2k\pi M \frac{\omega_1}{\omega_c} \right) \times \right. \\ \left. \{ \sin[(n\omega_c + k\omega_1 - p\omega_2)t - (n\omega_c + k\omega_1)\tau_o] \} \right\} \quad (\text{II.20})$$

Appendix -3

Cross-talk in the TDM-PPM System

Consider the case when two PPM channels with identical characteristics are multiplexed in the time domain. The timing diagram is shown in Fig. III.1. Due to the limitation in the transmission bandwidth, the actual pulse shapes tend to overlap. This resulting in cross-talk between the two PPM channels. This cross-talk depends on the guard time T_g .

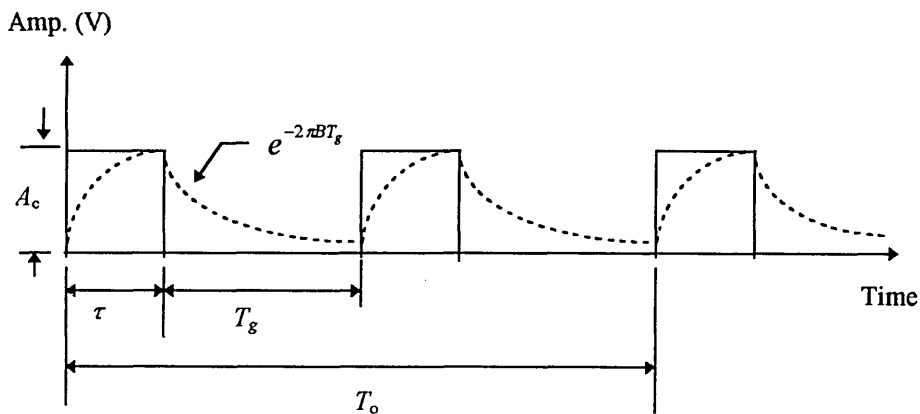


Fig. III.1 Time diagram of TDM-PPM waveform.

For a quantitative estimate of cross-talk, it is known that the pulses decay exponentially with time constant of order $1/2\pi B$ where B is the 3 dB bandwidth of the channel. Therefore, the cross-talk factor can be given as;

$$k \equiv \left(\frac{A_c}{A}\right)^2 = e^{-4\pi BT_g} \approx -54.5BT_g \quad (\text{dB}) \quad (\text{III.1})$$

The above factor represents the strength of the cross-talk component at the signal channel. The maximum permitted displacement for each PM channel is given as;

$$t_{o1,2} = \frac{1}{2} \left\{ \frac{T_o}{2} - \tau - T_g \right\} \quad (\text{III.2})$$

Therefore the modulation index for either the first or the second channel can be determined as;

$$M_{1,2} = \frac{2t_{o1,2}}{T_o} = \frac{1}{2} - \frac{\tau}{T_o} - \frac{T_g}{T_o} \quad (\text{III.3})$$

Substitute equation III1 into III3, the cross-talk factor from the first channel to the second channel can be calculated as;

$$k = -54.5BT \left\{ M - \frac{1}{2} - \frac{\tau}{T_o} \right\} \quad (\text{in dB}) \quad (\text{III.4})$$

The signal power at the demodulator output can be given as;

$$S_1 = \frac{1}{2} \left(\frac{t_{o1}}{T_o} \right)^2 \quad (\text{III.5})$$

Substituting equation III.3 into III.5, the later can be rewritten as;

$$S_1 = \frac{M_1^2}{8} = 10 \log \left(\frac{M_1^2}{8} \right) \quad (\text{in dB}) \quad (\text{III.6})$$

Therefore the cross-talk in the second channel due to the first can be given as;

$$\text{Cross-talk}(dB) = -54.5BT \left(M_2 - \frac{1}{2} - \frac{\tau}{T_o} \right) - 10 \log \left(\frac{M_{1_1}^2}{8} \right) \quad (\text{III.6})$$

The above equation could be rewritten in terms of the pulse rise time by substituting for $B=1/2t_R$, this leads to;

$$\text{Cross-talk}(dB) = -\frac{27.25T}{t_R} \left(M_2 - \frac{1}{2} - \frac{\tau}{T_o} \right) - 10 \log \left(\frac{M_{1_1}^2}{8} \right) \quad (\text{III.7})$$